



**HAL**  
open science

# Generation of high drug loading amorphous solid dispersions by different manufacturing processes

Bhianca Lins de Azevedo Costa

► **To cite this version:**

Bhianca Lins de Azevedo Costa. Generation of high drug loading amorphous solid dispersions by different manufacturing processes. Chemical and Process Engineering. Ecole des Mines d'Albi-Carmaux, 2018. English. NNT : 2018EMAC0012 . tel-02180544

**HAL Id: tel-02180544**

**<https://theses.hal.science/tel-02180544>**

Submitted on 11 Jul 2019

**HAL** is a multi-disciplinary open access archive for the deposit and dissemination of scientific research documents, whether they are published or not. The documents may come from teaching and research institutions in France or abroad, or from public or private research centers.

L'archive ouverte pluridisciplinaire **HAL**, est destinée au dépôt et à la diffusion de documents scientifiques de niveau recherche, publiés ou non, émanant des établissements d'enseignement et de recherche français ou étrangers, des laboratoires publics ou privés.



# THÈSE

En vue de l'obtention du

## DOCTORAT DE L'UNIVERSITÉ DE TOULOUSE

Délivré par :

IMT - École Nationale Supérieure des Mines d'Albi-Carmaux

---

**Présentée et soutenue par :**

**Bhianca LINS DE AZEVEDO COSTA**

le 13/12/2018

**Titre :**

Generation of high drug loading amorphous solid dispersions by different manufacturing processes

---

**École doctorale et discipline ou spécialité :**

ED MEGEP : Génie des procédés et de l'Environnement

**Unité de recherche :**

Centre RAPSODEE, UMR CNRS 5302, IMT Mines Albi

**Directeur/trice(s) de Thèse :**

Maria Inês RÉ, Directrice de Recherche HDR, IMT Mines Albi

Martial SAUCEAU, Maître-assistant, IMT Mines Albi

**Jury :**

Bernard BATAILLE, Professeur, Université de Montpellier, Président  
Eric BEYSSAC, Professeur, Université d'Auvergne Clermont-Ferrand, Rapporteur  
Jean-François WILLART, Professeur, Université de Lille, Rapporteur  
Romain SESCOUSSE, Maître-assistant, IMT Mines Albi, Examineur  
Jérôme MENEGOTTO, Evotec Toulouse, Invité



**Com amor,**

*Aos meus avôs, Zenilda e José Barros, que se tornaram meus anjos no céu nesse último ano de tese.*

*À toda minha família, por ter aberto meus caminhos e me deixado voar sendo sempre minha melhor companhia e meu porto seguro.*

*Aos meus amigos brasileiros e todos os amigos que a França me deu, por todo apoio, amor, ajuda e por ter sido muitas vezes a minha família aqui.*

**Em especial,**

*Aos meus orientadores, Inês, Martial e Romain, por seu apoio contínuo, paciência, motivação, entusiasmo e imenso conhecimento.*

*À IMT Mines Albi e ao Centro RAPSODEE, por todo o suporte, ensinamentos e ajuda durante esses anos de tese.*

**With love,**

*To my grandparents, Zenilda and José Barros, who became my angels in heaven in this last year of thesis.*

*To all my family, for having opened my ways and let me fly being always my best company and my safe harbor.*

*To my Brazilian friends and all the friends that France has given me, for all the support, love, help and for having been my family here in many times.*

**In particular,**

*To my supervisors, Inês, Martial and Romain, for their continued support, patience, motivation, enthusiasm and immense knowledge.*

*To IMT Mines Albi and the RAPSODEE Center, for all the support, teachings and help during these years of thesis.*

**Avec amour,**

*À mes grands-parents, Zenilda et José Barros, qui sont devenus mes anges au paradis lors de cette dernière année de thèse.*

*À toute ma famille, pour m'avoir ouvert la voie et m'avoir laissée voler de mes propres ailes tout en restant ma meilleure compagnie et mon refuge.*

*À mes amis brésiliens et à tous les amis que la France m'a apportés, pour tout le soutien, l'amour, l'aide et pour avoir été ma famille ici plusieurs fois.*

**En particulier,**

*À mes encadrants, Inês, Martial et Romain, pour leur soutien continu, leur patience, leur motivation, leur enthousiasme et leur immense connaissance.*

*À IMT Mines Albi et le Centre RAPSODEE, pour tout le soutien, les enseignements et l'aide durant ces années de thèse.*



## Résumé

La principale difficulté lors de l'administration orale d'un ingrédient pharmaceutique actif (API) est de garantir que la dose clinique de l'API sera dissoute dans le volume disponible de liquides gastro-intestinaux. Toutefois, environ 40% des API sur le marché et près de 90% des molécules en cours de développement sont peu solubles dans l'eau et présentent une faible absorption par voie orale, ce qui entraîne une faible biodisponibilité. Les dispersions solides amorphes (ASD) sont considérées comme l'une des stratégies plus efficaces pour résoudre des problèmes de solubilité des principes actifs peu solubles dans l'eau et, ainsi, améliorer leur biodisponibilité orale. En dépit de leur introduction il y a plus de 50 ans comme stratégie pour améliorer l'administration orale des API, la formation et la stabilité physique des ASD font toujours l'objet de recherches approfondies. En effet, plusieurs facteurs peuvent influencer sur la stabilité physique des ASD pendant le stockage, parmi lesquels la température de transition vitreuse du mélange binaire API-polymère, la solubilité apparente de l'API dans le polymère, les interactions entre l'API et le polymère et le procédé de fabrication. Cette thèse consistait en deux parties qui avaient pour objectif le développement de nouvelles formulations sous forme d'ASD d'un antirétroviral, l'Efavirenz (EFV), dispersé dans un polymère amphiphile, le Soluplus, en utilisant deux procédés différents, le séchage par atomisation (SD) et l'extrusion à chaud (HME). EFV est l'API BCS de classe II de notre choix car c'est un API qui représente un défi pour les nouvelles formulations. En effet, il a besoin d'ASD plus fortement concentrées, pour lesquelles la stabilité chimique et physique pendant le stockage et la dissolution seront essentielles. Dans le but de développer de manière rationnelle les ASDs EFV-Soluplus à forte concentration, la première partie s'est concentrée sur la construction d'un diagramme de phases EFV-Soluplus en fonction de la composition et de la température. Le diagramme de phases a été construit à partir d'une étude thermique de recristallisation d'un ASD sursaturé (85 %m EFV), générée par séchage par atomisation. À notre connaissance, il s'agit de la première étude à présenter un diagramme de phase pour ce système binaire. Ce diagramme de phases est très utile et démontre que la solubilité de l'EFV dans les solutions varie de 20 %m (25 °C) à 30 %m (40 °C). Les ASD de EFV dans le Soluplus contenant plus de 30 %m d'EFV doivent être surveillées pendant le stockage dans des conditions typiques de température. Ce diagramme de phases peut être considéré comme un outil de pré-formulation pour les chercheurs qui étudient de nouvelles ASD d'EFV dans le Soluplus afin de prédire la stabilité (thermodynamique et cinétique). Les ASD préparées par différentes techniques peuvent afficher des différences dans leurs propriétés physicochimiques. La deuxième partie de cette thèse portait sur la fabrication d'ASD par des procédés HME et SD. Cette étude montre clairement que la formation d'ASD est une stratégie de formulation utile pour améliorer la solubilité dans l'eau et la vitesse de dissolution de l'EFV à partir de mélanges binaires EFV-Soluplus. Les procédés de fabrication (HME et SD) se sont révélés efficaces pour générer des ASD dans une large gamme de compositions en EFV. L'optimisation du ratio EFV-Soluplus peut être utilisée pour adapter la libération cinétique des ASD. Le choix d'une charge EFV élevée dépassant la solubilité thermodynamique de l'EFV dans le Soluplus est possible, mais il convient de prendre en compte sa stabilité cinétique dans le temps.

**Mots clés :** *Dispersion solides amorphes, séchage par atomisation, extrusion à chaud, amélioration de la solubilité, diagramme de phase, libération de principe actif, Efavirenz, Soluplus.*



# Table of contents

<b>Table of contents</b> .....	<b>7</b>
<b>List of figures</b> .....	<b>11</b>
<b>List of tables</b> .....	<b>17</b>
<b>List of abbreviations</b> .....	<b>19</b>
<b>Chapter 1 - Introduction</b> .....	<b>23</b>
1. Background .....	25
2. Objectives .....	29
<b>Chapter 2 – Theoretical Section</b> .....	<b>33</b>
1. Poorly water soluble APIs .....	35
1.1. A general view on the solubility problem for oral pharmaceutical formulation .....	35
1.1.1. The oral route .....	35
1.1.2. Solubility challenges and reasons for poor solubility .....	37
1.2. Formulation approaches for solubility/dissolution rate enhancement .....	39
1.2.1. Solubilization/Complexation .....	39
1.2.2. Crystal engineering .....	40
1.3. Solid dispersions engineering .....	42
1.3.1. Definition and types of solid dispersions .....	42
1.3.2. The amorphous state .....	43
1.3.3. Effect “Spring and parachute” .....	46
1.3.4. Mechanisms of API release from ASDs .....	47
1.3.5. Stability .....	49
1.3.6. Characterization of amorphous solid dispersions (ASDs) .....	52
1.3.6.1. Thermal analysis .....	52
1.3.6.2. X-ray diffraction .....	54
1.3.6.3. Spectroscopic methods: Raman (RM) and Fourier-transform infrared spectroscopy (FTIR) .....	54
1.3.6.4. Scanning electron microscopy (SEM) .....	55
1.3.6.5. Dynamic vapor sorption (DVS) .....	55
1.3.6.6. Apparent kinetic solubility .....	56
1.3.6.7. Dissolution .....	57
1.3.7. Manufacturing amorphous solid dispersions (ASDs) .....	66
1.3.8. Manufacturing processes .....	70
1.3.8.1. Spray drying (SD) .....	70
1.3.8.2. Hot-Melt extrusion (HME) .....	74
1.3.8.3. Comparison of manufacturing processes .....	80
2. Rational development of amorphous solid dispersions .....	83

2.1. Screening of carrier .....	83
2.1.1. API-carrier miscibility .....	83
2.1.2. Temperature-composition phase diagrams .....	84
2.1.2.1. Equilibrium equations.....	89
3. Amorphous solid dispersion of Efavirenz (API) and Soluplus® (carrier) .....	92
3.1. Active Pharmaceutical Ingredient (API) - Efavirenz .....	92
3.2. Carrier - Soluplus® .....	95
3.3. Efavirenz- Soluplus miscibility .....	98
4. References .....	99
<b>Chapter 3-Efavirenz/Soluplus® properties and solubility measurements.....</b>	<b>113</b>
1. Introduction .....	115
2. Materials and Methods .....	116
2.1. Materials.....	116
2.2. Methods.....	116
2.2.1. Characterization of pure compounds .....	116
2.2.1.1. Shape and morphology (SEM) .....	116
2.2.1.2. True density .....	116
2.2.1.3. Solid state (XRD) .....	116
2.2.1.4. Thermal properties (DSC) .....	117
2.2.1.5. Characterization of Soluplus® micelles .....	117
2.2.1.6. Solubility of crystalline EFV in aqueous medium.....	117
2.2.1.7. Solubility of crystalline EFV in the presence of Soluplus® .....	118
2.2.2. Temperature-composition EFV-Soluplus phase diagram.....	118
2.2.2.1. Preparation of a supersaturated EFV-Soluplus solid dispersion by spray drying .....	118
2.2.2.2. Determination of EFV solubility in Soluplus by recrystallization .....	119
3. Results .....	121
3.1. Characterization of pure compounds.....	121
3.1.1. Efavirenz.....	121
3.1.2. Soluplus® .....	123
3.1.3. Solubility of crystalline EFV in the presence of Soluplus® in water.....	126
3.2. API-polymer solubility determination by recrystallization.....	127
4. Conclusion .....	133
5. References .....	135
<b>Chapter 4 -Efavirenz/Soluplus® amorphous solid dispersions manufactured by Spray Drying .....</b>	<b>137</b>
1. Introduction .....	139
2. Generation of EFV-SOL binary mixtures .....	140
2.1. Preparation methods .....	140

3. Characterization techniques.....	141
3.1. Raman Mapping (RM) .....	141
3.2. Fourier Transform Infrared Spectroscopy (FTIR) .....	141
3.3. Performance behavior .....	141
3.3.1. In vitro drug release dissolution tests.....	141
4. Results .....	144
4.1. Characterization of ASDs.....	144
4.1.1. SEM images .....	144
4.1.3. Raman Mapping.....	147
4.1.4. Solid state (XRD).....	149
4.1.5. Glass transition temperature of binary mixtures (DSC) .....	149
4.1.6. Fourier Transform Infrared Spectroscopy (FTIR) .....	151
4.2. Performance behavior .....	153
4.2.1. Solubility studies.....	153
4.2.2. Dissolution studies .....	156
4.2.3. Physical Stability .....	160
5. Conclusion .....	167
6. References .....	169

## **Chapter 5 -Efavirenz/Soluplus® amorphous solid dispersions manufactured by Hot-melt**

<b>Extrusion .....</b>	<b>173</b>
1. Introduction .....	175
2. Generation of EFV-SOL binary mixtures .....	176
2.1. Preparation methods .....	176
3. Characterization techniques.....	178
4. Results .....	179
4.1. Characterization of ASDs.....	179
4.1.1. Microscopic observations .....	179
4.1.2. Raman Spectroscopy.....	180
4.1.3. Solid state (DRX).....	181
4.1.4. Glass transition temperature of binary mixtures (DSC) .....	181
4.1.5. Fourier Transform Infrared Spectroscopy (FTIR) .....	182
4.2. Performance behavior .....	183
4.2.1. Solubility studies.....	183
4.2.2. In vitro dissolution studies .....	186
4.2.3. Physical stability .....	190
5. Effect of the manufacturing process on the ASD properties .....	195
5.1. Solid dispersion characteristics .....	196
5.1.1. Solid state, homogeneity, spatial distribution of EFV .....	196
5.1.2. EFV-Soluplus interactions .....	198

5.2. Performance behavior .....	199
5.2.1. Solubility studies.....	199
5.2.2. Dissolution studies .....	201
5.2.3. Physical Stability .....	204
6. Conclusion .....	207
7. References .....	209
<b>Chapter 6 -General conclusion and perspectives .....</b>	<b>211</b>
<b>General conclusion and perspectives.....</b>	<b>213</b>
<b>Chapter 7 – Résumé étendu en français.....</b>	<b>217</b>
<b>Résumé étendu en français.....</b>	<b>219</b>
<b>Références bibliographiques .....</b>	<b>229</b>
<b>Chapter 8 – Works made from this thesis.....</b>	<b>233</b>
<b>Appendix .....</b>	<b>241</b>
Appendix 1- Contribution values of functional groups (Van Krevelen & Te Nijenhuis, 2009) .....	241
Appendix 2 – Approved procedure to EFV quantification by HPLC (Monograph posted on the Pharmacopeia USP) .....	243
Appendix 3 – API release fitting described mathematically by Korsmeyer-Peppas (KP) model.....	245

## List of figures

FIGURE 1. SUMMARY ABOUT THE THESIS OUTLINE AND THE MAIN TOPICS DISCUSSED ON THIS THESIS .....	31
FIGURE 2. SCHEMATIC REPRESENTATION OF ORAL ADMINISTRATION FOR API ABSORPTION AND SYSTEMIC EFFECTS [2]–[4]. .....	35
FIGURE 3. THE BIOPHARMACEUTICAL CLASSIFICATION SYSTEM (BCS) [5] AND THE SUBDIVISION OF CLASS II [11].....	36
FIGURE 4. SOLUBILITY CHALLENGES IN THE ORAL API DEVELOPMENT. A) MARKETED APIs AND B) APIs IN DEVELOPMENT [3] .....	37
FIGURE 5. SCHEMATIC REPRESENTATION OF THE BREAKDOWN OF THE SOLID-STATE BONDS WITHIN A CRYSTAL .....	38
FIGURE 6. SCHEMATIC REPRESENTATION OF THE SOLVATION OF THE INDIVIDUALIZED SPECIES (API MOLECULES/IONS/ATOMS) SURROUNDED BY A SHELL OF WATER MOLECULES. ....	39
FIGURE 7. PLOT OF ENTHALPY, ENTROPY OR FREE VOLUME IN FUNCTION OF TEMPERATURE FOR MOLECULAR SUBSTANCES AT CONSTANT PRESSURE. $T^G$ IS THE GLASS TRANSITION TEMPERATURE AND $T^M$ IS THE MELTING POINT. ADAPTED FROM [43] .....	44
FIGURE 8. COMPARISON OF ENERGY LANDSCAPES OF AMORPHOUS FORM, ASD AND CRYSTALLINE FORM. $M$ IS THE CHEMICAL POTENTIAL WHILE $E_A$ IS THE ACTIVATION ENERGY BARRIER FOR CRYSTALLIZATION. DIAGRAM IS NOT TO SCALE. ADAPTED FROM [53] .....	45
FIGURE 9. API PROFILE DISSOLUTION BASED ON THE AQUEOUS SOLUBILITY OF AMORPHOUS AND CRYSTALLINE API AND AMORPHOUS SOLID DISPERSIONS. ADAPTED FROM [9], [42].....	46
FIGURE 10. REPRESENTATIVE SCHEME OF A MICELLAR SOLUBILIZATION .....	48
FIGURE 11. SOLID DISPERSIONS BASED ON AMORPHOUS POLYMERIC CARRIERS, WITH API CONCENTRATION EXCEEDING OR NOT THE SOLUBILITY OF THE API IN THE CARRIER. A) UNDERSATURATED ASD AND (B) OVERSATURATED ASD .....	51
FIGURE 12. SUMMARY OF ASDS TECHNIQUES OF CHARACTERIZATION.....	52
FIGURE 13. SCHEMATIC REPRESENTATION OF A DSC THERMOGRAM WITH THE MAIN ENDOTHERMIC AND EXOTHERMIC PROCESSES. TAKEN FROM [84] .....	53
FIGURE 14. SCHEMATIC REPRESENTATION OF KINETIC SOLUBILITY FOR AMORPHOUS MATERIALS. ....	56
FIGURE 15. EXAMPLE OF IN VITRO DISSOLUTION PROFILE FOR PERFECT SINK CONDITIONS .....	58

FIGURE 16. IN VITRO DISSOLUTION PROFILES FOR A) INTERMEDIATE NON-SINK CONDITIONS AND B) EXTREMELY NON-SINK CONDITIONS .....	59
FIGURE 17. SCHEMATIC REPRESENTATION OF FORMATION OF ASD THROUGH MELTING AND SOLVENT EVAPORATION METHODS. ADAPTED FROM [77].....	67
FIGURE 18. SUMMARY ABOUT WORKS USING AMORPHOUS SOLID DISPERSIONS (ASDs) IN THIS CENTURY (SOURCE – WEB OF SCIENCE-KEYWORDS: AMORPHOUS SOLID DISPERSIONS. ACCESSED IN: 18/07/2018).....	68
FIGURE 19. GENERATION PROCESSES OF ASDs USED IN THIS CENTURY (2000-2017) (SOURCE – WEB OF SCIENCE; KEYWORDS: AMORPHOUS SOLID DISPERSIONS, PROCESS AND DRUG. ACCESSED IN: 18/07/2018).....	68
FIGURE 20. THE SPRAY DRYING PROCESS OCCURRING IN SUCCESSIVE STEPS: 1. NEBULIZATION OF A LIQUID FORMULATION; 2. LIQUID DROPLETS (SPRAY) - HOT DRYING GAS STREAM CONTACT (MIXING AND FLOW); 3. DRYING OF SPRAY (SOLVENT EVAPORATION); 4) SEPARATION OF DRIED PRODUCT FROM THE AIR. ....	70
FIGURE 21. SCHEMATIC REPRESENTATION OF A HOT MELT EXTRUSION PROCESS .....	74
FIGURE 22. SCHEMA OF HOT-MELT EXTRUSION FOR PHARMACEUTICAL APPLICATION.....	75
FIGURE 23. INPUT AND DEPENDENT VARIABLES IN THE HME PROCESS.....	77
FIGURE 24. SCHEMATIC PHASE-DIAGRAM OF AN API/CARRIER MIXTURE. IT REPRESENTS THE EVOLUTION OF EQUILIBRIUM CONCENTRATIONS AS A FUNCTION OF TEMPERATURE (GREEN LINE) AND THE EVOLUTION OF THE GLASS TRANSITION TEMPERATURE OF MIXTURE (RED LINE) AS A FUNCTION OF TEMPERATURE. THEY DELIMIT ZONES OF STABILITY REPRESENTED BY 1, 2, 3 AND 4.....	85
FIGURE 25. ILLUSTRATION OF EXTRAPOLATED ONSET OF MELTING OF NIFEDIPINE (TRIANGLE) AND FELODIPINE (CIRCLES) AS DEMONSTRATED BY MARSAC ET AL. TAKE FROM [158]. ...	87
FIGURE 26. SCHEMATIC TIME AND PROCESS EVOLUTION OF THE GLASS TRANSITION TEMPERATURE OF AN API-POLYMER MIXTURE WHEN REACHING ITS EQUILIBRIUM SOLUBILITY IN AN ANNEALING. ADAPTED FROM [115].....	89
FIGURE 27. EXAMPLE OF LITERATURE HOW TO PREDICT THE FLORY-HUGGINS SOLUBILITY PARAMETER $\chi$ . $\phi_{POLYMER2}$ IS THE VOLUME FRACTION OF POLYMER. TAKE FROM [158]. ..	92
FIGURE 28. THE STRUCTURE OF SOLUPLUS®. THE THREE DIFFERENT BLOCK POLYMERS SHOWN ARE PVCL, PVAc, AND PEG, AND THEIR RESPECTIVE MONOMER RATIOS 57:30:13.....	96
FIGURE 29. MICELLES FORMATION OF SOLUPLUS IN WATER AND ENTRAPMENT OF API .....	97
FIGURE 30. SOLUBILITY OF SEVERAL APIs WITH AND WITHOUT SOLUPLUS® (10 WT%), ADAPTED FROM BASF [185] .....	97
FIGURE 31. EXPERIMENTAL APPARATUS FOR SOLUBILITY TESTS (37°C).....	118

FIGURE 32. PRINCIPLE OF DSC ANALYSIS FOR RECRYSTALLIZATION METHOD.....	120
FIGURE 33. SEM IMAGE OF UNPROCESSED EFV CRYSTALS.....	121
FIGURE 34. XRD DIFFRACTOGRAM FOR UNPROCESSED CRYSTALS OF EFV.....	122
FIGURE 35. MDSC THERMOGRAMME FOR EFV. (A) UNPROCESSED EFV (B) AMORPHOUS EFV OBTAINED BY SPRAY DRYING ALREADY DETERMINED BY OUR GROUP IN PREVIOUS STUDIES [16]. .....	123
FIGURE 36. XRD DIFFRACTOGRAM FOR UNPROCESSED SOLUPLUS POLYMER.....	124
FIGURE 37. MDSC THERMOGRAMME FOR SOLUPLUS® .....	124
FIGURE 38. EXAMPLE OF SIZE DISTRIBUTION OF COMMERCIAL SOLUPLUS® MICELLES .....	126
FIGURE 39. REVERSE HEAT FLOW OF SPRAY-DRIED 85%EFV-15%SOL ASD. ....	128
FIGURE 40. A) ESTIMATION OF FLORY-HUGGINS PARAMETER X BY LINEAR REGRESSION B) PHASE DIAGRAM OF EFV-SOL .....	131
FIGURE 41. SCHEMATIC EFV-SOL PHASE DIAGRAM WITH ALL ASDs .....	133
FIGURE 42. A DISSOLUTION TESTER DT 60 (TYPE II DISSOLUTION APPARATUS).....	142
FIGURE 43. SEM IMAGES OF ASDs. (A) SPRAY-DRIED SOL; (B) 20%EFV-80%SOL; (C) 40%EFV-60%SOL AND (D) 70%EFV-30%SOL.....	147
FIGURE 44. SPECTRA FROM RAMAN SPECTROSCOPY OF EFV, SOL AND ASDs .....	148
FIGURE 45. XRD DIFFRACTOGRAMS FOR PURE EFV AND SOLUPLUS AND FOR ALL STUDIED SPRAY-DRIED ASDs .....	149
FIGURE 46. MIXTURE GLASS TRANSITION TEMPERATURE (T <sub>MIXG</sub> ): MEASURED (GREEN ASTERISKS – SD AND BLUE DIAMOND - PM) AND THEORETICAL VALUES BY GT MODEL (RED LINE). 151	
FIGURE 47. FTIR SPECTRA FOR PURE COMPONENTS, PHYSICAL MIXTURE AND ASDs. ....	152
FIGURE 48. KINETIC SOLUBILITY PROFILES FOR ASDs GENERATED BY SPRAY DRYING WITH SEVERAL API-CARRIER MASS PROPORTIONS LOADINGS (30 WT% TO 80 WT% OF CARRIER). .....	153
FIGURE 49. COMPARISON BETWEEN KINETIC SOLUBILITY PROFILES FOR SPRAY-DRIED ASDs AND PHYSICAL MIXTURES (PM) WITH SIMILAR API-CARRIER COMPOSITIONS .....	155
FIGURE 50. KINETIC SOLUBILITY PROFILES FOR ALL SPRAY-DRIED ASDs.....	156
FIGURE 51. IN VITRO DISSOLUTION PROFILES FOR ALL ASDs. (A) SINK CONDITIONS (B) NON- SINK CONDITIONS.....	157
FIGURE 52. DVS SORPTION ISOTHERMS AT 25°C FOR SPRAY DRIED SAMPLES, DEMONSTRATING THE WEIGHT CHANGE (%) AS A FUNCTION OF THE RELATIVE HUMIDITY (%) FOR EACH SAMPLE: (A) EFV; (B) SOLUPLUS; (C) 40%EFV-60%SOL ASD; (D) 60%EFV-40%SOL ASD; (E) 70%EFV-30%SOL ASD. ....	163

FIGURE 53. WATER MASS CHANGE OF THE ASDs COMPARED WITH THEORETICAL WATER SORPTION AT 95% RH. ....	165
FIGURE 54. (A) THERMO-FISHER PHARMA 16 EXTRUDER AND (B) POWDER MIXER TURBULA T2F .....	177
FIGURE 55. SCHEMATIC REPRESENTATION OF HME CONFIGURATION U FOR EXTRUDED ASDs GENERATION .....	178
FIGURE 56. IMAGES OF EXTRUDED ASD WITH A CHARGE OF 70%EFV-30%SOL A) FROM SEM ANALYSIS AND B) FROM OPTICAL MICROSCOPY. ....	180
FIGURE 57. SPECTRA FROM RAMAN SPECTROSCOPY FOR EXTRUDED EFV-SOLUPLUS ASDs .	180
FIGURE 58. XRD DIFFRACTOGRAMS FOR EXTRUDED EFV-SOL ASDs.....	181
FIGURE 59. MIXTURE GLASS TRANSITION TEMPERATURE ( $T_{MIXG}$ ): MEASURED (GREEN ASTERISKS – HME AND BLUE DIAMOND - PM) AND THEORETICAL VALUES BY GT MODEL (RED LINE). ....	182
FIGURE 60. FTIR SPECTRA FOR PURE COMPONENTS, PHYSICAL MIXTURE AND ASDs. ....	183
FIGURE 61. SOLUBILITY PROFILE FOR DIFFERENT ASD COMPOSITIONS GENERATED BY HOT MELT EXTRUSION .....	184
FIGURE 62. COMPARISON BETWEEN KINETIC SOLUBILITY OF EXTRUDED ASDs, AND SOLUBILITY OF CRYSTALLINE EFV, PURE OR PHYSICALLY MIXED WITH SOLUPLUS. ....	185
FIGURE 63. KINETIC SOLUBILITY PROFILES FOR ALL EXTRUDED ASDs .....	186
FIGURE 64. IN VITRO DISSOLUTION PROFILES OF ALL SAMPLES INCLUDING CRYSTALLINE EFV AND ASD'S. (A) UNDER SINK DISSOLUTION CONDITIONS (B) UNDER NON-SINK DISSOLUTION CONDITIONS.....	187
FIGURE 65. DVS ISOTHERMS AT 25°C FOR EXTRUDED SAMPLES, DEMONSTRATING THE WEIGHT CHANGE (%) AS A FUNCTION OF THE RELATIVE HUMIDITY (%) FOR EACH SAMPLE: (A) EXTRUDED SOLUPLUS; (B) 20%EFV-80%SOL; (C) 40%EFV-60%SOL; (D) 60%EFV-40%SOL ASD; (E) 70%EFV-30%SOL ASD.....	193
FIGURE 66. WATER MASS CHANGE OF THE EXTRUDED ASDs COMPARED WITH THEORETICAL WATER SORPTION AT 95% RH. ....	194
FIGURE 67. COMPARATIVE OF XRD DIFFRACTOGRAMS FOR SPRAY-DRIED AND EXTRUDED ASDs. ....	196
FIGURE 68. MIXTURE GLASS TRANSITION TEMPERATURE ( $T_{MIXG}$ ): MEASURED (BLUE CIRCLES – HME AND GREEN DIAMONDS-SD) AND THEORETICAL VALUES BY GT MODEL (RED LINE). ....	197
FIGURE 69. RAMAN SPECTRA OF SPRAY-DRIED AND EXTRUDED 70%EFV-30%SOL ASD SYSTEMS.....	198

FIGURE 70. FTIR SPECTRA FOR PURE COMPONENTS, PHYSICAL MIXTURE AND ASDs GENERATED BY SD AND HME PROCESSES. ....	199
FIGURE 71. COMPARISON BETWEEN KINETIC SOLUBILITY PROFILES FOR SPRAY-DRIED AND EXTRUDED ASDs WITH SIMILAR API-CARRIER COMPOSITIONS .....	200
FIGURE 72. EFFECT OF SOLUPLUS IN THE ASDs GENERATED BY SD AND HME.....	201
FIGURE 73. IN VITRO DISSOLUTION PROFILES OF ALL SAMPLES INCLUDING CRYSTALLINE EFV, SPRAY-DRIED AND EXTRUDED ASDs. (A) SD ASD UNDER SINK DISSOLUTION CONDITIONS, (B) SD ASD UNDER NON-SINK DISSOLUTION CONDITIONS, (C) HME ASDs UNDER SINK DISSOLUTION CONDITIONS (D) HME ASD UNDER NON-SINK DISSOLUTION CONDITIONS. ....	203
FIGURE 74. WATER MASS CHANGE OF THE ASDs COMPARE WITH THEORETICAL WATER SORPTION AT 95% RH, 25°C FOR SPRAY-DRIED AND EXTRUDED ASDs. ....	205
FIGURE 75. REPRÉSENTATION SCHÉMATIQUE DU DEVENIR D’UN PA DANS L’ORGANISME APRÈS ADMINISTRATION ORALE [2]–[4]. ....	219
FIGURE 76. DÉFIS DE LA SOLUBILITÉ DANS LE DÉVELOPPEMENT DES PA POUR UNE ADMINISTRATION ORALE. A) PA COMMERCIALISÉS ET B) PA EN DÉVELOPPEMENT [3]..	220
FIGURE 77. FORMULATIONS STRATÉGIQUES UTILISÉES POUR TRAITER LA PROBLÉMATIQUE D’AMÉLIORATION DE LA BIODISPONIBILITÉ D’UN PRINCIPE ACTIF D’INTÉRÊT PHARMACEUTIQUE (CLASSE II BCS). ....	221
FIGURE 78. RÉSUMÉ (NON-EXHAUSTIF) DES TECHNIQUES DE CARACTÉRISATION DES ASD. ...	223
FIGURE 79. DIAGRAMME DE PHASE EFV(PA)/SOLUPLUS. LES FORMULATIONS DES ASD ÉTUDIÉES DANS CETTE THÈSE ONT ÉGALEMENT ÉTÉ REPRÉSENTÉES À LA TEMPÉRATURE DE T= 37°C (T UTILISÉE POUR LES ESSAIS DE SOLUBILITÉ ET DISSOLUTION) .....	225



## List of tables

TABLE 1. CLASSIFICATION OF SOLID DISPERSIONS BASED ON THE SOLID STATE OF API AND CARRIER .....	43
TABLE 2. INTERPRETATION OF RELEASE MECHANISMS FROM POLYMERIC MATRICES [97], [99], [100] .....	64
TABLE 3. SUMMARY ABOUT WORKS IN THE LITERATURE THAT HAVE USED KORSMEYER-PEPPAS MODEL TO FIT API RELEASE FROM SOLID DISPERSIONS. (WEB OF SCIENCE- KEYWORDS: SOLID DISPERSIONS, DISSOLUTION AND KORSMEYER-PEPPAS MODEL. ACCESSED IN 11/10/2018) .....	65
TABLE 4. SOME COMMERCIALY AVAILABLE MEDICINES USING AMORPHOUS SOLID DISPERSIONS TECHNOLOGIES. ADAPTED FROM [120] .....	69
TABLE 5. PROCESS AND FORMULATION PARAMETERS THAT INFLUENCE THE CHARACTERISTICS OF THE PARTICLE [123].....	71
TABLE 6. THE MAIN ADVANTAGES AND DISADVANTAGES OF SPRAY DRYING.....	72
TABLE 7. GENERAL TREND IN THE USE OF CARRIERS USED FOR THE PREPARATION OF ASDs OF POORLY WATER SOLUBLE APIs THAT ARE PUBLISHED OVER THE YEARS. ....	73
TABLE 8. DIFFERENT TYPES OF SCREW ELEMENTS. ADAPTED FROM [138] .....	76
TABLE 9. SUMMARY OF THE POLYMERS GENERALLY USED IN HME. ADAPTED FROM [110] .....	78
TABLE 10. THE MAIN ADVANTAGES AND DISADVANTAGES OF HOT-MELT EXTRUSION [110], [138], [139].....	80
TABLE 11. SUMMARY OF PHYSICOCHEMICAL CHARACTERISTICS OF EFAVIRENZ.....	93
TABLE 12. SUMMARY ABOUT EFAVIRENZ STUDIES (SOURCE-WEB OF SCIENCE. KEYWORDS: EFAVIRENZ AND DISSOLUTION. ACCESSED IN: 20/05/2018) .....	94
TABLE 13. HANSEN SOLUBILITY PARAMETERS FOR EFAVIRENZ AND SOLUPLUS .....	98
TABLE 14. SIZE OF MICELLES FOR DIFFERENT TYPES OF SOLUPLUS® .....	125
TABLE 15. EQUILIBRIUM SOLUBILITY OF EFAVIRENZ (EFV) IN PURIFIED WATER AND IN PRESENCE OF DISSOLVED POLYMERIC CARRIER (SOLUPLUS) .....	126
TABLE 16. GLASS TRANSITION TEMPERATURES OF SOLID DISPERSION AND PURE COMPONENTS DETERMINED BY DSC AND GORDON-TAYLOR EQUATION .....	127
TABLE 17. CALCULATED EQUILIBRIUM CONCENTRATIONS ( WPA) FROM SPRAY-DRIED 85% EFV IN SOL.....	129
TABLE 18. SPRAY DRYING PROCESS CONDITIONS USED TO GENERATE ASDs.....	140

TABLE 19. SUMMARY OF DISSOLUTION KEY PARAMETERS UNDER SINK AND NON-SINK CONDITIONS.....	158
TABLE 20. EFV CUMULATIVE PERCENTAGE RELEASED IN THE DISSOLUTION MEDIUM IN 15 MIN .....	159
TABLE 21. SUMMARY OF RESULTS OBTAINED AFTER AFTER THE KINETIC FITTING BY KORSMEYER-PEPPAS MODEL.....	160
TABLE 22. SUMMARY OF WATER UPTAKE (%) FOR SPRAY DRIED ASDs IN THE DIFFERENT RELATIVE HUMIDITY (60%, 75%, 85% AND 95% RH) AT 25°C. ....	164
TABLE 23. STABILITY RESULTS UNDER STRESS CONDITIONS (40 °C/75 % RH) FOR EFV-SOL ASDs WITH API LOADS OF 40WT % AND 70 WT%.....	166
TABLE 24. TEMPERATURE PROFILE FOR ASDs PRODUCTION BY HOT-MELT EXTRUSION PROCESS .....	178
TABLE 25. SUMMARY OF DISSOLUTION KEY PARAMETERS UNDER SINK AND NON-SINK CONDITIONS.....	188
TABLE 26. EFV CUMULATIVE PERCENTAGE RELEASED IN THE DISSOLUTION MEDIUM IN 30 MIN .....	189
TABLE 27. SUMMARY OF RESULTS OBTAINED AFTER AFTER THE KINETIC FITTING BY KORSMEYER-PEPPAS MODEL.....	190
TABLE 28. SUMMARY OF WATER UPTAKE (%) EXTRUDED ASDs IN THE DIFFERENT RELATIVE HUMIDITY (60%, 75%, 85% AND 95% RH) AT 25°C.....	194
TABLE 29. STABILITY RESULTS UNDER STRESS CONDITIONS (40 °C/75 % RH) FOR EFV-SOL ASDs WITH DRUG LOADS OF 40 % AND 70 % .....	195
TABLE 30. COMPARATIVE OF APPARENT SOLUBILITY ENHANCEMENT FOR PM, HME AND SD SAMPLES.....	200
TABLE 31. SUMMARY OF DISSOLUTION KEY PARAMETERS UNDER SINK AND NON-SINK CONDITIONS FOR SPRAY-DRIED AND .....	204

## List of abbreviations

<b>A</b>	Surface area
<b>Affinisol® HPMC</b>	Hydroxypropylmethyl cellulose
<b>AIC</b>	Akaike's information criterion
<b>API</b>	Active pharmaceutical ingredient
<b>ASD</b>	Amorphous solid dispersion
<b>BCS</b>	Biopharmaceutical Classification System
<b>C<sub>max</sub></b>	Maximum solubility
<b>CMC</b>	Critical micelle concentration
<b>CP</b>	Co-precipitation
<b>C<sup>p</sup></b>	Heat capacity
<b>C<sub>s</sub></b>	Solubility
<b>DE</b>	Dissolution efficiency
<b>DSC</b>	Differential scanning calorimetry
<b>DVS</b>	Dynamic vapor sorption
<b>EFV</b>	Efavirenz
<b>EMA</b>	European Medicine Agency
<b>Ethocel®</b>	Ethyl cellulose
<b>Eudragit® E</b>	Copolymer of poly(butyl methacrylate), poly((2-dimethylaminoethyl) methacrylate) and poly(methyl methacrylate) 1:2:1
<b>Eudragit® L</b>	Copolymer of poly(methyl acrylate) and poly(methyl methacrylate) 1:1

<b>Eudragit® RL</b>	Copolymer of poly(ethyl acrylate) poly(methyl methacrylate) and poly(trimethylammonioethyl methacrylate chloride) 1:2:0.2
<b>Eudragit® RS</b>	Copolymer of poly(ethyl acrylate), poly(methyl methacrylate) and poly(trimethylammonioethyl methacrylate chloride) 1:2:0.1
<b>Eudragit® S</b>	Copolymer of poly(methyl acrylate) and poly(methyl methacrylate) 1:2
<b>FDA</b>	Food and Drug Administration
<b>FDC</b>	Fixed-dose combination
<b>FTIR</b>	Fourier-transform infrared spectroscopy
<b>GI tract</b>	Gastrointestinal tract
<b>HME</b>	Hot - melt extrusion
<b>HPC</b>	Hydroxypropylmethyl cellulose
<b>HPMC-AS</b>	Hydroxypropylmethyl cellulose acetate succinate
<b>HPMCP</b>	Hydroxypropylmethyl cellulose phthalate
<b>IDR</b>	Intrinsic dissolution rate
<b>Isomalt</b>	6- <i>O</i> - $\alpha$ -D-Glucopyranosyl-D-glucitol mixed with 1- <i>O</i> - $\alpha$ -D-glucopyranosyl-D-mannitol
<b>IUPAC</b>	International Union of Pure and Applied Chemistry
<b>Kollicoat® IR</b>	Poly(ethylene glycol) grafted with poly(vinyl alcohol)
<b>Kollicoat® MAE100P</b>	Copolymer of poly(methyl acrylate) and poly(ethyl acrylate) 1:1
<b>Kollicoat® Protect</b>	Poly(ethylene glycol) grafted with poly(vinyl alcohol) + poly(vinyl alcohol)

<b>Kollidon® 12 PF</b>	Poly(vinyl pyrrolidone)
<b>Kollidon® VA 64</b>	Copolymer of poly(vinyl pyrrolidone) and poly(vinyl acetate)
<b>KP</b>	Korsmeyer-Peppas
<b>LCST</b>	lower critical solution temperature
<b>mDSC</b>	Modulated differential scanning calorimetry
<b>Methocel®</b>	Methyl cellulose
<b>PA</b>	Active pharmaceutical Ingredient
<b>PABA</b>	Para Amino Benzoic Acid
<b>Parteck® MXP</b>	Milled polyvinyl alcohol
<b>PEG 6000</b>	Polyethylene glycol 6000
<b>pH</b>	Hydrogen potential
<b>PLGA</b>	Poly (lactic-co-glycolic acid)
<b>PM</b>	Physical mixture
<b>Poloxamer 188 / Kolliphor® P188</b>	Poly(ethylene glycol)- <i>block</i> -poly(propylene glycol)- <i>block</i> -poly(ethylene glycol)
<b>PVAc</b>	Poly(vinyl acetate)
<b>PVCL</b>	Poly(vinyl caprolactam)
<b>RH</b>	Relative humidity
<b>RM</b>	Raman spectroscopy
<b>RMSE</b>	Root mean square error
<b>SD</b>	Spray – drying
<b>SEDDS</b>	Self-emulsifying delivery systems
<b>SI</b>	Sink index
<b>SLS</b>	Sodium lauryl sulfate

<b>SMEDDS</b>	Self-microemulsifying delivery systems
<b>SNEDDS</b>	Self-nanoemulsifying delivery systems
<b>SOL</b>	Soluplus
<b>Soluplus®</b>	Poly (ethylene glycol)grafted with a copolymer of poly (vynil caprolactam) and poly(vinyl acetate)
<b>T<sup>degradation</sup></b>	Degradation temperature
<b>T<sup>g</sup></b>	Glass transition temperature
<b>T<sup>m</sup></b>	Melting point
<b>wt</b>	Weight total
<b>XRD</b>	X-ray diffraction

# Chapter 1 - Introduction

---



## 1. Background

In oral active pharmaceutical ingredients (API) delivery, the bioavailability of active pharmaceutical ingredients (APIs) depends on the absorption through the gastrointestinal tract. Physicochemical obstacles to oral bioavailability include low aqueous solubility (a thermodynamic and form-dependent property) and a slow rate of dissolution (a kinetic property). Low aqueous solubility of an API can therefore limit the API concentration in the intestinal lumen and result in low absorption from the intestine. A slow rate of dissolution can also limit absorption, particularly when the solubility of the API is sufficiently low that is necessary to maintain the concentration of API near its solubility in order for API absorption to be complete over the limited time that the API transits the GI tract.

The emerging trends in the combinatorial chemistry and API design have led to the development of API candidates with greater lipophilicity and poor water solubility. About 40% of APIs with market approval and nearly 90% of molecules in the discovery pipeline are poorly water-soluble. Most of these compounds belong to class II according to the Biopharmaceutical Classification System (BCS). Class II compounds are characterized by a low aqueous solubility and high effective permeability.

Different approaches (solid-state modifications, solubilization/complexation) have been developed to formulate oral dosage forms of poorly water-soluble APIs. Over the last decades, solid dispersions, which involves the dispersion of a poorly water-soluble compound in a hydrophilic or amphiphilic carrier, appeared as a promising strategy.

Several types of solid dispersions have been developed that are not all equal regarding the physical state of the API in the carrier matrix. The most common and attractive systems are the amorphous solid suspension or solution, where the active compound is in an amorphous form or molecularly dispersed, respectively. The amorphous state or the molecular dispersion of an API typically show higher oral bioavailability compared to the crystalline form.

Various methods are employed for manufacturing amorphous solid dispersions (solution or suspension), nevertheless, hot-melt extrusion (HME) and spray drying (SD) are the most popular manufacturing processes. Spray drying is a solvent-based process where the crystal lattice structure of the API is destroyed completely during the preparation process by its solubilization generally in an organic solvent. It is a very efficient solvent-evaporation-based technology since it allows for extremely rapid solvent evaporation, leading to a fast transformation of the API to the amorphized form dispersed within solid carrier particles. Hot-melt extrusion is a solvent-free process, in which the crystal lattice structure of the API is

destroyed by high temperatures and by mechanical stress. Both are attractive manufacturing processes considering scale-up possibilities, however imperfect amorphization in the extruded solid dispersions due to the presence of remaining nuclei or small crystals, or the presence of residual solvents in spray-dried solid dispersions may lead to crystallization after preparation, are some critical points to be controlled or monitored during solid suspension or solution preparation by these processes.

Amorphous solid dispersion (ASD) provides a potential advantage in stabilizing an API amorphous form, however, the conversion of this technological approach to successful commercial products is still a challenge. Challenges such as poor stability as a result of hygroscopicity, deviations from expected dissolution behavior, and poor processability may limit their utility as a viable formulation strategy.

The performance of amorphous solid dispersions (solubility and dissolution kinetics, chemical and physical stability) is known to be affected by formulation and process variables. Carriers, generally polymers, play an important role in stabilization through various mechanisms including antiplasticization, specific intermolecular interactions on reduction in molecular mobility of the amorphous API. Molecular aspects of miscibility and interaction between API and carrier should be thus considered when formulating solid suspensions or solutions. Moreover, proper selection of the carrier, composition of the solid form, and the manufacturing process can aid in formulating a stable amorphous system but the careful control of these parameters is still a scientific challenge, exacerbated by a need for higher dosed formulations in the market. In fact, the API load in these solid structures is another critical parameter. In order to achieve adequate stabilization, they are often produced with a relatively low API load (<30 wt%). The problem is that low API loads requires large doses of the formulation to ensure therapeutic efficacy. Furthermore, the insertion of high loaded-API amorphous solid dispersions on the market may reduce dosage amounts as well as decrease the production in the pharmaceutical industries to supply cost savings.

Each API represents a specific case and the adaptation of a technology to an active material is generally not obvious. Efavirenz (EFV) is the API of choice for the development of this thesis because it is a challenging API for new formulations: EFV is an API classified as a class II of the Biopharmaceutical Classification System (BCS), i.e., it has low aqueous solubility (less than 9 µg/mL at room temperature), resulting in poor gastrointestinal absorption and, consequently, poor oral bioavailability. Some research results have been published focusing on enhancement of solubility/dissolution rate of EFV, among them, amorphous solid dispersions. They have been developed using different polymeric carriers and manufacturing

processes. The amorphous solid formulations are not comparable in chemical composition and physical structures. Research data demonstrating the potential of this type of formulation strategy to enhance the kinetic and dissolution kinetics have been published. The physical stability is studied under specific conditions, but the behavior is not always understood. EFV also needs more high-dosed amorphous solid dispersions, for which chemical and physical stability during storage and dissolution will be critical.



## 2. Objectives

A previous study carried out in our laboratory was focused on amorphous solid dispersions of EFV and Soluplus [1]. In the mentioned, ASDs with three different EFV loads (10, 17 and 44 wt%) were produced by spray drying as manufacturing process. All formulations provided a solubility enhancement for EFV (6-9 fold in water; 1.5-2 in FeSSIF medium) compared to the crystalline state and, their physical stability up to 12 months under storage conditions (22°C, 25%RH) was confirmed. However, some remaining questions were related to:

- The real impact on physical stability of the ASDs generated: are they thermodynamically or kinetically controlled? The phase diagram API/polymer binary mixture could be a useful preformulation tool to answer this question.
- The feasibility to generate ASDs of high-EFV loadings (up to 40 wt% EFV) to go deeper on the understanding of this study case of ASD.
- The effect of manufacturing process (spray drying and hot melt extrusion) on ASDs structure, the level of molecular interactions between API and carrier and the ASDs performance behavior.

This thesis aims to answer these questions.

- Thesis outline

Chapter 2 provides a background and is divided into 3 major sections. Firstly, it presents a brief introduction on the API oral bioavailability problems related to an inadequate water solubility, then gives an overview on formulation strategies existing to enhance solubility/dissolution rate of these molecules, before moving to a more detailed topic on amorphous solid dispersions. In this topic, the basic concepts of amorphous systems such as glass transition temperature and the solubility advantage are provided. Additionally, information on types of carriers used for the development of amorphous solid dispersions, their structural attributes and mechanisms of API dissolution and stabilization are introduced. Molecular aspects of API-polymer miscibility and API polymer interactions are also discussed. Finally, API (EFV) and carrier (Soluplus® - SOL) used in this thesis are presented.

Chapter 3 is divided in three major sections. The first section one presents the techniques of characterizations and also the results of the characterization of pure compounds that will be

essential to understand the behavior of these compounds in the binary mixtures. A second presents the supersaturated ASD (85 wt% EFV) that it was generated by spray drying and then the details of the recrystallization protocol used to determine API-polymer solubility. Indeed, the phase diagram for EFV-SOL mixture is predicted by extrapolation of data obtained through several annealing temperatures using Flory-Huggins or polynomial models, whereas the mixture glass transition temperature ( $T_{MIX}^g$ ) was calculated by Gordon-Taylor equation.

Chapter 4 presents the methodologies employed for the preparation and characterization of a large range of EFV-Soluplus concentration (20 wt% until 85 wt% in EFV) and has been divided into 3 main parts. In the first one, it presents more details about the process and parameters to generate the ASDs by Spray drying and their physical mixtures. Indeed, detailed information about the techniques of characterization and their control parameters are also presented. Following, once manufactured the spray dried ASDs, their solid-state structure and their performance behavior (solubility, physical stability and in vitro API release by Sink and non Sink conditions) will be evaluated and provided in the results.

Chapter 5 focuses on the manufacturing process of Hot melt extrusion. This chapter is divided in two main parts. The first one is exactly the same structure and discussion of the Chapter 4, followed by one part that will be the comparison between the both processes: Spray drying and hot-melt extrusion.

Chapter 6 provides an overall summary and conclusions of the work presented in this thesis and the scope for future work.

Chapter 7 contains references to published work cited within the thesis.

Figure 1 summarizes an overview about all the chapters of results in this thesis and the main topics to be discussed.

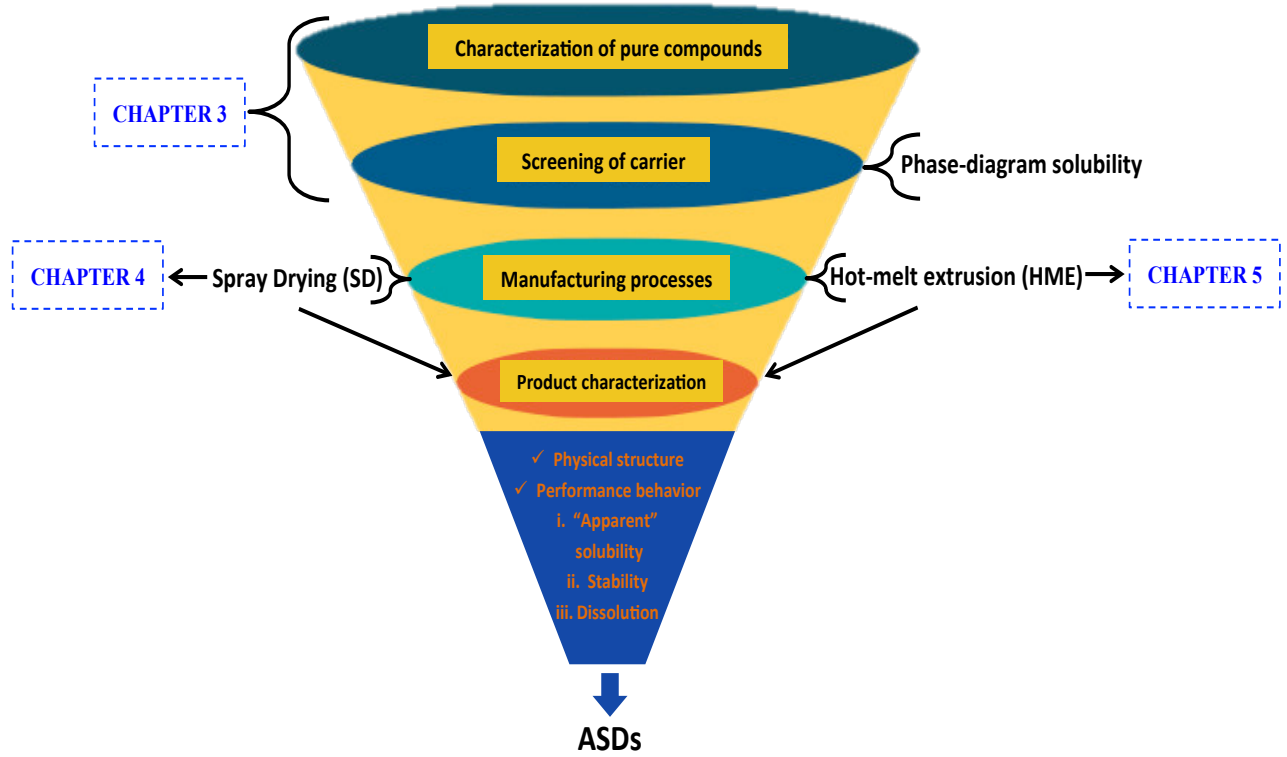


Figure 1. Summary about the thesis outline and the main topics discussed on this thesis



# Chapter 2 – Theoretical Section

---



## 1. Poorly water soluble APIs

### 1.1. A general view on the solubility problem for oral pharmaceutical formulation

#### 1.1.1. The oral route

The oral route is the simplest, most convenient route for API administration. Oral dosage forms are intended usually for systemic effects resulting from API absorption through the various epithelia and mucosa of the gastrointestinal tract (Figure 2).

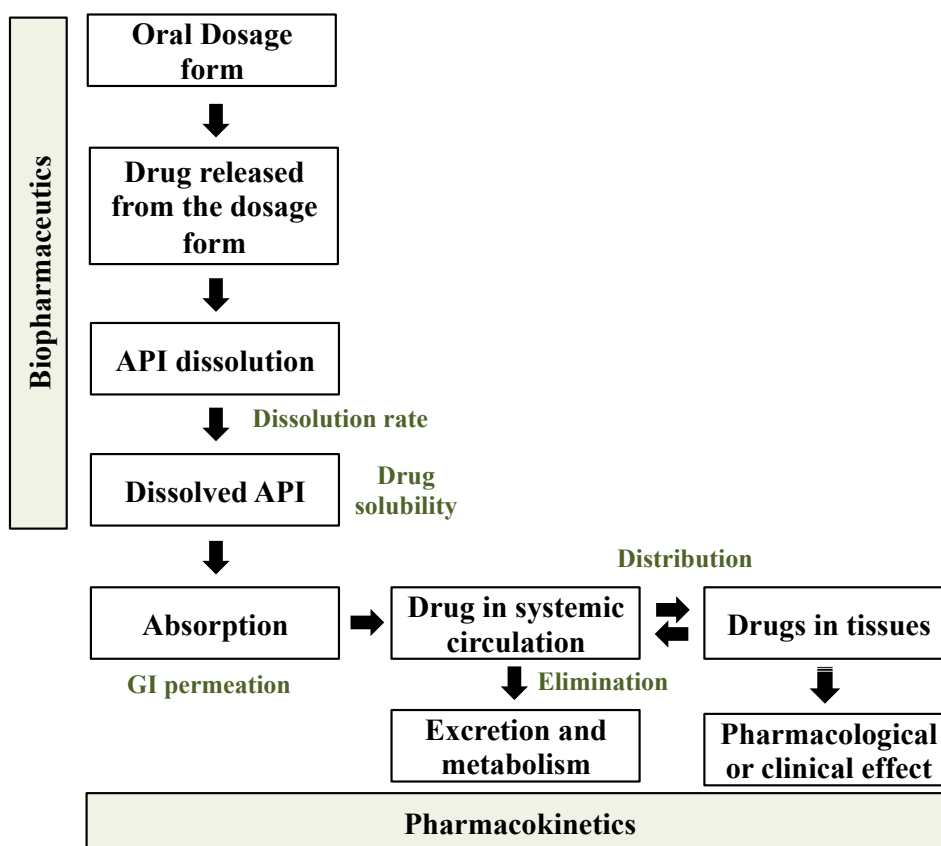


Figure 2. Schematic representation of oral administration for API absorption and systemic effects [2]–[4].

Once administered by oral route, the dosage form (tablets, capsules or granules) might lead to the API released. Progressing, the API released should be dissolved in the gastrointestinal fluids to be finally available for absorption through the various epithelia and mucosa of the gastrointestinal (GI) tract.

Physicochemical obstacles to oral bioavailability include low aqueous solubility and a slow rate of dissolution. Low aqueous solubility of a API (a thermodynamic and form-

dependent property) can therefore limit the API concentration in the intestinal lumen and result in low absorption from the intestine. A slow rate of dissolution (a kinetic property) can also limit absorption, as the API may pass its absorption site before complete dissolution.

The proportion of an API reaching the system circulation, and being available to be absorbed by the intended site of action, is called bioavailability [5]. The oral bioavailability is influenced by water solubility, GI permeability and dissolution rate of the API. The clinical effectiveness depends on the bioavailability [6]. For this biological barrier, the Biopharmaceutical Classification system (BCS) of Amidon et al (1995) provides a framework for relating oral API absorption to gastric permeability and API water solubility (Figure 3). Solubility is based on the highest-dose strength of an immediate release product. A drug is considered highly soluble when the highest dose is soluble in 250 mL or less of aqueous media over the pH ranging from 1 to 7.5 at 37 ± 0.5 °C. The estimated volume of 250 mL is derived from typical bioequivalence study protocols that prescribe administration of a drug product to fasting human volunteers [7], [8]. When more than 85% of the administered API is absorbed through the intestinal barrier, it exhibits a high permeability [9], [10].

The four categories of BSC include Class I (high solubility and high permeability), II (low solubility and good permeability), III (good solubility and low permeability) and IV (low solubility and low permeability) (Figure 3). In 2009, a new subdivision in Class II was proposed to better identify the factor limiting oral absorption: dissolution rate (class IIa) or API solubility (Class IIb) [11].

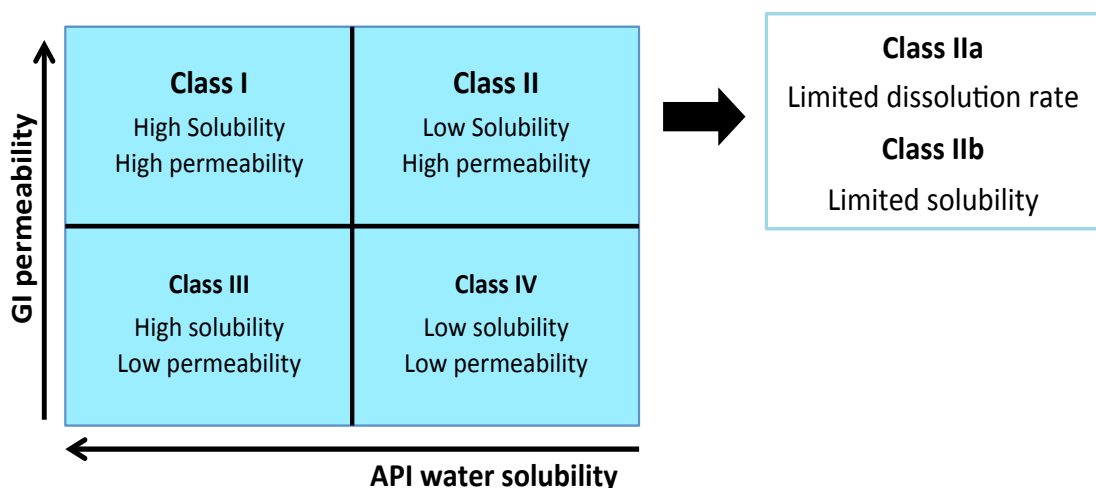
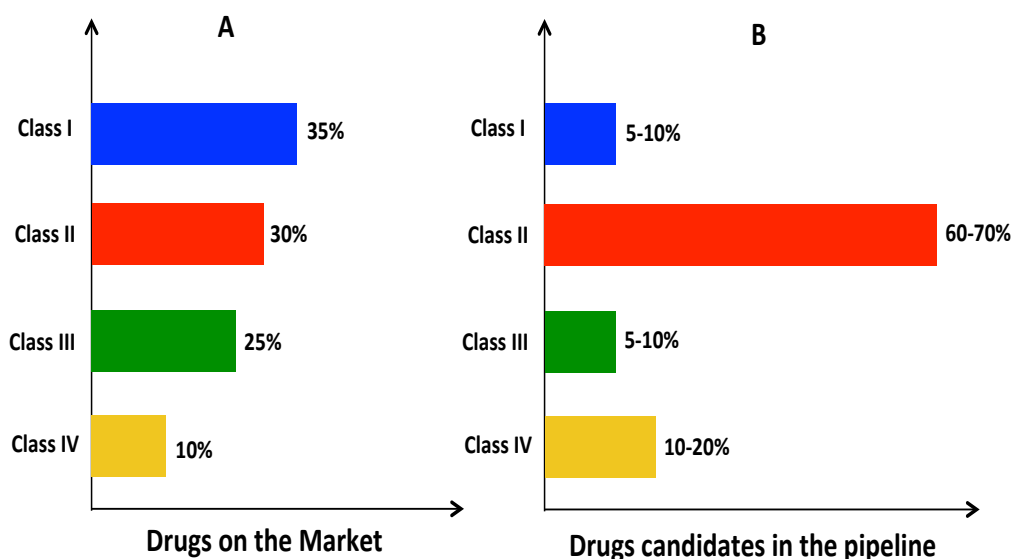


Figure 3. The Biopharmaceutical Classification System (BCS) [5] and the subdivision of Class II [11]

### 1.1.2. Solubility challenges and reasons for poor solubility

Poorly water-soluble APIs have steadily grown on the global pharmaceutical industry. The graphics in Figure 4 show the estimated distribution of marketed and pipeline APIs by BCS classes [3]. APIs on the market show a fairly uniform distribution between the BCS classes, with class I compounds expectedly ranking the highest (35%). However, a strong trend towards API candidates is found with low aqueous solubility. Indeed, looking at Figure 4, only 5-10% of potential API candidates fall under class I, and the vast majority (60-70%) are Class II. It is also important to note that up to 90% of pipeline APIs are in class II or IV categories, where APIs have poor water solubility. Low solubility of API candidates can translate in clinical use, to poor bioavailability that might result in limited therapeutic potential and insufficient clinical outcomes. Low solubility can contribute to the increasing cost of API development.



*Figure 4. Solubility challenges in the oral API development. A) marketed APIs and B) APIs in development [3]*

The observed trend towards poor water solubility can be attributed to some tools such as genomics and molecular biology, combinatorial chemistry and computational API design methodologies, which have been helping the biomedical and pharmaceutical research looking for APIs exhibiting high potency to treat diseases. The driving force of API-receptor binding is often composed of hydrophobic interactions. Consequently, many of these pipeline APIs possess high lipophilicity limiting their oral delivery applicability [3], [12], [13].

The process of solubilization involves the breaking of inter-ionic or intermolecular bonds in the solute, the separation of the molecules of the solvent to provide space in the solvent for the solute, interaction between the solvent and the solute molecule or ion. APIs have different physico-chemical properties and poor water solubility can be attributed to different factors:

- **The solubility of the compounds in water is restricted due to strong intermolecular bonds within the crystal structure.**

Physicochemical stability and high purity are advantages of crystalline form. However, high thermodynamic driving force energy is required to overcome the dissolution barrier [9], [14]. To start the solubilisation process, a large amount of external energy is required to break the API crystal lattice (Figure 5). A high crystal lattice energy, which generally increases with increasing melting temperature of a compound, results in low solubility in essentially all solvents.

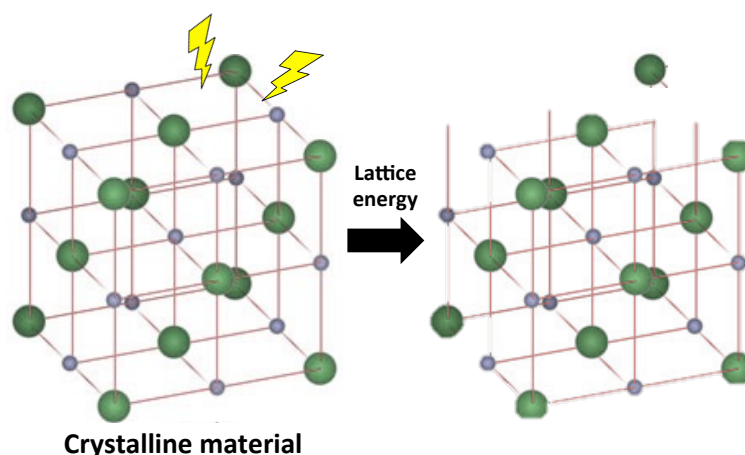


*Figure 5. Schematic representation of the breakdown of the solid-state bonds within a crystal*

- **The solubility of the compounds in water is limited because they cannot form bonds with water molecules**, thus, their solubility is limited by the solvation process. The aqueous solvation generally decreases with increasing log P value of a compound, i.e., lipophilicity (Figure 6).

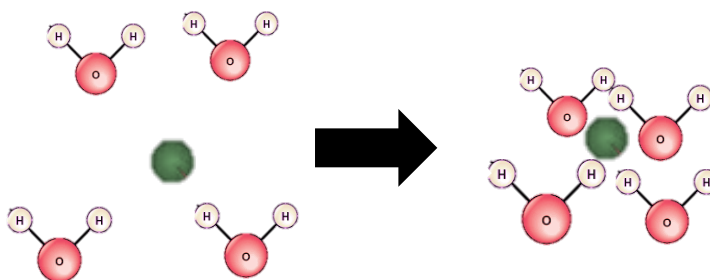


*Figure 6. Schematic representation of the solvation of the individualized species (API molecules/ions/atoms) surrounded by a shell of water molecules.*

- **A combination of both**, where the impact of high crystal energy on solubility is exacerbated by low solvation energy.

## 1.2. Formulation approaches for solubility/dissolution rate enhancement

Different approaches have been developed over the last few decades to overcome solubility and/or dissolution rate of API molecules. An overview of commonly used ways, although non-exhaustive, is given here after.

### 1.2.1. Solubilization/Complexation

- Co-solvency

It is well-known that the addition of an water-miscible organic solvent to water can dramatically change the solubility of poorly water soluble APIs [15], [16]. Most co-solvents have hydrogen bond donor and/or acceptor groups as well as small hydrocarbon regions. Their hydrophilic hydrogen bonding groups ensure water miscibility, while their hydrophobic hydrocarbon regions interfere with waters hydrogen bonding network, reducing the overall intermolecular attraction of water. By disrupting waters self-association, co-solvents reduce waters ability to squeeze out non-polar, hydrophobic compounds, thus increasing solubility [17].

- Solubilization by surfactants

Surfactants are molecules with distinct polar and nonpolar regions. Most surfactants consist of a hydrocarbon segment connected to a polar group [18]. Surfactants can reduce surface tension and improve the dissolution of lipophilic APIs in aqueous medium. When the

concentration of surfactants exceeds their critical micelle concentration (CMC) it entraps the API within the micelles improving the dissolution performance of poorly soluble APIs [19]–[21].

- *Inclusion complexes/complexation with cyclodextrins*

Cyclodextrins are a group of cyclic oligosaccharides that have a polar cavity and hydrophilic external surface [22]. In aqueous solutions, cyclodextrins are able to form inclusion complexes with many APIs by taking up the API molecule or some lipophilic moiety of the molecule into the central cavity. No covalent bonds are formed or broken during complex formation and the molecules in complex are in rapid equilibrium with free molecules in the solution [22], [23]. These inclusion complexes can be formed simply by adding the poorly water soluble API and cyclodextrin together, resulting in enhanced apparent API solubility.

- *Lipid-based systems*

Encapsulating or solubilizing a poorly water soluble API in lipid excipients can lead to increased solubilization and oral absorption, due to their spontaneous emulsification and formation of an emulsion, microemulsion or nanoemulsion in aqueous media [24]–[26].

Lipid formulations, such as self-emulsifying (SEDDS), self-microemulsifying (SMEDDS) and self-nanoemulsifying API delivery systems (SNEDDS) were explored in many studies as an efficient approach for improving the bioavailability and dissolution rate of poorly water-soluble APIs [25], [27], [28].

### ***1.2.2. Crystal engineering***

A range of different API properties, including solubility and dissolution rate might be improved by modifying its crystalline state.

- *Salts*

The selection of an appropriate salt form is frequently the primary approach to increase solubility and dissolution rate of weakly acidic and basic poorly soluble APIs [29]–[31]. Pharmaceutical salts comprise charged species of crystal structure, free bases and acids are made up of uncharged species.

To dissolve a crystal, it has to be attacked by water molecules that knock API molecules or counter out of the crystal lattice. This process is facilitated as the interaction between water molecules and the crystal surface becomes stronger. Therefore pharmaceutical salts exhibiting polar crystal surfaces in many cases show superior dissolution behavior compared to the

respective free base or free acid. The API solubility as function of pH dictates whether salt formation might be suitable.

- Pro-APIs

A pro-moiety, called pro-group is covalently linked to the API, to improve its lipophilicity and absorption [24]–[26]. The biological activity of the native API substance is obtained when the pro-API is metabolized in-vivo and is chemically or enzymatically converted to the native API substance.

- Modification of the crystal habit

Polymorphism is the ability of an element or compound to crystallize in more than one crystalline form. Different polymorphs of APIs are chemically identical, but they exhibit different physicochemical properties including solubility, melting point, density, texture, stability etc [34]–[36].

- Cocrystals

Crystal composed of at least two molecular species, an API and a conformer, held together by non-covalent forces. The solubility of cocrystals is determined by a range of conformer properties and possible interactions with the API crystal [12], [32], [37], [38].

- Particle size reduction

The size of the solid API particle influences firstly the dissolution rate because as a particle becomes smaller, the surface area to volume ratio, available for solvation, increases. The larger surface area allows a greater interaction with the solvent. The effect of the particle size on solubility can be expressed by the equation:

$$\log \frac{S}{S_0} = \frac{2 \gamma v}{2.303 RT r} \quad (1)$$

Where, **S** is the solubility of infinitely large particles, **S<sub>0</sub>** is the solubility of fine particles, **v** is molar volume, **γ** is the surface tension of the solid, **R** is the radius of the fine particle and **T** is the temperature in Kelvin.

The particle reduction can attain micro or nano levels by high-pressure homogenization or spraying methods, as well [12]. Milling is the most famous method by using ball milling, jet milling, hammer milling or cryomilling to reduce particle size [32], [39], [40]. API particles, preferably in nanometer size scale, exhibit increased dissolution rate due to higher surface area and also increased solubility under critical particle size [20], [40], [41].

- *Amorphous solid dispersions*

The crystalline form of an API offers advantages in terms of high purity and physical/chemical stability. However, constraints contributed by lattice energy must be overcome to allow solute molecules to dissolve.

The amorphous state exhibits a disordered structure in comparison to the crystalline state and possesses higher free energy. Thus it offers enhanced apparent solubility, dissolution rate and oral bioavailability [9], [42]–[45]. Pure amorphous APIs are rarely developed alone into medicinal products because of their inherent physical/chemical instability.

This has encouraged investigation of the stability of ASDs and thus led to advances have been made in recent years. ASDs are defined as solid systems consisting of API and carrier excipient(s) prepared using thermal and/or solvent based methods. A variety of excipients such as polymers and surfactants may be used to prepare and stabilize the amorphous form of API [3], [42], [43], [45]–[47].

ASDs will be the main object of study in this thesis. The next section reviews the main theoretical and technical aspects of ASDs, focusing on generation, performance and stability of these systems.

### **1.3. Solid dispersions engineering**

#### ***1.3.1. Definition and types of solid dispersions***

Chiou and Reigelman introduced the term, solid dispersion, in 1971. It is defined as a dispersion of one or more API's in an inert carrier at the solid state, prepared using thermal and/or solvent based methods [42], [48], [49]. This definition indicates that there are several types of solid dispersions.

Solid dispersions have been classified based on the distribution of solute molecules within the carrier matrix as eutectic mixtures, crystalline or amorphous dispersions and solid solutions.

*Table 1. Classification of solid dispersions based on the solid state of API and carrier*

Type of solid dispersion	Matrix (carrier)	API	Phases
1. Eutetics	Crystalline	Crystalline	2
2. Amorphous precipitates in crystalline matrix	Crystalline	Amorphous	2
3. Solid solutions	Crystalline	Molecularly dissolved	-
4. Glass suspension	Amorphous	Crystalline	2
5. Glass suspension	Amorphous	Amorphous	2
6. Glass solution	Amorphous	Molecularly dissolved	1

Table 1 shows six different types of solid dispersions. The first generation of solid dispersions used crystalline carriers and two types of solid dispersions were obtained differing in the API state, crystalline API (type 1) or amorphous API (type 2). The second generation employed natural or synthetic amorphous polymeric carriers, with crystalline (type 4) or amorphous APIs (types 3 and 5).

Type 4 is classified as a crystalline glass suspension, type 5 as an amorphous glass suspension. Type 4 is achieved if the API is dispersed as crystals in the amorphous polymer phase. This is a two-phase system. This type of solid dispersion is very stable since the API remains in its crystalline state.

Type 5 means that the API is transformed into an amorphous state but is not molecularly dispersed in the carrier matrix. This type of glass suspension is usually metastable. This means that, in the case of a too large amorphous API cluster, nuclei formation and hence nuclei growth resulting in fast recrystallization is likely to occur.

In case of type 6, the solid dispersion of the API is molecularly dispersed in the carrier. This results in a single-phase system. To obtain a glass solution, a certain degree of solubility of one component in the other is required. This means that the API can dissolve in the carrier up to a certain degree [21], [42], [48].

A wide range of pharmaceutical excipients such as polymers [19], [21], [46], lipids [24]–[27] and surfactants [18], [50], [51] may be used to prepare and stabilize the amorphous form of APIs.

### ***1.3.2. The amorphous state***

The crystalline state is characterized by a long range order of molecular arrangements in the crystal lattice [52]. In contrast, the amorphous form possesses only short range order in their

molecular arrangement. Because of this higher disorder, amorphous solids (or glasses) possess higher molecular mobility and increased thermodynamic properties such as enthalpy, entropy and free energy, compared to the crystalline state [42], [52]. This phenomenon is visualized in Figure 7 where enthalpy, entropy or volume for molecular substances are plotted in function of temperature at constant pressure.

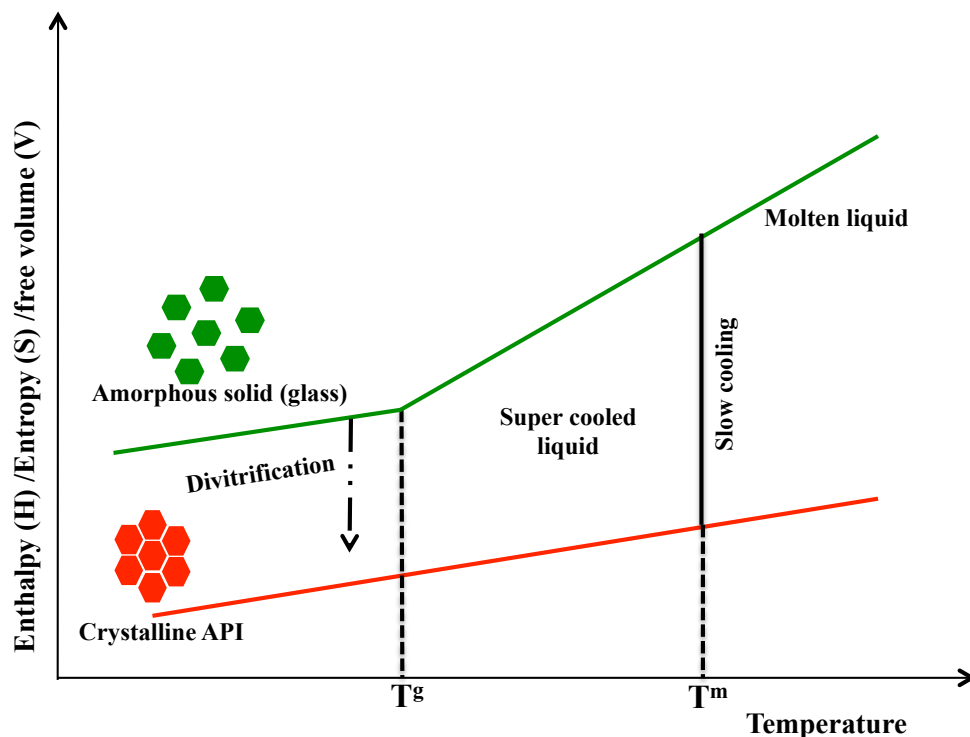


*Figure 7. Plot of enthalpy, entropy or free volume in function of temperature for molecular substances at constant pressure.  $T^g$  is the glass transition temperature and  $T^m$  is the melting point. Adapted from [43]*

In order to well understand the differences between crystalline and amorphous material, let's consider the crystalline state shown in Figure 7. When a crystalline solid is heated, it will melt and become a liquid at  $T^m$ , which is the melting temperature. Melting is a first order transition and the liquid state is reached by a step change in enthalpy, entropy and free volume values compared to the crystalline state [53]. When the molten liquid is cooled slowly, it will allow for sufficient time for the molecules to reorganize and regenerate a crystalline structure. In contrast, if the same molten liquid is cooled rapidly, it may attain a temperature lower than  $T^m$  without crystallizing, going to a supercooled liquid state, which is in equilibrium with the molten liquid state [9]. The system on further cooling continues to be in equilibrium until glass transition temperature ( $T^g$ ) is attained, where the system enters into a non-equilibrium state.  $T^g$  is marked by a significant decrease in molecular mobility and viscosity. There is a sudden decrease in kinetic energy of the system [52].

As shown in the previous paragraphs, amorphous solids have higher free energy compared to a crystal and lack the highly ordered crystal lattice. This gives them a benefit in solubility since they don't have to overcome lattice energy.

However, their excess properties also confer physical instability on the amorphous system that has a tendency to convert to a stable crystalline state. Due to their inherent instability and propensity to crystallize, amorphous forms of APIs are rarely formulated alone.

An amorphous form can be stabilized primarily by minimizing its molecular mobility in order to prevent crystallization. The simplest approach is to store an amorphous form below its  $T_g$ . An empirical rule known described in the literature recommends a storage of the amorphous form at temperature  $50^\circ\text{C}$  below its  $T_g$ . This retards the molecular mobility of the amorphous state making it sufficiently stable to provide a practical shelf life [54], [55]. However, this strategy has limited applications as it affects stability during shelf life only. It has no effect on subsequent events during dissolution.

As mentioned previously, a more practical approach towards stabilizing the amorphous form is formulating an ASD wherein the amorphous API is incorporated into a matrix of excipient(s). Figure 8 shows the energy landscape of a crystalline form, an amorphous form and an ASD. Formulation of an amorphous API into an ASD lowers the free energy of the amorphous form closer to the energy level of crystalline form [56].

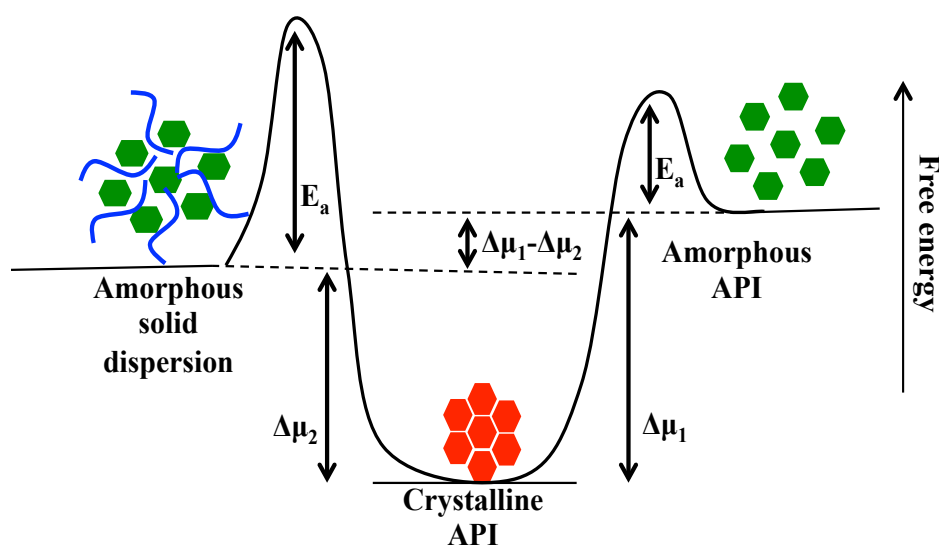


Figure 8. Comparison of energy landscapes of amorphous form, ASD and crystalline form.  $M$  is the chemical potential while  $E_a$  is the activation energy barrier for crystallization. Diagram is not to scale. Adapted from [53]

### 1.3.3. Effect “Spring and parachute”

IUPAC has defined solubilization as a process by which an agent increases the solubility or the rate of dissolution of a solid solute (IUPAC) [57].

The general solubilization mechanism of ASDs is called ‘spring and parachute’ concept. The spring and parachute concept is the usual strategy associated with API release from solid dispersions.

Considering a dissolution medium (Figure 9), a crystalline API is capable to be dissolved until the concentration attains the API thermodynamic solubility. In other words, so far, it reaches the equilibrium saturation, at which the concentration remains constant. In comparison, immediately upon contact with aqueous medium, the amorphous form of the same API dissolves more rapidly, reaches the supersaturation in the dissolution medium. This first step of dissolution is named “spring” effect. Because of the poor physical stability of the amorphous state, the concentration of dissolved API decreases quickly to achieve the equilibrium saturation [9], [23], [42], [58], [59]. The supersaturation is short-lived, because it depends on the interplay between the dissolution and crystallization rates of the API [42].

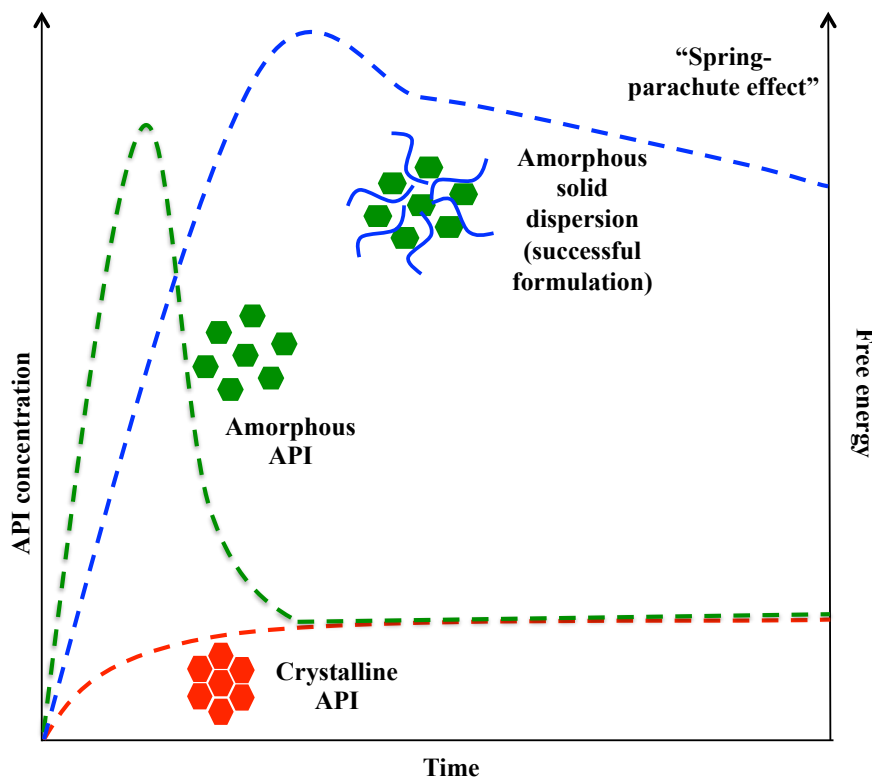


Figure 9. API profile dissolution based on the aqueous solubility of amorphous and crystalline API and amorphous solid dispersions. Adapted from [9], [42]

The success of the ASD depends on the ability of the carrier, usually a soluble polymer, to function as stabilizing agent and thus maintain supersaturated concentrations achieved during dissolution. The combination of a rapidly dissolving and supersaturating "spring" with a precipitation retarding "parachute" for a period of hours while API is being absorbed (parachute effect) [42], [58] has often been pursued as an effective formulation strategy for ASDs to enhance the rate and extent of oral absorption.

#### *1.3.4. Mechanisms of API release from ASDs*

Despite the significant advance in the design of ASDs, the API release from these solid structures has been shown to be complex involving several mechanisms by which the carrier prolongs the API supersaturation in the dissolution medium. Possible mechanisms of enhanced dissolution include the following:

- Wettability

When a solid enter in contact with a liquid, a strong affinity between them can occur and then, liquids might form a film over the surface of the solid. However, if this affinity is nonexistent or weak, the liquid has difficulty to disperse the air and a bigger angle of contact appears between the liquid and the solid [60]. This contact angle is determined from a balance between adhesive and cohesive forces involving three interface tensions: (i) liquid and vapor phase, (ii) solid and liquid phase and (iii) solid and vapor phase. If this angle is small, the solid surface increases and then, wettability increases. Thus, the contact angle provides an inverse measure of wettability [61]. In literature, the dissolution properties of individual materials have been correlated with the process of wetting and wetting kinetics [62]–[64]. The mechanism of improved solubility and dissolution rate of an API may involves its enhanced wettability in a polymer-rich microenvironment as the polymer dissolves [65].

- Carrier nature

The nature of a carrier, i.e., hydrophilic, hydrophobic or amphiphilic may influence the dissolution release of the API. The incorporation of poorly water-soluble API into a water-insoluble carrier leads to delay the API release from matrix. On the other hand, if a poorly water soluble API is added into a water-soluble carrier, the impact is inverse and the dissolution rate is improved [66].

Micellar solubilization is an intrinsic characteristic of surfactants with amphiphilic behavior. To be amphiphilic means to be composed by a hydrophilic unit (contact with aqueous media) and a hydrophobic unit (contact with the API) and thus to be capable to perform a micellar solubilization [67]. In aqueous medium, the micellar solubilisation (Figure 10) can be explained as follows: the hydrophilic part generates hydrogen bonds with water allowing the dissolution, while the hydrophobic part forms hydrophobic niches where the API molecules can come housing.

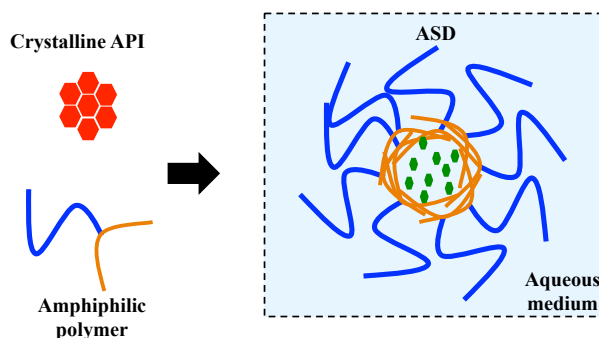


*Figure 10. Representative scheme of a micellar solubilization*

- API-carrier ratio

The optimization of carrier to API ratio is important in the design and development of solid dispersions for poorly water soluble APIs since carrier dissolution is a crucial component in API release from these systems.

High polymer to API ratio can produce better wettability resulting in an enhanced solubility possibly due to a more homogenous dispersion of the API within the polymer matrix [66], [68]. In contrast, it is always more advantageous for the industry (cost-effectiveness) and patient (by reducing dosage form) if the carrier is used in minimal amounts.

- API-carrier interaction

In addition to the ability of carrier matrix to improve local solubility and wettability of APIs, carriers also contribute to enhance their aqueous solubility and dissolution rate through specific interactions (like hydrogen bonds and/or hydrophobic interactions) with API functional groups.

API precipitation (or recrystallization) might occur in two stages: nucleation and crystal growth. When carriers (polymers in most cases) are added to API to generate solid dispersions,

they may interfere in one or both of these processes through formation of hydrogen bonds or hydrophobic interactions with API [43], [69].

In literature, different studies of ASDs have identified and discussed API-carrier interactions. For example, in the case of indomethacin (API) and ethylcellulose (carrier), a delayed release rate from ASD was related to strong indomethacin-ethylcellulose interactions occurring during dissolution at acid pH [70]. In another example, ASDs containing Ketoconazole and different carriers (PVP, PVP-VA, HPMC or HPMC-AS) demonstrated that the presence of interaction between API and polymer at the molecular level plays a big role in the API release rate [58].

It is important to mention here that the free API concentration in the dissolution medium is dependent on the aqueous solubility of the crystalline or amorphous API, which in turn depends on many factors including API crystallization rate but also API-carrier interactions.

### ***1.3.5. Stability***

Long-term stability has always been the main concern of formulation scientists on amorphous solid dispersions [42], [71].

The apparent solubility and dissolution behavior of ASDs must remain unchanged during storage. The best way to guarantee this is by maintaining their physical state. Physical instability of solid dispersions such as phase separation and subsequent crystallization may reduce the dissolution rate of the active ingredients. Since many solid dispersions contain amorphous or molecularly dispersed APIs, they are often susceptible to crystallization during storage [56]. Similarly, certain carriers may exist in thermodynamically unstable states in solid dispersions and undergo changes with time [66], [70].

The physical stability of ASDs should be related not only to API crystallization but to any change in molecular structure including the distribution of API within the ASDs [21], [43], [56], [72], [73]. For optimal stability of ASDs, the molecular mobility should be as low as possible.

A relevant quantity of factors has been noticed to influence the physical storage stability of ASDs, among them, the crystallization tendency, the molecular mobility of APIs, the anti-plasticization effect of ASDs in the API, API-carrier interactions and the manufacturing process [44], [56], [74], [75], besides the storage environment (temperature and humidity). In particular, moisture might facilitate the crystallization of amorphous APIs and for this reason solid dispersions should be protected from moisture. Various studies reported reduced dissolution rates of APIs in ASDs upon ageing [48], [54], [76].

- The anti-plasticization effect

This effect is based on a thermodynamic approach that means an increase in the glass transition temperature of a binary mixture (API and carrier). Typically, the polymer has a high glass transition temperature and would have an antiplasticization effect on the API compound [77]. An amorphous solid dispersion usually has a higher glass transition temperature than the pure API compound. The increase in the glass transition temperature of the amorphous system can often result in the amorphous system being in the glassy state at room temperature. This effectively reduces the molecular mobility of the system and the crystallization rate.

For an ideally mixed binary mixture, the glass transition temperature of the binary mixture ( $T_{MIX}^g$ ) can be estimated from several equations such as Fox equation, Gordon-Taylor equation, Couchman-Karasz or Kwei [77].

From Gordon-Taylor equation,  $T_{MIX}^g$  is calculated based on the individual contributions of weight fraction and glass transition temperature of each component in the binary mixture, without considering the intermolecular interactions between them:

$$T_{MIX}^g = \frac{W_{PA} \cdot T_{PA}^g + K \cdot (1 - W_{PA}) \cdot T_{PO}^g}{W_{PA} + K \cdot (1 - W_{PA})} \quad (2)$$

$T_{PA}^g$  and  $T_{PO}^g$  are the API and polymer glass transition temperatures, respectively.  $W_{PA}$  is the API mass fraction in the mixture. K can be defined as a parameter characterizing the intermolecular interactions between both components resulting in the curvature of the evolution and is defined by equation 3 [78]. A value of 1 for K means that the interactions between both components are similar to the ones of the pure components.

$$K = \frac{T_{PA}^g \cdot \rho_{PA}}{T_{PO}^g \cdot \rho_{PO}} \quad (3)$$

$\rho_{PA}$  and  $\rho_{PO}$  are the densities of API and polymer, respectively.

- Crystallization tendency

Recrystallization is the major disadvantage of ASDs. As already discussed, amorphous systems are thermodynamically unstable and have the tendency to change to a more stable state under recrystallization. Molecular mobility is a key factor governing the stability of amorphous phases, because, even at high viscosities, below  $T^g$ , there is enough mobility for an amorphous

system to crystallize over pharmaceutically relevant time scales. Molecular mobility of the amorphous system depends not only on its composition, but also on the manufacturing process [79].

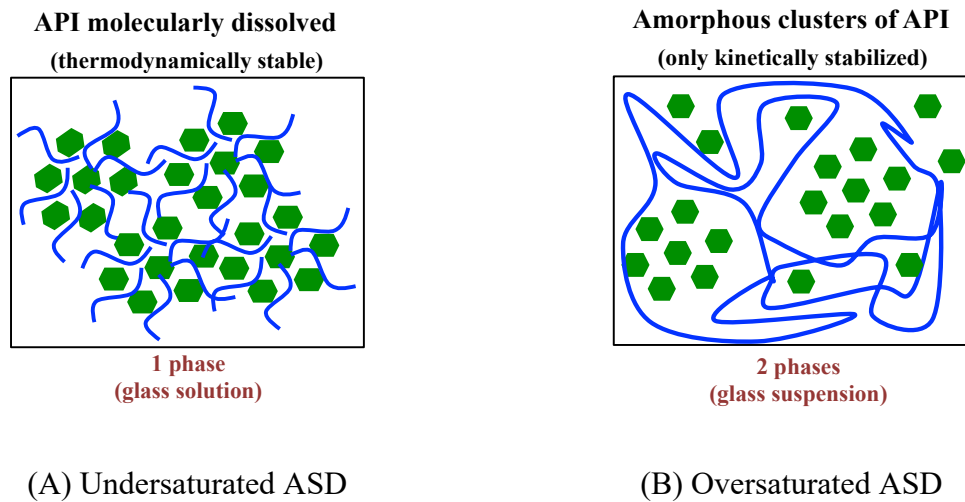


**Figure 11.** Solid dispersions based on amorphous polymeric carriers, with API concentration exceeding or not the solubility of the API in the carrier. A) Undersaturated ASD and B) oversaturated ASD

Figure 11 (A) illustrates an ASD where the amorphous API is molecularly dissolved in the carrier, i.e, the binary mixture is undersaturated in API. This system is thermodynamically stable.

Figure 11 (B) shows that the API is in an amorphous state but is not molecularly dispersed in the carrier matrix. This type of glass suspension is usually metastable. This means that, in case of too large amorphous API clusters, nuclei formation and hence nuclei growth resulting in fast recrystallization is likely to occur. If the clusters of the amorphous API are small, i.e. they do not contain a sufficient number of API molecules to recrystallize, the immobilization of API in the matrix, as an amorphous glass suspension can be sufficient to ensure a kinetic control of the physical stability. Since water acts as a plasticizer and lowers the glass transition temperature, moisture absorption needs to be avoided in the case of ASD type B shown in Figure 11 in order to maintain sufficient stability. Also, ASD of type B are more susceptible to evolve in its solid structure under unfavorable storage conditions such as elevated temperature and humidity and other stress conditions such as compression, that is an important stage of tablet manufacturing of ASDs [80].

### 1.3.6. Characterization of amorphous solid dispersions (ASDs)

The aim of the characterization of an ASD is to exhibit the feasibility of this complex system to enhance API solubility, dissolution rate and also, to maintain the supersaturated solution performance in terms of stability, controlling/reducing its tendency to recrystallize [81]. To achieve this aim, several techniques have been used in order to explore the physical structure, molecular interaction and behavior of ASDs [45], [81], [82] and some of them are summarized in Figure 12.

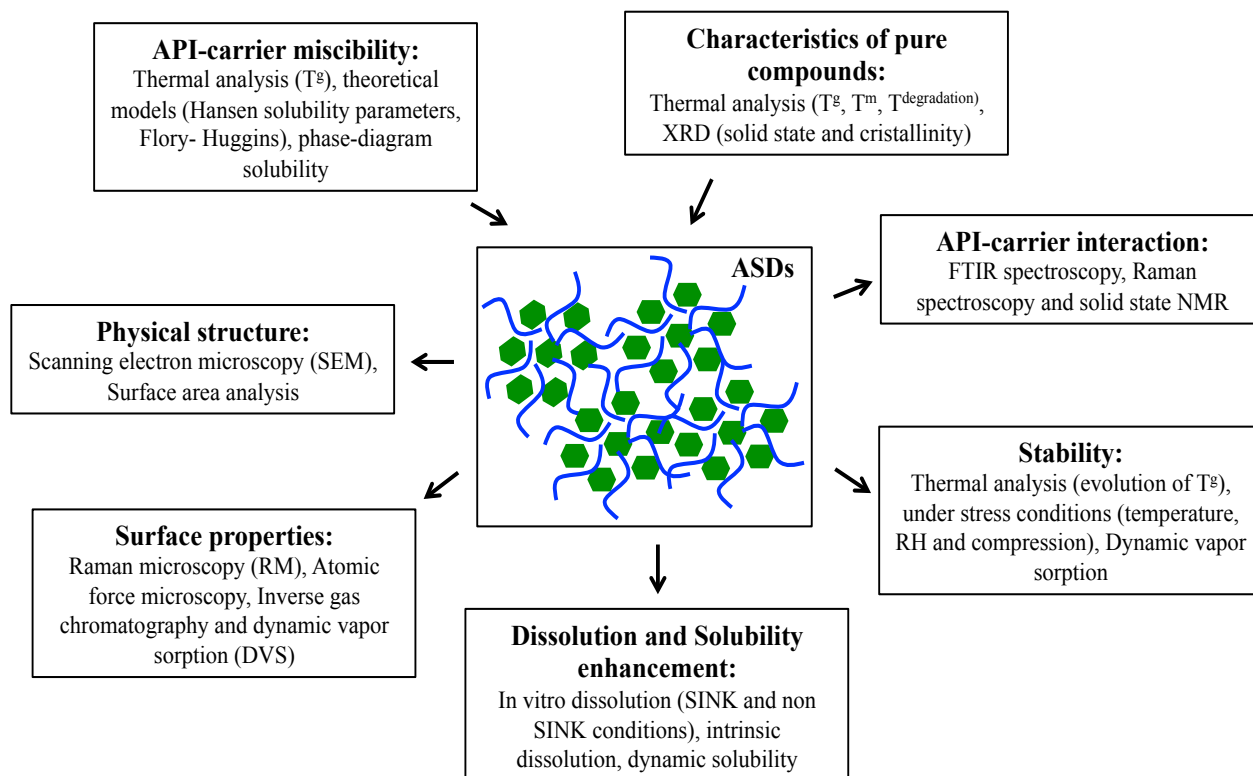


Figure 12. Summary of ASDs techniques of characterization.

Techniques that will be used in this thesis are the following:

#### 1.3.6.1. Thermal analysis

Thermal analysis might be the most essential routine tool for the ASD characterization. They are commonly used to monitor phase transformation through exothermic processes (e.g., crystallization, chemical degradation) and endothermic processes (e.g., glass transition, melting point). The most widely thermal methods are Differential Scanning Calorimetry (DSC) and modulated differential scanning calorimetry (mDSC) [78], [81], [83].

In these methods, the material is heated, and then the energy associated with its transformation can be measured in order to detect thermal transitions such as the glass transition temperature, polymorphic transformation, melting point and recrystallization [81].

Figure 13 shows an example of DSC thermogram, where the thermal transformations are represented. Crystalline materials, once heated, attain the melting temperature ( $T^m$ ) and consequently, they pass by an endothermic transformation corresponding to melting. On the contrary, amorphous materials, once heated, reach the glass transition temperature ( $T^g$ ) instead of  $T^m$ . Indeed, an amorphous material can also show an exothermic event (recrystallization), which is then followed by an endothermic melting one.

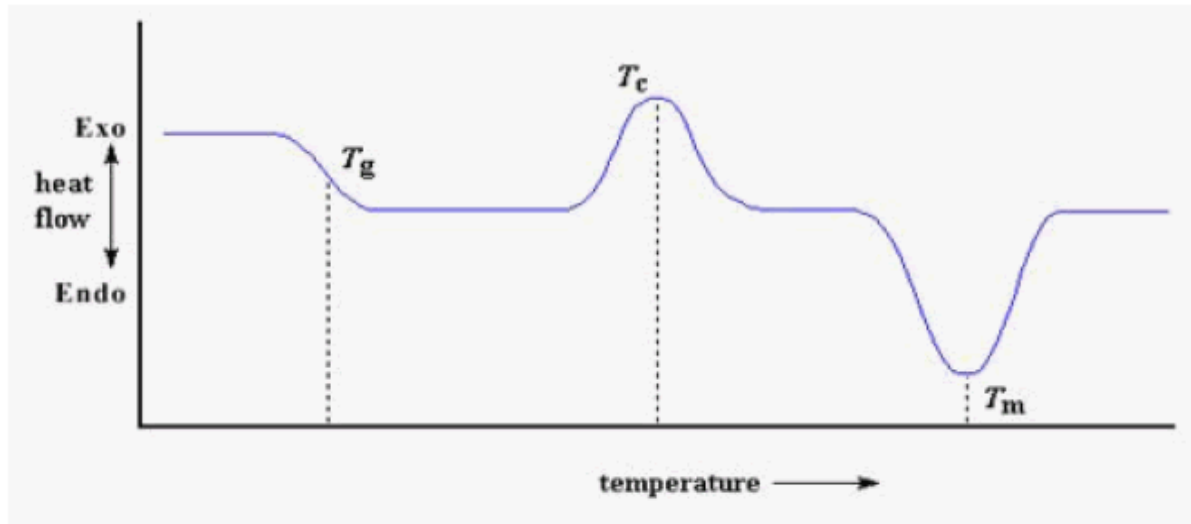


*Figure 13. Schematic representation of a DSC thermogram with the main endothermic and exothermic processes. Taken from [84]*

Sometimes, DSC analysis can exhibit some limitations to detect the thermal transitions because they are weak or overlap another event, for example, water evaporation occurring at the same time. mDSC is then, applied to overcome these limitations by separation of overlapping thermal events if it is possible and this method has higher sensitivity in measuring heat capacity (CP) [81]. mDSC has been used to measure the APIs crystallization tendency, glass transition, API-polymer miscibility, crystallinity/crystallization (e.g. crystal growth rate, crystallinity degree) and molecular mobility (e.g. structural relaxation and viscosity) [78]. mDSC provides the ability to enhance interpretation of complex thermal curves. To perform mDSC analysis, a sinusoid is added on the ramp of T by a software that is coupled to the conventional DSC, allowing the separation of the signal of total heat flow in:

- Reverse heat flow (reversing): which contains heat capacity related events such as the glass transition;
- Non-reversing heat flow: which contains kinetic events such as crystallization, crystal perfection and reorganization, cure and decomposition.

Heat capacity ( $C^P$ ) of a system is the amount of heat (often expressed in SI by  $J.kg^{-1}.K^{-1}$ ) needed to raise the system's temperature by 1K. Usually the specific heat is not measured during first order transitions in the physical state (e.g. melting), where it can be infinitely large. The measurement of  $C^P$  by DSC for crystalline and amorphous form is distinctive. For the first one, the measure occurs before melting point (crystalline compound) and after melting point (liquid). For amorphous material,  $C^P$  might be measured before glass transition to ensure that it will be a measure corresponding to all material because the increase in temperature stimulates the appearance of other thermal events, such as recrystallization [1].

Concerning API-polymer miscibility, the homogeneity between the compounds is an important factor for stability. A unique  $T^g$  for the mixture, placed between the  $T^g$ 's of the pure compounds, can indicate homogeneity between the compounds at molecular level corresponding to a single phase. The  $T^g$  of the pure compounds should be quite different of, at least,  $10^\circ C$  in order to exhibit a true analyze by DSC or mDSC [56].

#### 1.3.6.2. X-ray diffraction

XRD has been used to study and identify, the presence or change in crystallinity (or amorphicity) and polymorphism in ASDs [42], [78], [85]. Also, XRD has proven to be a valuable tool to assess the storage stability of amorphous systems [86].

This technique of characterization is based on Bragg's Law defined by the equation:

$$n\lambda = 2 d \sin(\theta) \quad (4)$$

$\lambda$  is the wavelength radiation,  $d$  the distance between atomic planes,  $\theta$  the Bragg angle and  $n$  the diffraction order.

This technique deals with the incidence of parallel X-rays, which attack the crystalline planes and are then diffracted at angles related to the spacing between the planes of molecules lattice. Characteristic peaks in the diffraction pattern evidence crystallinity, which can be determined. On the other hand, amorphous state is detected by the absence of characteristic Bragg's peaks [86].

#### 1.3.6.3. Spectroscopic methods: Raman (RM) and Fourier-transform infrared spectroscopy (FTIR)

When the material is exposed to electromagnetic radiation, changes, such as electronic transitions, vibrational transitions and nuclear spin transitions on the molecular and atomic-level, can occur. This phenomenon represents the base of spectroscopic methods and can be divided into, for example, Raman Spectroscopy or Infrared spectroscopy, based on the energy

gap between the ground and excited states [81]. These techniques allow the identification of substances due to fingerprints that are specific to each substance.

For ASDs, the spectroscopy imaging might provide essential molecular-level information about local structure in amorphous solids, such as API-polymer interaction, phase separation and crystallization. Infrared (IR) is based on the absorption, reflection and emission of light and Raman (RM) is based on the phenomenon of light scattering. They are complementary techniques.

FTIR can be used to identify specific interactions between API and polymer, such as electrostatic interactions, hydrogen bonds, dipole interactions and forces of van der Waals by observing changes in peak shape or position (disappearance, appearance or peak displacement).

RM is an important supplemental technique of FTIR to evaluate the miscibility in API-polymer systems since it provides localized compositional information that is distinctive from the bulk characterization [49], [56]. RAMAN spectroscopy offers the advantage to make possible to obtain chemical detailed information on the spatial distribution of the sample constituents. When coupled to microscopy, high-resolution chemical images of the spatial distribution of sample components can be obtained through RAMAN mapping [1].

#### 1.3.6.4. Scanning electron microscopy (SEM)

This technique is based on the emission of monochromatic electron beam to probe the surface and near-surface area of materials at a higher magnification and resolution than a traditional light microscopy [81]. SEM provides high-resolution images from the application of a potential difference in a Tungsten filament, which will interact with the surface of the material to be analyzed, which in response produce secondary electrons that will be detected forming the image of the micrograph [1]. SEM have been widely applied in the ASDs characterization examining the effects of manufacture process on particle morphology and homogeneity of samples. It can also be used to investigate the morphology of ASDs after dissolution or a physical stability tests [81].

#### 1.3.6.5. Dynamic vapor sorption (DVS)

Water vapor sorption is an established method, used to study the affinity of powders and their physical mixtures towards water. A water sorption isotherm reflects the interaction between a powder material and water by relating the humidity of air in equilibrium with water content of the solid material at a constant temperature and pressure [87].

The measurement of this affinity is evidenced by the degree of hygroscopicity of the carrier used in the ASD formulations. If the carrier (polymer) is hydrophilic, the interaction with water increases. Due to the plasticizing effect of water, the mixture glass transition decreases, higher molecular mobility is detected and consequently, the recrystallization tendency is stimulated [48].

DVS has been applied to study the effect of water uptake in amorphous systems through sorption/desorption isotherms of ASDs [88].

#### 1.3.6.6. Apparent kinetic solubility

Thermodynamic solubility is normally measured according to the method of Higuchi and Connors [89]. In this method, an excess amount of API is suspended in an aqueous buffer or solvent and rotated or shaken for an extended period of time, typically, 24 to 48 hours, to ensure the attainment of equilibrium. At the end of the equilibration, the solution is filtered or centrifuged and the concentration of the filtrate is measured using ultraviolet light absorption spectroscopy or high performance liquid chromatography and compared to a standard.

Unlike crystalline APIs, equilibrium solubility cannot be determined for amorphous materials because, at equilibrium, API solubility using the crystalline or amorphous form is similar, by definition. If we accept the fact that precipitation follows supersaturation, then concentration of API from ASDs at the peak of the solubilisation could be used for the determination of apparent (kinetic) solubility ( $C_{max}$ ) as represented in Figure 14.

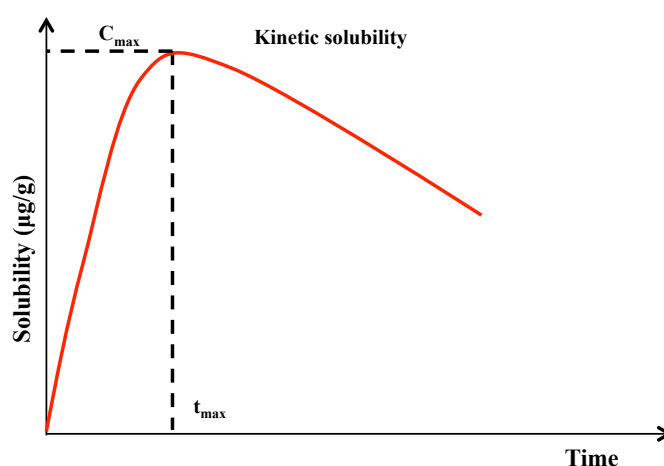


*Figure 14. Schematic representation of kinetic solubility for amorphous materials.*

### 1.3.6.7. Dissolution

As already discussed in topic 1.3.3., upon dispersion of an API in a carrier matrix, a true solid solution will result if the API and polymer are completely miscible to yield a single phase. In an ASD where the API concentration exceeds its own solubility in the carrier matrix, the resulting supersaturation will induce crystallization in the solid state what, depending on the crystallization induction period, may compromise the solubility advantage of the dispersion.

The rate at which an API goes into solution (dissolution rate) is an essential pre-requisite for the absorption process. Dissolution is hence an important aspect of formulation development of ASDs. Essentially, the apparent solubility advantage of ASDs determines the probability of success of improving bioavailability *in vivo*. Typically, the apparent solubility behaviors of ASDs are evaluated by dissolution studies. Not only the peak concentration achieved but also the duration of supersaturation is biorelevant.

The scientific literature is enriched with a great number of studies on the dissolution assessment of amorphous dispersions. Majority of them are using powder dissolution to elucidate the mechanism of the dissolution behaviors of amorphous dispersions.

Dissolution method development for these formulations has faced challenges due to their unstable supersaturation state in aqueous media. The rate of dissolution can be expressed by using Noyes-Whitney equation, which provides various parameters that can help the improvement of dissolution rate of a poorly water-soluble API, to minimize the limitations of oral availability:

$$\frac{dX}{dt} = \frac{DA}{h} (C_s - \frac{X}{V}) \quad (5)$$

$\frac{dX}{dt}$  is the dissolution rate, **A** is the surface area available for dissolution, **D** is the diffusion coefficient of the API particle, **h** is the thickness of the diffusion layer adjacent to the dissolving API particle surface, **C<sub>s</sub>** is the saturation solubility of the API particle in diffusion layer, **X** is the amount of API particle dissolved at time **t** and **V** is the volume of dissolution medium [72].

As ASD disintegrates, the increased solubility (C<sub>s</sub>) of the amorphous form will yield a higher dissolution rate relative to the corresponding stable (crystalline) form, as well the increased surface area (A) resulting from size reduction of the API particles during solid dispersion process to the molecular or nearly molecular scale.

However, rapid dissolution of the amorphous API will quickly lead to attainment of a high supersaturation level with respect to the more stable form, which will start to crystallise immediately or after a certain induction period.

Broadly, there are two types of crystallization which may affect the dissolution profiles of ASDs [9], [90] namely, (I) crystallization from solution and (II) conversion of amorphous state into crystalline state in the undissolved material due to the plasticizing effect of water.

The dissolution behavior of ASDs is governed by the degree of supersaturation ( $C > C_s$ ). Then, crystallization can take place under supersaturated conditions and the rate of this transformation is affected by the degree of supersaturation besides factors like API physicochemical properties and API-carrier interactions.

- *Defining Dissolution in Sink/Non-Sink conditions*

Based on kinetic (apparent) solubility, dissolution conditions can be varied with regard to dose, volume and composition of dissolution medium. In the European Pharmacopeia [8], sink conditions are defined as a volume of dissolution medium that is at least three to ten times the saturation volume. In other words, the volume of dissolution medium has to be sufficient to dissolve, into the dissolution vessel, 100% API loaded (Dose) in the studied formulation. This condition is based on the determined thermodynamic solubility and the dissolution is not limited by diffusion [90]. A typical dissolution profile under sink condition is shown in Figure 15.

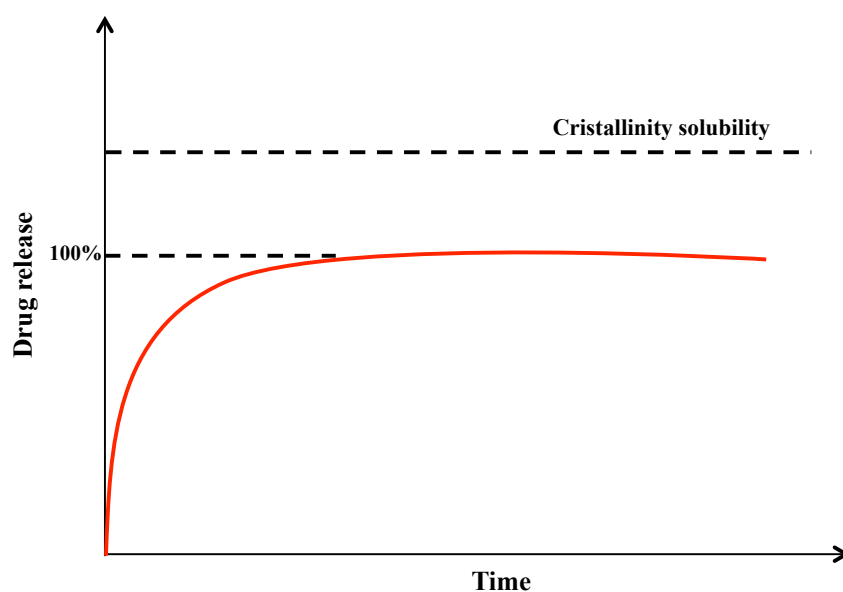


*Figure 15. Example of in vitro dissolution profile for perfect Sink conditions*

To observe the supersaturation effect of amorphous SDs, *in vitro* dissolution studies should be conducted under non-sink conditions as is commonly encountered on entering the gastrointestinal (GI) tract [90].

Two types of dissolution kinetics could be expected under non-sink conditions. They are represented in Figure 16.

A (Fig. 16 A): Supersaturation is sustained over time during whole experiment and crystallization is unnoticed. In this case, the dissolution profile shows a supersaturation behavior with concentrations higher than the equilibrium solubility of crystalline API;

B (Fig. 16 B): The dissolution profile leads to a supersaturation solution followed by crystallisation [90].

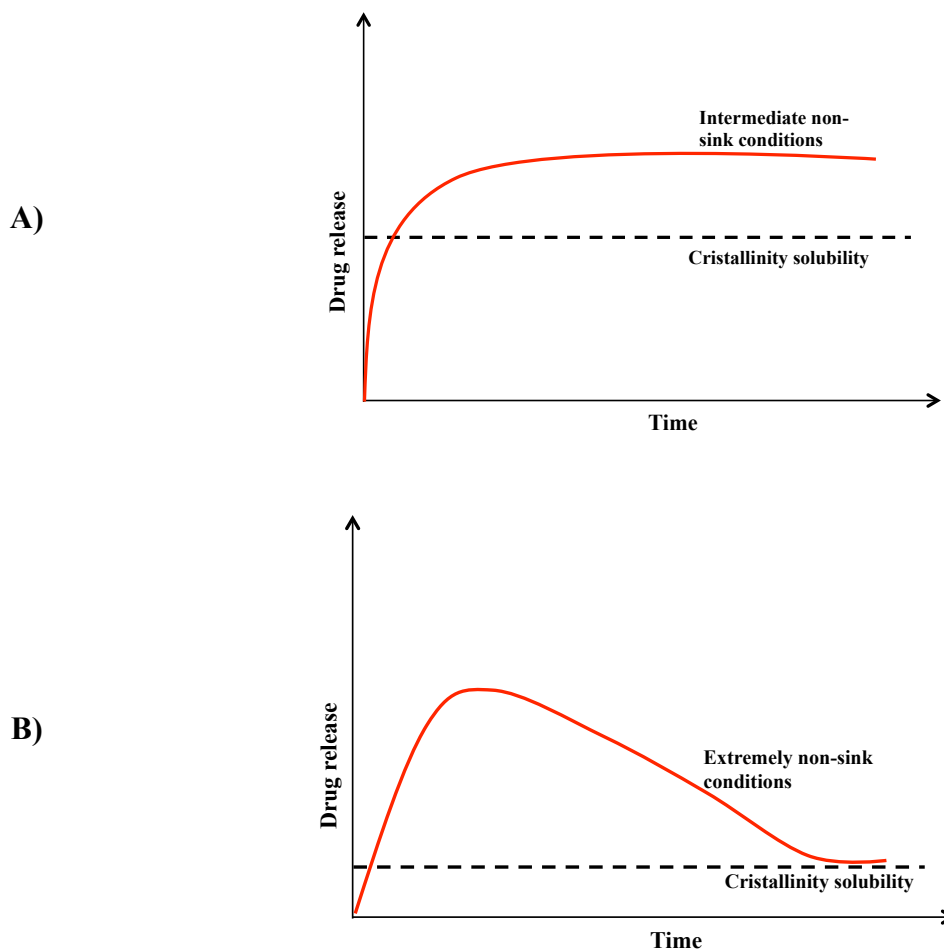


**Figure 16. *In vitro* dissolution profiles for A) Intermediate non-Sink conditions and B) Extremely non-Sink conditions**

For supersaturating formulations, the maintenance of supersaturation over dissolution time depends on the level of ‘stress’ imposed to the formulation under dissolution. Therefore,

the degree (%) of supersaturation in the dissolution medium can provide an efficient way to screen formulations, since the ability for a formulation to maintain a temporary supersaturation in the dissolution medium depends on the dissolution of the powder and the ability of the carrier to inhibit API recrystallization [43], [90], [91].

Based on this, the sink index (SI) was introduced [90], which is defined as follows [90]:

$$SI = \frac{C_s}{\frac{Dose}{V}} \quad (6)$$

$C_s$  is the solubility of crystalline API,  $V$  the volume of dissolution medium and **Dose** is the total amount of API in the test sample. In order, to establish in vitro-in vivo correlation of API dissolution and absorption, Dose can be defined as  $Dose = \frac{M_o/V_o}{C_s}$  (7), where  $M_o$  is the dose and  $V_o$  the initial gastric volume, 250 mL. In general, SI is a dimensionless number equivalent to the inverse of the maximum theoretical supersaturation ratio. This number can be at least 3 (up to 10) for dissolution Sink conditions and about 0.1 for dissolution non-Sink conditions.

- Studies comparing dissolution under sink and non-sink conditions

It is still a challenge compare sink and non-sink conditions due to the several factors affecting supersaturated solutions [18]. So far, few studies have reported the effect of sink and non-sink conditions in dissolution release from solid dispersions. A recent review on this topic was provided by Sun [90]. Some of the more relevant results are summarized here: França et al. performed solid dispersions with chlorthalidone and polymer (Soluplus®) – surfactant (sodium lauryl sulfate – SLS) complex. API release was evaluated using sink and non-sink conditions in different dissolution media (pure water and biorelevant medium) and the results showed differences between the dissolution kinetics carried out under the two different dissolution conditions, even if a high level of supersaturation (up to 6-fold the crystalline solubility) was maintained for 6 drug in biorelevant medium [18].

Another example is the work performed by Huo et al. who generated solid dispersions of tacrolimus with HPMC and poloxamer 188 as carrier materials [92]. It was found that all the solid dispersions showed favorable dissolution rate under sink conditions. However, the release of tacrolimus was hampered in non-sink conditions, being also influenced by the pH of the medium in the non-sink environment.

Finally, Newman et al. has already commented that, for in vitro dissolution testing of ASD formulations, few studies have clearly specified ‘sink’ or ‘non-sink’ dissolution

conditions [93]. Additionally, some authors claim that, ideally, formulations should be able to maintain the high supersaturation level or prolong the induction period for crystallization for at least 2-3 hours [94].

- Mathematical analysis of API release kinetics

To further understand the release mechanism from ASDs, experimental data can be subjected to mathematical analysis to determine release/dissolution profile characteristics from the formulations.

API release profiles can be analyzed using independent [dissolution efficiency - DE] and model-dependent (curve-fitting) approaches.

- Dissolution efficiency (DE)

Model-independent methods generate a single value from a dissolution profile, thus allowing data to be compared directly.

Model-independent methods include the dissolution efficiency percentage (DE). This concept has been presented by Khan and Rhodes in 1972 [95]. For each sample, the percentage dissolution efficiency is calculated as the percentage ratio of the area under the dissolution curve up to time  $t$  to that of the area of the rectangle described by 100% dissolution at the same time point, and is defined as follows:

$$DE = \frac{\int_{t_1}^{t_2} y dt}{y_{100} (t_2 - t_1)} 100\% \quad (8)$$

$y$  is the percentage of dissolved product. **DE** is then the area under dissolution curve between time points  $t_1$  and  $t_2$  expressed as the percentage of the curve maximum dissolution. **100**, over the same period.

The dissolution efficiency (DE) has been used to evaluate API release performance from different API delivery systems (solid dispersions and others) under different formulations and test conditions with a 100% of drug delivery.

- Curve-fitting model

Model-dependent methods explore the mathematical equations governing the liberation profile as a function of certain parameters related to the pharmaceutical dosage form. These models allow an easy quantitative interpretation of data. A large number of mathematical

models were developed to describe the release rate of APIs from different API delivery systems. Some of the important models are [96]:

1. Diffusion model
2. Zero order kinetics model
3. First order kinetics model
4. Higuchi model
5. Korsmeyer-Peppas model

- Diffusion model

Two laws can explain the diffusion mechanism: Fick's first law of diffusion and Fick's second law of diffusion.

- In Fick's first law of diffusion, the diffusion flux occurs from regions of high concentration to regions of low concentration, with a magnitude that is proportional to the concentration gradient. The law can be defined:

$$J = -D \frac{dC}{dx} \quad (9)$$

Where, **J** is the amount of substance passing perpendicularly through a unit surface area per time, **D** is the diffusion coefficient and  $\frac{dC}{dx}$  is the concentration gradient.

The negative sign in the equation is to illustrate that the diffusion occurs in the direction opposite to the increasing concentration.

- In Fick's second law of diffusion, concentration changes with time. This law is derived from Fick's first law and illustrates that the change rate in concentration in a volume within the diffusional field is proportional to the rate of change in spatial concentration gradient at that point in the field.

$$\frac{dC}{dt} = -D \frac{d^2C}{dx^2} \quad (10)$$

The diffusion models are applied to find flux and concentration across membranes. Fickian diffusion generally occurs in polymeric matrices in which the value of the vitreous transition temperature of polymer ( $T_g$ ) is less than the temperature of the environment. When the polymer is in the rubbery state, polymeric chains have high mobility, enabling easy solvent penetration [97].

- Zero order kinetics model

This model represents a slow release of API from dosage forms that do not disaggregate. It is represented by

$$Q_0 - Q_s = K_0 t \quad (11)$$

$Q_0$  is the initial amount of API in the solution (most times,  $Q_0=0$ ),  $Q_s$  is the amount of API dissolved in time  $t$  and  $K_0$  is the zero order constant.

This model is applied to describe the API dissolution of several types of modified pharmaceutical dosage forms, such as, transdermal systems, matrix tablets with low soluble API in coated forms, osmotic systems, etc.

- First order kinetics model

This model is used to describe absorption and elimination of some APIs. The release can be expressed by the equation:

$$\frac{dC}{dt} = -KC \quad (12)$$

Where,  $K$  is the first order rate constant.

This model can be used to describe the API dissolution in pharmaceutical dosage forms such as those containing water-soluble APIs in porous matrices. There are a variety of therapeutic systems that display this type of first-order release. For soluble active agents incorporated in a porous matrix, the amount of drug released is proportional to the amount of remaining drug in the matrix. Thus, the amount of active released tends to decrease in function of time [97].

- Higuchi model

In 1961, this model was proposed by Higuchi in order to describe the API release from matrix systems. The hypothesis was based on:

- (i) Initial API concentration in the matrix is much higher than API solubility;
- (ii) API diffusion takes place only in one dimension (edge effect must be negligible);
- (iii) API particles are much smaller than system thickness;
- (iv) Matrix swelling and dissolution are negligible;
- (v) API diffusivity is constant and
- (vi) Perfect sink conditions are always attained in the release environment.

Higuchi model is given by the equation:

$$Q = K_H t_{1/2} \quad (13)$$

$Q$  is the amount of API released in time  $t$  per unit area  $A$  and  $K_H$  is the Higuchi dissolution constant.

This model is applicable to describe API dissolution from several modified release dosage forms like, some transdermal systems and matrix tablets with water soluble APIs.

- Korsmeyer-Peppas model (Power law)

Korsmeyer et al. (1983) derived a simple relationship to observe and understand the API release mechanism from polymeric system. *In vitro* release data was converted into the fraction of API or polymer released from the solid dispersions and plotted against time [98]. This plot was then fitted to the model described in Peppas equation.

$$Q = K_K t^n \quad \text{with} \quad Q = \frac{Q_t}{Q_\infty} \quad (14)$$

$Q_t$  is the amount of API dissolved in time  $t$  and  $Q_\infty$  is the maximum amount of API dissolved in time  $t$ ,  $K_K$  is a constant of Korsmeyer-Peppas,  $n$  is an important parameter in Korsmeyer-Peppas model, which characterizes the release mechanism as summarized in Table 2. The ( $n$ ) value is used to characterize different release for cylindrical or spherical shaped matrices.

*Table 2. Interpretation of release mechanisms from polymeric matrices [97], [99], [100]*

Release exponent (n)	API transport mechanism	Description
0.45 (cylinder) 0.43 (sphere)	Fick diffusion	Solvent transport rate or diffusion >> Polymeric chain relaxation
0.45 < n < 0.89 (cylinder) 0.43 < n < 0.85 (sphere)	Non-Fickian and anomalous transport	Diffusion and Swelling. The rearrangement of polymeric chains is slow.
<b>0.89</b> (cylinder) 0.85 (sphere)	Case II – Non-Fickian	Swelling or relaxation of polymeric chains
n > 0.89 (cylinder) n > 0.85 (sphere)	Super Case II – Non-Fickian	Tension of the polymers chain

This model has been frequently used to describe API release from several modified release dosage forms.

- Selection of the model for release study

There are various criteria for the selection of the mathematical models. The most widely used method employs the coefficient of determination  $R^2$  to assess the fit of the model equation.

Other criteria can also be used like least square fit, i.e. AIC (Akaike’s information criterion) and RMSE (root mean square error).

In general, the release models with major application are the Higuchi model, zero order model and Korsmeyer-Peppas law. The Higuchi and zero order model represents two limit cases in the transport and API release phenomena and Korsmeyer-Peppas model can be the decision parameter between these two models [101].

Korsmeyer-Peppas model has described well the dissolution behavior of solid dispersions of various APIs, polymers and manufacturing processes as shown in Table 3.

**Table 3. Summary about works in the literature that have used Korsmeyer-Peppas model to fit API release from solid dispersions. (Web of science- Keywords: solid dispersions, dissolution and Korsmeyer-Peppas model. Accessed in 11/10/2018)**

API	Carrier	Manufacturing processes							References
		Melting methods	Solvent evaporation	Freeze-drying	Co-precipitation	Kneading technique	Fusion method	Co-grinding	
Artemisinin	Succinic acid		X	X					[102]
Efavirenz	Soluplus®		X						[103]
Pelubiprofen	Eudragit® RL/RS PO + Aminoclay		X						[104]
PABA esters	PVP K15, K30 and K90		X						[105]
Clopidogrel bisulphate	PEG-4000						X		[106]
Allopurinol	Polyethylene glycol 6000	X	X		X	X		X	[107]

### ***1.3.7. Manufacturing amorphous solid dispersions (ASDs)***

As already discussed earlier in the Chapter, a more practical approach towards stabilizing an amorphous form is formulating ASDs.

Melting or solubilization of API and a carrier in a suitable solvent or solvent mixture are the basic principles of the transformation of the API in an amorphous stabilized form. The steps of this transformation is schematically represented in Figure 17 [77].

In the melting process showed in Figure 17, also called solvent-free method, API and carrier, generally a polymer, are pre-mixed and heated to melt the API. The polymer is firstly heated at temperatures above its glass transition temperature (if amorphous) or above its melting temperature (if crystalline). We will focus here on amorphous polymers. Above the  $T_g$ , the mobility in relatively long segments of polymer chains occurs freely. The crystal lattice structure of API can be destroyed by high temperatures (above its melting point) and it can then interact with the mobile polymer chains. The binary mixture is subsequently rapid cooled to 'freeze out' the solid state API-polymer in an amorphous solid structure.

On the other hand, i.e., starting from a solution of API and carrier in a common solvent or solvent mixture, the named 'solvent evaporation' method (Figure 17), the lattice crystal structure is completely destroyed during the solution preparation step. API molecules that are solubilized in the solvent are incorporated into the loosened polymer chains. The common solvent in the multi-constituent solution is subsequently eliminated generally by a rapid evaporation to 'freeze out' the solid state API-polymer in the resulting amorphous solid structure.

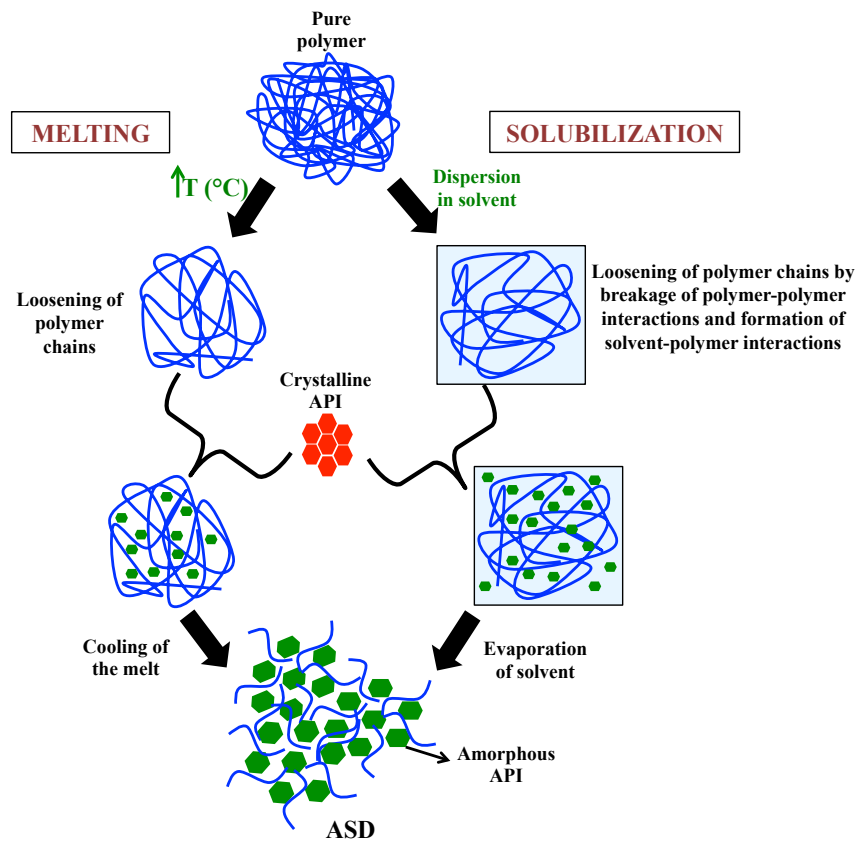


Figure 17. Schematic representation of formation of ASD through melting and solvent evaporation methods. Adapted from [77]

In the last two decades, ASDs have attracted an increasing attention in the works as showed in Figure 18, being a well-established strategy for overcoming limited aqueous solubility and poor oral bioavailability of APIs, by dispersing them in carriers, usually amorphous polymers. In the majority of published studies, ASDs have been produced by different preparation methods such as freeze-drying [67], [108]; hot-melt extrusion [109], [110],[1],[49]; rotary solvent evaporation [14]; film casting [112], [113]; ball milling [114]; cryo-milling [115]; super-cooling [116] and spray drying [46], [111], [117]–[119]. In these studies, the final product (ASD) obtained by each process is characterized and then, depending on the studied parameters (process conditions, composition), compared for evaluation of the preparation method efficiency, solid state, physical stability, solubility and dissolution enhancement.

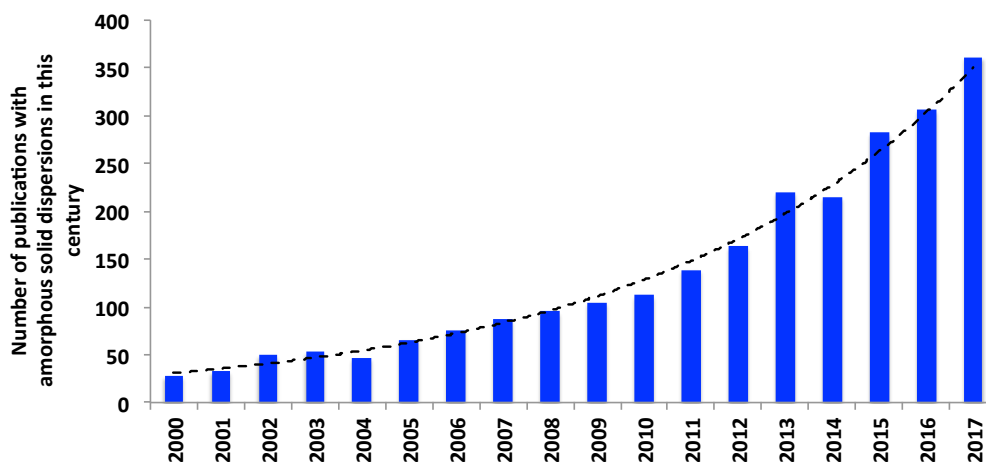


Figure 18. Summary about works using amorphous solid dispersions (ASDs) in this century (Source – Web of Science-keywords: Amorphous solid dispersions. Accessed in: 18/07/2018)

As shown in Figure 19, spray drying (SD) and Hot-melt extrusion (HME) have been the most used processes in the published studies. Both are also largely applied in the industrial research to attend industrial criteria such as cost-effectiveness and efficient scale-up from a small-scale laboratory. Table 4 shows some commercially available medicines using amorphous solid dispersions technologies. It highlights the preference for SD and HME as ASDs manufacturing processes.

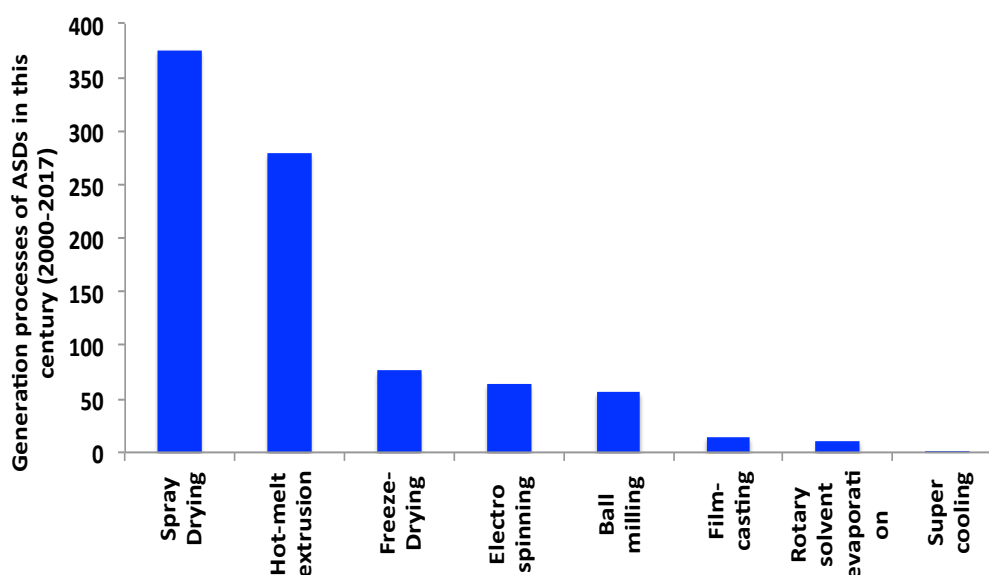


Figure 19. Generation Processes of ASDs used in this century (2000-2017) (Source – Web of Science; keywords: amorphous solid dispersions, process and drug. Accessed in: 18/07/2018)

*Table 4. Some commercially available medicines using amorphous solid dispersions technologies. Adapted from [120]*

Commercial name	API substance	Polymers	Preparation method	Year of approval
Isoptin® ER-E	Verapamil	HPC/HPMC	Hot-melt extrusion	1981
Cesamet®	Nabilone	PVP	Solvent evaporation	1985 (FDA)
Nivadil®	Nilvadipine	HPC/HPMC	Solvent evaporation	1989
Sporonax®	Itraconazole	HPMC	Spray drying on sugar beads	1992
Prograf®	Tacrolimus	HPMC	Spray Drying	1994 (FDA)
Gris-PEG™	Griseofluvin	PEG	Hot-melt extrusion	2000 (FDA)
Crestor®	Rosuvastatin	HPMC	Spray Drying	2004 (EMA)/ 2002 (FDA)
Cymbalta®	Duloxetine	HPMCAS	N/A	2004 (EMA/FDA)
Kaletra®	Lopinavir/ Ritonavir	PVP/VA	Hot-melt extrusion	2005 (FDA)/ 2001 (EMA)
Eucreas® Galvumet™	Vildagliptin/ Metformin HCL	HPC	Hot-melt extrusion	2007 (EMA)
Intelence®	Etravirine	HPMC	Spray Drying	2008 (EMA/FDA)
Modigraf®	Tacrolimus	HPMC	Spray Drying	2009 (EMA)
Samscar®	Tolvaptan	N/A	Granulation	2009 (EMA/FDA)
Certican®/ Votubia®/ Zotress™	Everolimus	HPMC	Spray Drying	2010 (EMA/FDA)
Onmel™	Itraconazole	HPMC	Hot-melt extrusion	2010 (FDA)
Fenoglide™	Fenofibrate	PEG/ Polaxamer 188	Hot-melt extrusion/ Spray drying	2010 (FDA)
Novir®	Ritonavir	PVP/VA	Hot-melt extrusion	2010 (FDA)/ 2009 (EMA)
Incivek™/Incivo®	Telaprevir	HPMCAS	Spray Drying	2011 (EMA/FDA)
Zelboraf®	Vemurafenib	HPMCAS	Coprecipitation	2012 (EMA) 2011 (FDA)
Kalydeco®	Ivacaftor	HPMCAS	Spray Drying	2012 (EMA/FDA)
Noxafil®	Posaconazole	HPMCAS	Hot melt extrusion	2014 (EMA) 2013 (FDA)
Viekira™/ Viekirax®	Ombitasvir/ Paritaprevir/ Ritonavir	PVP-VA/TPGS	Hot melt extrusion	2014 (EMA/FDA)
Orkambi®	Lumacaftor/ Ivacaftor	HPMCAS	Spray Drying	2015 (EMA/FDA)

### 1.3.8. Manufacturing processes

#### 1.3.8.1. Spray drying (SD)

A very efficient solvent-evaporation-based technology is spray drying since it allows for extremely rapid solvent evaporation, leading to a fast transformation of an API-carrier solution to solid API-carrier particles [121].

The spray drying process, schematically shown in Figure 20 is conceptually simple, involving the droplet formation from a liquid state by a solidification process driven by solvent evaporation. The process consists of three basic stages: nebulization of the liquid formulation, mixing of the liquid with the drying hot gas, evaporation of the liquid and separation of the dried particles from the gas. The solvent is mostly aqueous, but in case of solid dispersion preparation, organic solvents are mainly used. In case of using organic solvents in the feed, inert drying gases are required (e.g. dry nitrogen) in combination with a closed-cycle setup. The use of organic solvents involves also some restrictions and particular measures for safe and environmentally friendly use [121].

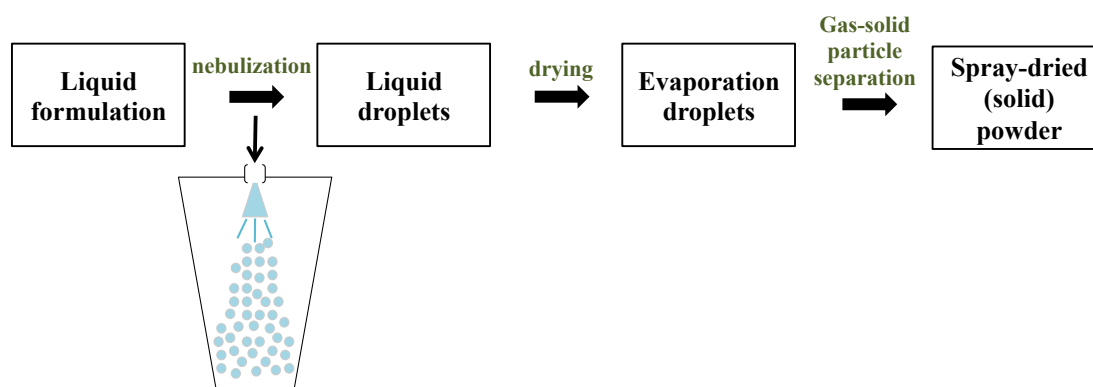


**Figure 20.** The spray drying process occurring in successive steps: 1. Nebulization of a liquid formulation; 2. Liquid droplets (spray) - hot drying gas stream contact (mixing and flow); 3. Drying of spray (solvent evaporation); 4) Separation of dried product from the air.

Solvent evaporation kinetics certainly contribute to formation of amorphous solid dispersions but also other factors such as the physical properties of feed, equipment components and processing parameters showing in Table 5 will influence the final physical structure of the obtained solid dispersion particles. For example, parameters influencing the initial droplet size (and the evaporation rate and also the spray-dried particle size) not only include formulations variables such as viscosity, surface tension and density, but also the nebulizing conditions. The

nebulizing conditions can be designed from several nozzles available on the market, which use different kinds of forces input to obtain fine droplets [1], [122].

The balance between liquid properties and process parameters is key parameter to design the desired particle characteristics. By modifying the spray drying processing conditions and feed formulation it is possible to alter and control over the properties of spray-dried powders such as particle size, shape, morphology, bulk density and moisture content besides functional properties such as solubility, flowability and dispersibility [72], [73], [121], [123].

Despite the energy of the hot drying gas transferred to the droplets, the most of this energy is used to vaporize the solvent, being this process available for thermolabile APIs in spray-dried ASDs.

*Table 5. Process and formulation parameters that influence the characteristics of the particle [123]*

<b>Formulation variables</b>	<b>Nebulizing conditions</b>	<b>Drying conditions</b>	<b>Spray-dried powder properties</b>
<ul style="list-style-type: none"> <li>• Flow rate</li> <li>• Temperature</li> <li>• Solid content</li> <li>• Viscosity</li> <li>• Type of solvent</li> </ul>	<ul style="list-style-type: none"> <li>• Nebulizing technique (two-fluid, pressurized or rotary nozzle)</li> <li>• Flow rate and type of drying gas</li> </ul>	<ul style="list-style-type: none"> <li>• Input temperature</li> <li>• Relative humidity</li> <li>• Drying gas flow rate</li> </ul>	<ul style="list-style-type: none"> <li>• Morphology</li> <li>• Particle size</li> <li>• Solubility</li> <li>• Dissolution rate</li> <li>• Hygroscopicity</li> <li>• Density</li> <li>• Residual moisture</li> </ul>

The spray-dried solid formation typically occurs within parts of a second to a few seconds. This high speed evaporation also avoids crystallization of the API during solid formation. It is an advantage in comparison to other slower evaporation processes such as film casting, where the time required for complete drying is in the range of minutes rather than seconds, during which the API may crystallize with the increase of API concentration in the solution.

In addition, the main advantages and disadvantages of the spray drying processes for the production of ASDs are summarized in Table 6.

*Table 6. The main advantages and disadvantages of Spray drying*

<b>Advantages</b>	<b>Disadvantages</b>
<ul style="list-style-type: none"> <li>● A one-step process from liquid to powder</li> <li>● Low thermal stress</li> <li>● Fast process</li> <li>● Quick drying avoids intermediate crystallization of the API during solid formation</li> <li>● Resulting powder can be directly formulated into solid oral dosage forms</li> <li>● Flexible particle sizes</li> <li>● Scalable process</li> </ul>	<ul style="list-style-type: none"> <li>● High costs of raw materials (solvent, nitrogen) and energetic cost</li> <li>● Residual solvents may remain in the powder</li> <li>● The powder is sensitive to moisture (high surface area and, depending of the hygroscopicity of the formulation, it will take up moisture affecting physical stability)</li> </ul>

- *Carriers for manufacturing ASDs of poorly soluble APIs by spray drying*

After selecting spray drying as the process for preparation of ASDs of a poorly soluble API, it is crucial to select the right carrier for the suitable API-carrier binary mixture. Most of the carriers used for amorphous solid dispersion formulations are hydrophilic polymeric compounds that primarily serve as crystallization inhibitor by decreasing the molecular mobility (anti-plasticization) of the amorphous form of an API dispersed in the matrices. The aim is to enhance solubility by maintaining the super saturation generated during dissolution in the gastrointestinal fluids [77], [119].

For manufacturing a solid solution by spray drying, a solution of API and a suitable carrier in an appropriate solvent or a mixture of solvents has to be prepared first. Sometimes it is not easy to find an appropriate and common solvent for both components. Typical solvents for spray drying are ethanol, isopropanol, methanol, acetone, ethyl acetate, methylene chloride [122], [124], [125]. However, the suitable solvent is a regularly used volatile organic solvent to project the viability of the process up to a commercial scale.

The solids concentration of the organic solutions is limited by viscosity since highly viscous solutions can no longer be nebulized properly. This also restricts the range of polymers, which can be employed, even if viscosities of polymers in organic solvents are commonly lower than in aqueous solvents [126].

Spray drying conditions have to be adjusted to avoid thermal stress of the API in the liquid formulation and to yields a dry product with very low levels of residual solvent. Besides safety considerations, residual solvents can avoid recrystallization [127].

**Table 7. General trend in the use of carriers used for the preparation of ASDs of poorly water soluble APIs that are published over the years.**

<b>Trend name</b>	<b>Polymer</b>	<b>Water soluble?</b>	<b>T<sup>g</sup> (°C)</b>	<b>T<sup>m</sup> (°C)</b>	<b>API</b>	<b>Reference</b>
Soluplus®	Poly (ethylene glycol)grafted with a copolymer of poly (vynil caprolactam) and poly(vinyl acetate)	Yes	79	-	Efavirenz	[103]
HPMC-AS	Hydroxypropyrylmethyl cellulose acetate succinate	Yes at pH>5.5	130	-	Probucol Danazol Phenytoin	[128]
PVP <sup>1</sup> and Isomalt <sup>2</sup>	<sup>1</sup> Polyvinylpyrrolidone <sup>2</sup> 6- <i>O</i> - $\alpha$ -D-Glucopyranosyl-D-glucitol mixed with 1- <i>O</i> - $\alpha$ -D-glucopyranosyl-D-mannitol	Yes	173 <sup>1</sup> and 63.6	145- 150 <sup>2</sup>	Celecoxib	[117]
PVP K-30	Polyvinylpyrrolidone	Yes	63.6	-	Nifedipine	[129]
PEG 6000	Polyethylene glycol 6000	Yes	-22.7	60	Sulfametho xazole and Nifedipine	[130]
PLGA	Poly (lactic-co-glycolic acid)	Yes	42-50	-	Celecoxib	[131]

### 1.3.8.2. Hot-Melt extrusion (HME)

Since the 1930's, hot-melt extrusion (HME) has been applied in several industrial fields, mostly in the plastic and food industry. The technology itself can be described as a process in which a material melts or softens under elevated temperature and pressure and is forced through a die by rotating screws [132]. The process set-up consists basically of three distinct parts: a conveying and kneading system for material transport and mixing; a die for forming the extrudates and downstream auxiliary equipment (cooling, shaping and collecting) as shown in Figure 21 [129].

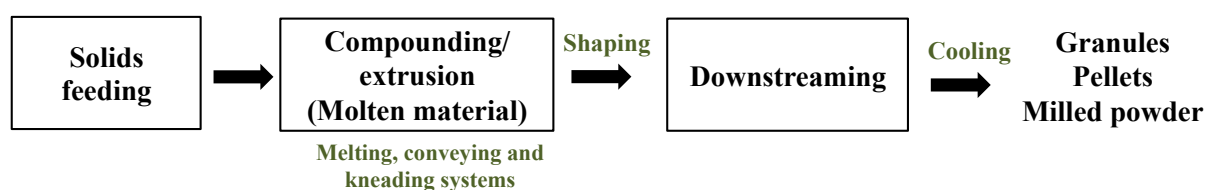


*Figure 21. Schematic representation of a hot melt extrusion process*

Academic and industrial researches have demonstrated HME processes as being an attractive alternative to traditional processing methods for preparation of complex API delivery systems, including granules, pellets, sustained release tablets, implants [133]. HME has become a popular process to prepare amorphous solid dispersions for the improvement of solubility and dissolution rates of poorly soluble APIs [48], [134]. During the melt extrusion process, the API dissolution into the polymer matrix is accelerated under the influence of shear and heat.

#### - Process configuration

HME process can be operated in two different configurations: single and twin-screw extruders. The single-screw extruder has been most commonly used in the plastic industry because it is more simple and cheaper. Twin-screw extruders are more common for pharmaceutical applications and it has several advantages over single-screw extruder, such as: easier material feeding, higher kneading and dispersing capacities, less tendency to over-heat and shorter residence times (which prevents degradation of heat-sensitive components) [133], [135]. The biggest difference between a plastic and pharmaceutical extruder is the contact between the product and metal parts in the machine. For a pharmaceutical extruder, regulatory requirements should be applied, such as, they must be not reactive, or absorptive with the product. Most screws are made from surface coated stainless steel with reduced friction. The

equipment is configured for the cleaning and validation requirements associated with a pharmaceutical environment [86], [136].

The basic components of an extruder shown in Figure 22 are the feeder, barrel, control panel, torque sensors, heating/cooling device, and assorted dies. The raw material can be volumetric or gravimetric fed into the barrel.

The feedstock will reach the conveying section in the barrel where the conveying elements move the material to the die section. The efficiency in this step can be improved by adapting the geometry of conveying elements. The next step is the melting section. In this step, the material is softening and melting by conductive thermal and mechanical energy input via preheated barrel and screws, respectively. It is a relevant pass to remove residual moisture or gas that might have been entrapped during intense mixing and melting. Following the process, the molten extrudate is pushed by pressure through the die, which defines the product shape (e.g. film, annular and circular). Finally, a conveyor belt is often employed for the cooling of the extrudate [86], [110], [133], [135], [137].

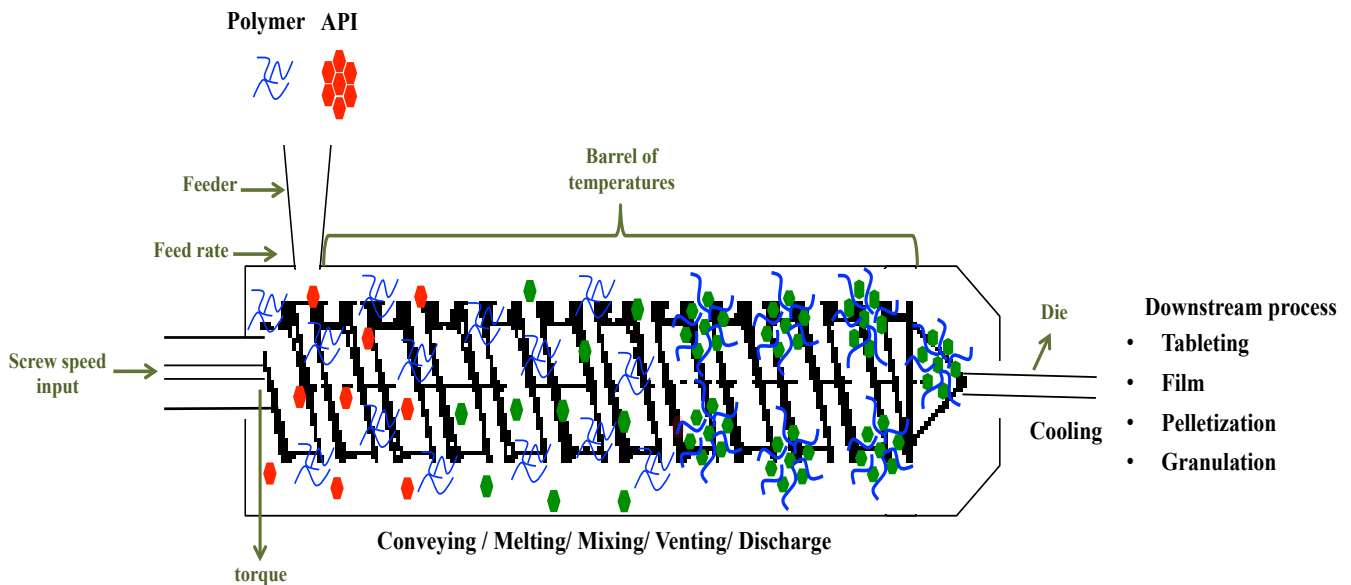


Figure 22. Schema of Hot-melt extrusion for pharmaceutical application

- Screw configuration

HME screws are segmented and can be configured as desired to meet various application requirements [110]. As already said, the most common application of screw configurations is

conveying, melting, mixing and shaping. Table 8 illustrates the different types of screw elements that are currently used in a HME process.

*Table 8. Different types of screw elements. Adapted from [138]*

SCREW ELEMENTS	APPLICATION
	Conveying
	Mixing
	Distributive flow
	Discharge feed screws

Conveying elements are used in the feeding, conveying and venting sections. They have a self-wiping lead geometry.

Mixing elements are composed of a combination of single mixing elements with offsets of 30, 60 or 90°. High offset leads to low conveying but high mixing properties.

Distributive flow elements are used to generate low energy mixing when liquids are added to the melt in the barrel. The elements are composed of an outer grooved and inner plain diameter disk.

Finally, discharge feed screws have a single lead geometry to generate the extrusion pressure to shape the final product at the die [86], [135], [139].

- Process variables and parameters

Versatility is one of the most attractive attributes of the HME technology. This characteristic is due to the high number of adjustable variables and parameters involved in this process (Figure 23), which gives the operator many possibilities to optimize the qualities of a certain formulation.

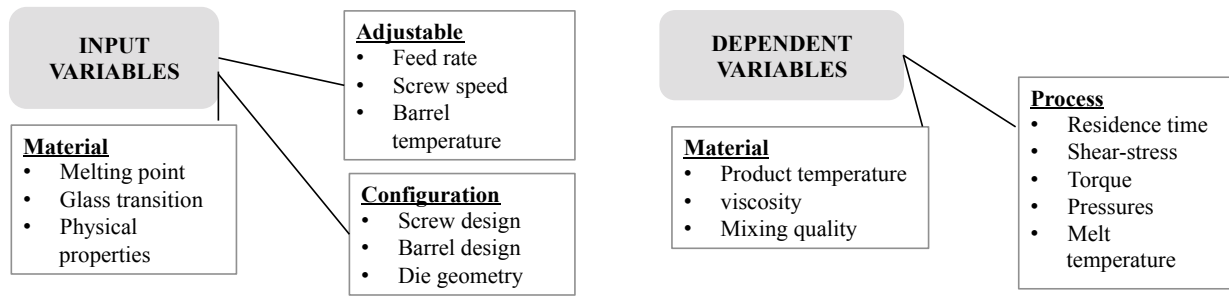


Figure 23. Input and dependent variables in the HME process

The input variables are set directly by the operator, whereas the dependent variables are not directly controlled but are important data to the reproducibility of a given process. For example, the segmented screw elements allow agitator designs to be easily optimized to suit a particular application; die plates can also be easily exchanged to alter the extrudate diameter and hence the spheroid diameter [140]. Consequently, a single machine is able to process many different formulations only by changing its parameters and process variables, not requiring space- and time-consuming solutions.

Most extruders have a modular design to facilitate different screw configurations [126]. The screw profile appears to have a significant impact on the extrusion process [86]. The operator is able to adapt the screw configuration by varying the number and arrangement of conveying and kneading elements (Table 8). Its design aims to achieve either a high or a low shear. One can arrange the kneading elements in order to obtain 30, 60 or 90° offset between consecutive elements, so to provide plasticizing, mixing and dispersing actions to the melt. The higher the angle, the higher the shear and mixing power provided to the flow at that point and the lower the transport action.

Distributive mixing refers to the content uniformity of a particular ingredient, as the API, while dispersive mixing relates to the size reduction and distribution [136]. The distributive screw element leads to a state of homogeneity whereas the dispersive mixing elements apply more shear stress and have less conveying capability, and therefore break down any agglomerates to a molecular level depending on their geometry. The distributive mixing elements avoid the formation of API clusters (oversaturated stages of the API in the polymer melt). This combined action assists the formation of the desired molecular dispersion. The larger the angle, the more mixing action takes place due to more leakage streams generation and residence time reduction [126].

- Carriers for HME

A prerequisite of the polymer to be used in HME is appropriate thermoplastic behavior. In addition, it should be solid at room temperature ( $T^g > \text{room temperature}$ ) for handle use, and have low hygroscopicity. Polymer has to be processed above its glass transition temperature ( $T^g$ ) but below its degradation temperature ( $T^{\text{degradation}}$ ). The same should be attributed for the API. In this case, the process can occur below or above its melting point ( $T^m$ ) depending on whether a miscibility regime or a solubilization, respectively is being used [141].

Table 9 presents a number of polymers that have been employed in HME process to produce ASDs. The number of polymers approved for pharmaceutical use is limited.

*Table 9. Summary of the polymers generally used in HME. Adapted from [110]*

<b>Trend name</b>	<b>Polymer</b>	<b>Water soluble?</b>	<b>T<sup>g</sup> (°C)</b>	<b>T<sup>m</sup> (°C)</b>	<b>T<sup>degradation</sup></b>
Soluplus®	Poly (ethylene glycol)grafted with a copolymer of poly (vynil caprolactam) and poly(vinyl acetate)	Yes	79	-	280
Kollidon® VA 64	Copolymer of poly(vinyl pyrrolidone) and poly(vinyl acetate)	Yes	105	-	260
Kollidon® 12 PF	Poly(vinyl pyrrolidone)	Yes	82	-	300
Affinisol® HPMC	Hidroxypropyrylmethyl cellulose	Yes	127	-	300
Kolliphor® P188	Poloxamer 188	Yes	-	54	350
Eudragit® RS	Copolymer of poly(ethyl acrylate), poly(methyl methacrylate) and poly(trimethylammonioethyl methacrylate chloride) 1:2:0.1	No	65	-	170
Eudragit® E	Copolymer of poly(butyl methacrylate), poly((2-dimethylaminoethyl) methacrylate) and poly(methyl methacrylate) 1:2:1	Yes at pH<5	55	-	250
Eudragit® RL	Copolymer of poly(ethyl acrylate) poly(methyl methacrylate) and	No	65	-	170

	poly(trimethylammonioethyl methacrylate chloride) 1:2:0.2				
Eudragit® L	Copolymer of poly(methyl acrylate) and poly(methyl methacrylate) 1:1	Yes at pH>7	190	-	190
Eudragit® S	Copolymer of poly(methyl acrylate) and poly(methyl methacrylate) 1:2	Yes at pH>6	180	-	180
Kollicoat® MAE100P	Copolymer of poly(methyl acrylate) and poly(ethyl acrylate) 1:1	Yes at pH>5.5	114	-	175
Kollicoat® IR	Poly(ethylene glycol) grafted with poly(vinyl alcohol)	Yes	45	-	200
Kollicoat® Protect	Poly(ethylene glycol) grafted with poly(vinyl alcohol) + poly(vinyl alcohol)	Yes	45	-	200
HPMC-AS	Hydroxypropylmethyl cellulose acetate succinate	Yes at pH>5.5	130	-	250*
HPMCP	Hydroxypropylmethyl cellulose phtalate	Yes	190	-	250*
Methocel®	Methyl cellulose	Yes	190	-	250
Ethocel®	Ethyl cellulose	No	130	-	300
Parteck® MXP	Milled polyvinyl alcohol	Yes	40-45	170	>250

In addition, the main advantages and disadvantages of HME process are given in Table 10.

*Table 10. The main advantages and disadvantages of Hot-melt extrusion [110], [138], [139]*

Advantages	Disadvantages
<ul style="list-style-type: none"> <li>• Solvent-free</li> <li>• Environmentally-friendly</li> <li>• Shorter and more efficient process time</li> <li>• Good controlled temperature system</li> <li>• Easier material feeding</li> <li>• High kneading</li> <li>• Dispersing capacities</li> <li>• Variety of shapes possible</li> </ul>	<ul style="list-style-type: none"> <li>• High temperature of process</li> <li>• High energy from the shear forces</li> <li>• Downstream processing</li> <li>• Not suitable for thermally labile APIs (such as proteins, peptides, etc)</li> <li>• Must be relatively moisture free</li> </ul>

### 1.3.8.3. Comparison of manufacturing processes

ASDs prepared by different methods do not necessarily exhibit the same physical or physicochemical characteristics, which might affect product performance such as dissolution behavior, solubility, including physical stability [142].

The dissolution behavior of ASDs is known to be affected by many variables, such as the aqueous solubility of components, the type of carrier and API-carrier ratio, but also by some characteristics of the solid forms such as particle size (surface area of contact with the dissolution medium), wettability and API-carrier interactions. The last three mentioned characteristics can be influenced by the manufacturing process, as demonstrated through some of the few examples found in the literature.

One example highlighting differences in physical stability and dissolution behavior was the study case performed by Dong et al. providing a comparative between ASDs with a compound A synthesized in-house, generated by hot-melt extrusion (HME) and by solvent co-precipitation (CP) process [143]. The carrier was the polymer HPMC-AS. The CP product was prepared by precipitation of Compound A and HPMC-AS from their solution and was dried under vacuum. The CP product was also milled prior to use. Both the HME and the CP products have the same API loading (40 wt%). Both CP and HME processes produced amorphous solid dispersions of Compound A which have the following in common: spectroscopic properties, powder X-ray diffraction, true density, and water vapor sorption/desorption behavior. In addition, the API was uniformly dispersed in both products as indicated by the single glass

transition temperature in DSC thermographs. However, CP process produced solid dispersion with larger specific surface area, which provided a faster dissolution compared with the HME process. Although both bulk products showed acceptable physical stability for three months in the 40°C/75% RH chamber, their stability was also evaluated in a suspension form. The two products were stored in 40°C/75% RH chamber for 3 months to monitor potential crystallization of Compound A from the products using XRD. In addition, suspensions of the HME and CP products were prepared in an aqueous vehicle (2% hydroxypropyl cellulose) at 25 mg/mL of concentration. After agitation for several days, the suspensions were collected, filtered and dried and the solid product was analyzed by XRD. The CP product was physically less stable, which was attributed to the surface area differences.

Another study reported differences in the onset of crystallization as a function of the preparation method for an amorphous solid dispersion model system containing Itraconazole (API) and the polymer Eudragit E100. ASDs with API loadings from 5 to 60 wt% were prepared by spray drying and film casting [144]. The crystallization temperature of Itraconazole reported from modulated differential scanning calorimetry (mDSC) analysis for the two processing methods indicate that Itraconazole crystallized more easily upon heating from film-casted samples than from spray-dried samples. This meant that the solid dispersions prepared by this process were less stable influencing the crystallization behavior of the API in the polymer. In brief the two methods produced dispersions of equal composition but different properties such as the kinetics of phase separation.

Some works have compared hot-melt extrusion and spray drying [46], [145]–[149]. Most of these studies employed a downstream processing like jet milling [46], ball milling [145], [150], mortar and pestle [149], [151] or co-milling [82] in order to reduce differences in particle size (surface area) between spray-dried powders and milled extrudates. The focus is generally a comparative between dissolution behavior and physical stability of ASDs produced by SD and HME.

Among them, Kelleher et al., 2018 [148] investigated the application of these two processes to the production of fixed-dose combination (FDC) monolithic systems comprising of Hydrochlorothiazide and Ramipril for the treatment of hypertension. Identical FDC formulations (APIs and carrier, with 5wt% API loading) were manufactured by hot-melt extrusion and spray drying and characterized using powder X-ray diffraction (XRD) and mDSC. Two polymers were used as immediate-release carriers: Kollidon® VA 64 and Soluplus®. Differences in the API solid state were observed between spray-dried (amorphous) and extruded (partially crystalline) ASDs. This result is not surprising, since the temperature in

the HME process was limited by the degradation temperature of Ramipril (123°C), which was below the melting point of the second API, Hydrochlorothiazide (272°C).

SD formulations offered greater long-term amorphous stability than the HME formulations under the particular stability test conditions chosen (10%RH and 75%RH at 25°C). The authors explained that since SD products were found to be completely amorphous and HME products to be partially crystalline, the crystal components may have encouraged further crystal growth to occur throughout the product as time progresses, leading to decreased amorphous stability in the HME products when compared to SD products. Initial  $T_g$ 's were also relatively lower for HME products when compared to SD products, which could result in decreased amorphous stability. Generally, a system with a higher  $T_g$  results in longer-term amorphous stability when compared to a system with a lower  $T_g$ .

In contrast, Agrawal et al.; 2013 [82] and Mahmah et al., 2014 [146] narrated the opposite. Agrawal et al. prepared solid dispersions of a compound X and PVP-VA64 in a concentration of 30 wt% of API, whereas Mahmah et al. developed solid dispersions of Felodipine (API loadings of 50, 30 and 25 wt%) in HPMC-AS or PVP. In both systems, HME offered greater long-term amorphous stability than the SD formulations under specific stress conditions (40°C/75%RH and 50°C/51%RH). This trend was attributed, on the one hand, to the possible presence of residual solvent in the spray-dried ASDs that may enhance crystallization and to different physical characteristics between them, and on the other hand, to the highly dense product provided by HME in comparison with SD, which led to better product stability [146].

Moreover, considering in vitro dissolution behaviors, two different tendencies have been observed comparing ASDs of same composition prepared by SD and HME processes: a faster dissolution rate for spray-dried ASDs [146], [150] or the opposite [148]. These results are attributed mainly to different physical characteristics of ASDs or the level of molecular interactions between API and polymer and chemical arrangements in the ASDs. An interesting result was shown by Agrawal et al. [82], who have noticed that similar dissolution performance was found for samples (Compound X in PVP-VA64) of ASDs produced by SD and HME processes, in spite of their large differences in surface area (22 times). They attributed the similar dissolution performance to a same level of molecular interactions between the components in the samples produced by both processes.

Based on these works, it is evident that the choice of the manufacturing process and its specific parameters of control might have a direct impact in the ASDs structure, generating

particles with different characteristics such as the level of molecular interactions between API and carrier.

## 2. Rational development of amorphous solid dispersions

A rational selection of appropriate carriers needs the support of thermodynamic and experimental methods to predict ASD formation from API-carrier miscibility estimation and, physical stability from temperature-composition phase-diagram of the API/carrier system.

### 2.1. Screening of carrier

#### 2.1.1. API-carrier miscibility

The miscibility between an API and a polymer can be calculated using the solubility parameter ( $\delta$ ) introduced by Hildebrand and Hansen [152], [153]. This parameter is based on the cohesive energy of each component calculated from a group contribution of dispersion forces ( $\delta_d$ ), polar interactions ( $\delta_p$ ) and hydrogen bonding ( $\delta_h$ ) (Equation 15) defined by Hoftyzer and Van Krevelen. The solubility parameter is expressed in  $(\text{J}/\text{cm}^3)^{1/2}$  or  $\text{MPa}^{1/2}$ .

$$\delta = (\delta_d^2 + \delta_p^2 + \delta_h^2)^{1/2} \quad (15)$$

where:

$$\delta_d = \frac{\sum F_{di}}{v}; \quad \delta_p = \frac{\sqrt{\sum F_{pi}^2}}{v}; \quad \delta_h = \frac{\sqrt{\sum E_{hi}}}{v} \quad (16)$$

In this equation,  $i$  is the structural chemical groups of component,  $F_{di}$  is molar attraction constant due to dispersion component,  $F_{pi}$  is molar attraction constant due to polar component,  $E_{hi}$  is the hydrogen bonding energy and  $v$  is the molar volume. The values of  $F_{di}$ ,  $E_{hi}$  and  $F_{pi}$  were determined by group contribution methods using the table described in Appendix 1.

These three parameters are used to position the compounds in a three-dimensional frame. Then, around the API is defined a sphere of solubility of radius ( $\Delta\delta_0$ ), which corresponds to the radius of interaction in the space of Hansen. Thanks to the values of  $\Delta\delta_d$ ,  $\Delta\delta_p$  and  $\Delta\delta_h$ , the distance between the API and the carrier,  $\Delta\delta$ , can be calculated. Any carrier molecule that is included in the sphere around the API (so with a API/carrier distance  $\Delta\delta$  less than  $\Delta\delta_0$ ) will be miscible with the API. This distance is expressed [153]:

$$\Delta\delta^2 = (\delta_d^1 - \delta_d^2)^2 + (\delta_p^1 - \delta_p^2)^2 + (\delta_h^1 - \delta_h^2)^2 \quad (17)$$

The API-polymer miscibility can be classified according to the difference between the solubility parameter  $\delta$  of the individual components in the mixture  $\Delta\delta$  [56], [86], [154].  $\Delta\delta < 7 \text{ MPa}^{1/2}$  indicates miscibility between the two compounds whereas  $\Delta\delta > 10 \text{ MPa}^{1/2}$  indicates an immiscibility. A value between these ranges may result in partial miscibility [56], [86], [154].

Solubility parameters have been used as a rapid screening tool for the selection of potential carrier polymers in solid dispersions, predicting if one material (API) will dissolve in another (carrier) to form a solution. However, it presents some limitations. Perhaps the most significant limitation is the purely thermodynamic foundation of the theory. Solid dispersions are not limited to the thermodynamically stable API-carrier binary mixture but kinetically stable mixtures can be equally useful for the improvement of apparent aqueous solubility. This method also neglects the entropy of mixing.

### ***2.1.2. Temperature-composition phase diagrams***

The physical stability of an ASD is strongly dependent on its glass-transition temperature and on the API solubility in the carrier matrix. Consequently, for the rational development of ASDs, it is essential to know the solubility of the API in the carrier because this value determines the maximal API load without a risk of phase separation and recrystallization [42], [71], [86].

Determining a phase-diagram of an API/carrier system means to establish a relation between temperature and API concentration and, consequently, represents the limits of stability (thermodynamic and kinetic) of the various phases in a chemical system at equilibrium [155].

In Figure 24 a typical phase-diagram is represented. The full (green) curve represents the solubility of the crystalline API in the carrier (single polymer or polymer blend). The dashed (red) curve marks the glass-transition temperature of the amorphous API-carrier binary mixture. The curve divides the phase diagram into four areas:

- Zone 1 and 2: thermodynamically stable,
- Zone 3: Unstable (demixing + recrystallization),
- Zone 4: Unstable (slow kinetic of demixing).

If the API load in ASD is lower than the API solubility in the carrier (left of the solubility curve), the amorphous system will be a thermodynamically stable, one-phase system. It can be

a melt (zone 1, above the glass-transition temperature curve) or a glass (zone 2, below the glass-transition temperature curve). For an ASD, if the API is molecularly dispersed in the carrier at concentrations below the API solubility at a fixed temperature, this system is, in theory, thermodynamically stable [42], [71], [86].

ASD systems with API loads to the right of the solubility curve are supersaturated and, thus, thermodynamically unstable. Clearly, kinetic effects are greater at temperature lower than  $T^g$  [156]. Zone 3 is the most unstable region where, above the glass-transition temperature curve, API recrystallization has a high probability to occur due to the higher molecular mobility in the supersaturated state (kinetically unstable). In zone 4, the supersaturated ASD systems are unstable but they can be kinetically stable because, due to the lower molecular mobility (region below the glass transition temperature curve), there is a weak tendency for demixing and recrystallization of API in excess.

The two curves represented in Figure 24 might be determined by mathematical or experimental approaches.

Gordon-Taylor equation is generally used to estimate the theoretical glass transition temperature of API-carrier mixture  $T_{MIX}^g$ . This equation was previously presented in Chapter 2 (section 1.3.5).

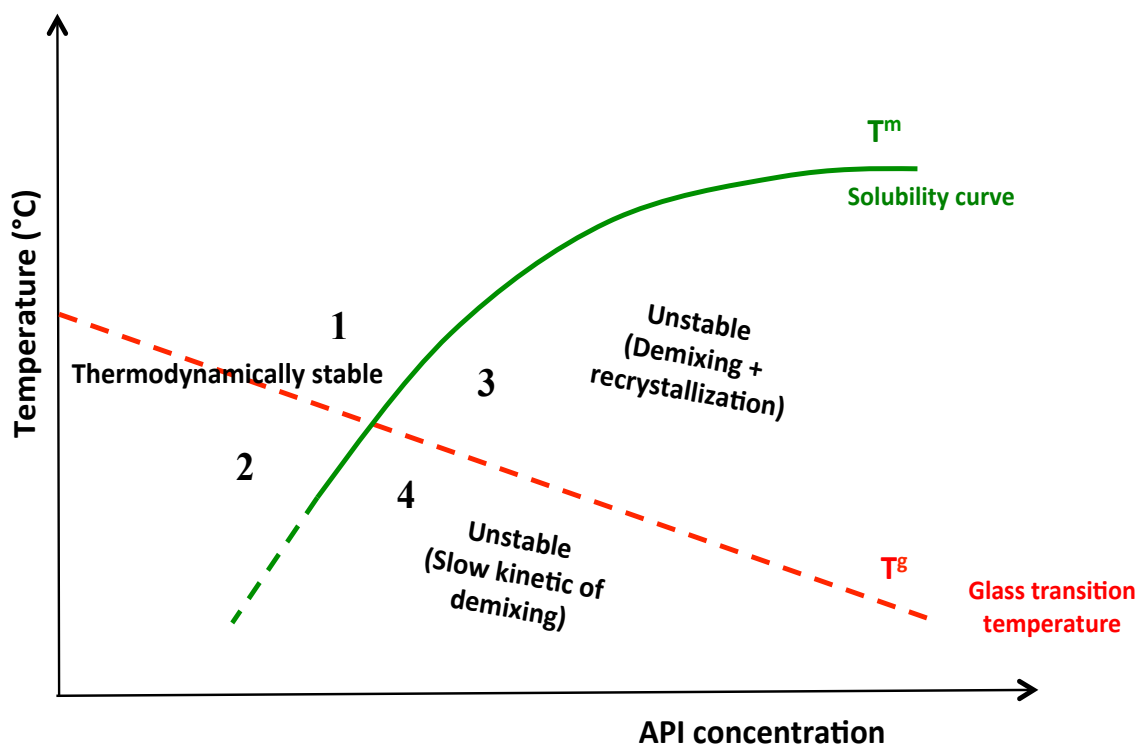


Figure 24. Schematic phase-diagram of an API/carrier mixture. It represents the evolution of equilibrium concentrations as a function of temperature (green line) and the evolution of the glass transition

*temperature of mixture (red line) as a function of temperature. They delimit zones of stability represented by 1, 2, 3 and 4.*

Measuring the crystalline API solubility in polymers (solubility curve) is still a challenge due to the high viscosity of polymeric solutions that hampers the solubility equilibrium achievement (equilibrium between a crystalline solid and its solution with a polymer), and makes difficult the experimental construction of solubility curves in a low time consuming and, consequently, the construction of a phase diagram API-polymer [109]. To overcome this difficulty and produce a solubility curve, different methods have been developed, among them:

- Estimation of the solubility of an API in a polymer from the solubility of the API in a low molecular weight liquid, chemically analogue to the polymer [157];
- Methods based on thermal analysis such as the melting point depression method [158], the dissolution end point method [159] and recrystallization methods [76], [109], [115]. These methods, schematically represented in Figure 26, will be presented in more details.

Theoretically, melting of a crystalline API occurs at the temperature ( $T^m$ ) when the chemical potential of the crystalline API equals to the chemical potential of the molten API. The melting point depression method explores the depressed melting point of the API in the presence of a miscible polymer [157]. The onset of the melting endotherm is considered as the equilibrium solubility temperature of the given composition. Marsac et al. showed a study of melting point depression optimization between Nifedipine or Felodipine in PVP K12. Their group reported that after method, which involved reducing the scan rate and controlling particle size, substantial melting point depression was verified for a increase in the polymer composition as seen in Figure 25 [158]. The choice of the melting onset eliminates the impact on  $T^m$  of particle size and preparation method of the physical mixtures. However, the onset only marks the beginning of the API dissolution in the polymer but does not provide information concerning the amount of API in the binary mixture that can be dissolved at that respective temperature [157].

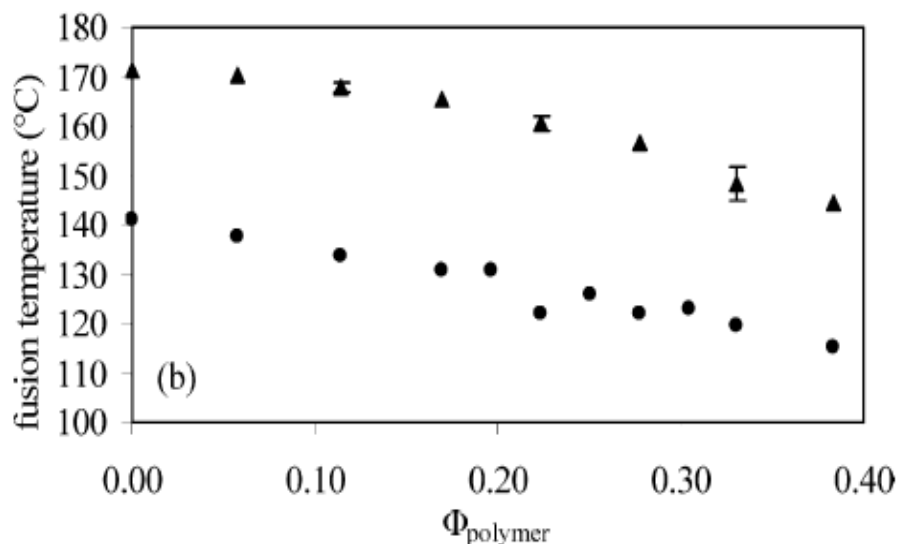


Figure 25. Illustration of extrapolated onset of melting of nifedipine (triangle) and felodipine (circles) as demonstrated by Marsac et al. Taken from [158].

Progressing the protocol for thermal analysis, the cryomilling of the physical mixtures was proposed in order to compensate the slow dissolution kinetics by reducing the size crystals prior to DSC experiments [85]. However, cryomilling is a longstanding process and have some limitations to control and to standardize particle characteristics such as size, morphology, shape and surface properties [160]. In contrast, the dissolution endpoint method enables the measurement of the endpoint of the dissolution step and thus might be more accurate [161]. The end point value represents the melting point of the final composition, assuming complete mixing has occurred. The disadvantage of this method is its strong dependence on the particle size. If the particle size is not sufficiently small, the melt is not able to reach its equilibrium state during heating. This may result in a higher dissolution end point, leading to underestimation of the API-polymer solubility.

The described methods follow the dissolution kinetics of APIs into polymers at under saturated concentration solutions (Figure 26). Another way to determine the API-polymer solubility is to reach the equilibrium solubility by following the recrystallization (recrystallization method) of the API from a supersaturated homogeneous API-polymer solid solution [115], [157]. The demixing kinetics of APIs from supersaturated systems is expected to be much faster than the dissolution kinetics of APIs into under saturated systems. This difference arises directly from the molecular mobility in the polymer matrix, which is higher in supersaturated API-polymer solutions than in undersaturated ones.

The supersaturation of the API into the polymer can be obtained from a physical mixture of crystalline API and polymer carrier by different techniques such as film casting method [157] and cryomilling [115], [161] that forces the miscibility of the two compounds to reach supersaturation as seen in Figure 26. The supersaturated glass solution is then loaded in a DSC analyzer and annealed above its  $T^g$  during a sufficient time to complete the demixing process, i.e., to release the excess of API in the mixture to reach the equilibrium solution concentration at the annealing temperature. The new equilibrium dissolution concentration of the API remaining dispersed in the polymer was then determined by applying another cooling-heating cycle to measure the  $T^g$  of the equilibrium phase obtained. Finally, this new  $T^g$  is associated to an equilibrium concentration using the Gordon-Taylor equation [78], [162].

Annealing temperature and annealing time are essential parameters and play an important role in the recrystallization method. At lower annealing temperatures, a longer time is required to reach the equilibrium state. The reason is probably a slower demixing kinetics due to an insufficient molecular mobility, leading consequently to slower API diffusion in the polymer matrix [115].

Binary interactions between polymer and API are commonly described by Flory-Huggins parameter ( $\chi$ ) obtained from the solubility curve. Immiscibility between the components is represented by a positive  $\chi$ , while miscibility is indicated by a negative  $\chi$  [52], [96], [102].

Flory-Huggins model will be deduced in the next section.

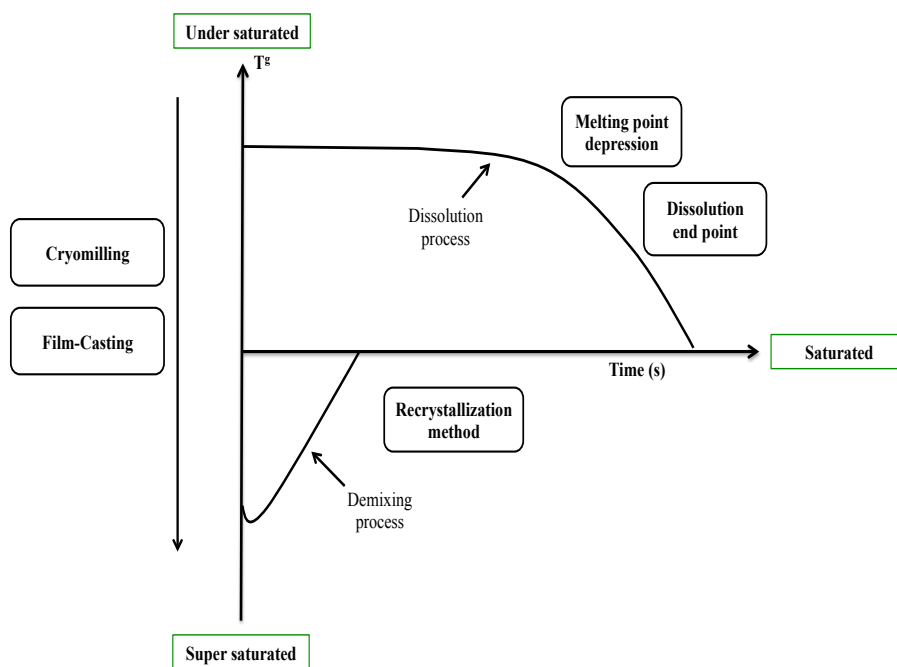


**Figure 26.** Schematic time and process evolution of the glass transition temperature of an API-polymer mixture when reaching its equilibrium solubility in an annealing. Adapted from [115]

#### 2.1.2.1. Equilibrium equations

Solubility is an intrinsic property of solids or fluids that can act as a solute dissolved in a solvent. This dissolution will happen until the system achieves the equilibrium and forms, consequently, a homogeneous solution. Equilibrium occurs under dynamic conditions when the two, simultaneous and opposing processes of dissolution and solids precipitation, happens at a constant rate [20]. Pressure, temperature, intermolecular interaction, crystal lattice and the molecular structure are properties that influence the solubility.

Considering our system as been an API dispersed in a polymer, it is essential to implement a thermodynamic approach to well understand the solubility and molecular interactions of this system. The thermodynamic study of polymer solutions has been investigated in order to explain the mixing-demixing phenomena of binary systems since 1940s by Flory and Huggins [164], [165]. They developed the rigid lattice theory: the system is represented by (equation 18):

$$N_0 = N_S + \lambda N_o \quad (18)$$

The molecules of the pure liquids in their mixture are distributed over  $N_0$  lattice sites and should be equal to the addition of the number of solvent molecules,  $N_S$ , and the number of polymer repeated units,  $\lambda N_o$ , where:

$$\lambda = \frac{V_P}{V_S} \quad (19)$$

is the ratio of the molar volume of the polymer  $V_o$  to the one of the solvent  $V_S$ . Based on this, Flory and Huggins obtained the expression for the entropy of mixing ( $S_m$ ) by counting the possible number of conformations taken by a first chain in the empty lattice.

$$S_m = -K (N_o \ln \quad + N_s \ln \quad) \quad (20)$$

$K$  is the constant of Boltzmann.  $\quad$  and  $\quad$  are the volume fractions of the polymer and the solvent respectively, which can be calculated by:

$$= \frac{N_S}{N_S + N_P} \text{ a d } = 1 - \quad (21)$$

Assuming that the API dissolved in the polymer matrix is equivalent to the solvent, previous equations can be rewritten by replacing index “S” by the index “PA” corresponding to the API. As combinatorial aspects are not sufficient, Flory and Huggins have introduced a new parameter  $\chi$ , which takes into account the specific interactions between API and polymer:

$$\chi = \frac{\Delta H_m}{KT N_P v_{PA}} \quad (22)$$

$H_m$  is the enthalpy of mixing and  $T$  the temperature. Immiscibility between the components is represented by a positive value of  $\chi$ , while miscibility is indicated by a negative  $\chi$  [56], [115], [163].

The Gibbs free energy of mixing  $\quad_m$  can be written:

$$\frac{\Delta G_m}{KT} = N_A \ln \quad + N_o \ln \quad + \chi N_o \quad (23)$$

This equation can be derived partially with respect to  $N_A$  to give the following equation for the variation of the PA chemical potential (expressed per mole unit):

$$\frac{\Delta \mu_{PA}}{RT} = \ln(1 - v_{PO}) + \left(1 - \frac{1}{\lambda}\right) v_{PO} + \chi v_{PO}^2 \quad (24)$$

$R$  is the gas constant (8.314 J/mol/K). The expression above will be essential to demonstrate the phase equilibrium for an API-polymer binary mixture.

In a thermodynamic approach, the solubility can be defined by the equality of the chemical potentials of the phases in equilibrium [88], [103]. In our case, we have to consider a phase constituted of polymer saturated in API and a solid crystalline phase of API. Presuming that the solid API is pure and can be considered as an incompressible fluid, the expression for the variation of the solid API chemical potential can be written [167]:

$$\mu_A = (C_A^L - C_A^S) \left( T_A^m - T - T \ln \left( \frac{T_{PA}^m}{T} \right) \right) - \Delta H_{PA}^m(T_A^m, P_0) \left( 1 - \frac{T}{T_{PA}^m} \right) + (P_0 - P)(V_A^L - V_A^S) \quad (25)$$

From this equation, some remarks and simplifications can be done. Assuming no variation in the pressure ( $P_0 = P$ ) and equality of the liquid and solid heat capacities ( $C_A^L = C_A^S$ ), the variation of the solid API chemical potential can be written:

$$\frac{\Delta \mu_{PA}}{RT} = - \frac{\Delta H_{PA}^m(T_{PA}^m, P_0)}{R} \left( \frac{1}{T} - \frac{1}{T_{PA}^m} \right) \quad (26)$$

$\Delta H_{PA}^m$  is the melting enthalpy of API at the pressure  $P_0$  and the melting temperature of API  $T_{PA}^m$  (in J/mol). Finally, for a binary mixture having a melting temperature equal to  $T_{MIX}^m$ , the equilibrium between the polymer phase saturated in API and the solid API phase leads to the following equality:

$$\frac{1}{T_{MIX}^m} - \frac{1}{T_{PA}^m} = - \frac{R}{\Delta H_{PA}^m} \left( 1 - (1 - \nu_{PO}) + (1 - \frac{1}{\lambda})\nu_{PO} + \chi \cdot \nu_{PO}^2 \right) \quad (27)$$

The polymer volume fraction  $\nu_{PO}$  can be calculated according Equation 28:

$$\nu_{PO} = \frac{\frac{W_P}{\rho_P}}{\frac{1 - W_P}{\rho_{PA}} + \frac{W_P}{\rho_{PO}}} \quad (28)$$

$W_{PO}$  is the polymer mass fraction and  $\rho_i$  is the density of the compound  $i$ .

The Equation 27 can be used to predict the Flory-Huggins parameter  $\chi$ . Indeed, knowing the melting temperatures  $T_{MIX}^m$  of mixtures at different polymer mass fractions  $W_{PO}$ , it is possible to plot  $-\frac{\Delta H_{PA}^m}{R} \left( \frac{1}{T_{MIX}^m} - \frac{1}{T_{PA}^m} \right) - \left( 1 - (1 - \nu_{PO}) + (1 - \frac{1}{\lambda})\nu_{PO} \right)$  as a function of  $\nu_{PO}^2$  and the slope of the obtained line (at least at low mass fraction) is equal to  $\chi$  [168] as represented in Figure 27.

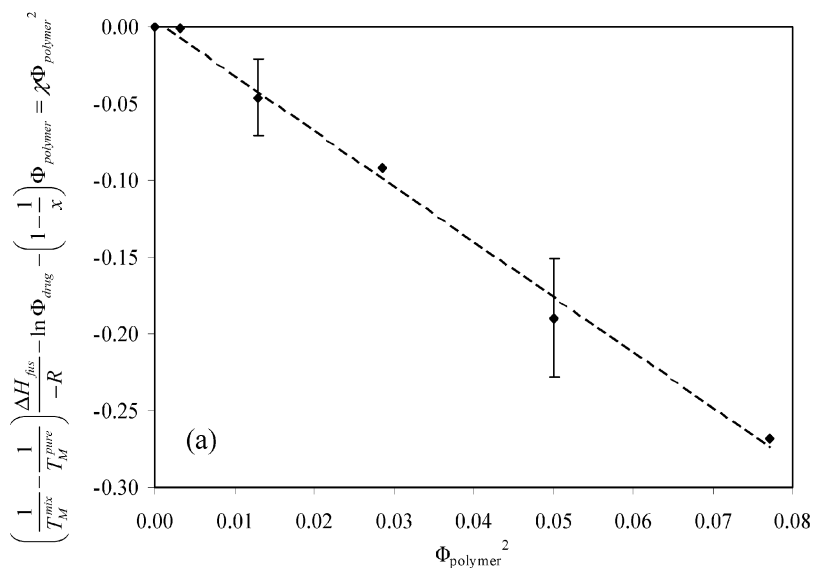


Figure 27. Example of literature how to predict the Flory-Huggins solubility parameter  $\chi$ .  $\Phi_{polymer}$  is the volume fraction of polymer. Taken from [158].

### 3. Amorphous solid dispersion of Efavirenz (API) and Soluplus® (carrier)

#### 3.1. Active Pharmaceutical Ingredient (API) - Efavirenz

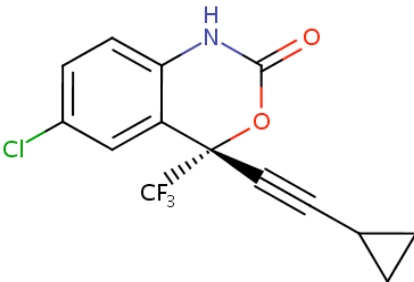
HIV continues to be a major global public health disease, reaching more than 35 million people so far. In terms of statistics, approximately 1.0 million people came to death as victim from HIV and 1.8 million people became newly infected with this disease in 2016 [169].

Efavirenz (EFV) ((S)-6-chloro-4-(cyclopropylethynyl)-1,4-dihydro-4-(trifluoromethyl)-2H-3,1-benzoxazin-2-one, the molecule of choice of this thesis, is recommended by World Health Organization (WHO) as an alternative first-line treatment of Human immunodeficiency virus (HIV) [169].

EFV is a non-nucleoside transcriptase inhibitor (NNRTI), used as part of high activity antiretroviral therapy (HAART) to ensure the amount of HIV at low levels in the organism of humans [170]. The recommended oral dose ranges from 50 to 600 mg, given once daily. Due to a narrow therapeutic window [171], its therapeutic monitoring is recommended to prevent collateral effects and discontinuation of the treatment.

The molecular formula of EFV is  $C_{19}H_{19}ClF_3NO_2$  (315.68 g/mol). A summary of its physicochemical characteristics is presented in Table 11.

Table 11. Summary of physicochemical characteristics of Efavirenz

<b>Molecular weight</b>	315.68g/mol	<b>Chemical structure</b> 
<b>Melting point</b>	139-141 °C	
<b>pKa</b>	10.2	
<b>LogP</b>	4.6	
<b>Aqueous solubility</b>	1-9 µg/mL (25°C)	
<b>DRUG- acceptors</b>	5	
<b>DRUG-donors</b>	1	

EFV is classified as a class II of the Biopharmaceutical Classification System (BCS), i.e., it has low aqueous solubility (1-9 µg/mL at room temperature), resulting in poor gastrointestinal absorption and, consequently, poor bioavailability [45][22], [172]–[174].

EFV has an intrinsic dissolution rate (IDR) of 0.037 mg/(cm<sup>2</sup>/min) [45], [175]. IDR of 0.1 mg/(cm<sup>2</sup>.min) is considered the low threshold limit for oral API absorption [176]. Dissolution rate is thus a limiting factor for oral absorption of EFV. In addition, EFV is highly lipophilic (log P = 5.4) [177]. In connection with reasons for low solubility of APIs discussed in topic 1.1.2, its low solubility in water is probably limited by the solvation process (log P > 4).

Some research results have been published focusing on enhancement of solubility/dissolution rate for EFV such as polymeric micelles [171] microcrystals [178] or organogels [179]. Other studies, grouped in Table 12, have focused on solid dispersions, crystalline physical mixtures of crystals or nanocrystals dispersed in polymer matrix) or amorphous (ASDs) [179].

Table 12 also shows that different polymer carriers (cellulosic polymers, polyvinylpyrrolidone - PVP, hydroxypropylcelluloses - Klucel, polyethylenoglycol, HPMCAS, Eudragits and Soluplus) have been used to generate solid formulations with enhanced solubility or dissolution rate, by using different manufacturing processes.

*Table 12. Summary about Efavirenz studies (Source-Web of science. Keywords: Efavirenz and dissolution. Accessed in: 20/05/2018)*

Reference	Carrier	API state	Formulation	Concentration in EFV (wt%)	Process
[180]	Cellulose acetate based	Amorphous	Nanoparticles solid dispersion	25	Dialysis and then, Freeze Drying
[64]	Cellulosic polymers matrices	Amorphous	ASD	15	Solvent Casting and Gridding
[175]	Klucel LF, Klucel ELF and HPMC	Crystalline	Suspension	10	Colloidal mill and then, freeze drying or spray drying
[103]	Soluplus®	Amorphous	ASD	10, 17 and 44	Spray-drying
[181]	PVP K-30	Amorphous	ASD	30,50 and 60	Freeze Drying
[182]	Soluplus® and HPMCA's	Amorphous	ASD	30	Hot-melt extrusion
[183]	PVP K-30	Amorphous	ASD	30,50 and 60	Spray Drying
[177]	PVP K-30	Crystalline	Nanocrystals solid dispersion	2 and 4	High-pressure homogenization and Hot-melt extrusion
[173]	Nicotinamide	Crystalline	Binary physical mixture	50	Solid state and solvent dropped grinding
[22]	PVP K-30 and Cyclodextrins	Amorphous	ASD	1, 5, 10 and 30	Kneading process
[184]	PVP K-30	Crystalline	Solid dispersion	20	Kneading and Solvent evaporation
[174]	Polyethylene glycol 8000 and PVP K-30	Amorphous	ASD	6, 9 and 17	Fusion and solvent method
[172]	Eudragit EPO	Amorphous and Crystalline	Solid dispersion	10, 25, 50, 60 and 70	Hot-melt extrusion
[45]	Eudragit EPO	Amorphous	ASD	50	Hot-melt extrusion

The majority of these works have demonstrated solubility and dissolution enhancement compared with the unprocessed EFV crystals. Mazumder et al. showed that the solubility increased 10-20 fold compared with the crystalline EFV alone in a potassium phosphate buffer at pH 6.8 [180]. Indeed, Lavra et al. indicated a solubility increase of 6 fold in water and 1.5-2 fold in FeSSIF (fed state simulating intestinal fluid – pH 5.0) in comparison with crystalline EFV [103]. Sathigari et al. showed a dissolution enhancement of the HME formulation with Eudragit EPO of approximately 2 fold higher than EFV alone and the corresponding physical mixture [45].

### **3.2. Carrier - Soluplus®**

The choice of a carrier is a critical parameter for ASDs because it impacts a number of factors such as molecular mobility, preparation methods and the physical/chemical stability of the amorphous form [71].

Soluplus® has gained much attention in ASDs area, because it acts as a solubilizing agent for APIs with low aqueous solubility, inhibiting recrystallization during dissolution [19].

Soluplus® is a block graft copolymer with poly(vinyl acetate) PVAc and poly(vinyl caprolactam) PVCL block grafted on a poly(ethylene glycol) PEG backbone in a ratio of 30:57:13 respectively.

Its average molecular weight is in the range of 90 000-140 000 g/mol and its chemical structure is shown in Figure 28. It is amorphous, with a glass temperature transition around 80 °C [185].

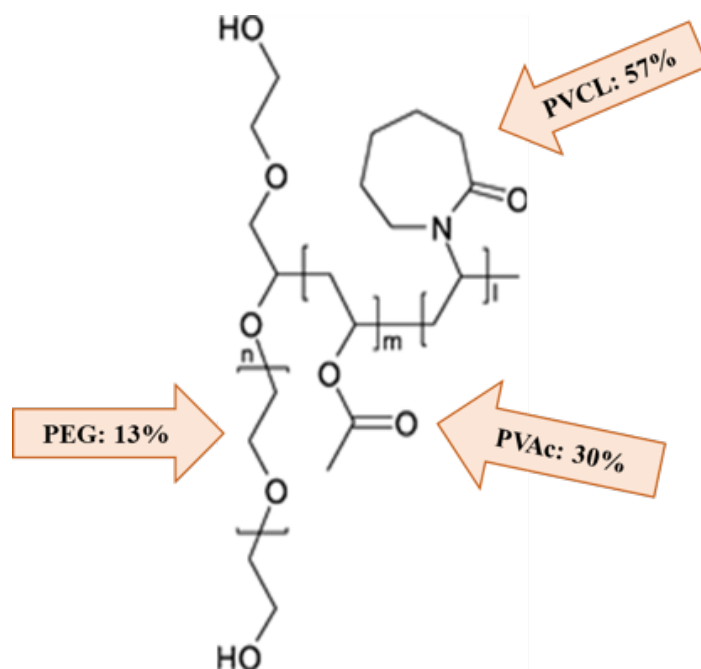


**Figure 28.** The structure of Soluplus®. The three different block polymers shown are PVCL, PVAc, and PEG, and their respective monomer ratios 57:30:13.

The composition of Soluplus® (Figure 28) allows the polymer molecule to self-assemble and to form molecular micelles. The graft copolymer provides a polyethylene glycol backbone as hydrophilic part and vinylcaprolactam/vinyl acetate side chains as lipophilic structure. It forms micelles in aqueous solution above the CMC of 7.6 mg/L [18].

The size of micelle formed by Soluplus® alone was found to be in the range of 65 nm to 70 nm with unimodal size distribution [186], [187] at a temperature of 25 °C, whatever the polymer concentration. However, at 37°C the micelle size increases with increasing concentration [187].

As noticed previously, due to its amphiphilic structure, Soluplus® forms micelles in aqueous solution which can solubilize poorly soluble APIs, as schematically represented in Figure 29. The hydrophilic domain (polyethylene glycol) of Soluplus® serves as a flexible outer shell of the core-shell structure in aqueous solution while the hydrophobic domain (polyvinyl caprolactam) forms the solid inner core, which will entrap the hydrophobic API in its interior.

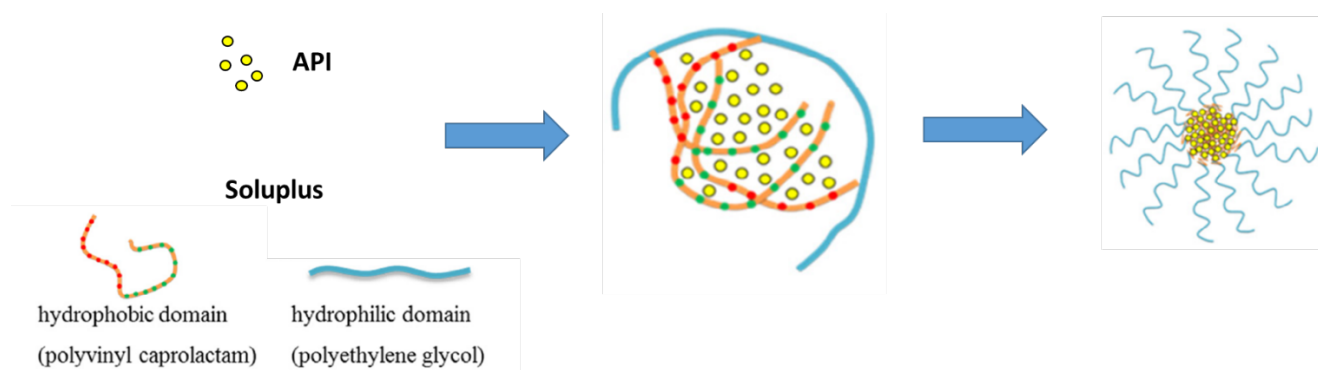


Figure 29. Micelles formation of Soluplus in water and entrapment of API

Due to this solubilizing action, it was shown that Soluplus® enables a many fold supersaturation for several APIs (Figure 30).

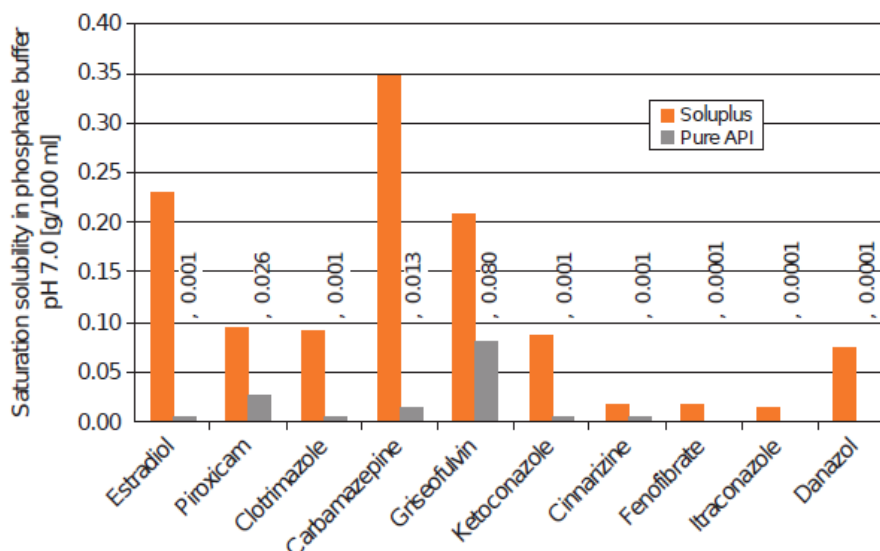


Figure 30. Solubility of several APIs with and without Soluplus® (10 wt%), adapted from BASF [185]

Soluplus® is a thermoresponsive polymer. Thermoresponsive polymers are a class of smart materials that exhibit change in their physical properties with temperature [188]. In aqueous solutions they exhibit a critical solution temperature (LCST), where phase separation is induced by a small change in temperature. The temperature at which the polymer solution starts to phase-separate, thus becomes cloudy is known as cloud point. Soluplus® exhibits a lower critical solution temperature (LCST) near 40°C [187], [189], above which it aggregates into larger micelles and displays gel-forming ability. This process is reversible upon cooling the polymer solution.

### 3.3. Efavirenz- Soluplus miscibility

API-polymer miscibility is a requirement to proper amorphous solid dispersions formation. A qualitative estimation of EFV-Soluplus miscibility was already demonstrated by our group using the Hansen solubility parameter approach [1]. The different structural groups present in EFV and Soluplus were discriminated from their known chemical structures and allowed estimation of solubility parameter components and subsequently total solubility parameter given in Table 13. The difference between the miscibility parameters of EFV and Soluplus is  $4.7 \text{ MPa}^{1/2}$ , suggesting miscibility between the two compounds [1]. However, it is important to keep in mind that this is a prediction to orientate in polymer choices but does not guarantee miscibility.

*Table 13. Hansen solubility parameters for Efavirenz and Soluplus*

<b>API and carrier</b>	<b>EFV</b>	<b>Soluplus</b>
Hansen parameter $\delta$ ( $\text{MPa}^{1/2}$ )	24,5	19.8
$\Delta\delta$ ( $\text{MPa}^{1/2}$ )	4.7	

## 4. References

- [1] M. Lavra and Z. Maria, *Incremento da solubilidade e da cinética de dissolução do fármaco Efavirenz através da obtenção de misturas binárias amorfas com matrizes poliméricas*. Ecole nationale des Mines d’Albi-Carmaux, 2016.
- [2] 19 November and 2007, ‘The administration of medicines’, *Nursing Times*. [Online]. Available: <https://www.nursingtimes.net/clinical-archive/medicine-management/the-administration-of-medicines/288560.article>. [Accessed: 01-Oct-2018].
- [3] J. M. Ting, W. W. Porter, J. M. Mecca, F. S. Bates, and T. M. Reineke, ‘Advances in Polymer Design for Enhancing Oral Drug Solubility and Delivery’, *Bioconjug. Chem.*, vol. 29, no. 4, pp. 939–952, Apr. 2018.
- [4] J. M. Ting *et al.*, ‘High-Throughput Excipient Discovery Enables Oral Delivery of Poorly Soluble Pharmaceuticals’, *ACS Cent. Sci.*, vol. 2, no. 10, pp. 748–755, Oct. 2016.
- [5] G. L. Amidon, H. Lennernäs, V. P. Shah, and J. R. Crison, ‘A theoretical basis for a biopharmaceutical drug classification: the correlation of in vitro drug product dissolution and in vivo bioavailability’, *Pharm. Res.*, vol. 12, no. 3, pp. 413–420, Mar. 1995.
- [6] A. Dokoumetzidis and P. Macheras, ‘A century of dissolution research: from Noyes and Whitney to the biopharmaceutics classification system’, *Int. J. Pharm.*, vol. 321, no. 1–2, pp. 1–11, Sep. 2006.
- [7] C. for D. E. and Research, ‘Development Resources - Dissolution Methods Database Frequently Asked Questions’. [Online]. Available: <https://www.fda.gov/Drugs/DevelopmentApprovalProcess/DevelopmentResources/ucm073197.htm>. [Accessed: 07-Oct-2018].
- [8] H. D. Friedel *et al.*, ‘FIP Guidelines for Dissolution Testing of Solid Oral Products’, *J. Pharm. Sci.*, Aug. 2018.
- [9] S. Baghel, H. Cathcart, and N. J. O’Reilly, ‘Polymeric Amorphous Solid Dispersions: A Review of Amorphization, Crystallization, Stabilization, Solid-State Characterization, and Aqueous Solubilization of Biopharmaceutical Classification System Class II Drugs’, *J. Pharm. Sci.*, vol. 105, no. 9, pp. 2527–2544, Sep. 2016.
- [10] L. X. Yu *et al.*, ‘Biopharmaceutics classification system: the scientific basis for biowaiver extensions’, *Pharm. Res.*, vol. 19, no. 7, pp. 921–925, Jul. 2002.
- [11] J. M. Butler and J. B. Dressman, ‘The developability classification system: application of biopharmaceutics concepts to formulation development’, *J. Pharm. Sci.*, vol. 99, no. 12, pp. 4940–4954, Dec. 2010.
- [12] E. Gué, *Formes galéniques polymériques avec cinétiques de libération améliorée pour le kétoprofène et le fénofibrate*. Lille 2, 2013.
- [13] D. M. Oh, R. L. Curl, and G. L. Amidon, ‘Estimating the fraction dose absorbed from suspensions of poorly soluble compounds in humans: a mathematical model’, *Pharm. Res.*, vol. 10, no. 2, pp. 264–270, Feb. 1993.
- [14] T. Xie and L. S. Taylor, ‘Dissolution Performance of High Drug Loading

Celecoxib Amorphous Solid Dispersions Formulated with Polymer Combinations', *Pharm. Res.*, vol. 33, no. 3, pp. 739–750, Mar. 2016.

[15] H. Lieberman and N. Murti Vemuri, 'Chapter 32 - Chemical and Physicochemical Approaches to Solve Formulation Problems', in *The Practice of Medicinal Chemistry (Fourth Edition)*, C. G. Wermuth, D. Aldous, P. Raboisson, and D. Rognan, Eds. San Diego: Academic Press, 2015, pp. 767–791.

[16] A. K. Nayak and P. P. Panigrahi, 'Solubility Enhancement of Etoricoxib by Cosolvency Approach', *International Scholarly Research Notices*, 2012. [Online]. Available: <https://www.hindawi.com/journals/isrn/2012/820653/>. [Accessed: 07-Oct-2018].

[17] J. T. Rubino and S. H. Yalkowsky, 'Cosolvency and cosolvent polarity', *Pharm. Res.*, vol. 4, no. 3, pp. 220–230, Jun. 1987.

[18] M. T. França, R. Nicolay Pereira, M. Klüppel Riekes, J. Munari Oliveira Pinto, and H. K. Stulzer, 'Investigation of novel supersaturating drug delivery systems of chlorthalidone: The use of polymer-surfactant complex as an effective carrier in solid dispersions', *Eur. J. Pharm. Sci. Off. J. Eur. Fed. Pharm. Sci.*, vol. 111, pp. 142–152, Jan. 2018.

[19] R. N. Shamma and M. Basha, 'Soluplus®: A novel polymeric solubilizer for optimization of Carvedilol solid dispersions: Formulation design and effect of method of preparation', *Powder Technol.*, vol. 237, pp. 406–414, Mar. 2013.

[20] K. T. Savjani, A. K. Gajjar, and J. K. Savjani, 'Drug Solubility: Importance and Enhancement Techniques', *ISRN Pharm.*, vol. 2012, Jul. 2012.

[21] S. Baghel, H. Cathcart, and N. J. O'Reilly, 'Polymeric Amorphous Solid Dispersions: A Review of Amorphization, Crystallization, Stabilization, Solid-State Characterization, and Aqueous Solubilization of Biopharmaceutical Classification System Class II Drugs', *J. Pharm. Sci.*, vol. 105, no. 9, pp. 2527–2544, Sep. 2016.

[22] A. C. C. Vieira *et al.*, 'Multicomponent systems with cyclodextrins and hydrophilic polymers for the delivery of Efavirenz', *Carbohydr. Polym.*, vol. 130, pp. 133–140, Oct. 2015.

[23] M. E. Brewster, R. Vandecruys, G. Verreck, and J. Peeters, 'Supersaturating drug delivery systems: effect of hydrophilic cyclodextrins and other excipients on the formation and stabilization of supersaturated drug solutions', *Pharm.*, vol. 63, no. 3, pp. 217–220, Mar. 2008.

[24] B. Chauhan, S. Shimpi, and A. Paradkar, 'Preparation and characterization of etoricoxib solid dispersions using lipid carriers by spray drying technique', *AAPS PharmSciTech*, vol. 6, no. 3, pp. E405–E409, Sep. 2005.

[25] S. Kamboj, S. Sethi, and V. Rana, 'Lipid based delivery of Efavirenz: An answer to its erratic absorption and food effect', *Eur. J. Pharm. Sci.*, vol. 123, pp. 199–216, Oct. 2018.

[26] K. Cerpnjak, A. Zvonar, M. Gašperlin, and F. Vrečer, 'Lipid-based systems as a promising approach for enhancing the bioavailability of poorly water-soluble drugs', *Acta Pharm. Zagreb Croat.*, vol. 63, no. 4, pp. 427–445, Dec. 2013.

[27] S. Kalepu, M. Manthina, and V. Padavala, 'Oral lipid-based drug delivery

systems – an overview’, *Acta Pharm. Sin. B*, vol. 3, no. 6, pp. 361–372, Dec. 2013.

[28] R. N. Kamble, P. P. Mehta, and A. Kumar, ‘Efavirenz Self-Nano-Emulsifying Drug Delivery System: In Vitro and In Vivo Evaluation’, *AAPS PharmSciTech*, vol. 17, no. 5, pp. 1240–1247, Oct. 2016.

[29] P. Khadka *et al.*, ‘Pharmaceutical particle technologies: An approach to improve drug solubility, dissolution and bioavailability’, *Asian J. Pharm. Sci.*, vol. 9, no. 6, pp. 304–316, Dec. 2014.

[30] A. T. M. Serajuddin, ‘Salt formation to improve drug solubility’, *Adv. Drug Deliv. Rev.*, vol. 59, no. 7, pp. 603–616, Jul. 2007.

[31] S. J. Dengale, H. Grohganz, T. Rades, and K. Löbmann, ‘Recent advances in co-amorphous drug formulations’, *Adv. Drug Deliv. Rev.*, vol. 100, pp. 116–125, May 2016.

[32] H. D. Williams *et al.*, ‘Strategies to Address Low Drug Solubility in Discovery and Development’, *Pharmacol. Rev.*, vol. 65, no. 1, pp. 315–499, Jan. 2013.

[33] P. Karande, J. P. Trasatti, and D. Chandra, ‘Chapter 4 - Novel Approaches for the Delivery of Biologics to the Central Nervous System’, in *Novel Approaches and Strategies for Biologics, Vaccines and Cancer Therapies*, M. Singh and M. Salnikova, Eds. San Diego: Academic Press, 2015, pp. 59–88.

[34] R. Hilfiker, *Polymorphism: In the Pharmaceutical Industry*. Wiley, 2006.

[35] R. K. Harris, ‘Polymorphism Studied by Solid-state NMR’, in *Encyclopedia of Spectroscopy and Spectrometry (Second Edition)*, J. C. Lindon, Ed. Oxford: Academic Press, 2010, pp. 2237–2246.

[36] D. D. Le Pevelen and G. E. Tranter, ‘FT-IR and Raman Spectroscopies, Polymorphism Applications’, in *Encyclopedia of Spectroscopy and Spectrometry (Third Edition)*, J. C. Lindon, G. E. Tranter, and D. W. Koppenaal, Eds. Oxford: Academic Press, 2017, pp. 750–761.

[37] J. Deng, S. Staufienbiel, and R. Bodmeier, ‘Evaluation of a biphasic in vitro dissolution test for estimating the bioavailability of carbamazepine polymorphic forms’, *Eur. J. Pharm. Sci.*, vol. 105, pp. 64–70, Jul. 2017.

[38] I. Sathisaran and S. V. Dalvi, ‘Engineering Cocrystals of Poorly Water-Soluble Drugs to Enhance Dissolution in Aqueous Medium’, *Pharmaceutics*, vol. 10, no. 3, Jul. 2018.

[39] C. M. Keck and R. H. Müller, ‘Drug nanocrystals of poorly soluble drugs produced by high pressure homogenisation’, *Eur. J. Pharm. Biopharm. Off. J. Arbeitsgemeinschaft Pharm. Verfahrenstechnik EV*, vol. 62, no. 1, pp. 3–16, Jan. 2006.

[40] E. M. Merisko-Liversidge and G. G. Liversidge, ‘Drug nanoparticles: formulating poorly water-soluble compounds’, *Toxicol. Pathol.*, vol. 36, no. 1, pp. 43–48, Jan. 2008.

[41] J. Sun *et al.*, ‘Effect of particle size on solubility, dissolution rate, and oral bioavailability: evaluation using coenzyme Q10 as naked nanocrystals’, *Int. J. Nanomedicine*, vol. 7, pp. 5733–5744, 2012.

[42] N. Shah, H. Sandhu, D. S. Choi, H. Chokshi, and A. W. Malick, *Amorphous*

*Solid Dispersions: Theory and Practice*. Springer, 2014.

[43] S. Baghel, H. Cathcart, and N. J. O'Reilly, 'Understanding the generation and maintenance of supersaturation during the dissolution of amorphous solid dispersions using modulated DSC and <sup>1</sup>H NMR', *Int. J. Pharm.*, vol. 536, no. 1, pp. 414–425, Jan. 2018.

[44] X. Lin *et al.*, 'Physical Stability of Amorphous Solid Dispersions: a Physicochemical Perspective with Thermodynamic, Kinetic and Environmental Aspects', *Pharm. Res.*, vol. 35, no. 6, p. 125, Apr. 2018.

[45] S. K. Sathigari, V. K. Radhakrishnan, V. A. Davis, D. L. Parsons, and R. J. Babu, 'Amorphous-state characterization of efavirenz—polymer hot-melt extrusion systems for dissolution enhancement', *J. Pharm. Sci.*, vol. 101, no. 9, pp. 3456–3464, Sep. 2012.

[46] N. Ogawa *et al.*, 'Improvement in the water solubility of drugs with a solid dispersion system by spray drying and hot-melt extrusion with using the amphiphilic polyvinyl caprolactam-polyvinyl acetate-polyethylene glycol graft copolymer and d-mannitol', *Eur. J. Pharm. Sci.*, vol. 111, pp. 205–214, Jan. 2018.

[47] M. M. Knopp *et al.*, 'Comparative Study of Different Methods for the Prediction of Drug–Polymer Solubility', *Mol. Pharm.*, vol. 12, no. 9, pp. 3408–3419, Sep. 2015.

[48] C. L.-N. Vo, C. Park, and B.-J. Lee, 'Current trends and future perspectives of solid dispersions containing poorly water-soluble drugs', *Eur. J. Pharm. Biopharm.*, vol. 85, no. 3, Part B, pp. 799–813, Nov. 2013.

[49] F. Qian *et al.*, 'Is a distinctive single T<sub>g</sub> a reliable indicator for the homogeneity of amorphous solid dispersion?', *Int. J. Pharm.*, vol. 395, no. 1–2, pp. 232–235, Aug. 2010.

[50] D. Feng *et al.*, 'Polymer–Surfactant System Based Amorphous Solid Dispersion: Precipitation Inhibition and Bioavailability Enhancement of Itraconazole', *Pharmaceutics*, vol. 10, no. 2, p. 53, Apr. 2018.

[51] A. N. Ghebremeskel, C. Vemavarapu, and M. Lodaya, 'Use of surfactants as plasticizers in preparing solid dispersions of poorly soluble API: stability testing of selected solid dispersions', *Pharm. Res.*, vol. 23, no. 8, pp. 1928–1936, Aug. 2006.

[52] Z. Yang, 'Development of Methods to Predict and Enhance the Physical Stability of Hot Melt Extruded Solid Dispersions', doctoral, University of East Anglia, 2013.

[53] P. Kanaujia, P. Poovizhi, W. K. Ng, and R. B. H. Tan, 'Amorphous formulations for dissolution and bioavailability enhancement of poorly soluble APIs', *Powder Technol.*, vol. 285, pp. 2–15, Nov. 2015.

[54] F. Theil, J. Milsmann, S. O. Kyeremateng, S. Anantharaman, J. Rosenberg, and H. van Lishaut, 'Extraordinary Long-Term-Stability in Kinetically Stabilized Amorphous Solid Dispersions of Fenofibrate', *Mol. Pharm.*, vol. 14, no. 12, pp. 4636–4647, Dec. 2017.

[55] T. W. Y. Lee, N. A. Boersen, H. W. Hui, S. F. Chow, K. Y. Wan, and A. H. L. Chow, 'Delivery of poorly soluble compounds by amorphous solid dispersions', *Curr. Pharm. Des.*, vol. 20, no. 3, pp. 303–324, 2014.

[56] F. Meng, V. Dave, and H. Chauhan, 'Qualitative and quantitative methods to determine miscibility in amorphous drug-polymer systems', *Eur. J. Pharm. Sci. Off. J. Eur.*

*Fed. Pharm. Sci.*, vol. 77, pp. 106–111, Sep. 2015.

[57] I. U. of P. and A. Chemistry, 'IUPAC Gold Book - molecule'. [Online]. Available: <https://goldbook.iupac.org/html/M/M04002.html>. [Accessed: 12-Oct-2018].

[58] Y. Chen *et al.*, 'Initial Drug Dissolution from Amorphous Solid Dispersions Controlled by Polymer Dissolution and Drug-Polymer Interaction', *Pharm. Res.*, vol. 33, no. 10, pp. 2445–2458, 2016.

[59] N.-Q. Shi *et al.*, 'Self-micellizing solid dispersions enhance the properties and therapeutic potential of fenofibrate: Advantages, profiles and mechanisms', *Int. J. Pharm.*, vol. 528, no. 1, pp. 563–577, Aug. 2017.

[60] S. Verma and V. S. Rudraraju, 'Wetting Kinetics: an Alternative Approach Towards Understanding the Enhanced Dissolution Rate for Amorphous Solid Dispersion of a Poorly Soluble Drug', *AAPS PharmSciTech*, vol. 16, no. 5, pp. 1079–1090, Feb. 2015.

[61] E. G. Shafrin and W. A. Zisman, 'CONSTITUTIVE RELATIONS IN THE WETTING OF LOW ENERGY SURFACES AND THE THEORY OF THE RETRACTION METHOD OF PREPARING MONOLAYERS<sup>1</sup>', *J. Phys. Chem.*, vol. 64, no. 5, pp. 519–524, May 1960.

[62] O. I. Corrigan and C. T. Stanley, 'Mechanism of drug dissolution rate enhancement from  $\beta$ -cyclodextrin-drug systems', *J. Pharm. Pharmacol.*, vol. 34, no. 10, pp. 621–626, Oct. 1982.

[63] S. Qi, D. Marchaud, and D. Q. M. Craig, 'An investigation into the mechanism of dissolution rate enhancement of poorly water-soluble drugs from spray chilled gelucire 50/13 microspheres', *J. Pharm. Sci.*, vol. 99, no. 1, pp. 262–274, Jan. 2010.

[64] H. Ç. Arca, L. I. Mosquera-Giraldo, D. Dahal, L. S. Taylor, and K. J. Edgar, 'Multidrug, Anti-HIV Amorphous Solid Dispersions: Nature and Mechanisms of Impacts of Drugs on Each Other's Solution Concentrations', *Mol. Pharm.*, vol. 14, no. 11, pp. 3617–3627, Nov. 2017.

[65] S. Verheyen, N. Blaton, R. Kinget, and G. Van den Mooter, 'Mechanism of increased dissolution of diazepam and temazepam from polyethylene glycol 6000 solid dispersions', *Int. J. Pharm.*, vol. 249, no. 1–2, pp. 45–58, Dec. 2002.

[66] S. Sh, S. Sb, K. As, and A. Nh, 'SOLID DISPERSION: A NOVEL APPROACH FOR POORLY WATER SOLUBLE DRUGS', *Int. J. Curr. Pharm. Res.*, vol. 7, no. 4, pp. 1–8, 2015.

[67] Y. Kojo, S. Matsunaga, H. Suzuki, H. Sato, Y. Seto, and S. Onoue, 'Improved oral absorption profile of itraconazole in hypochlorhydria by self-micellizing solid dispersion approach', *Eur. J. Pharm. Sci. Off. J. Eur. Fed. Pharm. Sci.*, vol. 97, pp. 55–61, Jan. 2017.

[68] D. Q. M. Craig and J. M. Newton, 'The dissolution of nortriptyline HCl from polyethylene glycol solid dispersions', *Int. J. Pharm.*, vol. 78, no. 1, pp. 175–182, Jan. 1992.

[69] S. A. Raina *et al.*, 'Trends in the Precipitation and Crystallization Behavior of Supersaturated Aqueous Solutions of Poorly Water-Soluble Drugs Assessed Using Synchrotron Radiation', *J. Pharm. Sci.*, vol. 104, no. 6, pp. 1981–1992, Jun. 2015.

- [70] T. Ohara, S. Kitamura, T. Kitagawa, and K. Terada, 'Dissolution mechanism of poorly water-soluble drug from extended release solid dispersion system with ethylcellulose and hydroxypropylmethylcellulose', *Int. J. Pharm.*, vol. 302, no. 1–2, pp. 95–102, Sep. 2005.
- [71] S. B. Murdande, M. J. Pikal, R. M. Shanker, and R. H. Bogner, 'Aqueous solubility of crystalline and amorphous drugs: Challenges in measurement', *Pharm. Dev. Technol.*, vol. 16, no. 3, pp. 187–200, Jun. 2011.
- [72] B. B. Patel, J. K. Patel, S. Chakraborty, and D. Shukla, 'Revealing facts behind spray dried solid dispersion technology used for solubility enhancement', *Saudi Pharm. J.*, vol. 23, no. 4, pp. 352–365, Sep. 2015.
- [73] A. Singh and G. Van den Mooter, 'Spray drying formulation of amorphous solid dispersions', *Adv. Drug Deliv. Rev.*, vol. 100, pp. 27–50, May 2016.
- [74] M. Mehta, K. Kothari, V. Ragoonanan, and R. Suryanarayanan, 'Effect of Water on Molecular Mobility and Physical Stability of Amorphous Pharmaceuticals', *Mol. Pharm.*, vol. 13, no. 4, pp. 1339–1346, Apr. 2016.
- [75] K. Lehmkemper, S. O. Kyeremateng, M. Bartels, M. Degenhardt, and G. Sadowski, 'Physical stability of API/polymer-blend amorphous solid dispersions', *Eur. J. Pharm. Biopharm.*, vol. 124, pp. 147–157, Mar. 2018.
- [76] K. Lehmkemper, S. O. Kyeremateng, O. Heinzerling, M. Degenhardt, and G. Sadowski, 'Long-Term Physical Stability of PVP- and PVPVA-Amorphous Solid Dispersions', *Mol. Pharm.*, vol. 14, no. 1, pp. 157–171, Jan. 2017.
- [77] S. B. Teja, S. P. Patil, G. Shete, S. Patel, and A. K. Bansal, 'Drug-excipient behavior in polymeric amorphous solid dispersions', *J. Excip. Food Chem.*, vol. 4, no. 3, pp. 70–94, Sep. 2013.
- [78] J. A. Baird and L. S. Taylor, 'Evaluation of amorphous solid dispersion properties using thermal analysis techniques', *Adv. Drug Deliv. Rev.*, vol. 64, no. 5, pp. 396–421, Apr. 2012.
- [79] S. Sapkal, M. Babhulkar, A. Rathi, G. Mehetre, and M. Narkhede, 'An overview on the mechanisms of solubility and dissolution rate enhancement in solid dispersion', *Int. J. PharmTech Res.*, vol. 5, pp. 31–39, Jan. 2013.
- [80] Z. Ayenew, A. Paudel, and G. Van den Mooter, 'Can compression induce demixing in amorphous solid dispersions? A case study of naproxen-PVP K25', *Eur. J. Pharm. Biopharm. Off. J. Arbeitsgemeinschaft Pharm. Verfahrenstechnik EV*, vol. 81, no. 1, pp. 207–213, May 2012.
- [81] X. Liu, X. Feng, R. O. Williams, and F. Zhang, 'Characterization of amorphous solid dispersions', *J. Pharm. Investig.*, vol. 48, no. 1, pp. 19–41, Jan. 2018.
- [82] A. M. Agrawal, M. S. Dudhedia, A. D. Patel, and M. S. Raikes, 'Characterization and performance assessment of solid dispersions prepared by hot melt extrusion and spray drying process', *Int. J. Pharm.*, vol. 457, no. 1, pp. 71–81, Nov. 2013.
- [83] J. S. LaFontaine, J. W. McGinity, and R. O. Williams, 'Challenges and Strategies in Thermal Processing of Amorphous Solid Dispersions: A Review', *AAPS*

*PharmSciTech*, vol. 17, no. 1, pp. 43–55, Feb. 2016.

[84] K. Kv, A. Sr, Y. Pr, P. Ry, and B. Vu, ‘Differential Scanning Calorimetry: A Review.’, *Res. Rev. J. Pharm. Anal.*, vol. 3, no. 3, pp. 11–22, Dec. 2014.

[85] Y. Sun, J. Tao, G. G. Z. Zhang, and L. Yu, ‘Solubilities of crystalline drugs in polymers: an improved analytical method and comparison of solubilities of indomethacin and nifedipine in PVP, PVP/VA, and PVAc’, *J. Pharm. Sci.*, vol. 99, no. 9, pp. 4023–4031, Sep. 2010.

[86] S. Shah, S. Maddineni, J. Lu, and M. A. Repka, ‘Melt extrusion with poorly soluble drugs’, *Int. J. Pharm.*, vol. 453, no. 1, pp. 233–252, Aug. 2013.

[87] M.-J. Chang, A. S. Myerson, and T. K. Kwei, ‘The effect of hydrogen bonding on vapor diffusion in water-soluble polymers’, *J. Appl. Polym. Sci.*, vol. 66, no. 2, pp. 279–291, Oct. 1997.

[88] K. Punčochová, J. Y. Y. Heng, J. Beránek, and F. Stěpánek, ‘Investigation of drug-polymer interaction in solid dispersions by vapour sorption methods’, *Int. J. Pharm.*, vol. 469, no. 1, pp. 159–167, Jul. 2014.

[89] H. M. C. Marques, J. Hadgraft, and I. W. Kellaway, ‘Studies of cyclodextrin inclusion complexes. I. The salbutamol-cyclodextrin complex as studied by phase solubility and DSC’, *Int. J. Pharm.*, vol. 63, no. 3, pp. 259–266, Sep. 1990.

[90] D. D. Sun, H. Wen, and L. S. Taylor, ‘Non-Sink Dissolution Conditions for Predicting Product Quality and In Vivo Performance of Supersaturating Drug Delivery Systems’, *J. Pharm. Sci.*, vol. 105, no. 9, pp. 2477–2488, 2016.

[91] N. Li and L. S. Taylor, ‘Tailoring supersaturation from amorphous solid dispersions’, *J. Controlled Release*, vol. 279, pp. 114–125, Jun. 2018.

[92] T. Huo *et al.*, ‘Preparation and comparison of tacrolimus-loaded solid dispersion and self-microemulsifying drug delivery system by in vitro/in vivo evaluation’, *Eur. J. Pharm. Sci.*, vol. 114, pp. 74–83, Mar. 2018.

[93] A. Newman, G. Knipp, and G. Zografí, ‘Assessing the performance of amorphous solid dispersions’, *J. Pharm. Sci.*, vol. 101, no. 4, pp. 1355–1377, Apr. 2012.

[94] N. Shah, H. Sandhu, D. S. Choi, O. Kalb, S. Page, and N. Wyttenbach, ‘Structured Development Approach for Amorphous Systems’, in *Formulating Poorly Water Soluble Drugs*, R. O. Williams III, A. B. Watts, and D. A. Miller, Eds. New York, NY: Springer New York, 2012, pp. 267–310.

[95] K. A. Khan and C. T. Rhodes, ‘Effect of compaction pressure on the dissolution efficiency of some direct compression systems’, *Pharm. Acta Helv.*, vol. 47, no. 10, pp. 594–607, Oct. 1972.

[96] S. Dash, P. N. Murthy, L. Nath, and P. Chowdhury, ‘Kinetic modeling on drug release from controlled drug delivery systems’, *Acta Pol. Pharm.*, vol. 67, no. 3, pp. 217–223, Jun. 2010.

[97] M. L. Bruschi, Ed., ‘5 - Mathematical models of drug release’, in *Strategies to Modify the Drug Release from Pharmaceutical Systems*, Woodhead Publishing, 2015, pp. 63–

[98] R. W. Korsmeyer, R. Gurny, E. Doelker, P. Buri, and N. A. Peppas, 'Mechanisms of solute release from porous hydrophilic polymers', *Int. J. Pharm.*, vol. 15, no. 1, pp. 25–35, May 1983.

[99] P. Costa and J. M. Sousa Lobo, 'Modeling and comparison of dissolution profiles', *Eur. J. Pharm. Sci.*, vol. 13, no. 2, pp. 123–133, May 2001.

[100] N. A. Peppas, 'Analysis of Fickian and non-Fickian drug release from polymers', *Pharm. Acta Helv.*, vol. 60, no. 4, pp. 110–111, 1985.

[101] M. J. Abdekhodaie and Y.-L. Cheng, 'Diffusional release of a dispersed solute from planar and spherical matrices into finite external volume', *J. Controlled Release*, vol. 43, no. 2, pp. 175–182, Jan. 1997.

[102] M. T. Ansari *et al.*, 'Improved physicochemical characteristics of artemisinin using succinic acid', *Acta Pol. Pharm.*, vol. 71, no. 3, pp. 451–462, Jun. 2014.

[103] Z. M. M. Lavra, D. Pereira de Santana, and M. I. Ré, 'Solubility and dissolution performances of spray-dried solid dispersion of Efavirenz in Soluplus', *Drug Dev. Ind. Pharm.*, vol. 43, no. 1, pp. 42–54, Jan. 2017.

[104] Y.-S. Lee, J. G. Song, S. H. Lee, and H.-K. Han, 'Sustained-release solid dispersion of pelubiprofen using the blended mixture of aminoclay and pH independent polymers: preparation and in vitro/in vivo characterization', *Drug Deliv.*, vol. 24, no. 1, pp. 1731–1739, Jan. 2017.

[105] Y. Wu, 'Release behavior of alkyl-p-aminobenzoate ester–PVP solid dispersions', *Theses Diss.*, Dec. 2015.

[106] A. Althaf S, 'Formulation, Evaluation and Mathematical Modelling of Clopidogrel Bisulphate & Aspirin Immediate Release Bilayer Tablets', *Pharm. Anal. Acta*, vol. 03, no. 09, 2012.

[107] J. S. Changdeo, M. Vinod, K. B. Shankar, and C. A. Rajaram, 'Physicochemical characterization and solubility enhancement studies of allopurinol solid dispersions', *Braz. J. Pharm. Sci.*, vol. 47, no. 3, pp. 513–523, Sep. 2011.

[108] J. Ihli, A. N. Kulak, and F. C. Meldrum, 'Freeze-drying yields stable and pure amorphous calcium carbonate (ACC)', *Chem. Commun. Camb. Engl.*, vol. 49, no. 30, pp. 3134–3136, Apr. 2013.

[109] S. O. Kyeremateng, M. Pudlas, and G. H. Woehrle, 'A Fast and Reliable Empirical Approach for Estimating Solubility of Crystalline Drugs in Polymers for Hot Melt Extrusion Formulations', *J. Pharm. Sci.*, vol. 103, no. 9, pp. 2847–2858, Sep. 2014.

[110] J. Thiry *et al.*, 'Continuous production of itraconazole-based solid dispersions by hot melt extrusion: Preformulation, optimization and design space determination', *Int. J. Pharm.*, vol. 515, no. 1–2, pp. 114–124, Dec. 2016.

[111] A. Haser, T. Cao, J. Lubach, T. Listro, L. Acquarulo, and F. Zhang, 'Melt extrusion vs. spray drying: The effect of processing methods on crystalline content of naproxen-povidone formulations', *Eur. J. Pharm. Sci. Off. J. Eur. Fed. Pharm. Sci.*, vol. 102, pp. 115–

125, May 2017.

[112] T. Parikh, S. S. Gupta, A. K. Meena, I. Vitez, N. Mahajan, and A. T. M. Serajuddin, ‘Application of Film-Casting Technique to Investigate Drug-Polymer Miscibility in Solid Dispersion and Hot-Melt Extrudate’, *J. Pharm. Sci.*, vol. 104, no. 7, pp. 2142–2152, Jul. 2015.

[113] K. Wlodarski *et al.*, ‘Physicochemical properties of tadalafil solid dispersions - Impact of polymer on the apparent solubility and dissolution rate of tadalafil’, *Eur. J. Pharm. Biopharm.*, vol. 94, pp. 106–115, Aug. 2015.

[114] V. Caron *et al.*, ‘Amorphous Solid Dispersions of Sulfonamide/Soluplus® and Sulfonamide/PVP Prepared by Ball Milling’, *AAPS PharmSciTech*, vol. 14, no. 1, pp. 464–474, Mar. 2013.

[115] A. Mahieu, J.-F. Willart, E. Dudognon, F. Danède, and M. Descamps, ‘A New Protocol To Determine the Solubility of Drugs into Polymer Matrixes’, *Mol. Pharm.*, vol. 10, no. 2, pp. 560–566, Feb. 2013.

[116] K. Semjonov *et al.*, ‘The formation and physical stability of two-phase solid dispersion systems of indomethacin in supercooled molten mixtures with different matrix formers’, *Eur. J. Pharm. Sci. Off. J. Eur. Fed. Pharm. Sci.*, vol. 97, pp. 237–246, Jan. 2017.

[117] R. Ghanavati, A. Taheri, and A. Homayouni, ‘Anomalous dissolution behavior of celecoxib in PVP/Isomalt solid dispersions prepared using spray drier’, *Mater. Sci. Eng. C*, vol. 72, pp. 501–511, Mar. 2017.

[118] K. Wlodarski, W. Sawicki, A. Kozyra, and L. Tajber, ‘Physical stability of solid dispersions with respect to thermodynamic solubility of tadalafil in PVP-VA’, *Eur. J. Pharm. Biopharm. Off. J. Arbeitsgemeinschaft Pharm. Verfahrenstechnik EV*, vol. 96, pp. 237–246, Oct. 2015.

[119] J. N. Pawar *et al.*, ‘Development of amorphous dispersions of artemether with hydrophilic polymers via spray drying: Physicochemical and in silico studies’, *Asian J. Pharm. Sci.*, vol. 11, no. 3, pp. 385–395, Jun. 2016.

[120] T. Vasconcelos, S. Marques, J. das Neves, and B. Sarmiento, ‘Amorphous solid dispersions: Rational selection of a manufacturing process’, *Adv. Drug Deliv. Rev.*, vol. 100, pp. 85–101, May 2016.

[121] A. Paudel, Z. A. Worku, J. Meeus, S. Guns, and G. Van den Mooter, ‘Manufacturing of solid dispersions of poorly water soluble drugs by spray drying: Formulation and process considerations’, *Int. J. Pharm.*, vol. 453, no. 1, pp. 253–284, Aug. 2013.

[122] ‘APPLICATION OF SPRAY DRYING TECHNIQUE FOR PREPARATION AMORPHOUS SOLID DISPERSION | INTERNATIONAL JOURNAL OF PHARMACEUTICAL SCIENCES AND RESEARCH’.

[123] M.-I. Ré, ‘Formulating Drug Delivery Systems by Spray Drying’, *Dry. Technol.*, vol. 24, no. 4, pp. 433–446, May 2006.

[124] A. Kauppinen *et al.*, ‘Efficient production of solid dispersions by spray drying solutions of high solid content using a 3-fluid nozzle’, *Eur. J. Pharm. Biopharm.*, vol. 123, pp.

50–58, Feb. 2018.

[125] O. NiÓgáin, L. Tajber, O. I. Corrigan, and A. M. Healy, ‘Spray drying from organic solvents to prepare nanoporous/nanoparticulate microparticles of protein: excipient composites designed for oral inhalation’, *J. Pharm. Pharmacol.*, vol. 64, no. 9, pp. 1275–1290, Sep. 2012.

[126] ‘Bioavailability enhancement using hot melt extrusion – with functional solutions from BASF’. [Online]. Available: <https://pharmaceutical.basf.com/en/Drug-Formulation/Hot-melt-extrusion.html>. [Accessed: 14-Oct-2018].

[127] K. Kawakami, ‘Current status of amorphous formulation and other special dosage forms as formulations for early clinical phases’, *J. Pharm. Sci.*, vol. 98, no. 9, pp. 2875–2885, Sep. 2009.

[128] M. Davis and G. Walker, ‘Recent strategies in spray drying for the enhanced bioavailability of poorly water-soluble drugs’, *J. Controlled Release*, vol. 269, pp. 110–127, Jan. 2018.

[129] E. D. Ikasari, A. Fudholi, S. Martono, and Marchaban, ‘Investigation of nifedipine solid dispersion with solvent PVP K-30’, *Int. J. Pharm. Pharm. Sci.*, vol. 7, pp. 389–392, Jan. 2015.

[130] M. A. Altamimi and S. H. Neau, ‘Investigation of the in vitro performance difference of drug-Soluplus® and drug-PEG 6000 dispersions when prepared using spray drying or lyophilization’, *Saudi Pharm. J. SPJ Off. Publ. Saudi Pharm. Soc.*, vol. 25, no. 3, pp. 419–439, Mar. 2017.

[131] F. Wan *et al.*, ‘Critical solvent properties affecting the particle formation process and characteristics of celecoxib-loaded plga microparticles via spray-drying’, *Pharm. Res.*, vol. 30, no. 4, pp. 1065–1076, Apr. 2013.

[132] J. G. Lyons *et al.*, ‘Preparation of monolithic matrices for oral drug delivery using a supercritical fluid assisted hot melt extrusion process’, *Int. J. Pharm.*, vol. 329, no. 1–2, pp. 62–71, Feb. 2007.

[133] A. Patel *et al.*, ‘A Review of Hot Melt Extrusion Technique’, *Int. J. Innov. Res. Sci. Eng. Technol.*, vol. 2, no. 6, pp. 2194–2198, Jan. 1970.

[134] E. A. Ashour *et al.*, ‘Hot Melt Extrusion as an Approach to Improve Solubility, Permeability, and Oral Absorption of a Psychoactive Natural Product, Piperine’, *J. Pharm. Pharmacol.*, vol. 68, no. 8, pp. 989–998, Aug. 2016.

[135] M. Maniruzzaman, D. Douroumis, J. S., and M. J., ‘Hot-Melt Extrusion (HME): From Process to Pharmaceutical Applications’, in *Recent Advances in Novel Drug Carrier Systems*, A. D. Sezer, Ed. InTech, 2012.

[136] M. A. Repka *et al.*, ‘Melt extrusion: process to product’, *Expert Opin. Drug Deliv.*, vol. 9, no. 1, pp. 105–125, Jan. 2012.

[137] N. Chomcharn and M. Xanthos, ‘Properties of aspirin modified enteric polymer prepared by hot-melt mixing’, *Int. J. Pharm.*, vol. 450, no. 1–2, pp. 259–267, Jun. 2013.

[138] D. Leister, T. Geilen, and T. Geissler, ‘Twin-screw Extruders for Pharmaceutical

Hot-melt Extrusion: Technology, Techniques and Practices’, in *Hot-Melt Extrusion: Pharmaceutical Applications*, Wiley-Blackwell, 2012, pp. 23–42.

[139] A. Almeida, B. Claeys, J. P. Remon, and C. Vervaet, ‘Hot-Melt Extrusion Developments in the Pharmaceutical Industry’, in *Hot-Melt Extrusion: Pharmaceutical Applications*, Wiley-Blackwell, 2012, pp. 43–69.

[140] J. Breitenbach, ‘Melt extrusion: from process to drug delivery technology’, *Eur. J. Pharm. Biopharm. Off. J. Arbeitsgemeinschaft Pharm. Verfahrenstechnik EV*, vol. 54, no. 2, pp. 107–117, Sep. 2002.

[141] J. Thiry, F. Krier, and B. Evrard, ‘A review of pharmaceutical extrusion: Critical process parameters and scaling-up’, *Int. J. Pharm.*, vol. 479, no. 1, pp. 227–240, Feb. 2015.

[142] M. Beneš *et al.*, ‘Methods for the preparation of amorphous solid dispersions – A comparative study’, *J. Drug Deliv. Sci. Technol.*, vol. 38, pp. 125–134, Apr. 2017.

[143] Z. Dong, A. Chatterji, H. Sandhu, D. S. Choi, H. Chokshi, and N. Shah, ‘Evaluation of solid state properties of solid dispersions prepared by hot-melt extrusion and solvent co-precipitation’, *Int. J. Pharm.*, vol. 355, no. 1, pp. 141–149, May 2008.

[144] S. Janssens, A. De Zeure, A. Paudel, J. Van Humbeeck, P. Rombaut, and G. Van den Mooter, ‘Influence of preparation methods on solid state supersaturation of amorphous solid dispersions: a case study with itraconazole and eudragit e100’, *Pharm. Res.*, vol. 27, no. 5, pp. 775–785, May 2010.

[145] Y. Song *et al.*, ‘Acid-base interactions in amorphous solid dispersions of lumefantrine prepared by spray-drying and hot-melt extrusion using X-ray photoelectron spectroscopy’, *Int. J. Pharm.*, vol. 514, no. 2, pp. 456–464, Dec. 2016.

[146] O. Mahmah, R. Tabbakh, A. Kelly, and A. Paradkar, ‘A comparative study of the effect of spray drying and hot-melt extrusion on the properties of amorphous solid dispersions containing felodipine’, *J. Pharm. Pharmacol.*, vol. 66, no. 2, pp. 275–284, Feb. 2014.

[147] S. H. Surasarang, J. M. Keen, S. Huang, F. Zhang, J. W. McGinity, and R. O. W. III, ‘Hot melt extrusion versus spray drying: hot melt extrusion degrades albendazole’, *Drug Dev. Ind. Pharm.*, vol. 43, no. 5, pp. 797–811, May 2017.

[148] J. F. Kelleher *et al.*, ‘A comparative study between hot-melt extrusion and spray-drying for the manufacture of anti-hypertension compatible monolithic fixed-dose combination products’, *Int. J. Pharm.*, vol. 545, no. 1–2, pp. 183–196, Jul. 2018.

[149] V. Bhardwaj, N. S. Trasi, D. Y. Zemlyanov, and L. S. Taylor, ‘Surface area normalized dissolution to study differences in itraconazole-copovidone solid dispersions prepared by spray-drying and hot melt extrusion’, *Int. J. Pharm.*, vol. 540, no. 1–2, pp. 106–119, Apr. 2018.

[150] M. T. Davis, C. B. Potter, and G. M. Walker, ‘Downstream processing of a ternary amorphous solid dispersion: The impacts of spray drying and hot melt extrusion on powder flow, compression and dissolution’, *Int. J. Pharm.*, vol. 544, no. 1, pp. 242–253, Jun. 2018.

- [151] K. Ramesh, B. R. C. Shekar, P. Khadgapathi, and D. V. R. N. Bhikshapathi, 'Design and evaluation of tolvaptan solid dispersions using hot-melt extrusion and spray drying technique – A comparative study', 2015. [Online]. Available: /paper/Design-and-evaluation-of-tolvaptan-solid-using-and-Ramesh-Shekar/a5ea09082c6c03dae58161b8f706481fd0a70e79. [Accessed: 08-Aug-2018].
- [152] J. Djuris, I. Nikolakakis, S. Ibric, Z. Djuric, and K. Kachrimanis, 'Preparation of carbamazepine-Soluplus solid dispersions by hot-melt extrusion, and prediction of drug-polymer miscibility by thermodynamic model fitting', *Eur. J. Pharm. Biopharm. Off. J. Arbeitsgemeinschaft Für Pharm. Verfahrenstechnik EV*, vol. 84, no. 1, pp. 228–237, May 2013.
- [153] D. W. van Krevelen and K. te Nijenhuis, *Properties of Polymers: Their Correlation with Chemical Structure; their Numerical Estimation and Prediction from Additive Group Contributions*. Elsevier, 2009.
- [154] A. L. Sarode, H. Sandhu, N. Shah, W. Malick, and H. Zia, 'Hot melt extrusion (HME) for amorphous solid dispersions: Predictive tools for processing and impact of drug-polymer interactions on supersaturation', *Eur. J. Pharm. Sci.*, vol. 48, no. 3, pp. 371–384, Feb. 2013.
- [155] Y. Sun, J. Tao, G. G. Z. Zhang, and L. Yu, 'Solubilities of crystalline drugs in polymers: an improved analytical method and comparison of solubilities of indomethacin and nifedipine in PVP, PVP/VA, and PVAc', *J. Pharm. Sci.*, vol. 99, no. 9, pp. 4023–4031, Sep. 2010.
- [156] Y. Tian, J. Booth, E. Meehan, D. S. Jones, S. Li, and G. P. Andrews, 'Construction of Drug-Polymer Thermodynamic Phase Diagrams Using Flory-Huggins Interaction Theory: Identifying the Relevance of Temperature and Drug Weight Fraction to Phase Separation within Solid Dispersions', *Mol. Pharm.*, vol. 10, no. 1, pp. 236–248, Jan. 2013.
- [157] M. M. Knopp *et al.*, 'Comparative Study of Different Methods for the Prediction of Drug-Polymer Solubility', *Mol. Pharm.*, vol. 12, no. 9, pp. 3408–3419, Sep. 2015.
- [158] P. J. Marsac, S. L. Shamblin, and L. S. Taylor, 'Theoretical and practical approaches for prediction of drug-polymer miscibility and solubility', *Pharm. Res.*, vol. 23, no. 10, pp. 2417–2426, Oct. 2006.
- [159] J. Tao, Y. Sun, G. G. Z. Zhang, and L. Yu, 'Solubility of Small-Molecule Crystals in Polymers: d-Mannitol in PVP, Indomethacin in PVP/VA, and Nifedipine in PVP/VA', *Pharm. Res.*, vol. 26, no. 4, pp. 855–864, Dec. 2008.
- [160] N. Kumar and K. Biswas, 'Cryomilling: An environment friendly approach of preparation large quantity ultra refined pure aluminium nanoparticles', *J. Mater. Res. Technol.*, Nov. 2017.
- [161] Z. Yang, K. Nollenberger, J. Albers, and S. Qi, 'Molecular implications of drug-polymer solubility in understanding the destabilization of solid dispersions by milling', *Mol. Pharm.*, vol. 11, no. 7, pp. 2453–2465, Jul. 2014.
- [162] R. Fule and P. Amin, 'Development and evaluation of lafutidine solid dispersion via hot melt extrusion: Investigating drug-polymer miscibility with advanced characterisation',

*Asian J. Pharm. Sci.*, vol. 9, no. 2, pp. 92–106, Apr. 2014.

[163] C. Donnelly, Y. Tian, C. Potter, D. S. Jones, and G. P. Andrews, ‘Probing the effects of experimental conditions on the character of drug-polymer phase diagrams constructed using Flory-Huggins theory’, *Pharm. Res.*, vol. 32, no. 1, pp. 167–179, Jan. 2015.

[164] B. Bouillot, *Approches thermodynamiques pour la prédiction de la solubilité de molécules d'intérêt pharmaceutique*. Toulouse, INPT, 2011.

[165] ‘Thermodynamique des solutions de polymère’, *Techniques de l'Ingénieur*. [Online]. Available: <https://www.techniques-ingenieur.fr/base-documentaire/materiaux-th11/plastochimie-et-analyse-physico-chimique-42139210/polymeres-en-solution-a3050/thermodynamique-des-solutions-de-polymere-a3050niv10001.html>. [Accessed: 10-Sep-2018].

[166] A. Mahieu, *Nouvelles méthodes de détermination des diagrammes de solubilité polymère / principe actif*. Lille 1, 2013.

[167] ‘Transformation liquide-vapeur ou solide-vapeur [Cristal Gemme]’. [Online]. Available: [http://nte.mines-albi.fr/CristalGemme/co/uc\\_ElvEsv.html](http://nte.mines-albi.fr/CristalGemme/co/uc_ElvEsv.html). [Accessed: 12-Sep-2018].

[168] P. J. Marsac, S. L. Shamblin, and L. S. Taylor, ‘Theoretical and practical approaches for prediction of drug-polymer miscibility and solubility’, *Pharm. Res.*, vol. 23, no. 10, pp. 2417–2426, Oct. 2006.

[169] ‘HIV/AIDS’, *World Health Organization*. [Online]. Available: <http://www.who.int/news-room/fact-sheets/detail/hiv-aids>. [Accessed: 29-May-2018].

[170] U. Wintergerst *et al.*, ‘Antiviral efficacy, tolerability and pharmacokinetics of efavirenz in an unselected cohort of HIV-infected children’, *J. Antimicrob. Chemother.*, vol. 61, no. 6, pp. 1336–1339, Jun. 2008.

[171] D. A. Chiappetta, C. Hocht, C. Taira, and A. Sosnik, ‘Efavirenz-loaded polymeric micelles for pediatric anti-HIV pharmacotherapy with significantly higher oral bioavailability’, *Nanomed.*, vol. 5, no. 1, pp. 11–23, Dec. 2009.

[172] A. Singh *et al.*, ‘Development and characterization of taste masked Efavirenz pellets utilizing hot melt extrusion’, *J. Drug Deliv. Sci. Technol.*, vol. 23, no. 2, pp. 157–163, Jan. 2013.

[173] E. Zaini, F. Rachmaini, F. Armin, and L. Fitriani, ‘Preparation and Characterization of Binary Mixture of Efavirenz and Nicotinamide’, *Orient. J. Chem.*, vol. 31, no. 4, pp. 2271–2276, Dec. 2015.

[174] P. T. Koh, J. N. Chuah, M. Talekar, A. Gorajana, and S. Garg, ‘Formulation Development and Dissolution Rate Enhancement of Efavirenz by Solid Dispersion Systems’, *Indian J. Pharm. Sci.*, vol. 75, no. 3, pp. 291–301, 2013.

[175] C. R. D. Hoffmeister *et al.*, ‘Efavirenz dissolution enhancement III: Colloid milling, pharmacokinetics and electronic tongue evaluation’, *Eur. J. Pharm. Sci. Off. J. Eur. Fed. Pharm. Sci.*, vol. 99, pp. 310–317, Mar. 2017.

[176] ‘intrinsic dissolution rate: Topics by Science.gov’. [Online]. Available:

<https://www.science.gov/topicpages/i/intrinsic+dissolution+rate.html>. [Accessed: 14-Oct-2018].

[177] X. Ye *et al.*, 'Conjugation of Hot-Melt Extrusion with High-Pressure Homogenization: a Novel Method of Continuously Preparing Nanocrystal Solid Dispersions', *AAPS PharmSciTech*, vol. 17, no. 1, pp. 78–88, Feb. 2016.

[178] M. A. da Costa, R. C. Seiceira, C. R. Rodrigues, C. R. D. Hoffmeister, L. M. Cabral, and H. V. A. Rocha, 'Efavirenz Dissolution Enhancement I: Co-Micronization', *Pharmaceutics*, vol. 5, no. 1, pp. 1–22, Dec. 2012.

[179] P. Camelo and S. Regina, *Encapsulation de molécules hydrophobes par des structures bi-gels générées par prilling : relation structure-propriétés*. Ecole nationale des Mines d'Albi-Carmaux, 2015.

[180] S. Mazumder, A. K. Dewangan, and N. Pavurala, 'Enhanced dissolution of poorly soluble antiviral drugs from nanoparticles of cellulose acetate based solid dispersion matrices', *Asian J. Pharm. Sci.*, vol. 12, no. 6, pp. 532–541, Nov. 2017.

[181] L. Fitriani, A. Haqi, and E. Zaini, 'Preparation and characterization of solid dispersion freeze-dried efavirenz u polyvinylpyrrolidone K-30', *J. Adv. Pharm. Technol. Res.*, vol. 7, no. 3, pp. 105–109, Sep. 2016.

[182] J. Pawar, A. Tayade, A. Gangurde, K. Moravkar, and P. Amin, 'Solubility and dissolution enhancement of efavirenz hot melt extruded amorphous solid dispersions using combination of polymeric blends: A QbD approach', *Eur. J. Pharm. Sci. Off. J. Eur. Fed. Pharm. Sci.*, vol. 88, pp. 37–49, Jun. 2016.

[183] L. Fitriani, M. Fadhila, and E. Zaini, 'Preparation of Efavirenz - PVP K-30 Solid Dispersion by Spray Drying Technique', *Res. J. Pharm. Biol. Chem. Sci.*, vol. 6, no. 6, pp. 925–930, Dec. 2015.

[184] L. D. Santos Alves *et al.*, 'Solid dispersion of efavirenz in PVP K-30 by conventional solvent and kneading methods', *Carbohydr. Polym.*, vol. 104, pp. 166–174, Apr. 2014.

[185] 'Soluplus - For better solubility & bioavailability', *BASF*. [Online]. Available: <https://pharmaceutical.basf.com/en/Drug-Formulation/Soluplus.html>. [Accessed: 14-Oct-2018].

[186] R. S. Bhuptani, 'Soluplus Based Polymeric Micelles and Mixed Micelles of Lornoxicam: Design, Characterization and In vivo Efficacy Studies in Rats', *Indian J. Pharm. Educ. Res.*, vol. 50, no. 2, pp. 277–286, 2016.

[187] M. Linn, 'In vitro characterization of the novel solubility enhancing excipient Soluplus®', *In vitro Charakterisierung des neuartigen Lösungsvermittlers Soluplus®*, 2011.

[188] J. Kost and R. Langer, 'Responsive polymeric delivery systems', *Adv. Drug Deliv. Rev.*, vol. 46, no. 1–3, pp. 125–148, Mar. 2001.

[189] A. Fini, C. Cavallari<sup>1</sup>, S. Ternullo<sup>2</sup>, F. Tarterini<sup>3</sup>, A. Fini<sup>1\*</sup>, and O. Internationals, 'Release Problems for Nifedipine in the Presence of Soluplus', *J. Pharm. Pharm.*, vol. 3, no. 2, pp. 0–0, Jun. 2016.

Chapter 3 -  
Efavirenz/Soluplus®  
properties and solubility  
measurements

---



## **1. Introduction**

Before designing amorphous solid dispersions systems, it is very important to characterize and correlate the physicochemical properties of API and carrier in an early stage of this development. In this work, some properties of API and polymer were firstly determined:

- Melting point of EFV, glass transition temperature of EFV and Soluplus;
- True density, shape and morphology of EFV unprocessed crystals;
- Soluplus micelles size, EFV solubility in aqueous media containing or not Soluplus.

As reviewed by DeBoyace et al [1], temperature-composition phase diagrams for very few APIs (indomethacin, felodipine, ketoconazole, aceclofenac) with carriers [2]–[6] have been published to date, despite their usefulness. In this thesis, a temperature-composition phase diagram of Efavirenz, and the polymer Soluplus® was determined and is presented in this Chapter. These phase-diagrams are essential to understand and predict the kinetic and thermodynamic stability of binary-mixture at a given composition and temperature. To this end, we propose an original method to rapidly produce a supersaturated solid solution of EFV in Soluplus by a spray drying process. Spray drying is one of the main processes capable of being scaled-up into large manufacturing scale to produce ASDs [7], [8] and was one of the manufacturing methods used in this work to produce EFV-Soluplus ASD systems as it will be shown in Chapter 4. However, it will be demonstrated in the present chapter that, preparing supersaturated API-polymer solid solutions by spray drying could also represent an alternative to determine API-carrier solubility from demixing, because it is a fast process (some seconds) compared to other ones commonly used as solvent casting or comilling, which are very time-consuming (hours).

## 2. Materials and Methods

### 2.1. Materials

Efavirenz was kindly provided by Cristalia Ltd (Itapira, Brazil).

Soluplus® was provided by BASF corporation (Ludwigshafen, Germany).

Ethanol used as organic solvent in the preparation of solid dispersions was purchased from Carlo ERBA Reagent (Italy). For the purpose of analysis, distilled and purified water was obtained by the purification system Milli-Q (classic Purelab DI, MK2, E3lga, UK).

### 2.2. Methods

#### *2.2.1. Characterization of pure compounds*

The pure compounds, API and carrier were firstly characterized.

##### 2.2.1.1. Shape and morphology (SEM)

SEM images of pure EFV and Soluplus were obtained using a scanning electron microscope Philips XL30 ESEM-FEG (Philips, USA) with acceleration voltage of 20 kV. Samples were fixed on a support using a double-sided adhesive and covered with platinum using a high-resolution SEM coated spray Polaron SC7640 (Quorum Technologies, England).

##### 2.2.1.2. True density

The true densities of EFV and Soluplus powders were determined in duplicate using a gas displacement pycnometer (Accupyc 1330, Micromeritics, UK). For these analyses, helium was injected at a known pressure into a cell containing the solid to be analyzed. The gas was then expanded in an expansion cell and its pressure in the cell was measured. The sample volume was calculated by the difference between the volume of the sample cell and the expansion cell with the pressure variation. The volumes of two cells were determined during calibration performed using stainless spheres of known weight and volume. Values and standard deviations were determined from 10 successive measurements.

##### 2.2.1.3. Solid state (XRD)

Powder X-ray diffraction patterns were obtained by X'Pert Panalytical X-ray diffractometer (Philips, USA) using CuK $\alpha$  radiation, putting 40 mA of current and 45 kV of

voltage. The recording spectral range was set at 7-50° with a measuring step (angular deviation between 2 consecutive points) of 0.0167° and an acquisition time of 100 s per point. In addition, the powder was rotated in its sample holder (1 revolution/s) during the acquisition of the results.

#### 2.2.1.4. Thermal properties (DSC)

Thermal analyses were performed using a DSC Q200 with the base module and mDSC (TA instruments, USA). A RCS90 cooling system was set up in order to control precisely the cooling rate. Nitrogen was used as the purging gas at 50 mL/min, the analysis was made in non-hermetic aluminum pans, indium standards were used for enthalpy and temperature calibration and an empty aluminum pan was used as a blank. Samples were heated with a rate of 2 °C/min, from 10 to 150 °C.

In mDSC analysis, sapphire was used to calibrate in heat capacity with constant pressure ( $C^P$ ). Experiments were carried out in order to determine the glass transition temperatures for Soluplus and EFV. In these analyzes, the samples were heated at 2 °C/min from 10 to 150 °C, with a modulation period of 40 s and an amplitude of 0.2 °C.

#### 2.2.1.5. Characterization of Soluplus® micelles

Aqueous solutions containing Soluplus at a concentration of 10 mg/L, higher than the critical micelle concentration (CMC=7.6 mg/L) [9], were prepared at 25°C.

Three different samples of polymer were used: the commercial product and two others processed by different manufacturing processes (spray drying and hot-melt extrusion). The micelle size was measured by dynamic light scattering (DLS). All measurements were performed using a Malvern Zetasizer Nano ZS.

#### 2.2.1.6. Solubility of crystalline EFV in aqueous medium

Solubility studies of unprocessed EFV crystals were determined following the standard shake flask method. For that purpose, an excess amount of samples was added into 30 mL of a dissolution medium containing purified water plus 0.25 wt % of Sodium Lauryl Sulfate (SLS) under magnetic agitation at 37 ± 0.5 °C in a water bath as recommended by Pharmacopeia USP [10], [11] (Figure 31). The USP specifications state aqueous solution containing 1% and 2% wt% of SLS as dissolution media for EFV. The concentration of SLS was chosen at 0.25 wt%, because this is a more biorelevant condition [12]. The addition of SLS 0.25 wt%, in the maximum limit of CMC was necessary to improve the wettability of EFV.

The samples of 2 mL were collected from 5 min until 48 h. Concentration of EFV in the medium was measured by HPLC system (Agilent 1100 Series) equipped with a UV-visible detector (Protocol to quantify EFV from the ASDs is described in appendix 2). The experiments were carried out in duplicate.



*Figure 31. Experimental apparatus for solubility tests (37°C)*

#### 2.2.1.7. Solubility of crystalline EFV in the presence of Soluplus®

To investigate the solubilizing power of Soluplus®, the equilibrium solubility of crystalline EFV in purified water containing 0.01 to 0.2 mg/mL of Soluplus at room temperature was determined and compared with the equilibrium solubility in the absence of the polymer in purified water.

The concentration range of Soluplus was chosen based on some preliminary experiments (data not shown), which demonstrated that at concentrations higher than 0.20 mg/mL, Soluplus exhibits absorbance at the same EFV wavelength ( $247 \text{ nm}^{-1}$ ) disturbing API quantification by UV spectroscopy.

#### ***2.2.2. Temperature-composition EFV-Soluplus phase diagram***

##### 2.2.2.1. Preparation of a supersaturated EFV-Soluplus solid dispersion by spray drying

A supersaturated amorphous solid dispersion was prepared by spray drying with an EFV load of 85 wt%. It will be named 85%EFV-15%SOL ASD system. The process conditions for its preparation and the results of the characterization study confirming its amorphous state will

be detailed in Chapter 4, which focuses on the generation of ASDs by spray drying, including the one discussed in this study. The present chapter is focused on the method used for determining the solubility of EFV in Soluplus from a spray-dried supersaturated amorphous solid dispersion of EFV in Soluplus, by employing a recrystallization method.

#### 2.2.2.2. Determination of EFV solubility in Soluplus by recrystallization

85%EFV-15%SOL ASD system was loaded into the DSC analyzer and annealed at different temperatures below the  $T^m$  (melting point) of EFV for 2-28 h, aiming to recrystallize the excess of API in the mixture and to reach the equilibrium solubility. After annealing, the sample was cooled to 10 °C and ramped at a rate of 2 °C/min to determine the  $T^g$  (glass transition temperature) of the annealed material.

The recrystallization method presented in Figure 32 illustrates a typical DSC running:

- Run 1 (first heat cycle) represents a change in the solid state evidenced by a unique glass transition temperature of the binary mixture, followed by an exothermic phenomenon (recrystallization).
- Run 2 (isotherm) aims to reach the equilibrium state for the sample at a given annealing temperature.
- Run 3 is the cooling to prepare the sample to follow the next cycle.
- Finishing the cycle, Run 4 (second heat cycle) gives the new glass transition temperature of the binary mixture, corresponding to the API amount that still remains dispersed in the polymer carrier at the equilibrium temperature, which corresponds to the melting temperature of this mixture  $T_{MIX}^g$ .

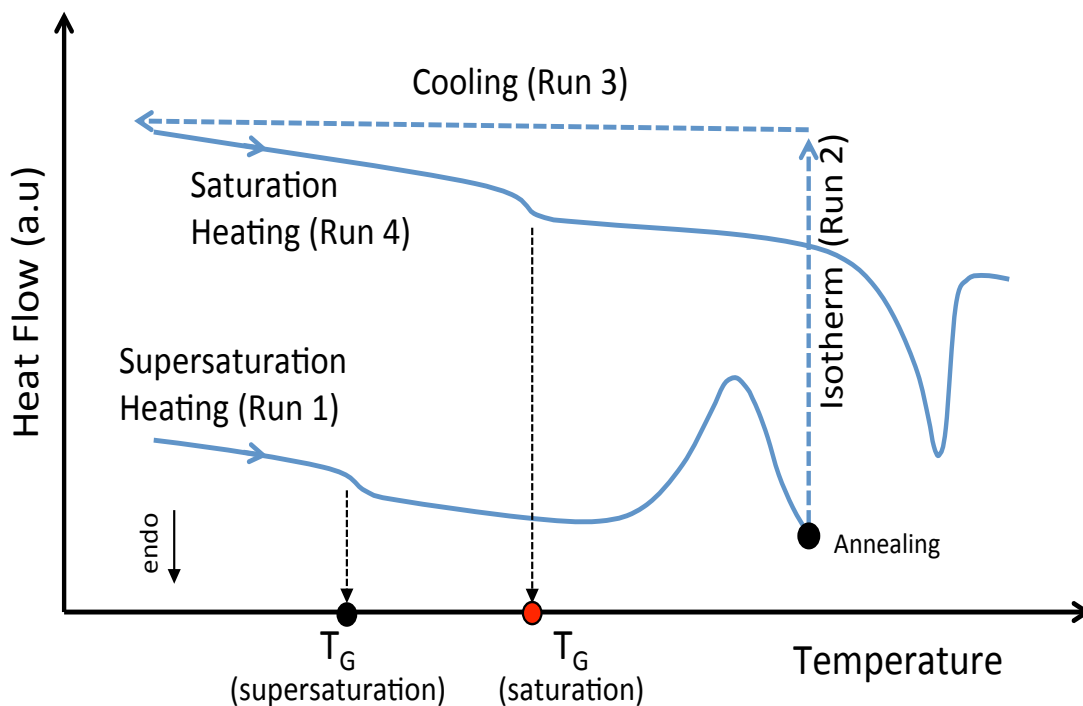


Figure 32. Principle of DSC analysis for recrystallization method

Annealing temperature and annealing time are essential parameters and play an important role in the recrystallization method. At lower annealing temperatures, a longer time is required to reach the equilibrium state. The reason is a slower demixing kinetics due to an insufficient molecular chain mobility, leading consequently to slower API diffusion in the polymer matrix [4]. Completing the DSC analysis, the new equilibrium dissolution concentration of the API remaining dispersed in the polymer was calculated using the Gordon-Taylor equation already introduced in Chapter 2 (section 1.3.5), following a procedure described in Chapter 2 (section 2.1.2).

#### 2.2.2.3. Theoretical considerations

- Prediction of Mixed Phase Glass Transition Temperature ( $T_{MIX}^g$ )

Gordon-Taylor equation is used to estimate the theoretical glass transition temperature of the mixture  $T_{MIX}^g$ . It is calculated based on the individual contributions of weight fraction and glass transition temperature of each component in the binary mixture, without considering the intermolecular interactions between them.

- Solubility curve fitting

Flory-Huggins modeling, already described in Chapter 2 (Equations 27 and 28, section 2.1.2.1) was used to construct the solubility curve and to estimate API solubility in polymer within the range of annealing temperature of 90 to 137°C. The calculated data were compared to the experimental results obtained with the DSC protocol.

Binary interactions between polymer and API are commonly described by Flory-Huggins parameter ( $\chi$ ) obtained from the solubility curve. Immiscibility between the components is represented by a positive  $\chi$ , while miscibility is indicated by a negative  $\chi$  [4], [6], [13].

### 3. Results

#### 3.1. Characterization of pure compounds

##### 3.1.1. Efavirenz

Cristallinity studies (XRD), thermal analysis (DSC) and surface morphology studies (SEM) were carried out to characterize the unprocessed EFV crystals.

In terms of morphology (SEM analysis), the unprocessed EFV crystals are long rods with regular and organized multi face geometry as seen in Figure 33. The true density of EFV particles determined experimentally by helium pycnometry is 1.39 g/cm<sup>3</sup>.

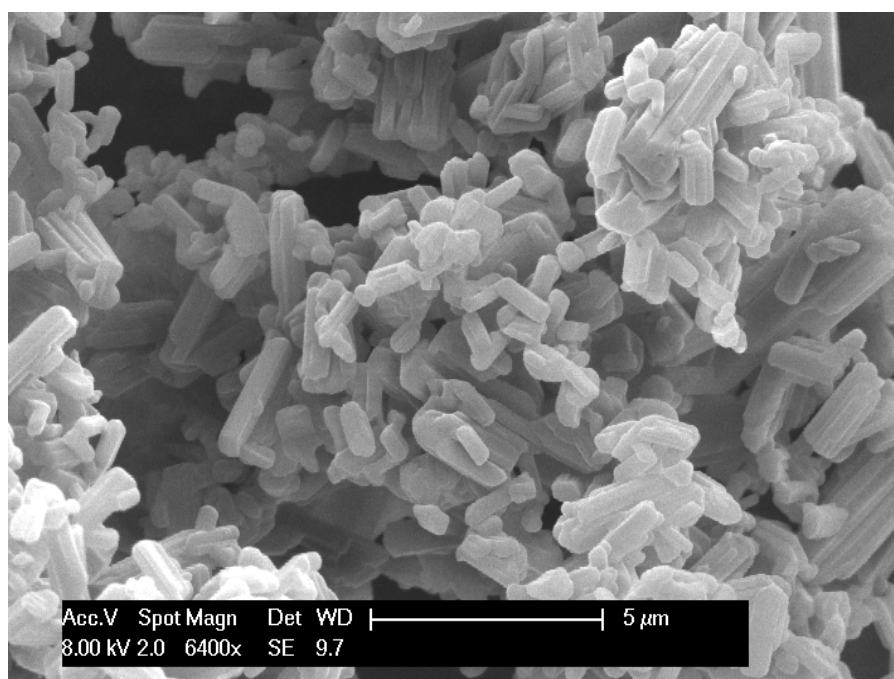
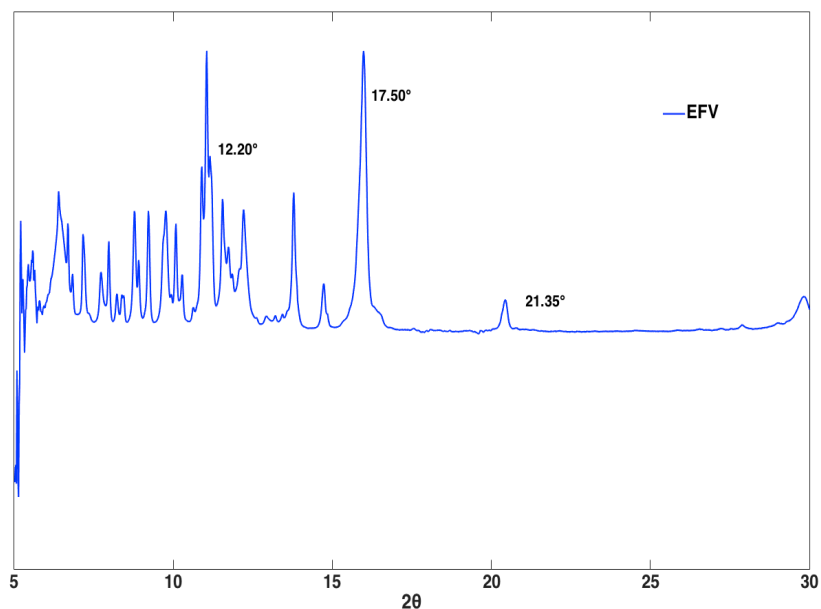


Figure 33. SEM image of unprocessed EFV crystals

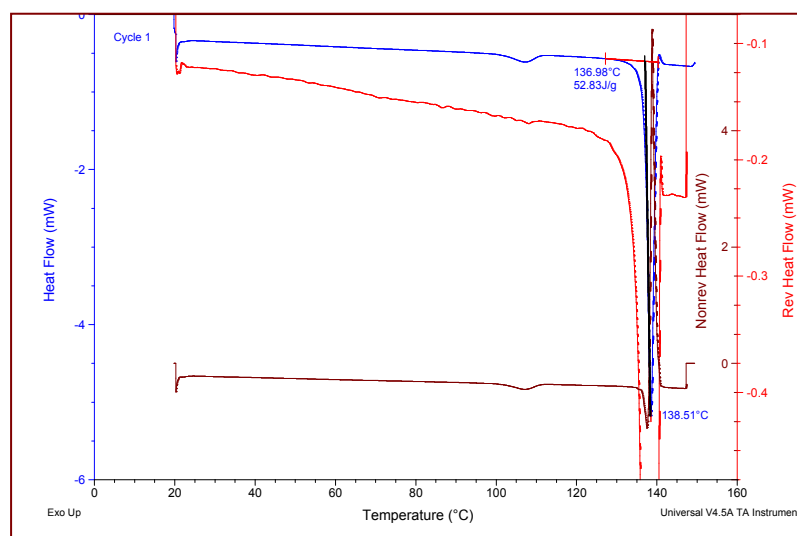
XRD spectra for unprocessed EFV crystals exhibit principal sharp diffraction peaks at  $2\theta$  of  $12.20^\circ$ ,  $17.50^\circ$  and  $21.35^\circ$  which represents characteristic peaks for crystalline nature of EFV in accordance to the literature [14], [15] (Figure 34).



*Figure 34. XRD diffractogram for unprocessed crystals of EFV*

mDSC shows in Figure 35 (A) a unique endothermic peak of  $138.5^\circ\text{C}$  (melting point) with an enthalpy of  $52.8\text{ J/g}$  for crystalline EFV. In Figure 35 (B), no endothermic peak was detected suggesting the amorphization of EFV. A glass transition temperature of  $36.1^\circ\text{C}$  was determined from atomized EFV through of DSC.

(A)



(B)

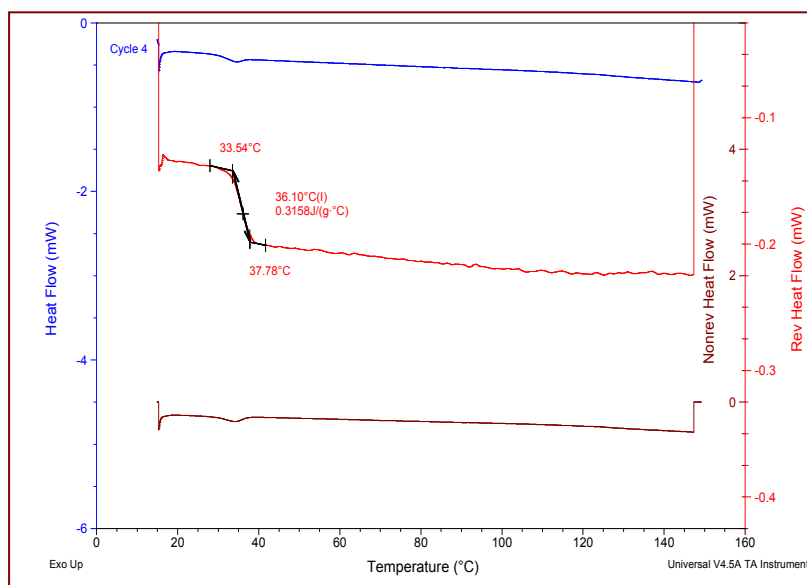


**Figure 35. mDSC thermogramme for EFV. (A) unprocessed EFV (B) amorphous EFV obtained by Spray Drying already determined by our group in previous studies [16].**

- Solubility of crystalline EFV in aqueous media

The saturation solubility of crystalline EFV at 37 ± 0.5 °C in pure water was measured as 3.80 ± 0.18 µg/g. This value is in the same order of magnitude of values already published, from 1 to 9 µg/mL at 25°C [17].

The solubility of EFV is greatly increased in presence of surfactants as shown by our measurements performed in an aqueous medium at 37°C containing 0.25wt% of SLS: 41.04 ± 9.38 µg/g, an increase of 10 fold compared to the EFV solubility in pure water.

### 3.1.2. Soluplus®

X-ray diffraction (XRD) and thermal analysis (DSC) were carried out to characterize the polymer Soluplus. From XRD, the absence of Bragg's peaks indicates the amorphous nature of this polymer (Figure 36).

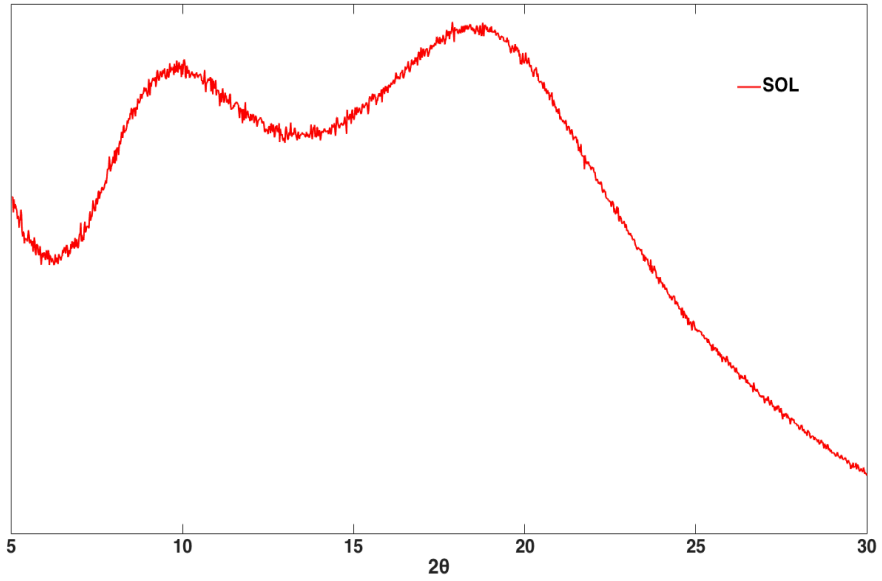


*Figure 36. XRD diffractogram for unprocessed Soluplus polymer*

Glass transition temperature of Soluplus, determined by mDSC (Figure 37) is 79.9 °C, and  $\Delta C_p = 0.246 \text{ j/g}\cdot^\circ\text{C}$ . In comparison to EFV amorphous mDSC thermogram, the signal is more noisy, and the glass transition is much larger (around 20°C)

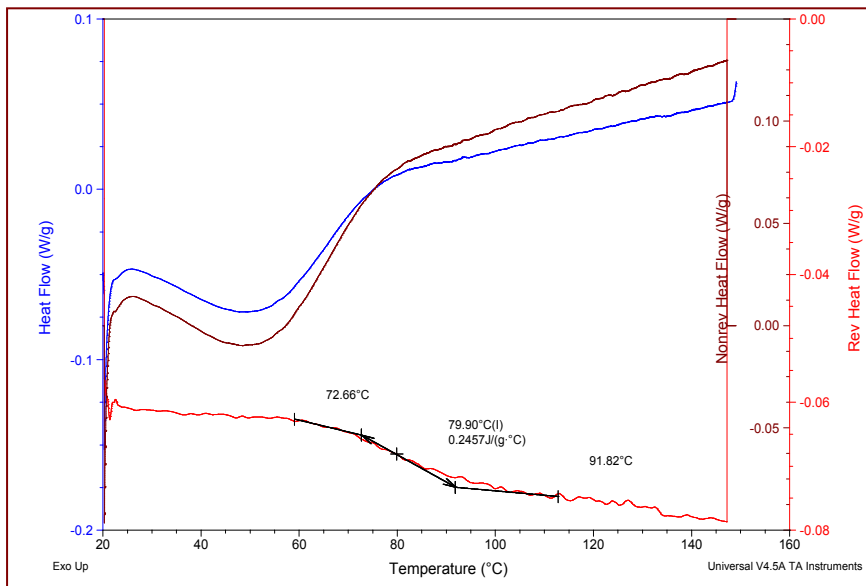


*Figure 37. mDSC thermogramme for Soluplus®*

The true density of Soluplus determined experimentally by helium pycnometry is 1.18 g/cm<sup>3</sup>. The true density of API and polymer are needed to calculate the glass transition temperature of mixture from Gordon-Taylor equation (equations 2 and 3, Chapter 2).

- Characterization of Soluplus® micelles

Using a DLS method, the formation of a colloidal micelle structure was found to be 62-67 nm at 25 °C (Table 14). The Soluplus micelles present a unimodal size distribution shown in Figure 38. The results are in accordance to previous measurements already published and discussed in Chapter 2. The micellar size had not changed after 1 month of storage under ambient conditions. This property (micelles formation) has been shown to improve the solubility and dissolution behavior of existent APIs from BCS Class II and Class IV [18]–[24].

Table 14 also shows that Soluplus processed by two different manufacturing processes, spray drying and hot-melt extrusion, present colloidal micelle structures similar to that of the unprocessed one.

*Table 14. Size of micelles for different types of Soluplus®*

Type of Soluplus®	Size of micelles (nm)*	
Spray-dried**	62.48	0.65
Extruded**	66.81	1.94
Commercial	65.82	0.62

\*Values represent the standard deviation, n = 3

\*\* The processing conditions used to produce spray-dried and extruded samples of Soluplus are given in Chapters 4 and 5, respectively.

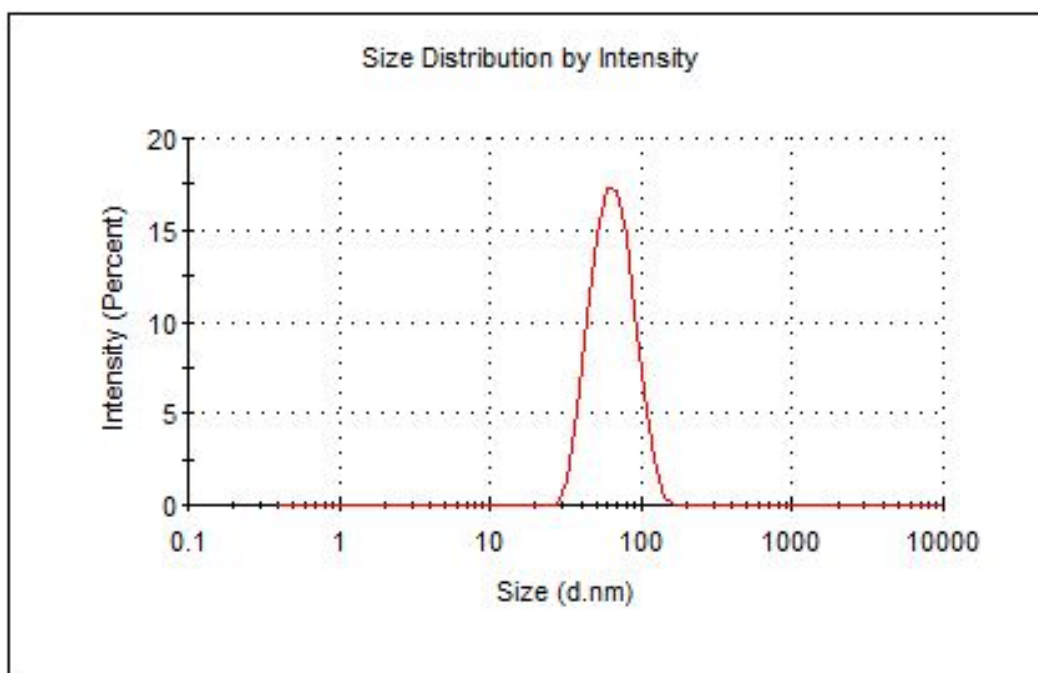


*Figure 38. Example of size distribution of commercial Soluplus® micelles*

### **3.1.3. Solubility of crystalline EFV in the presence of Soluplus® in water**

Table 15 shows that the equilibrium solubility of EFV changed significantly as a function of the polymer concentration in aqueous solution, in the range of 0.01 to 0.2 mg/g. These results indicate that, in the studied range of concentration (above the CMC of Soluplus®), the EFV solubility increase is probably due to a mechanism of micellar solubilization, i.e., inclusion of EFV molecules into the micellar structure of the polymeric carrier.

*Table 15. Equilibrium solubility of Efavirenz (EFV) in purified water and in presence of dissolved polymeric carrier (Soluplus)*

Solubility of EFV ( $\mu\text{g/g}$ )		SOL (mg/g)
3.80	0.18*	0
27.56	7.47	0.01
33.33	3.62	0.02
61.24	12.30	0.06
87.87	10.46	0.20

\*Values represent the standard deviation, n = 2

### 3.2. API-polymer solubility determination by recrystallization

85%EFV-15%SOL ASD system was successfully prepared by spray drying. The glass transition temperatures of ASD sample and pure compounds were determined by DSC (Table 16). ASD revealed a single and distinctive mixture glass transition temperature ( $T_{MIX}^g$ ) in the reversing heat flow signals, which indicates the formation of one-phase in the solid structure produced by spray-drying.

The experimental  $T_{MIX}^g$  is compared (Table 16) to the theoretical value calculated by the Gordon-Taylor equation previously detailed. The experimental  $T^g$  value is lower than the theoretical one obtained from Gordon-Taylor plot equation. This could be attributed to residual solvent effects on the spray-dried solid structure or due to molecular interactions between the components.

*Table 16. Glass transition temperatures of solid dispersion and pure components determined by DSC and Gordon-Taylor equation*

$W_{PA}$	$T_{MIX}^g$ (°C) ± 2 °C	
	Gordon Taylor equation	DSC
0.00	-	79.9
0.85	47.2	36.7
1.00	-	36.1

Other measurements (XRD and Raman mapping) that will be presented in the next chapter confirmed the amorphous state of the high API load ASD produced by spray drying. This sample was then annealed from 90 °C until 130 °C to promote the recrystallization of excess EFV amount. In order to use a reasonable annealing time, the lower limit of temperature range (90°C) was chosen far enough above the glass transition ( $\approx 79.9^\circ\text{C}$  for pure polymer,  $36.7^\circ\text{C}$  for the mixture), the molecular mobility reducing strongly as we approach  $T_{MIX}^g$ . The upper value of this range was chosen under the melting point of pure API ( $T_{PA}^m=138,5^\circ\text{C}$ ).

The reverse signal of mDSC scans corresponding to 120 °C annealing temperature is shown in Figure 39, as example. A mixture glass transition ( $T_{MIX}^g$ ) in Run 1 at  $36.7 \pm 3^\circ\text{C}$

followed by a recrystallization which starts at about 90 °C and is stopped at the annealing temperature of 120 °C.

In Run 2 (isotherm, not seen for clarity reasons), the sample is kept at 120°C during 2 h. This step is essential, because it favors the end of recrystallization of the remaining excess EFV in order to reach the equilibrium state.

Once reached the equilibrium state, the sample was cooled (Run 3, not seen for clarity reasons) and rescanned (Run 4) in the same conditions as the first run. It is detected a higher second mixture glass transition ( $T_{MIX}^g = 51.2 \pm 3 \text{ °C}$ ) by a decrease in  $C^p$  (0.32 J/g/K for Run 1 and 0.16 J/g/K for Run 4). This increase in the  $T_{MIX}^g$  value and the smaller amplitude of  $C^p$  is expected to be due to the reduction of amorphous API amount in the solid dispersion that recrystallized in comparison with the Run 1.

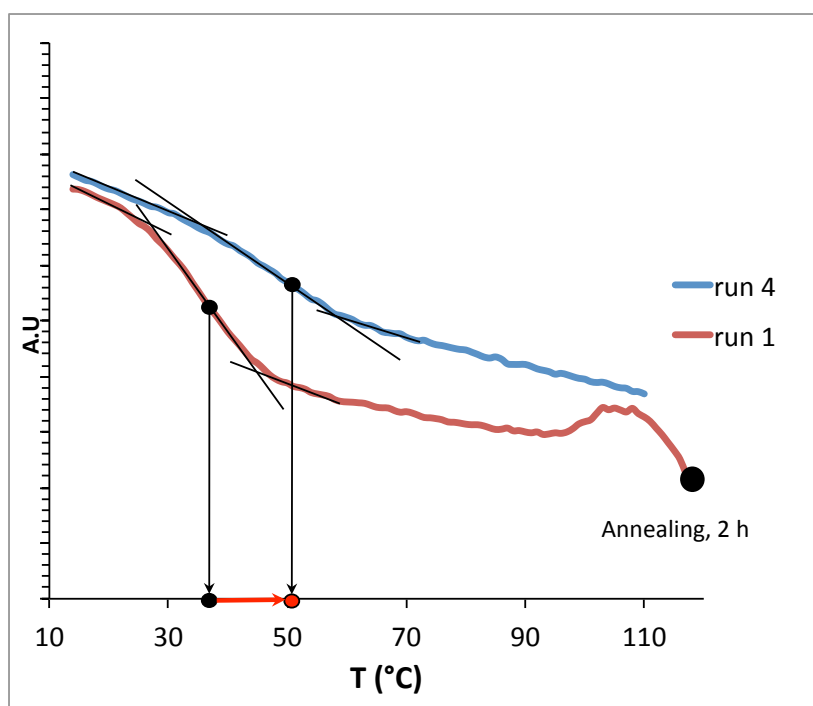


*Figure 39. Reverse heat flow of spray-dried 85%EFV-15%SOL ASD.*

The new EFV composition can be determined from Gordon-Taylor equation thanks to the  $T_{MIX}^g$  obtained in run 4. Table 17 regroups the saturated EFV concentrations at equilibrium obtained for all annealing temperatures.

Table 17. Calculated equilibrium concentrations ( $W_{PA}$ ) from spray-dried 85% EFV in SOL

Annealing temperature (°C)	Annealing time (h)	$T_{MIX}^g$ during Run 4 (°C)	$W_{PA}$
90	28	55.0	0.58
100	28	53.4	0.61
110	2	52.2	0.64
120	2	51.2	0.66
125	2	47.1	0.75
130	2	45.9	0.78
137	-	-	1.00

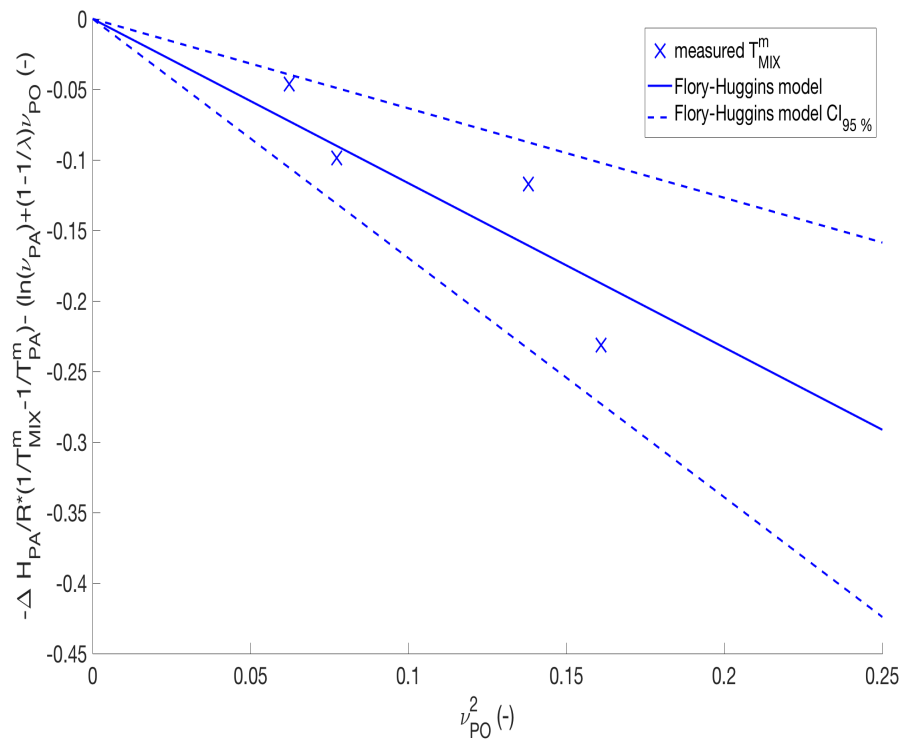
In the case of lower temperature than 110 °C, 2 h wasn't enough to reach the saturation equilibrium because of the slower kinetic of demixing. In that case, the time required to reach the saturation equilibrium had to be increased to 28 h.

Flory-Huggins model was used to estimate the  $\chi$  parameter by lowering of the  $T^g$  mixture temperature. This model is expressed in a linear form for which  $\chi$  is the slope of the obtained line (Figure 40 (A)). The full line represents the linear regression of the data obtained with the least squares method. The dashed lines in the same figure represent the limit of the 95 % confidence interval (CI<sub>95%</sub>) for the slope. The number of data used for the regression was decreased until all used data are in this confidence interval. Finally, the  $\chi$  parameter of Flory-Huggins obtained is -1.165 with CI<sub>95%</sub>=[-1.70;-0.63]. A negative  $\chi$  parameter represents attractive API-polymer interaction [25]. Figure 40 (B) presents the best fit of Flory-Huggins model with the corresponding limits of  $\chi$  confidence interval, as represented in Figure 40 (A). To refine these results, a polynomial fitting is also represented. The two fitting models are in good agreement between them for low temperatures and give the solubility curve of EFV in SOL. Thanks to these plots, it is possible to identify regions of kinetic and thermodynamic stability. For example, approximately 20 % (Flory-Huggins model) of EFV is soluble in Soluplus at room temperature (25 °C). It means that a thermodynamic stability should be achieved at room temperature for API loads lower than 20 %. In contrast, a high API load SD with 85 % of EFV might be phase separate and eventually recrystallize at 25 °C.

The lower temperature, the more difficult the determination of the solubility curve, since the time required to reach the saturation equilibrium is relevant due to slow kinetic of demixing. Although there is no thermodynamic stability, the sample was still stable from the kinetic point of view. As showed in Table 17, below 110 °C, the slow molecular mobility makes the demixing process slower and then, a longer time was required to reach the saturation equilibrium (28 h in our experiments).

This method can not be applied for the lowest temperature given by the crossing point between the solubility and Gordon-Taylor curves. In our case, the crossing point for the Flory-Huggins model is 63.4°C, what means that, if the annealing is done under this temperature, it would result in an abrupt reduction of molecular mobility and consequently of the demixing process avoiding the reach of saturation equilibrium [4].

(A)



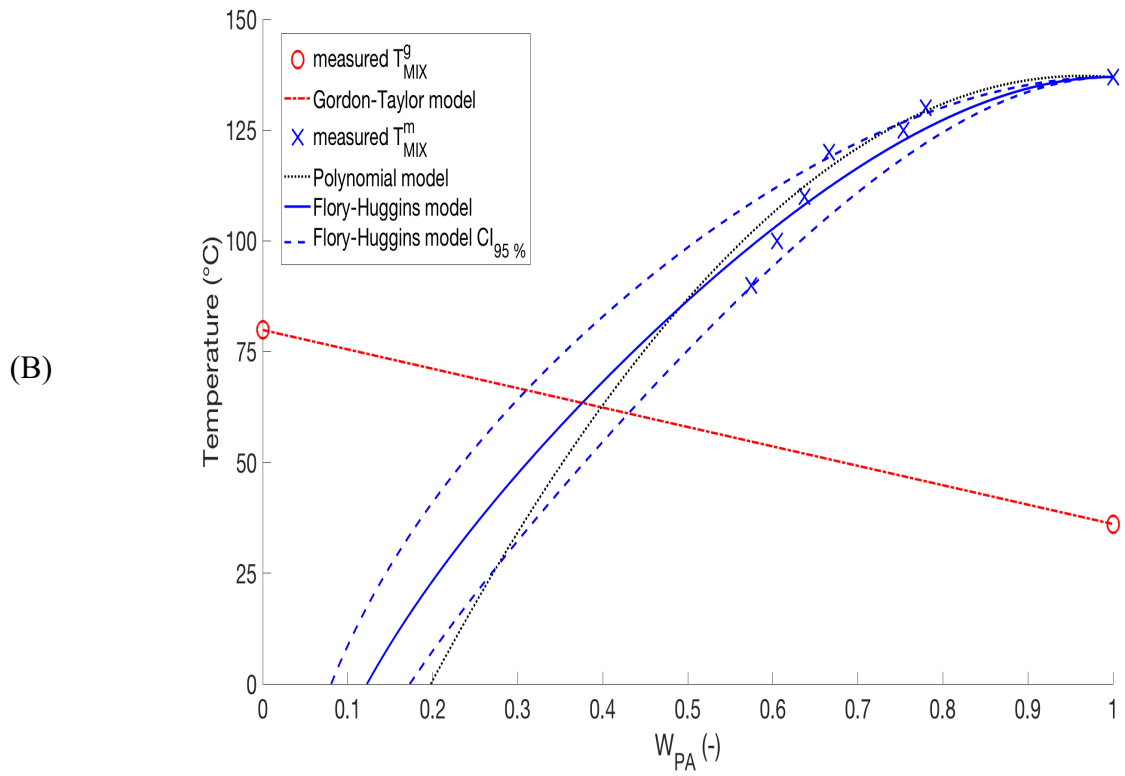


Figure 40. A) Estimation of Flory-Huggins parameter  $\chi$  by linear regression  
 B) Phase diagram of EFV-SOL



## 4. Conclusion

As expected, we confirm the very poor solubility of the crystalline form of EFV in pure water ( $3.80 \pm 0.18 \mu\text{g/g}$  at  $37^\circ\text{C}$ ). It could be demonstrated that its solubility is influenced by the presence of surfactants and of dissolved Soluplus. The measured values indicated an increase of 10 fold in 0.25% SLS and from 7 to 23 fold in presence of Soluplus concentrations from 0.01 to 0.2 mg/g, respectively.

It is, at our knowledge, the first study reporting a phase diagram of EFV and Soluplus, presented again in Figure 41, where it is possible to identify regions of kinetic and thermodynamic stability varying temperature and EFV concentration. It can be very useful (a preformulation tool) for researchers studying amorphous solid dispersions of Efavirenz in Soluplus, to assist for predicting the stability of EFV-Soluplus ASDs at different EFV loadings and under different thermal conditions.

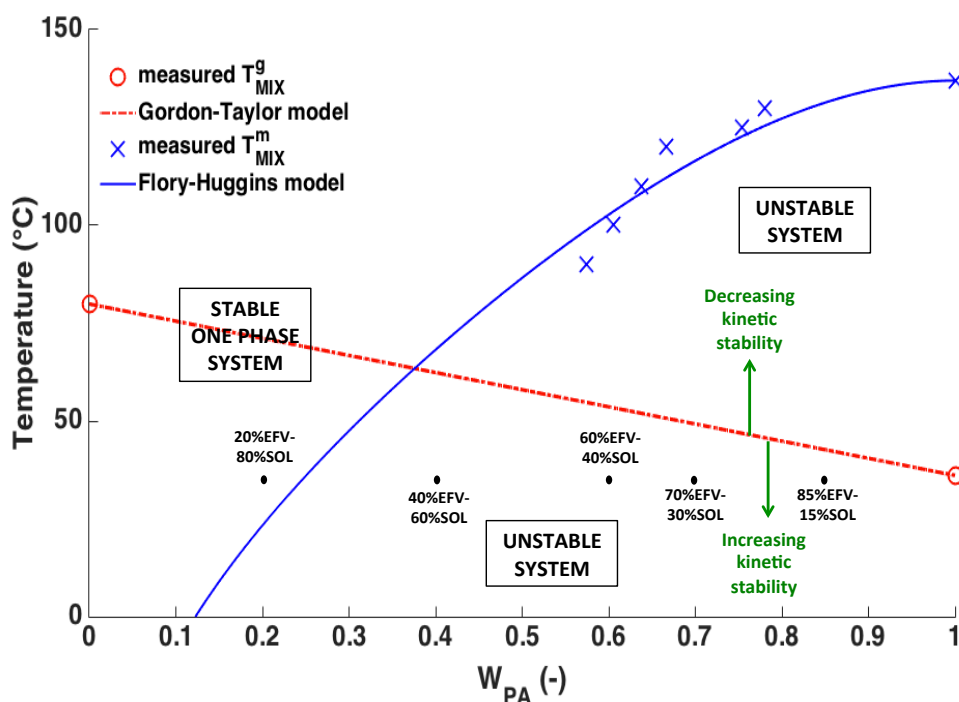


Figure 41. Schematic EFV-SOL phase diagram with all ASDs

API-polymer solubility and the glass transition temperature are the main factors that influence physical stability and performance behavior. The EFV-Soluplus phase-diagram is useful to predict the stability of amorphous binary-mixtures of different compositions under

different temperature conditions. For example, samples are stressed under different temperature conditions from room to 40°C in order to investigate physical stability. The EFV solubility in Soluplus ranges from 20 wt% (25°C) to 30 wt% (40°C). Amorphous solid dispersions of EFV in Soluplus containing more than 30% of EFV in mass are supersaturated and their stability should be monitored over storage from room to accelerated (40°C) temperature conditions.

From this point, the aim is to predict the physical stability (thermodynamically stable, kinetically stable or unstable) amorphous solid dispersions with a large range of composition (indicated in Figure 41), with the assistance of the EFV-Soluplus temperature-composition phase diagram.

In the chosen composition interval, only one ASD system (20%EFV-80%SOL) is placed in a thermodynamically stable glass region. The other ASD systems to be produced are in a kinetically stable glasses region, but thermodynamically unstable. In this region, physical stability against phase separation and recrystallization is a challenge.

## 5. References

- [1] K. DeBoyace and P. L. D. Wildfong, 'The Application of Modeling and Prediction to the Formation and Stability of Amorphous Solid Dispersions', *J. Pharm. Sci.*, vol. 107, no. 1, pp. 57–74, Jan. 2018.
- [2] T. Nishi and T. T. Wang, 'Melting Point Depression and Kinetic Effects of Cooling on Crystallization in Poly(vinylidene fluoride)-Poly(methyl methacrylate) Mixtures', *Macromolecules*, vol. 8, no. 6, pp. 909–915, Nov. 1975.
- [3] Y. Zhao, P. Inbar, H. P. Chokshi, A. W. Malick, and D. S. Choi, 'Prediction of the thermal phase diagram of amorphous solid dispersions by Flory-Huggins theory', *J. Pharm. Sci.*, vol. 100, no. 8, pp. 3196–3207, Aug. 2011.
- [4] A. Mahieu, J.-F. Willart, E. Dudognon, F. Danède, and M. Descamps, 'A New Protocol To Determine the Solubility of Drugs into Polymer Matrixes', *Mol. Pharm.*, vol. 10, no. 2, pp. 560–566, Feb. 2013.
- [5] M. M. Knopp *et al.*, 'Comparative Study of Different Methods for the Prediction of Drug-Polymer Solubility', *Mol. Pharm.*, vol. 12, no. 9, pp. 3408–3419, Sep. 2015.
- [6] C. Donnelly, Y. Tian, C. Potter, D. S. Jones, and G. P. Andrews, 'Probing the effects of experimental conditions on the character of drug-polymer phase diagrams constructed using Flory-Huggins theory', *Pharm. Res.*, vol. 32, no. 1, pp. 167–179, Jan. 2015.
- [7] B. B. Patel, J. K. Patel, S. Chakraborty, and D. Shukla, 'Revealing facts behind spray dried solid dispersion technology used for solubility enhancement', *Saudi Pharm. J.*, vol. 23, no. 4, pp. 352–365, Sep. 2015.
- [8] A. Sosnik and K. P. Seremeta, 'Advantages and challenges of the spray-drying technology for the production of pure drug particles and drug-loaded polymeric carriers', *Adv. Colloid Interface Sci.*, vol. 223, pp. 40–54, Sep. 2015.
- [9] 'Soluplus - For better solubility & bioavailability', *BASF*. [Online]. Available: <https://pharmaceutical.basf.com/en/Drug-Formulation/Soluplus.html>. [Accessed: 14-Oct-2018].
- [10] '| USP'. [Online]. Available: <http://www.usp.org/>. [Accessed: 13-Jun-2018].
- [11] 'Efavirenz racemic 1234114', *Sigma-Aldrich*. [Online]. Available: <https://www.sigmaaldrich.com/catalog/product/usp/1234114>. [Accessed: 27-Oct-2018].
- [12] C. Fandaruff *et al.*, 'Polymorphism of Anti-HIV Drug Efavirenz: Investigations on Thermodynamic and Dissolution Properties', *Cryst. Growth Des.*, vol. 14, no. 10, pp. 4968–4975, Oct. 2014.
- [13] F. Meng, V. Dave, and H. Chauhan, 'Qualitative and quantitative methods to determine miscibility in amorphous drug-polymer systems', *Eur. J. Pharm. Sci. Off. J. Eur. Fed. Pharm. Sci.*, vol. 77, pp. 106–111, Sep. 2015.
- [14] P. T. Koh, J. N. Chuah, M. Talekar, A. Gorajana, and S. Garg, 'Formulation Development and Dissolution Rate Enhancement of Efavirenz by Solid Dispersion Systems', *Indian J. Pharm. Sci.*, vol. 75, no. 3, pp. 291–301, 2013.

- [15] Z. M. M. Lavra, D. Pereira de Santana, and M. I. Ré, 'Solubility and dissolution performances of spray-dried solid dispersion of Efavirenz in Soluplus', *Drug Dev. Ind. Pharm.*, vol. 43, no. 1, pp. 42–54, Jan. 2017.
- [16] M. Lavra and Z. Maria, *Incremento da solubilidade e da cinética de dissolução do fármaco Efavirenz através da obtenção de misturas binárias amorfas com matrizes poliméricas*. Ecole nationale des Mines d'Albi-Carmaux, 2016.
- [17] 'Efavirenz | C<sub>14</sub>H<sub>9</sub>ClF<sub>3</sub>NO<sub>2</sub> - PubChem'. [Online]. Available: <https://pubchem.ncbi.nlm.nih.gov/compound/64139>. [Accessed: 08-Jun-2018].
- [18] J. Djuris, I. Nikolakakis, S. Ibric, Z. Djuric, and K. Kachrimanis, 'Preparation of carbamazepine-Soluplus solid dispersions by hot-melt extrusion, and prediction of drug-polymer miscibility by thermodynamic model fitting', *Eur. J. Pharm. Biopharm. Off. J. Arbeitsgemeinschaft Für Pharm. Verfahrenstechnik EV*, vol. 84, no. 1, pp. 228–237, May 2013.
- [19] S. Tanida, T. Kurokawa, H. Sato, K. Kadota, and Y. Tozuka, 'Evaluation of the Micellization Mechanism of an Amphipathic Graft Copolymer with Enhanced Solubility of Ipriflavone', *Chem. Pharm. Bull. (Tokyo)*, vol. 64, no. 1, pp. 68–72, 2016.
- [20] M. Linn, 'In vitro characterization of the novel solubility enhancing excipient Soluplus®', *In vitro Charakterisierung des neuartigen Lösungsvermittlers Soluplus®*, 2011.
- [21] R. N. Shamma and M. Basha, 'Soluplus®: A novel polymeric solubilizer for optimization of Carvedilol solid dispersions: Formulation design and effect of method of preparation', *Powder Technol.*, vol. 237, pp. 406–414, Mar. 2013.
- [22] Q. Zhang *et al.*, 'Preparation of curcumin self-micelle solid dispersion with enhanced bioavailability and cytotoxic activity by mechanochemistry', *Drug Deliv.*, vol. 25, no. 1, pp. 198–209, Nov. 2018.
- [23] Y. Zhang *et al.*, 'Extruded Soluplus/SIM as an oral delivery system: characterization, interactions, in vitro and in vivo evaluations', *Drug Deliv.*, vol. 23, no. 6, pp. 1902–1911, Jul. 2016.
- [24] X. Lian *et al.*, 'Soluplus(®) based 9-nitrocamptothecin solid dispersion for peroral administration: preparation, characterization, in vitro and in vivo evaluation', *Int. J. Pharm.*, vol. 477, no. 1–2, pp. 399–407, Dec. 2014.
- [25] S. O. Kyeremateng, M. Pudlas, and G. H. Woehrle, 'A Fast and Reliable Empirical Approach for Estimating Solubility of Crystalline Drugs in Polymers for Hot Melt Extrusion Formulations', *J. Pharm. Sci.*, vol. 103, no. 9, pp. 2847–2858, Sep. 2014.

Chapter 4 -  
Efavirenz/Soluplus®  
amorphous solid dispersions  
manufactured by Spray  
Drying

---



## **1. Introduction**

As introduced earlier in this thesis, spray drying is one of the main processes capable of being scaled-up into large manufacturing scale to produce amorphous solid dispersions and is one of the manufacturing methods used here to produce EFV-Soluplus ASD systems.

This chapter presents the methodologies employed for the preparation, by spray drying, and characterization of a large range of solid dispersion compositions (20 wt% until 85 wt% in EFV). Their solid-state structure, performance behavior (solubility, in-vitro dissolution) and physical stability under controlled conditions during storage are evaluated.

The large range of composition aimed:

- Firstly, to investigate the feasibility to generate high-API load amorphous solid dispersions of EFV in Soluplus.

ASDs are often produced with a relatively low API load (<30 wt%) dispersed in the carrier at molecular level [1]. The problem is that a low API-loaded amorphous solid dispersion requires a large dose to ensure therapeutic efficacy. The insertion of high API load formulations on the market is expected to meet patients demand for fixed, unique and smaller dosage combinations products. Furthermore, the supersaturated combinations may reduce dosage amounts as well as decrease the production in the pharmaceutical industries to supply cost savings [2]–[7].

- Secondly, to investigate the physical stability of high-API loaded ASDs produced by spray drying, taking in account their position in the EFV-Soluplus phase diagram presented in Chapter 3.

## 2. Generation of EFV-SOL binary mixtures

### 2.1. Preparation methods

EFV ASDs were prepared by spray drying.

A Buchi B-290 mini spray dryer (Buchi Labortechnik AG, Flawil, Switzerland) equipped with Inert Loop B-295 and an integrated two-fluid 0.7 mm nozzle was used to produce the ASD samples.

Solvent choice is an essential step in the spray dryer process and it was based on high solubility of API and polymer, generation of a feed solution with acceptable viscosity, low toxicity and high volatility to be easily evaporated during the drying of the liquid droplets. Ethanol respects these specifications was used as the common solvent. The feeding solution was prepared by dissolving EFV in a 10 wt % solution of Soluplus in absolute ethanol 99%. Compressed nitrogen was used as the drying/carrying gas with a flow rate of 600 L/h.

The other operation parameters are presented in Table 18.

*Table 18. Spray drying process conditions used to generate ASDs*

Sample	Feed rate (g/h)	Inlet temperature (°C)	Outlet temperature (°C)	Yield (%)
20%EFV-80%SOL-SD	172.8	74	59	56.4
40%EFV-60%SOL-SD	154.8	72	60	61.6
60%EFV-40%SOL-SD	187.2	80	61	31.8
70%EFV-30%SOL-SD	187.2	73	62	43.7
85%EFV-15%SOL-SD	288.1	80	57	38.8

The liquid feed rate and inlet gas temperature were the adjustable process variables. The inlet temperature was controlled at 72 to 80°C and the outlet temperature (57-62°C) was determined by the inlet temperature and relative factors such as gas and liquid flow rates.

Ethanol was continuously condensed in the process for further disposal. The dry powder was recovered in a cyclone. Yield was calculated according the follow equation:

$$\text{Yield (\%)} = \frac{\text{Total weight of solid dispersions}}{\text{Weight of EFV} + \text{Weight of Soluplus}} (100\%) \quad (1)$$

Aiming to compare and, if possible, to differentiate the behavior of ASD systems from a simple physical mixture of the same compounds, two physical mixtures with different compositions were also prepared: 20%EFV-80%SOL-PM (a physical binary mixture containing 20 wt% in EFV) and 40%EFV-60%SOL-PM (a physical binary mixture containing 40 wt% in EFV).

### **3. Characterization techniques**

ASDs were characterized to investigate their solid-state structure, API-carrier interactions and their performance behavior.

Some techniques already described in Chapter 3, i.e., X-ray diffraction (XRD), differential scanning calorimetry (DSC) and scanning electron microscopy (SEM), were also employed in this part of the work and are not presented here (see Chapter 3).

#### **3.1. Raman Mapping (RM)**

Raman mapping was performed using a Raman confocal microscope 300AR Alpha-AFM (Witec, Germany), equipped with a laser at a wavelength of 532 nm and the analyses were conducted at room temperature. Samples were analyzed by a 50x objective with a lateral resolution of 432 nm and an axial resolution of 1320 nm. A surface (10x10 µm) and deep mapping (12x10 µm) were used to predict drug and polymer distribution.

#### **3.2. Fourier Transform Infrared Spectroscopy (FTIR)**

FTIR investigations were realized on a Thermo Scientific Nicolet 5700 spectrometer. The samples were premixed with KBr using mortar and pestle at 10% of the samples in KBr and the discs were produced by compressing the powders at a working pressure of 10 ton. The scanning range was 4000-400 cm<sup>-1</sup> with a 4 cm<sup>-1</sup> resolution.

#### **3.3. Performance behavior**

##### ***3.3.1. In vitro drug release dissolution tests***

Dissolution rate of ASDs was studied using a six-station dissolution rate test type II apparatus (DT 60 ERWEKA, Germany, shown in Figure 42). Paddle stirrers at a speed of 50 rpm and temperature of 37 ± 0.5°C were used in each test. Poor powder wetting of APIs highly

lipophilic as EFV has been overcoming by addition SLS (0.25% to 1.0 wt%) in dissolution tests [8]–[11]. In this study, the dissolution medium was purified water containing 0.25 wt% SLS as wetting agent, as already explained in the section 2.2.1.6 of Chapter 3.

Tests were carried out in Sink and non-Sink conditions. The SI (Sink Index), defined as  $SI = \frac{C_s}{\frac{Dose}{V}}$ , was maintained at a constant value of 3 and 0.1, respectively, for Sink and non-Sink conditions in all dissolutions experiments, which was possible by adjusting the amount of ASDs in accordance to the measured equilibrium solubility of EFV in the dissolution medium. In other words:

- Sink conditions: 7 mg of EFV by sample in 500 mL of dissolution medium;
- Non-Sink conditions: 210 mg of EFV by sample in 500 mL of dissolution medium;

Samples of dissolution, i.e., 0.25wt% SLS aqueous medium (2 mL) were withdrawn at different time intervals (2, 5, 8, 10, 15, 20, 30, 60, 120, 240 and 360 min) and assayed for EFV by HPLC system (Agilent 1100 Series) equipped with a UV-visible detector. The dissolution experiments were conducted in triplicate.

Values were calculated based on protocol described in Appendix 1.



*Figure 42. A dissolution tester DT 60 (type II dissolution apparatus)*

- Methods used to compare EFV release profiles from spray dried ASD systems

EFV release profiles were analyzed using dissolution efficiency (DE) and curve-fitting respectively as independent and dependent-model approaches.

DE, already defined in the section 1.3.6.7 in Chapter 2, was calculated by the free open source software KinetDS® 3.0, according to Equation 8 (Chapter 2). KinetDS® 3.0 was also used to fit the release curves to the Korsmeyer–Peppas mathematical model (Equation 14, Chapter 2). The coefficient of determination ( $R^2$ ), Akaike's information criterion (AIC) and root mean square error (RMSE) are calculated by the following equations:

$$AIC = 2k + n(1 + \frac{\sum_{i=1}^n (y_{iobs} - y_{ipred})^2}{n}) \quad (2)$$

$$RMSE = \sqrt{\frac{\sum_{i=1}^n (y_{iobs} - y_{ipred})^2}{n}} \quad (3)$$

where,  $i$  is the data points,  $n$  is the number of data point,  $y_{iobs}$  is the observed value and  $y_{ipred}$  is the model predicted value.

### **3.3.2. Physical Stability studies**

Phase transformation from amorphous to crystalline or/and to amorphous phase separated systems can be induced by unfavorable storage conditions such as elevated temperature and humidity. In this study, we performed the physical stability assessment under different stress conditions:

- Monitoring the water sorption capacities of the powders using an automated water sorption (DVS)

Dynamic vapor sorption is a gravimetric technology which measures the water uptake of samples upon exposure to humidity as a function of time [12]. It is a powerful tool to study the kinetics of moisture uptake of samples. DVS is normally used in two modes to investigate the kinetics of water adsorption and absorption. The first one is termed as isohumidity whereby samples are exposed to certain humidity at a fixed temperature for a certain time length until the equilibrium is obtained. The second one is termed as isothermal, which involves a step increase of the provided humidity at a certain temperature and monitor the mass change of the sample against time. The second mode was applied in this study.

An automated water sorption analyzer (DVS-2, Surface measurement systems Ltd., London, UK) was used for the investigation of moisture uptake by samples. An isothermal test at 25°C was performed on spray-dried ASD samples, including Soluplus and EFV raw powders.

The relative humidity around the sample was controlled by mixing saturated and dry carrier gas streams using mass flow controllers. The temperature was kept constant at 25°C. Prior to being exposed to any water vapor, the sample was dried at 0% RH to remove any water present. Next, the sample was exposed to the desired relative humidity and the moisture uptake was measured. More specifically, approximately 50 mg of sample was weighed into the sample pan of the DVS and subjected to one 0–95% relative humidity (RH) sorption-desorption cycle, over 10% RH increments. During the measurements, the instrument was run in dm/dt mode (mass variation over time variation) to decide when equilibrium was reached. A fixed dm/dt value (0.01) was selected at each RH segment. This criterion permits the DVS software to automatically determine when equilibrium has been reached and complete a step. When the rate of change of mass falls below this threshold over a demanded period of time, the RH set point proceeded to the next programmed level.

- Following an International Conference on Harmonization ICH guideline (Q1A) for accelerated stability condition (40°C ± 2°C/75% RH ± 5% RH) during 15 days.

Spray-dried ASD samples in open containers were exposed at 40 °C and 75 % RH during 15 days. Every 3 days, they were analyzed by DSC to monitor changes in the physical state.

## 4. Results

### 4.1. Characterization of ASDs

#### 4.1.1. SEM images

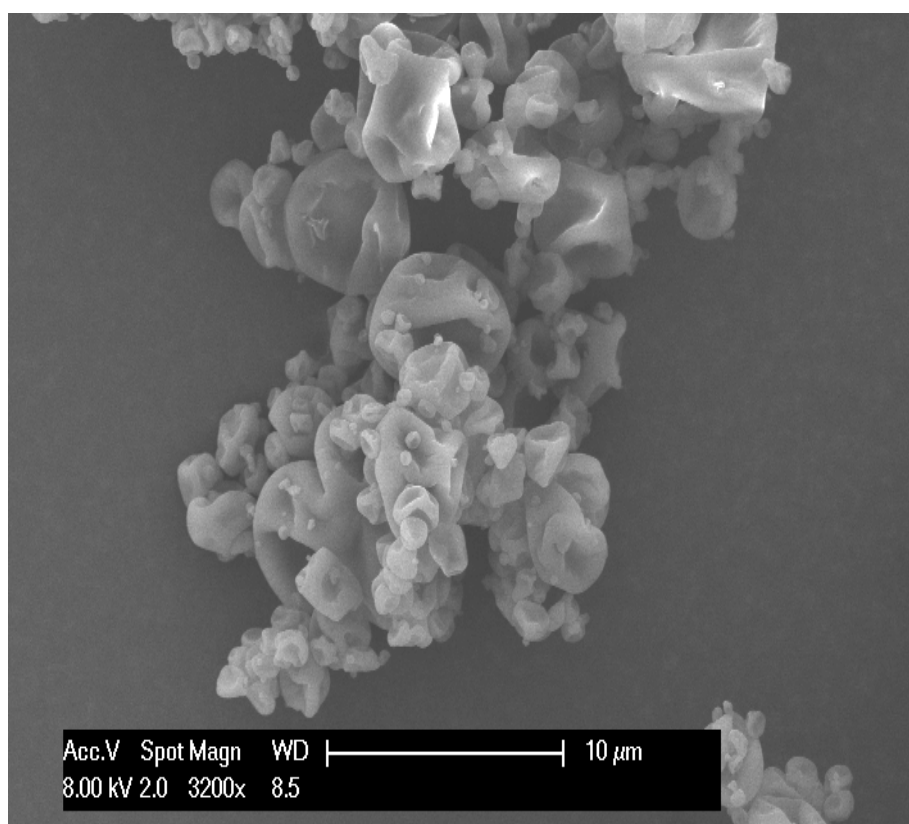
SEM analyses were carried out for all samples. SEM images of three spray-dried ASDs are presented in Figure 43. Firstly, from SEM analyses, it was not possible to distinguish the two components isolated in this new structure with uniform appearance, suggesting good mixture between both amorphous compounds. However, it was possible to observe that the physical appearance of the spray-dried particles was markedly influenced by EFV content in the binary mixture.

The SEM images revealed that the particles with higher concentration of polymer (80 wt%) have a physical shape closer to that of spray-dried particles of pure polymer (Figure 43 (A)), i.e., they have a less spherical shape and a wrinkled surface. In contrast, spray-dried ASD particles containing higher loads of EFV and then lower amounts of polymer (equal or less than 60 wt%, Figure 43 (C) and (D) respectively) are predominantly spherical with smoother surfaces.

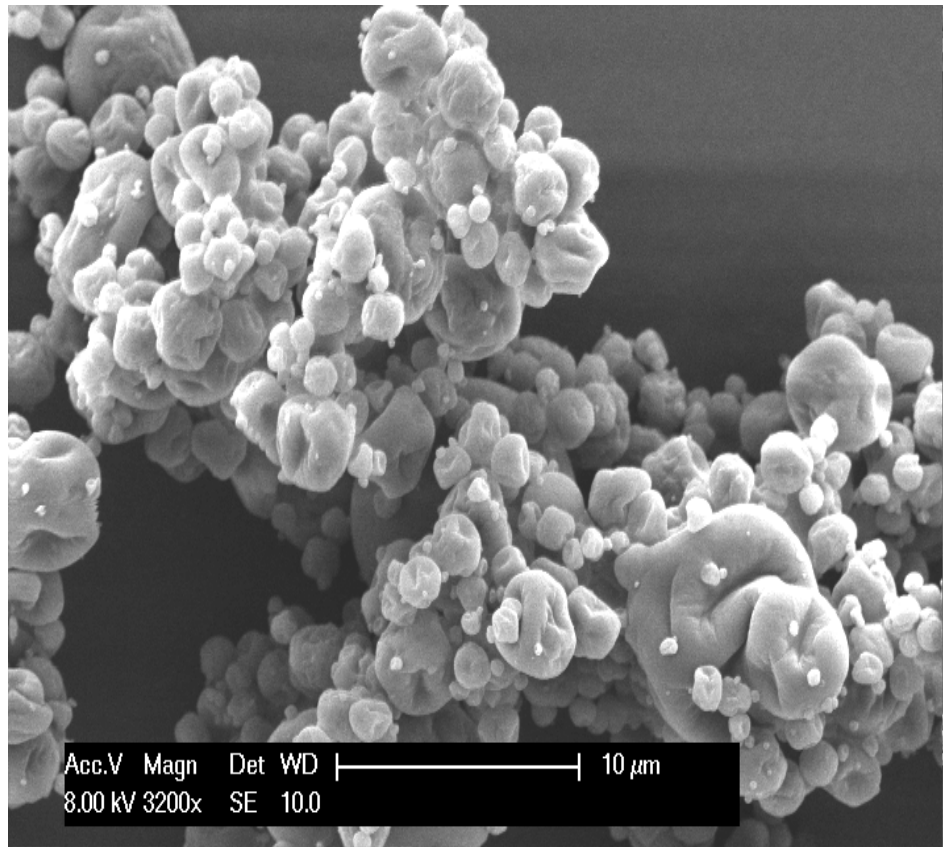
It is well known that feed concentration plays an important role in defining spray-dried morphology [13]. In order to explain the differences in physical appearances, let us consider the concentration in dissolved solids from each of these formulations before spray-drying: Spray-dried Soluplus particles (Figure 43 (A)) were generated from a liquid solution concentration of about 10 wt% in polymer. In this case, through the evaporation process of the liquid droplets with 10 wt% of dissolved polymer, their surface remained wet for a longer time creating hollow particles with a thin solid skin that could deflate resulting in a wrinkled morphology. For 20%EFV-80%SOL ASD (Figure 43 (B)) the behavior was the same due to the low total solid concentration (12.5 wt%) in the feed, as well.

In contrast, the liquid formulations generating ASDs with 40 wt% or more in EFV are more concentrated. For example, 40%EFV-60%SOL ASD (Figure 43 (C)) contains 34 wt% of total solid in the liquid feed. In this case, with higher initial liquid feed concentrations, the droplets dry with a solid surface being rapidly created, preventing further shrinkage. The same trend is expected with more concentrated liquid feeds as observed in Figure 43 (D) with 70%EFV-30%SOL ASD.

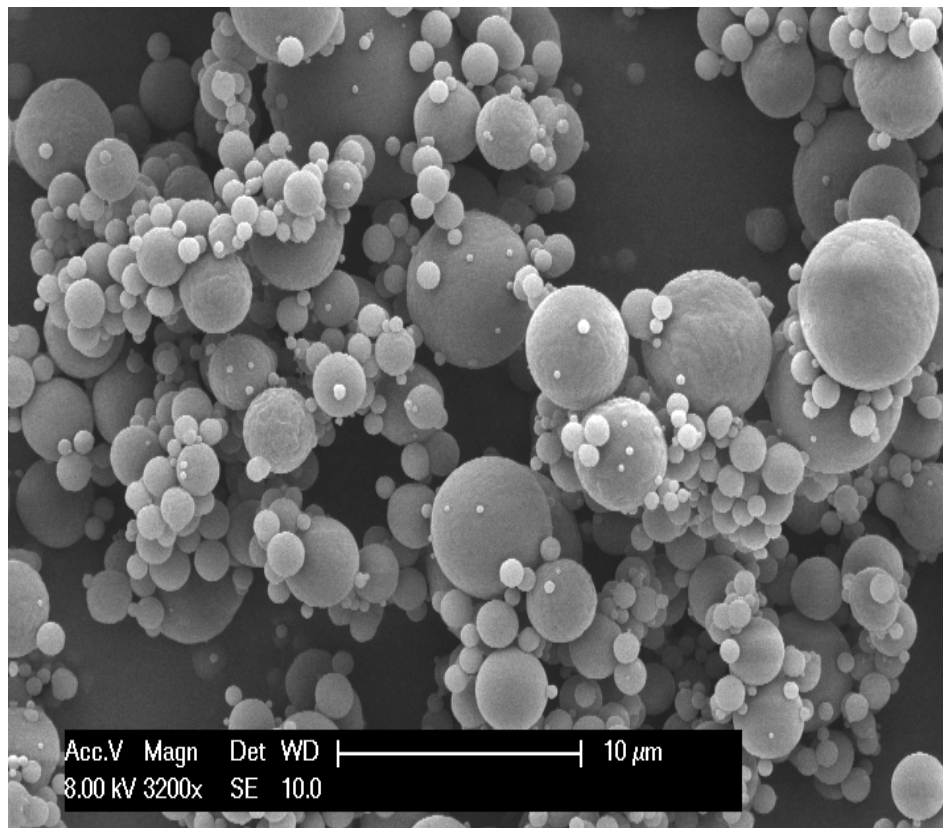
(A)



**(B)**



**(C)**



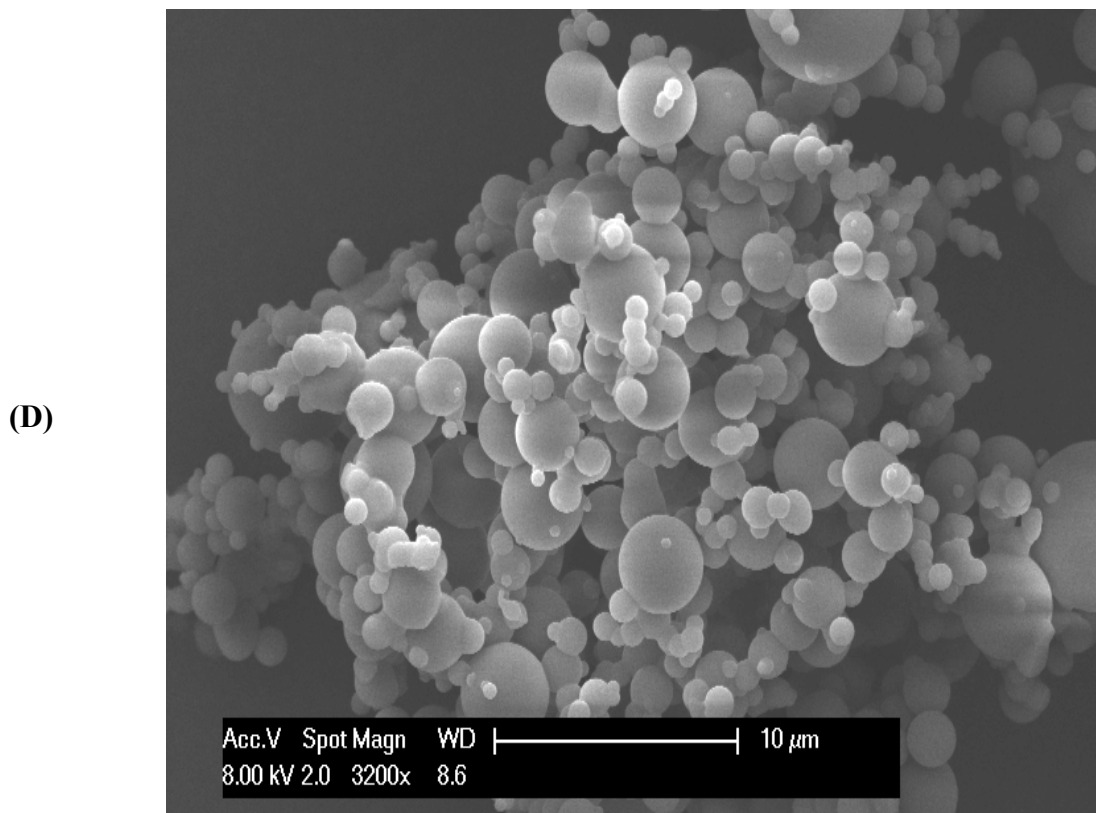


*Figure 43. SEM images of ASDs. (A) Spray-dried SOL; (B) 20%EFV-80%SOL; (C) 40%EFV-60%SOL and (D) 70%EFV-30%SOL*

#### **4.1.3. Raman Mapping**

A Raman mapping was performed to gain insight into the EFV distribution inside the polymer matrix. Figure 44 presents the Raman spectra for the spray-dried ASDs as well as for the individual components.

EFV spectrum show characteristic peaks at a wavelength around  $3100\text{ cm}^{-1}$  and  $2250\text{ cm}^{-1}$  due to amine group N-H and C-C triple bond respectively.

Soluplus spectrum show characteristic peaks around  $2987\text{ cm}^{-1}$  and  $2900\text{ cm}^{-1}$  due to C-H stretching bands. Raman spectrum revealed all EFV and Soluplus vibrations bands in the ASDs.

Still in Figure 44, 3D images represent a scan of the characteristic peak of each component in a SD sample region ( $10\text{ }\mu\text{m} \times 10\text{ }\mu\text{m}$ ). The similarity between these images for each ASD confirms the presence of Soluplus and EFV and their good distribution with a better uniformity for Soluplus. Moreover, the 3D images of the highest concentrated ASD (85%EFV-15%SOL) present a yellow area observed in 3D Raman imaging corresponding to EFV

characteristic Raman peak, not associated to Soluplus peaks as observed for the other ASD samples. This 'spot' of EFV could correspond to an API cluster in the sample, that could be expected considering the very high API load (85 wt%) in the solid analyzed.

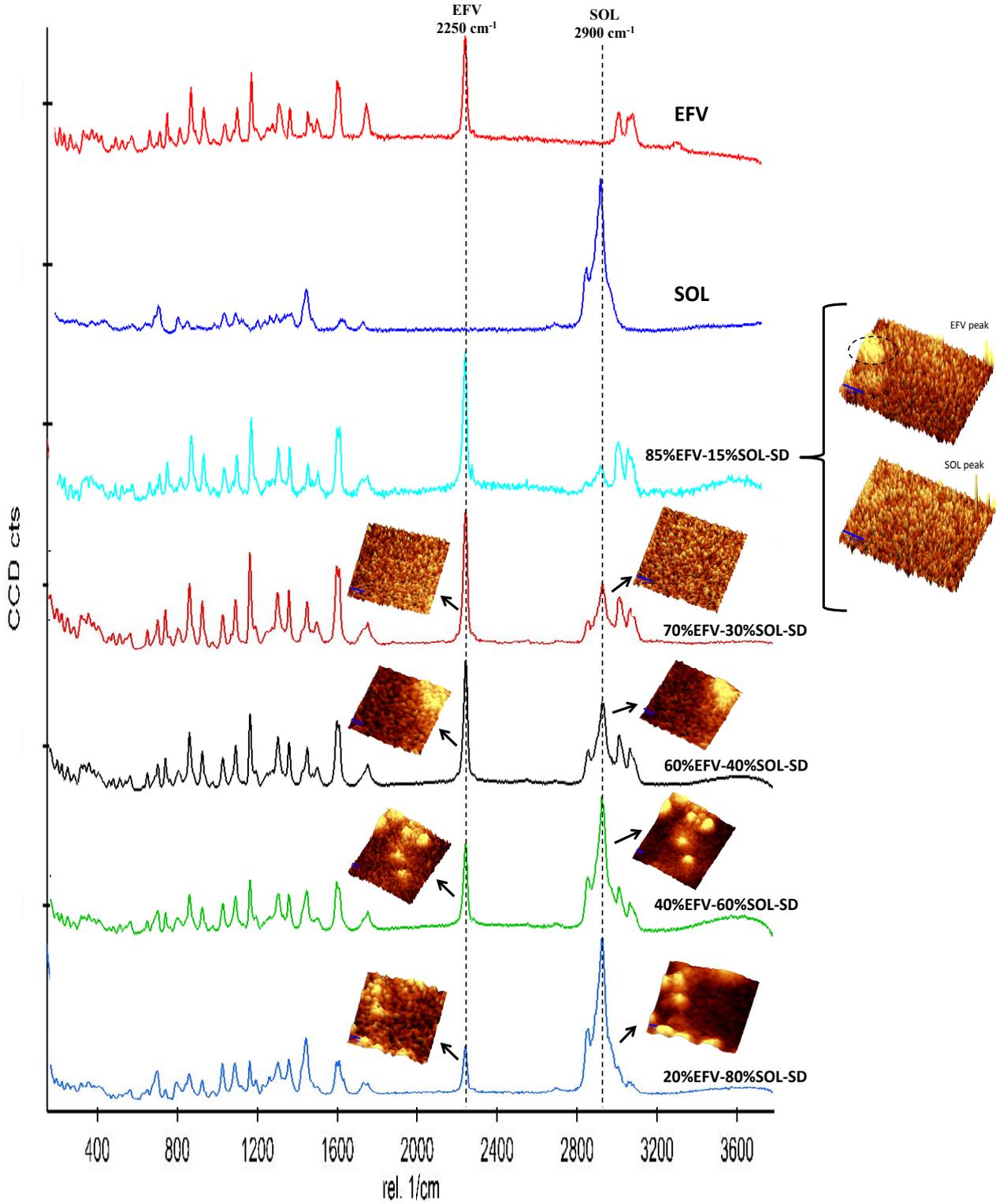


Figure 44. Spectra from Raman Spectroscopy of EFV, SOL and ASDs

#### 4.1.4. Solid state (XRD)

Solid states of ASDs were characterized by XRD analysis. XRD diffractograms for pure compounds were already presented in the previous section (Chapter 3, section 2.2.1.3). The XRD patterns obtained for all ASDs were depicted in Figure 45. In this figure, the characteristic Bragg's peaks of unprocessed EFV appeared in the  $2\theta$  range of  $5\text{--}35^\circ$  showing its high crystalline structure. However, these peaks disappeared in the spray-dried EFV-Soluplus formulations, which means that the EFV and Soluplus solubilization in ethanol, followed by the fast solvent evaporation and solidification process by spray-drying, resulted in the EFV amorphization in the binary mixture.

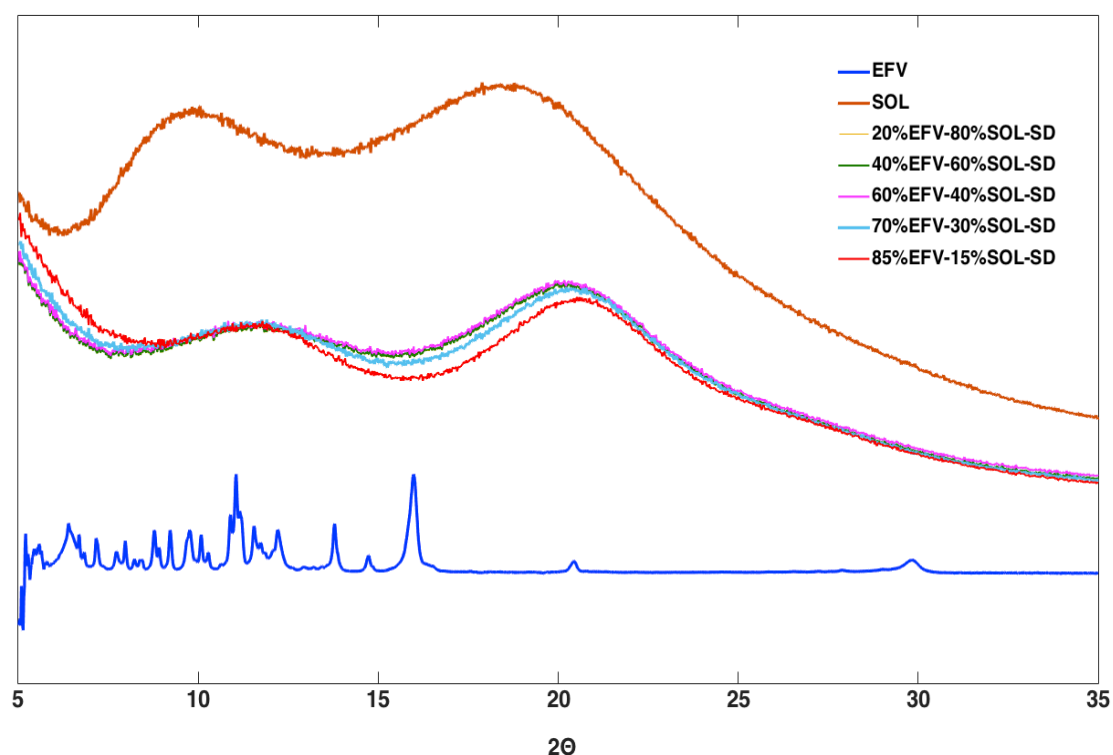


Figure 45. XRD diffractograms for pure EFV and Soluplus and for all studied spray-dried ASDs

#### 4.1.5. Glass transition temperature of binary mixtures (DSC)

$T_g$  of mixtures ( $T_{mix}^g$ ) are expected to be placed as an intermediary between the pure API and polymer values as calculated by Gordon-Taylor (GT) model already described in Chapter 2 (section 1.3.5).  $T_{mix}^g$  is calculated from GT equation based on the individual contributions of weight fraction and glass transition temperature of each component in the binary mixture,

without considering the intermolecular interactions between them. The true densities ( $\text{g}/\text{cm}^3$ ) of pure constituents were needed to calculate a value of 1.03 for K (equation 3, section 1.3.5, chapter 2).  $T_{mix}^g$  was firstly calculated for all binary mixture considered here (20 wt% to 85 wt% of EFV) and are shown in Figure 46.

EFV has a  $T_g$  close to  $36^\circ\text{C}$  that could compromise the stability of a pure amorphous phase under stability studies ( $40^\circ\text{C}$ ). The anti-plasticization effect of EFV-Soluplus binary mixtures is then demonstrated in Figure 46. They are expected to have higher glass transition temperature than the API compound by itself. The increase in the glass transition temperature of the amorphous system can result in the amorphous system being in the glassy state at room temperature. This effectively reduces the molecular mobility of the system and the crystallization rate.

Thermal analysis was also performed to determine the experimental glass transition temperature of the spray-dried mixed systems. Figure 46 shows the experimental values of  $T_{mix}^g$  obtained from reversing heat flow signals in mDSC analysis as a function of the EFV load in the spray-dried ASDs and physical mixtures of same compositions. The results showed only one  $T_{mix}^g$  for each spray-dried formulation in an intermediary band between  $T_g$  of the pure compounds, suggesting the existence of only one amorphous phase in ASDs produced by spray drying. The amorphous state of these mixtures was also demonstrated by the XRD analysis previously presented in this Chapter.

The Figure 46 also reveals, for two of the spray-dried ASDs (20%EFV-80%SOL-SD and 40%EFV-60%SOL-SD) a negative deviation of around (24% and 14%, respectively) between the experimental values of  $T_{mix}^g$  for spray-dried ASDs and the theoretical values calculated from GT model. In contrast, negative deviations from  $\text{GT}-T_{mix}^g$  were also observed for physical mixtures more concentrated in EFV (70%EFV-30%SOL-SD and 85%EFV-15%SOL-SD).

These negative deviations of experimental values from  $\text{GT}-T_{mix}^g$  could be attributed to different reasons:

- Molecular interactions between the compounds could explain this variation from the theoretical GT model as already discussed in the literature for similar findings [13];
- In the case of physical mixtures, some experimental errors in weighted amounts of individual constituents and physical composition of mixture due to the handling of small amount of powder (few mg);
- In the spray-dried samples, a plasticizing effect of water molecules adsorbed by amorphous systems;

- In the spray-dried samples, residual solvents leading to a plasticizing effect on amorphous systems.

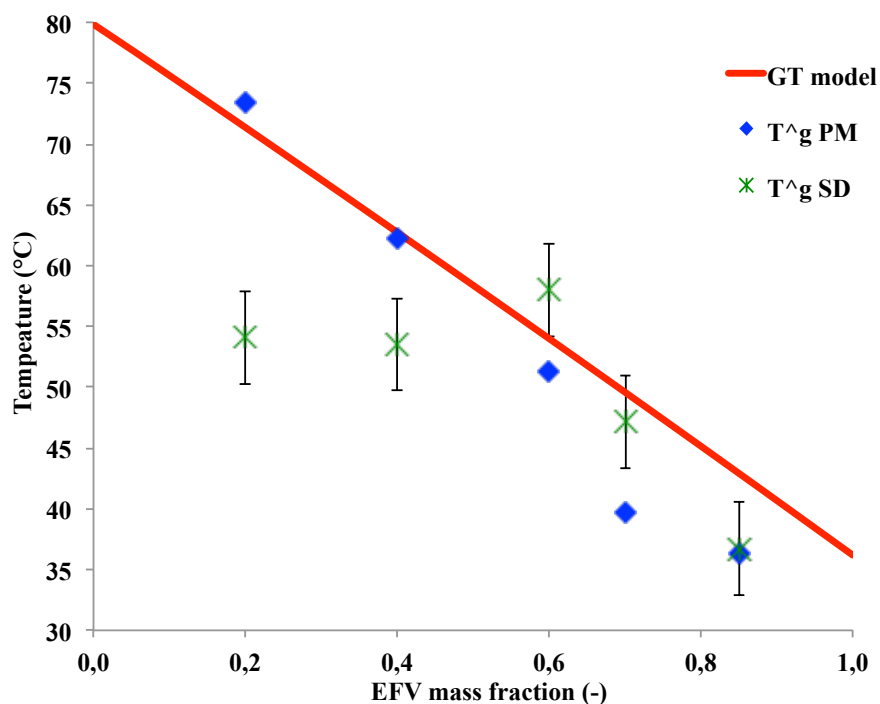


Figure 46. Mixture glass transition temperature ( $T_{mix}^g$ ): measured (green asterisks – SD and blue diamond – PM) and theoretical values by GT model (red line).

#### 4.1.6. Fourier Transform Infrared Spectroscopy (FTIR)

Figure 47 displays the FTIR spectra for ASDs, pure components and their physical mixture.

The main characteristic peaks previously reported for EFV [13]–[16] were also identified here: around 3320  $\text{cm}^{-1}$ , 2250  $\text{cm}^{-1}$ , 1750  $\text{cm}^{-1}$ , 1600  $\text{cm}^{-1}$  and 1250  $\text{cm}^{-1}$  due to the amine group N-H (stretching vibration), C-C triple bond (stretching vibration), C=O (stretching vibration), N-H (bending vibrations) and C-F stretching vibrations, respectively.

SOL spectra shows distinctive peaks in accordance to the literature [13], [17], [18]: around 3675  $\text{cm}^{-1}$  due to the hydrogen bonds O-H group, 2987  $\text{cm}^{-1}$  and 2900  $\text{cm}^{-1}$  due to C-H stretching bands, 1735  $\text{cm}^{-1}$  and 1635  $\text{cm}^{-1}$  corresponding to carbonyl bonds C=O group and 1406  $\text{cm}^{-1}$  to C-O-C stretching vibrations.

The spectral analysis of spray-dried ASDs presented some characteristic peaks of the pure components. However, some modifications can be observed in the region between 3700 – 2700  $\text{cm}^{-1}$ :

- A disappearance of a characteristic peak of Soluplus (3675  $\text{cm}^{-1}$  corresponding to O-H group) and of a characteristic peak of EFV (3320  $\text{cm}^{-1}$  corresponding to N-H);

- A broadening of Soluplus peaks at 2987  $\text{cm}^{-1}$  and 2900  $\text{cm}^{-1}$  due to C-H stretching bands.

Moreover, the characteristic peak of EFV at 1750  $\text{cm}^{-1}$ , corresponding to C=O (stretching vibration) and Soluplus peak at 1735  $\text{cm}^{-1}$  (C=O bond) are broadened in ASDs.

These changes in FTIR spectra observed in ASDs compared to the pure components or their physical mixture may be related to hydrogen bonds interaction between the proton donating groups (-NH) of EFV and the proton accepting groups (C=O) in the Soluplus®, as already proposed in literature [13].

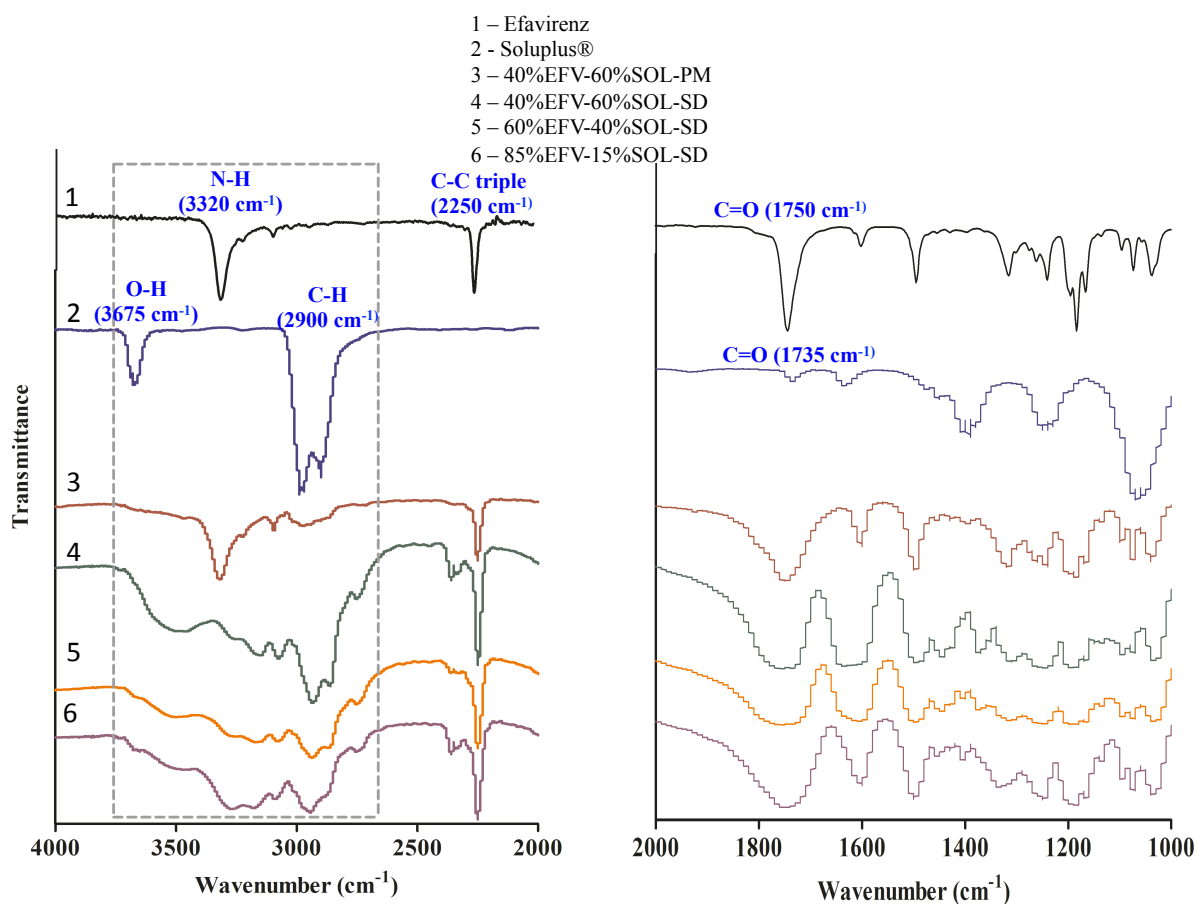
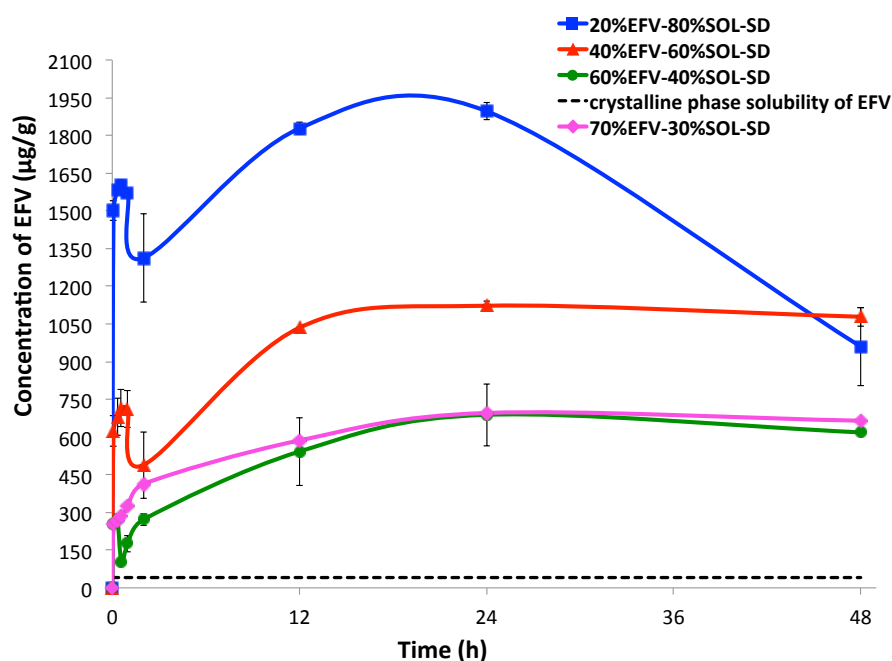


Figure 47. FTIR spectra for pure components, physical mixture and ASDs.

## 4.2. Performance behavior

### 4.2.1. Solubility studies

For the ASD to be effective in enhancing the API (kinetic) solubility in an aqueous medium, an appropriated API-carrier proportion is desired. It would be more advantageous if carrier is used in minimal amounts. The ability of the different spray-dried ASD compositions to generate and maintain supersaturated EFV solution was assessed by kinetic solubility measurements in an aqueous medium containing 0.25% SLS at 37°C and the results are presented in Figure 48.



*Figure 48. Kinetic Solubility profiles for ASDs generated by spray drying with several API-carrier mass proportions loadings (30 wt% to 80 wt% of carrier).*

It is evident the EFV apparent solubility is enhanced for all ASDs compared to the equilibrium solubility of the crystalline EFV also represented in Figure 48 (dark dashed line). However, before comparing the concentration of EFV in solution at predetermined time intervals to observe the solubilization effect of Soluplus, let us to start by analyzing the kinetic solubility profiles shown in Figure 48. This figure reveals that the solubilization of EFV from water-soluble Soluplus is almost instantaneous, resulting in an initial surge of EFV concentration followed by a sharp decline due to the nucleation and crystallization events triggered by the rapid build-up of API supersaturation. An oscillatory behavior is detected in the solubility profiles for ASDs with until 2h of experiment, for ASDs with EFV loads equal

and higher than 40 wt%. This behavior might be explained by an attempt of samples stabilization, owing to the samples exhibited the follow behavior: solubilization, recrystallization and solubilization.

Spray-dried ASDs with 30 wt% to 60 wt% carrier attained the higher supersaturation level in solution around 24h, which was maintained for at least 48h (end of the experiment). In contrast, the ASD with the highest amount of carrier (80 wt%) exhibited a spring-parachute effect not observed for the other ASD formulations: a maximum kinetic EFV solubility was attained around 24h, followed by a sharp reduction in the dissolved EFV amount in the medium.

Spring (initial dissolution step) and the parachute (supersaturation maintenance step) effects are two sequential and distinctive processes mediated by the API amorphous state properties (solubility, dissolution rate), carrier characteristics (solubilizing capacity, dissolution rate, amphiphilicity) and interaction between them [19], [20]. The reason for the less effectiveness of the 20%EFV-80%SOL ASD in maintaining the maximum supersaturated level of EFV in solution is probably related to concentration effects of Soluplus on micelle size and thermoresponsive behavior at the temperature of 37°C, nearly its LSCT (40°C) [21]. This assessment is based in some evidences found in literature: In an aqueous dissolution medium, Soluplus enters in the solution as a single polymer chains which then arrange into uni-chain polymer micelles [22], [23]. Linn (2011), in his PhD work, have characterized Soluplus micelles considering the effects of temperature (25°C and 37°C) and Soluplus concentration (0.01 to 100 mg/mL) on micelles size. It was observed that at 37°C the micelle size increased with increasing Soluplus concentration, leading to a beginning aggregation at this point (multi-chain polymer micelles), even lower its LCST. This trend was increased at Soluplus concentrations higher than 75 mg/mL [23].

As already discussed, due to hydrophilic and hydrophobic functionalities in its chains, Soluplus displays solubilizing properties through micelle formation in solution [22]. In polymer micelles the soluplus polycaprolactam moieties might create hydrophobic pockets to accommodate EFV molecules; polyethylene glycol groups located on the external surface of colloidal micelle usually provides to micelle solubility. As a consequence, the final result for this carrier, proposed to improve the release of the embedded API, could depend on the relative weight of these opposite parameters, as already demonstrated by Cavallari et al. [24] highlighted by the dynamic solubility profile of spray-dried ASD prepared with the highest Soluplus concentration (80%) shown in Figure 48.

Figure 49 (A and B) compares the solubilizing effect of spray-dried ASDs (20 wt% and 40 wt% EFV) with physical mixtures of EFV and Soluplus with similar compositions. Also,

for the corresponding physical mixture, the EFV solubility exhibited an increasing effect dependent on the carrier concentration, however, the markedly improvement in solubility of the API obtained with both ASDs can be mainly attributed to the amorphous dispersions (absence of crystal lattice to disrupt compared to crystalline EFV in the physical mixture), in addition to the solubilizing action of Soluplus, which helped EFV to achieve micelle solubilization.

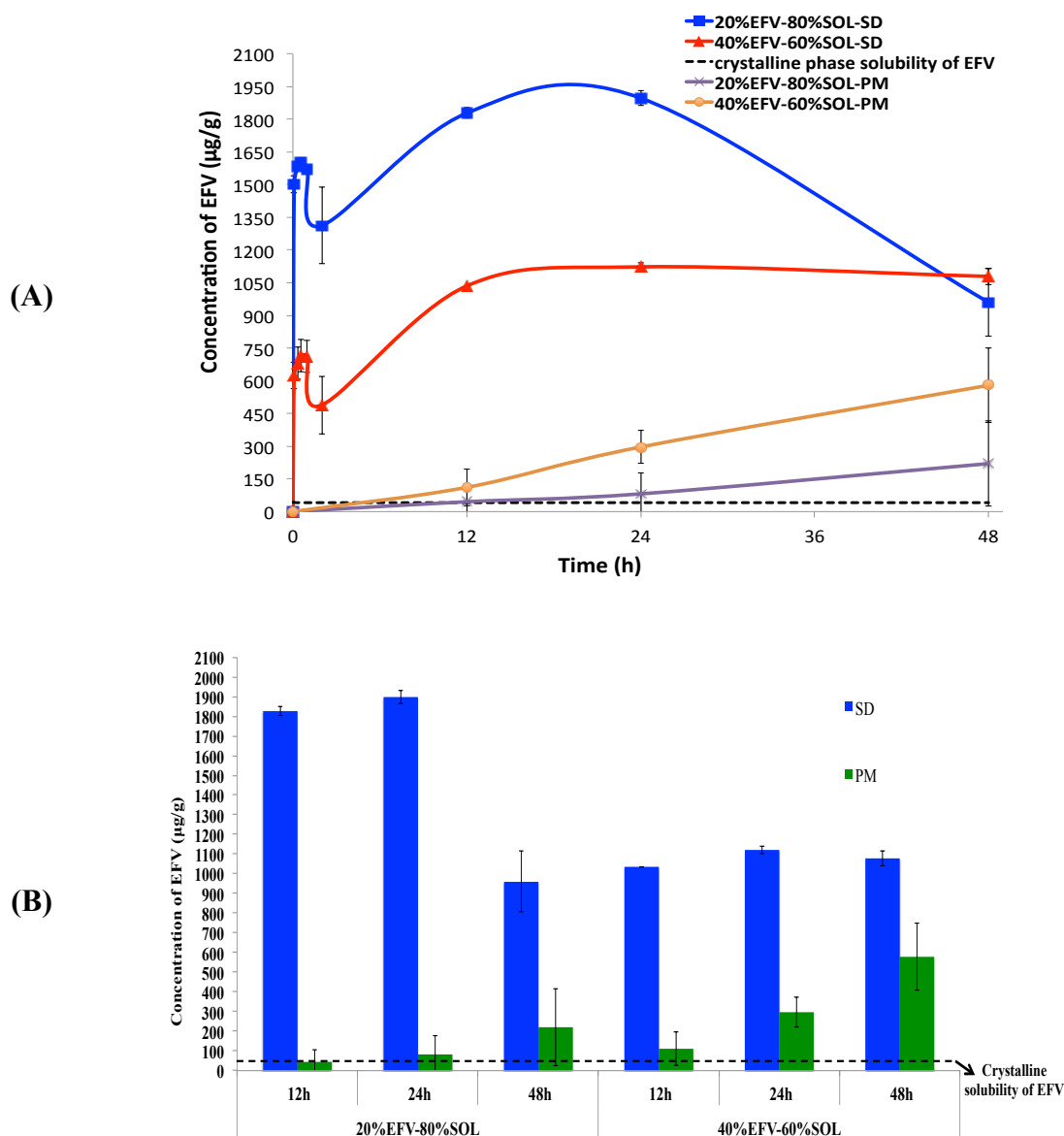


**Figure 49. Comparison between kinetic solubility profiles for spray-dried ASDs and physical mixtures (PM) with similar API-carrier compositions**

As so many works have reported, Soluplus has been efficient to improve the kinetic solubility of some APIs [13], [17], [24]–[27]. This trend is also confirmed by our results grouped in Figure 50 from all spray-dried ASDs as a function of time. Also the values declined

with an increase in the polymer concentrations, further illustrating the solubilization effect of Soluplus.

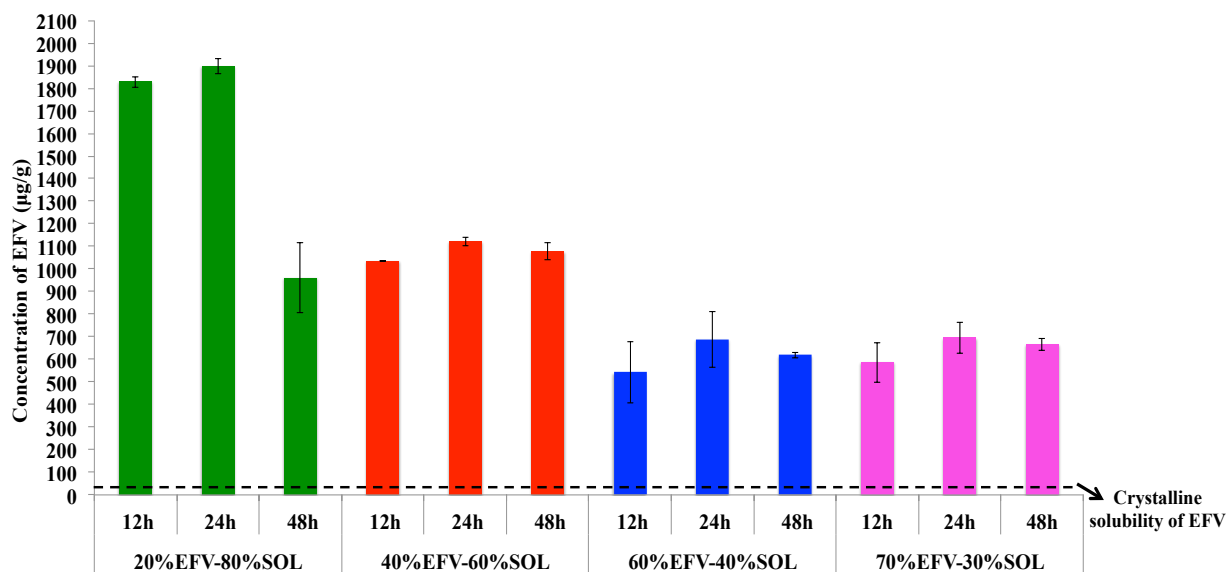


Figure 50. Kinetic solubility profiles for all spray-dried ASDs

#### 4.2.2. Dissolution studies

In order to evaluate the mechanisms of API release, dissolution tests were realized under sink and non-sink conditions. SI was previously calculated to define the dissolution conditions. The equilibrium solubility of crystalline EFV ( $C_S$ ), already presented in Chapter 3 (section 3.1.1), is 41.04 – 9.38 µg/g at 37.0 ± 0.5 °C in 0.25% SLS aqueous dissolution medium. In Figure 51, the dissolution profiles for all spray-dried ASDs studied are represented. Dissolution parameters such as percentage of EFV dissolved in 360 minutes and  $DE_{360}$  for the samples that attained 100 % of cumulative release are given in Table 19.

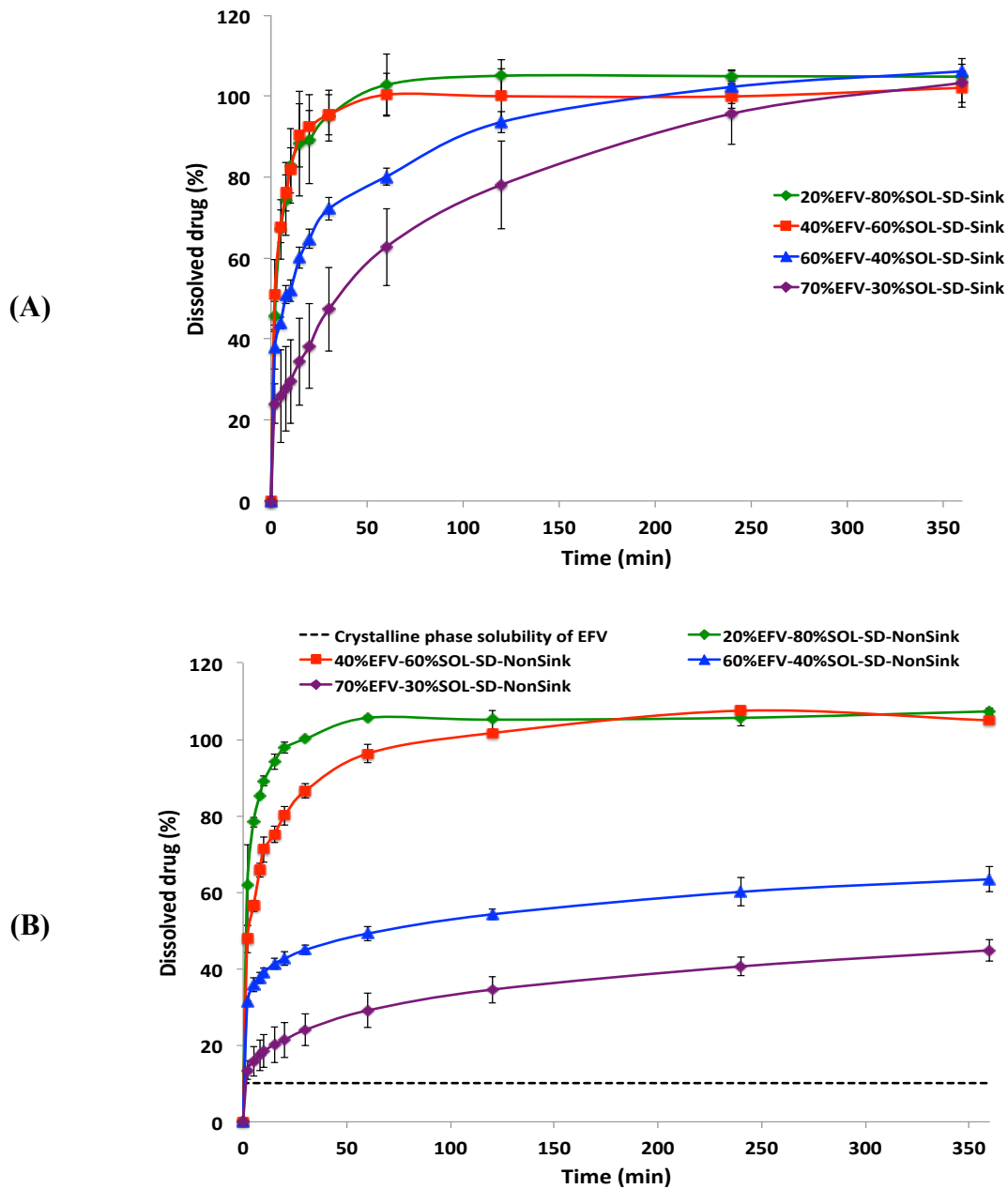


Figure 51. In vitro dissolution profiles for all ASDs. (A) Sink conditions (B) non-Sink conditions

*Table 19. Summary of dissolution key parameters under Sink and non-Sink conditions*

<b>Dissolution conditions</b>	<b>Sample</b>	<b>Cumulative Release<sub>360</sub> (%)</b>		<b>Dissolution Efficiency<sub>360</sub> (DE - %) (n=3)*</b>
<b>Sink</b>	20%EFV-80%SOL-Sink	104.83	3.0	98.07
	40%EFV-60%SOL -Sink	102.09	3.6	98.20
	60%EFV-40%SOL -Sink	106.14	0.2	91.10
	70%EFV-30%SOL -Sink	103.32	6.0	80.70
<b>Non-Sink</b>	20%EFV-80%SOL- NonSink	107.35	0.8	98.94
	40%EFV-60%SOL- NonSink	104.99	0.5	96.51
	60%EFV-40%SOL- NonSink	63.43	3.3	-
	70%EFV-30%SOL- NonSink	44.86	2.8	-

- Values represent the mean of three independent determinations.

Analyzing the Figure 51 and Table 20, in all cases, the spray-dried solid dispersions exhibited faster and almost complete dissolution under sink conditions (Figure 51 (A)). Indeed, the dissolution efficiency DE decreases gradually with increasing EFV load in ASD samples.

According to the Pharmacopeia, a compound can be considered soluble in an aqueous medium if 85 wt% of its highest clinical dose is dissolved in less than 30 min [28], [29]. To be considered as an immediate release, the API amount dissolved in the dissolution medium should be at least 80% in 15 min [23]. Table 20 presents the percentage of EFV released in 15 min.

Table 20 shows, for example, that ASD with 20%EFV-80%SOL presented a rapid and efficient release (more than 88 wt% of API) in 15 min, under both sink and non-sink conditions. For all other spray-dried ASD studied, the cumulative EFV release was dependent on the dissolution condition (sink or non-sink), being lower for non-sink conditions as observed for 60%EFV-40%SOL and 70%EFV-30%SOL ASDs. The reason could be the exposition of the dissolving solids to a medium with a high level of supersaturation, in which the release becomes controlled by dissolution of the API.

Few studies have reported the dissolution performance of EFV in Soluplus matrix [13], [30] and until now, no studies were realized comparing sink and non-sink dissolution. The transformation of amorphous state into crystalline structures during the dissolution process has

been considered a limiting factor in the development of amorphous solid dispersions since the recrystallization in the biological environment can directly influence the drug absorption present in these systems [13]. Non-sink conditions are better representative of the in vivo conditions.

*Table 20. EFV cumulative percentage released in the dissolution medium in 15 min*

Dissolution conditions	Sample	Cumulative Release (%)	
Sink (SI= 3)	20%EFV-80%SOL-Sink	88.24	12.90
	40%EFV-60%SOL -Sink	90.28	7.86
	60%EFV-40%SOL -Sink	60.09	2.58
	70%EFV-30%SOL -Sink	34.43	10.83
Non-Sink (SI= 0.1)	20%EFV-80%SOL- NonSink	94.24	2.04
	40%EFV-60%SOL- NonSink	78.15	2.18
	60%EFV-40%SOL- NonSink	41.32	1.37
	70%EFV-30%SOL- NonSink	20.20	4.69

To determine the mechanism of EFV release from spray-dried ADS systems, the first 60% drug release data from all SDS formulations were fitted by Korsmeyer–Peppas model (Equation 14, Chapter 2) [31]–[33] . Nonlinear regressions were applied for cumulative dissolved drug.

From the obtained results (Table 21) it is observed that EFV release from ASDs is well described mathematically by the Korsmeyer-Peppas, considering the values of  $R^2$ , AIC and RMSE determined using KinetDS 3.0 rev. 2010 software, Krakow, Poland.

*Table 21. Summary of results obtained after after the kinetic fitting by Korsmeyer-Peppas model*

	Sample	$K_K$ ( $\text{min}^{-n}$ )	$R^2$	n	AIC	RMSE
<b>Sink</b>	20%EFV-80%SOL-Sink	36.79	0.999	0.35	13.18	1.57
	40%EFV-60%SOL -Sink	42.20	0.999	0.29	5.36	0.59
	60%EFV-40%SOL -Sink	30.61	0.996	0.25	19.85	1.17
	70%EFV-30%SOL -Sink	13.97	0.993	0.36	41.41	2.66
<b>Non-Sink</b>	20%EFV-80%SOL- NonSink	51.72	0.999	0.26	-8.05	0.08
	40%EFV-60%SOL- NonSink	39.09	0.998	0.25	14.64	1.29
	60%EFV-40%SOL- NonSink	28.42	0.969	0.17	13.62	0.43
	70%EFV-30%SOL- NonSink	10.54	0.977	0.25	10.10	0.39

Korsmeyer-Peppas is a semi-empirical equation to describe drug release from pharmaceutical polymeric systems when the drug release involves more than one release phenomenon or unknown mechanisms. Based on this, the exponent (n) is used to characterize different release mechanisms. All values of exponent (n) determined from Korsmeyer-Peppas model were  $< 0.5$ , suggesting Fickian diffusion as the mechanism of drug release from all formulations. The penetration of the dissolution medium will be controlled by the diffusion through the polymer layer around the drug molecularly dispersed in the solid dispersions.

All the graphs for the fitting model are reunited in Appendix 3.

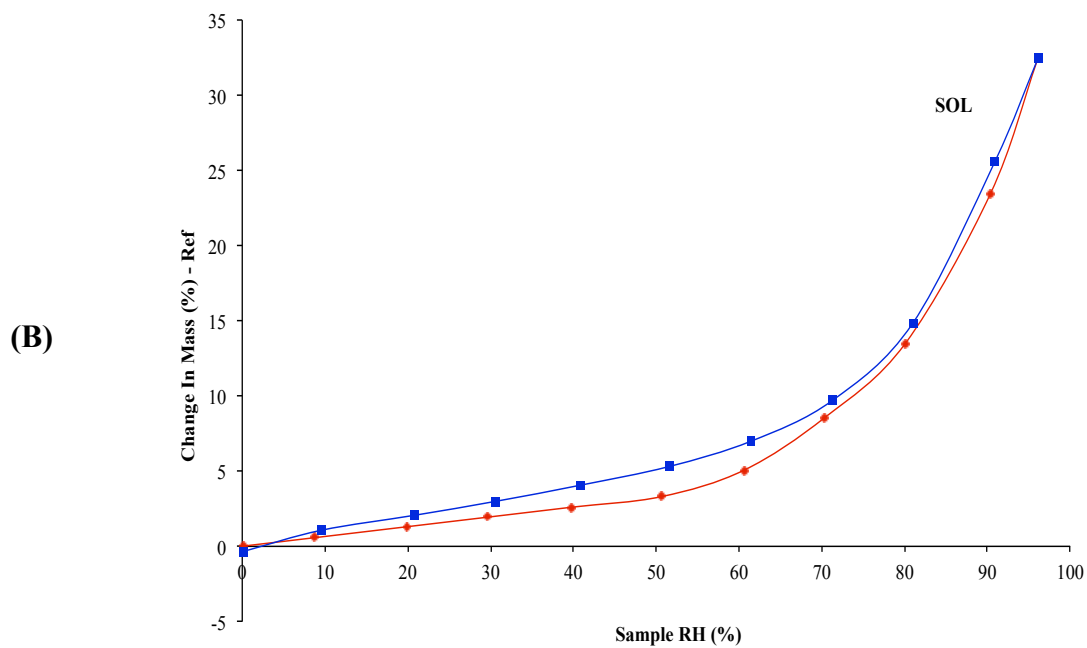
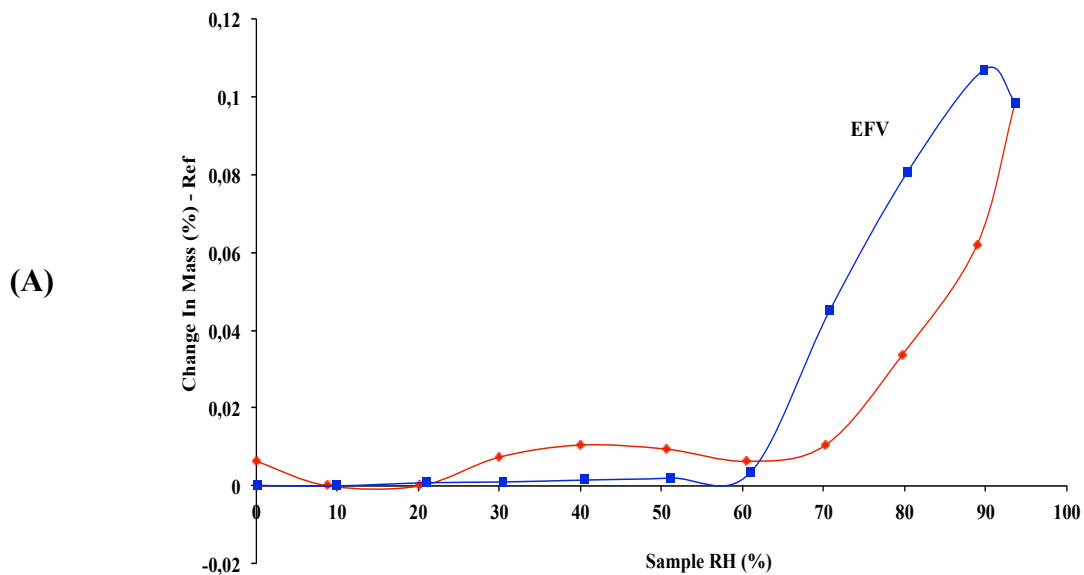
#### **4.2.3. Physical Stability**

Stability of ASDs can be directly influenced by water uptake during downstream processing and storage. The aim of this study was firstly to evaluate the effect of polymer carrier (Soluplus) and formulation parameters (EFV:Soluplus mass proportion) on the water uptake properties of the amorphous solid dispersions generated by spray drying.

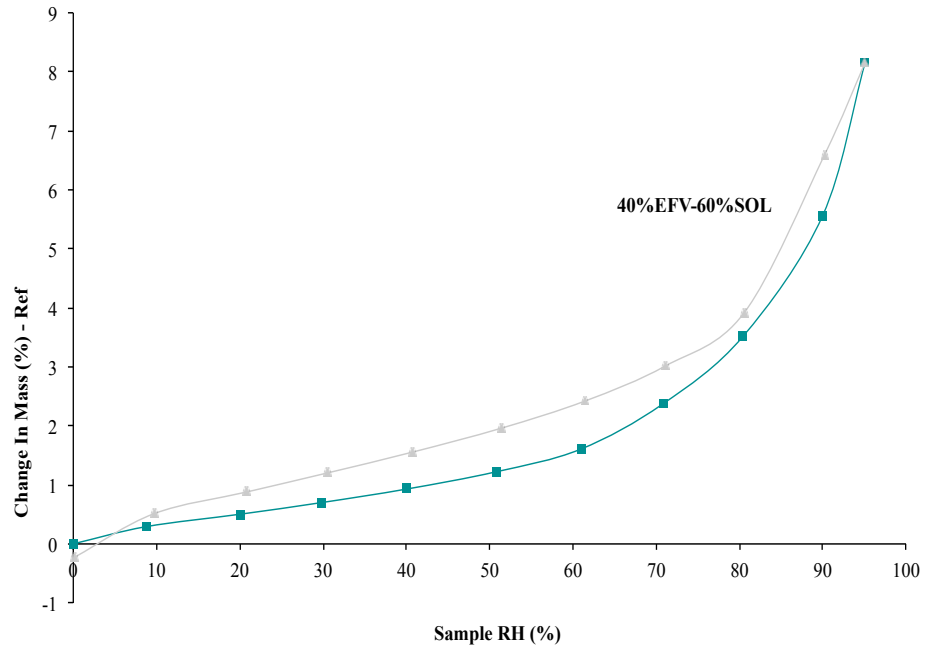
- Dynamic vapor sorption (DVS)

A water sorption isotherm at 25°C was used to obtain information about the affinity between the analyzed powders and water, upon exposure to stressed humidity. The general shape of the isotherm, reversibility of moisture uptake, presence and shape of a hysteresis loop provide information on the manner of interaction of the solid with water [34], [35]. Figure 52

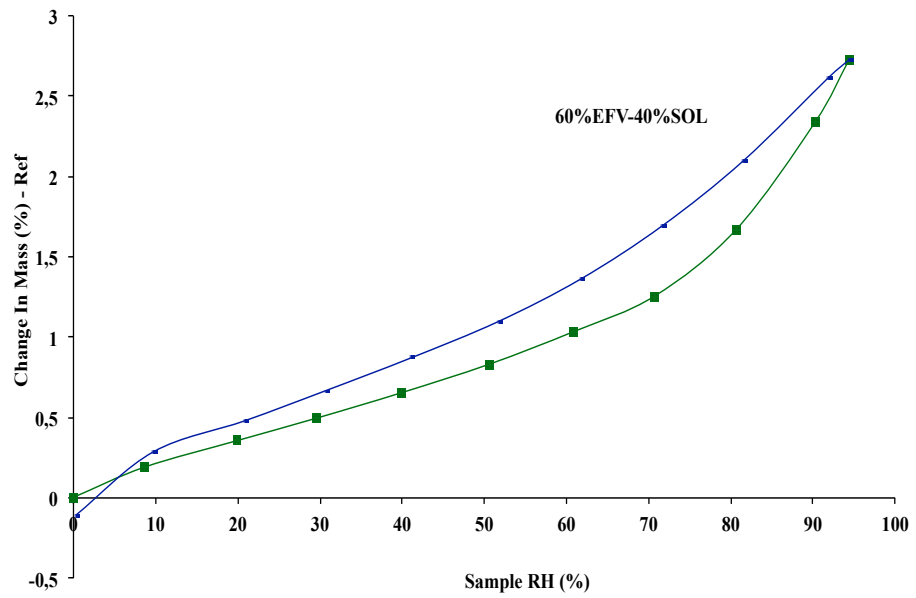
displays the DVS isotherm plots for the studied samples, showing the change in mass percentage as a function of changing relative humidity (RH) in the range 0% to 95%RH.



(C)



(D)



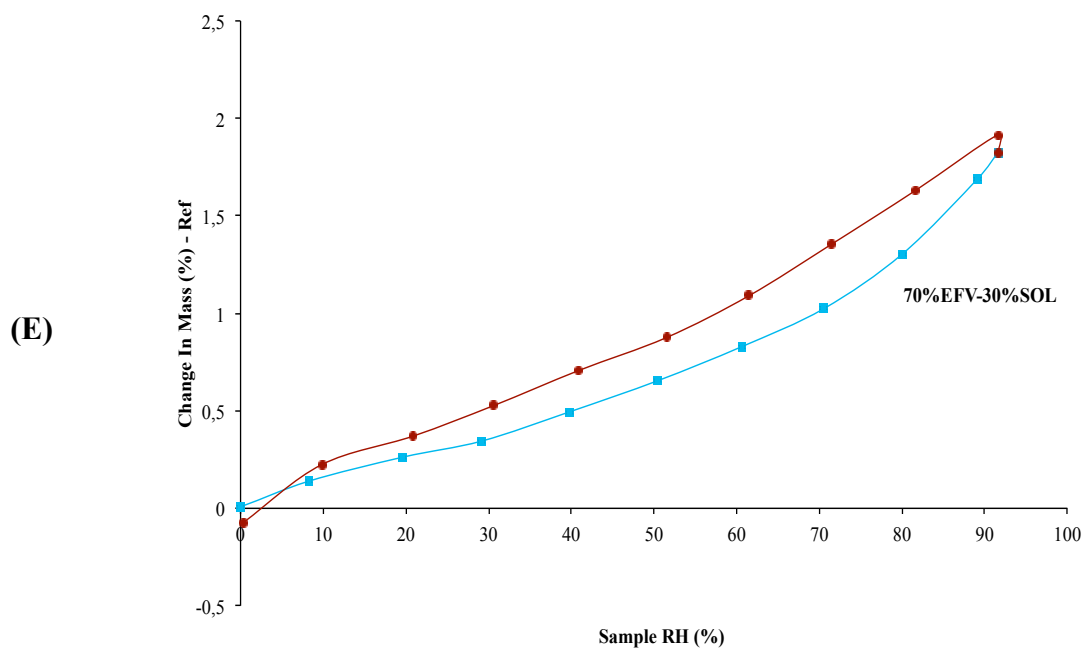


**Figure 52. DVS sorption isotherms at 25°C for spray dried samples, demonstrating the weight change (%) as a function of the relative humidity (%) for each sample: (A) EFV; (B) Soluplus; (C) 40%EFV-60%SOL ASD; (D) 60%EFV-40%SOL ASD; (E) 70%EFV-30%SOL ASD.**

Firstly, the hydrophobic character of the pure API was demonstrated by the low sorption of water in Figure 52 (A). Our results showed that the water content of pure API did not reach more than 0.1% change of mass at 95%RH. At 25°C, the sample is in its amorphous glassy state ( $T < T_g$ ) and the very low uptake level is mainly due to surface adsorption.

In contrast, amorphous solids like spray-dried Soluplus can absorb significant amounts of moisture as shown by its measured water sorption isotherm (32.4% change of mass at 95% RH, Figure 52 (B)). The measured sorption is a contribution of both adsorption (surface phenomenon) and absorption (volume phenomenon). Water vapor is absorbed into structure of amorphous solids and not simply adsorbed on the surface. Water absorbed can act as a plasticizer and increase molecular mobility due to the breakage of hydrogen bonds between molecules [36]. Although water vapor sorption is reversible, the hysteresis observed between the sorption and the desorption isotherm for the spray dried Soluplus is probably due to a slow diffusion-controlled bulk desorption process.

In turn, spray-dried ASDs were more sensitive to environmental moisture than the pure API. However, all ASDs sorbed little moisture (Table 22) over the RH 0-95%. As shown in Figure 52 (C) to Figure 52 (E), the % change in weight was not more than 1.60% at 60% relative

humidity and not more than 2.94% at 75% relative humidity for all studied spray-dried ASD systems.

**Table 22. Summary of water uptake (%) for spray dried ASDs in the different relative humidity (60%, 75%, 85% and 95% RH) at 25°C.**

Sample	Relative Humidity (RH), %			
	60	75	85	95
Efavirenz	0.01	0.02	0.05	0.10
Soluplus	5.07	11.04	18.49	32.43
40%EFV-60%SOL	1.60	2.94	4.54	8.16
60%EFV-40%SOL	1.03	1.46	2.00	2.73
70%EFV-30%SOL	0.83	1.17	1.50	1.83

The water sorption isotherm of binary mixtures can be predicted by assuming additivity of the individual component isotherms. Assuming that there is no interaction between the components, the moisture isotherm of an EFV-Soluplus binary mixture can be calculated using the equation:

$$W_{MIX} = \frac{W_{PA} m_{PA} + W_P m_P}{m_{PA} + m_P} \quad (4)$$

Where **W** is the mass of sorbed water per dry mass of solid and **m** is the component mass in the mixture [37]. On the other hand, if EFV and Soluplus interact with each other, a deviation from the ideal behavior implied by Equation 3 would be observed and the extent of the deviation can be regarded as a measure of the strength of the EFV-Soluplus interaction.

In fact, when the water amount up taken by the ASD systems are compared to the data calculated from Equation 3 using pure-components, a decrease of the amount of water up taken could be observed for all cases as represented in Figure 53. The lower sorption in the spray-dried ASDs compared to the predicted from Equation 3 for the EFV-Soluplus binary system, is possibly due to EFV-Soluplus interactions in the solid dispersions, already indicated by FTIR analysis.

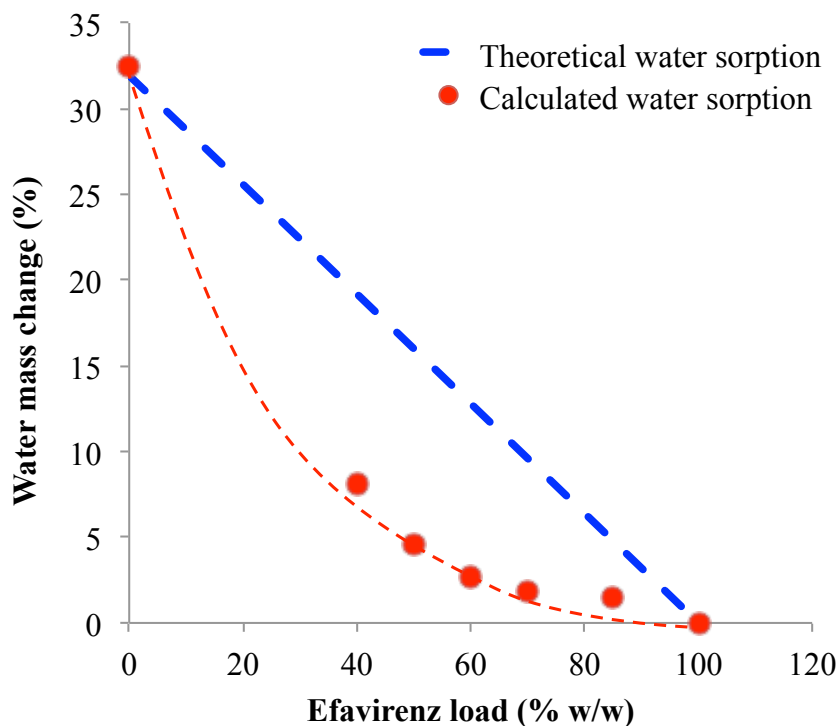


*Figure 53. Water mass change of the ASDs compared with theoretical water sorption at 95% RH.*

- Stability studies at accelerated stability condition (40°C/75% RH)

Stability studies were performed in accordance to the ICH guidelines at accelerated stability condition 40°C/75% RH with two spray-dried ASD samples containing different EFV loadings: 40 wt% and 70 wt%.

Samples were monitored by DSC analysis each 3 days, within 15 days. The results are grouped in Table 23. It is noticeable that the samples have evolved over time since  $T_{\text{mix}}^{\text{e}}$  increases in both cases.

This behavior suggests some variation in the amorphous mixture composition. However, any particular signs of amorphous phase separation like emerging of a second  $T_g$ , or drug recrystallization were detected by DSC analysis for the sample loaded with 40%EFV-60%SOL.

Contrarily, the 70%EFV-30%SOL sample revealed an evolution of crystallization enthalpy ( $\Delta H$ ) over time, corresponding to a partial EFV recrystallization. Considering  $\Delta H=52.83$  J/g for the unprocessed EFV crystals, it was possible to estimate the percentage of EFV recrystallized during the stability test duration. Table 23 also shows that, after 15 days of storage, approximately 7.79% of the amorphous EFV dispersed in soluplus recrystallized (calculated according Equation 1, Chapter 3).

**Table 23. Stability results under stress conditions (40 °C/75 % RH)  
for EFV-SOL ASDs with API loads of 40wt % and 70 wt%**

	<b>40 % EFV- 60% SOL- SD</b>	<b>70 % EFV-30% SOL- SD</b>		
<b>t (days)</b>	$T_{mix}^g$ (°C)	$T_{mix}^g$ (°C)	<b>Crystallization enthalpy <math>H_{PA}</math> (J/g)</b>	<b>Crystallization (%)</b>
3	59.8	51.4	1.3	2.89
6	64.9	53.4	2.6	5.79
9	64.1	55.9	2.8	6.24
15	67.2	57.7	3.5	7.79

## 5. Conclusion

Supersaturated ASDs, in a large range of API concentration, loaded up to 85 wt% in API, could be generated by spray drying. The amorphous state of all binary mixtures was confirmed by XRD and DSC analysis.

The two components seem to be well spatially distributed in most of the spray-dried ASDs as demonstrated by Raman mapping. However, high API loads might generate supersaturated systems in which the amorphous EFV in excess is distributed as amorphous clusters in the sample (as observed for 85%EFV-15%SOL-SD).

The solubilization effect of Soluplus and the ability of this carrier to generate and maintain supersaturated EFV solutions were demonstrated. However, this effect depends on the Soluplus concentration in the spray-dried ASD and can be limited if high concentrations of this carrier are used, as observed for the ASD containing 80% of Soluplus.

Different dissolution profiles were generated depending on the dissolution conditions (sink or non-sink). Although these differences, all spray-dried ASDs have not shown signs of recrystallization in non-sink conditions.

Physical stability demonstrated to be a critical parameter for ASDs. The spray-dried ASDs studied here present the following characteristics favoring physical stability:

- An antiplasticizing effect of the carrier used, confirmed by the increase of  $T_{\text{mix}}^{\text{g}}$  with the increased mass proportion of Soluplus in the binary mixtures;
- Possible interactions between EFV and Soluplus, related to hydrogen bonds interaction between the proton donating groups (-NH) of EFV and the proton accepting groups (C=O) in the Soluplus.

However, we could verify under stress tests that the stability depends on the level of supersaturation of the samples. A spray-dried ASD with 70% EFV (70%EFV-30%SOL ASD) started to recrystallize in a short time experiment (15 days) during exposition to 40°C and 75%RH.



## 6. References

- [1] N.-T. Tung, C.-S. Tran, T.-L. Nguyen, T. Hoang, T.-D. Trinh, and T.-N. Nguyen, 'Formulation and biopharmaceutical evaluation of bitter taste masking microparticles containing azithromycin loaded in dispersible tablets', *Innov. Process. Bio-Pharm. Poorly Water-Soluble API*, vol. 126, pp. 187–200, May 2018.
- [2] M. T. França, R. Nicolay Pereira, M. Klüppel Riekes, J. Munari Oliveira Pinto, and H. K. Stulzer, 'Investigation of novel supersaturating drug delivery systems of chlorthalidone: The use of polymer-surfactant complex as an effective carrier in solid dispersions', *Eur. J. Pharm. Sci. Off. J. Eur. Fed. Pharm. Sci.*, vol. 111, pp. 142–152, Jan. 2018.
- [3] S. Baghel, H. Cathcart, and N. J. O'Reilly, 'Understanding the generation and maintenance of supersaturation during the dissolution of amorphous solid dispersions using modulated DSC and 1H NMR', *Int. J. Pharm.*, vol. 536, no. 1, pp. 414–425, Jan. 2018.
- [4] G. Van den Mooter, 'The use of amorphous solid dispersions: A formulation strategy to overcome poor solubility and dissolution rate', *Drug Discov. Today Technol.*, vol. 9, no. 2, pp. e79–e85, 2012.
- [5] S. Motallae, A. Taheri, and A. Homayouni, 'Preparation and characterization of solid dispersions of celecoxib obtained by spray-drying ethanolic suspensions containing PVP-K30 or isomalt', *J. Drug Deliv. Sci. Technol.*, vol. 46, pp. 188–196, Aug. 2018.
- [6] F. L. Lopez, T. B. Ernest, C. Tuleu, and M. O. Gul, 'Formulation approaches to pediatric oral drug delivery: benefits and limitations of current platforms', *Expert Opin. Drug Deliv.*, vol. 12, no. 11, pp. 1727–1740, Nov. 2015.
- [7] F. Liu *et al.*, 'Patient-Centred Pharmaceutical Design to Improve Acceptability of Medicines: Similarities and Differences in Paediatric and Geriatric Populations', *Drugs*, vol. 74, no. 16, pp. 1871–1889, 2014.
- [8] 'USP'. [Online]. Available: <http://www.usp.org/>. [Accessed: 13-Jun-2018].
- [9] O. Mahmah, R. Tabbakh, A. Kelly, and A. Paradkar, 'A comparative study of the effect of spray drying and hot-melt extrusion on the properties of amorphous solid dispersions containing felodipine', *J. Pharm. Pharmacol.*, vol. 66, no. 2, pp. 275–284, Feb. 2014.
- [10] S. N. Bhattachar, J. A. Wesley, A. Fioritto, P. J. Martin, and S. R. Babu, 'Dissolution testing of a poorly soluble compound using the flow-through cell dissolution apparatus', *Int. J. Pharm.*, vol. 236, no. 1, pp. 135–143, Apr. 2002.
- [11] H. D. Friedel *et al.*, 'FIP Guidelines for Dissolution Testing of Solid Oral Products', *J. Pharm. Sci.*, Aug. 2018.
- [12] M.-J. Chang, A. S. Myerson, and T. K. Kwei, 'The effect of hydrogen bonding on vapor diffusion in water-soluble polymers', *J. Appl. Polym. Sci.*, vol. 66, no. 2, pp. 279–291, Oct. 1997.
- [13] Z. M. M. Lavra, D. Pereira de Santana, and M. I. Ré, 'Solubility and dissolution performances of spray-dried solid dispersion of Efavirenz in Soluplus', *Drug Dev. Ind. Pharm.*,

vol. 43, no. 1, pp. 42–54, Jan. 2017.

[14] P. T. Koh, J. N. Chuah, M. Talekar, A. Gorajana, and S. Garg, 'Formulation Development and Dissolution Rate Enhancement of Efavirenz by Solid Dispersion Systems', *Indian J. Pharm. Sci.*, vol. 75, no. 3, pp. 291–301, 2013.

[15] A. Singh *et al.*, 'Development and characterization of taste masked Efavirenz pellets utilizing hot melt extrusion', *J. Drug Deliv. Sci. Technol.*, vol. 23, no. 2, pp. 157–163, Jan. 2013.

[16] A. C. C. Vieira *et al.*, 'Multicomponent systems with cyclodextrins and hydrophilic polymers for the delivery of Efavirenz', *Carbohydr. Polym.*, vol. 130, pp. 133–140, Oct. 2015.

[17] R. N. Shamma and M. Basha, 'Soluplus®: A novel polymeric solubilizer for optimization of Carvedilol solid dispersions: Formulation design and effect of method of preparation', *Powder Technol.*, vol. 237, pp. 406–414, Mar. 2013.

[18] Yidan Lan, Shaukat Ali, and N. Langley, 'Characterization of Soluplus® by FTIR and Raman Spectroscopy', 2010.

[19] N. Shah, H. Sandhu, D. S. Choi, H. Chokshi, and A. W. Malick, *Amorphous Solid Dispersions: Theory and Practice*. Springer, 2014.

[20] Y. Chen *et al.*, 'Initial Drug Dissolution from Amorphous Solid Dispersions Controlled by Polymer Dissolution and Drug-Polymer Interaction', *Pharm. Res.*, vol. 33, no. 10, pp. 2445–2458, 2016.

[21] J. Kost and R. Langer, 'Responsive polymeric delivery systems', *Adv. Drug Deliv. Rev.*, vol. 46, no. 1–3, pp. 125–148, Mar. 2001.

[22] 'Soluplus - For better solubility & bioavailability'. [Online]. Available: <https://pharmaceutical.basf.com/en/Drug-Formulation/Soluplus.html>. [Accessed: 08-Jun-2018].

[23] M. Linn, 'In vitro characterization of the novel solubility enhancing excipient Soluplus®', *In vitro Charakterisierung des neuartigen Lösungsvermittlers Soluplus®*, 2011.

[24] A. Fini, C. Cavallari<sup>1</sup>, S. Ternullo<sup>2</sup>, F. Tarterini<sup>3</sup>, A. Fini<sup>1\*</sup>, and O. Internationals, 'Release Problems for Nifedipine in the Presence of Soluplus', *J. Pharm. Pharm.*, vol. 3, no. 2, pp. 0–0, Jun. 2016.

[25] J. F. Kelleher *et al.*, 'A comparative study between hot-melt extrusion and spray-drying for the manufacture of anti-hypertension compatible monolithic fixed-dose combination products', *Int. J. Pharm.*, vol. 545, no. 1–2, pp. 183–196, Jul. 2018.

[26] J. Djuris, I. Nikolakakis, S. Ibric, Z. Djuric, and K. Kachrimanis, 'Preparation of carbamazepine-Soluplus solid dispersions by hot-melt extrusion, and prediction of drug-polymer miscibility by thermodynamic model fitting', *Eur. J. Pharm. Biopharm. Off. J. Arbeitsgemeinschaft Für Pharm. Verfahrenstechnik EV*, vol. 84, no. 1, pp. 228–237, May 2013.

[27] Y. Zhang *et al.*, 'Extruded Soluplus/SIM as an oral delivery system: characterization, interactions, in vitro and in vivo evaluations', *Drug Deliv.*, vol. 23, no. 6, pp. 1902–1911, Jul. 2016.

[28] S. Baghel, H. Cathcart, and N. J. O'Reilly, 'Polymeric Amorphous Solid Dispersions: A Review of Amorphization, Crystallization, Stabilization, Solid-State Characterization, and Aqueous Solubilization of Biopharmaceutical Classification System Class II Drugs', *J. Pharm. Sci.*, vol. 105, no. 9, pp. 2527–2544, Sep. 2016.

[29] L. X. Yu *et al.*, 'Biopharmaceutics classification system: the scientific basis for biowaiver extensions', *Pharm. Res.*, vol. 19, no. 7, pp. 921–925, Jul. 2002.

[30] J. Pawar, A. Tayade, A. Gangurde, K. Moravkar, and P. Amin, 'Solubility and dissolution enhancement of efavirenz hot melt extruded amorphous solid dispersions using combination of polymeric blends: A QbD approach', *Eur. J. Pharm. Sci. Off. J. Eur. Fed. Pharm. Sci.*, vol. 88, pp. 37–49, Jun. 2016.

[31] R. W. Korsmeyer, R. Gurny, E. Doelker, P. Buri, and N. A. Peppas, 'Mechanisms of solute release from porous hydrophilic polymers', *Int. J. Pharm.*, vol. 15, no. 1, pp. 25–35, May 1983.

[32] M. L. Bruschi, Ed., '5 - Mathematical models of drug release', in *Strategies to Modify the Drug Release from Pharmaceutical Systems*, Woodhead Publishing, 2015, pp. 63–86.

[33] P. Costa and J. M. Sousa Lobo, 'Modeling and comparison of dissolution profiles', *Eur. J. Pharm. Sci.*, vol. 13, no. 2, pp. 123–133, May 2001.

[34] S. Airaksinen, *Role of excipients in moisture sorption and physical stability of solid pharmaceutical formulations*. Helsinki: University of Helsinki, 2005.

[35] S. Airaksinen *et al.*, 'Role of water in the physical stability of solid dosage formulations', *J. Pharm. Sci.*, vol. 94, no. 10, pp. 2147–2165, Oct. 2005.

[36] B. Démuth *et al.*, 'Development and tableting of directly compressible powder from electrospun nanofibrous amorphous solid dispersion', *Adv. Powder Technol.*, vol. 28, no. 6, pp. 1554–1563, Jun. 2017.

[37] K. Punčochová, J. Y. Y. Heng, J. Beránek, and F. Stěpánek, 'Investigation of drug-polymer interaction in solid dispersions by vapour sorption methods', *Int. J. Pharm.*, vol. 469, no. 1, pp. 159–167, Jul. 2014.



Chapter 5 -  
Efavirenz/Soluplus®  
amorphous solid dispersions  
manufactured by Hot-melt  
Extrusion

---



## **1. Introduction**

HME and SD are two of most common continuous processing techniques used to produce solid dispersions, with both techniques having their own associated advantages and disadvantages [1]–[3] [3]–[5].

In most cases, one of these methods is chosen and then formulation scientists modify the formulation until the desired characteristics of the solid dispersion are achieved. However, as already discussed in Chap 2, solid dispersions prepared by different techniques can display differences in their physicochemical properties [1], [3], [5]–[7] and because of that, during early stage development of a formulation, it may be important to understand the influence of the processing technique on the desired formulation.

The main objective of Chapter 5 is to present the methods applied and the results obtained from the study of generation, by HME, of amorphous solid dispersions with similar compositions to those already prepared by spray drying and presented in the previous chapter.

One of the main objectives of this thesis is to produce EFV- Soluplus ASDs by SD and HME and to investigate how these different manufacturing techniques affect physicochemical properties, product performance and physical stability. Chap 5 closes with a comparative analysis between extruded and spray-dried ASDs with similar compositions.

## 2. Generation of EFV-SOL binary mixtures

### 2.1. Preparation methods

A Thermo-Fisher pharma 16 Extruder (Thermo scientific™, Germany) equipped with a co-rotating twin-screw parallel with five heating zones, two mixing zones and a screw diameter (D) of 16 mm and L/D ratio equal to 40 (L being the length of barrel) was used to generate the extruded samples. This pilot, shown in Figure 54, is composed by:

- Two Brabender gravimetric feeders (Germany) with different capacities. The large dosing unit has a flow rate range from 0.5 to 10 kg/h and the small dosing unit has a flow rate range from 0.05 to 2.5 kg/h. To generate the ASDs, the small dosing unit was used due to the low powder feed rate implemented (maintained at 0.25 kg/h);
- Twin-screw configuration located in the sheath allows conveying and mixing the powder. The configuration used is based on the various application requirements. The most common application of screw configurations is conveying, melting, mixing and shaping. In the feeding, conveying and venting, conveying elements are used. Then, the angles between the mixing elements can take values of 30, 60 and 90°. To generate low energy mixing when liquids are added in the melt in the barrel, distributive flow rate are used. Finally, discharge feed screws have a single lead geometry to generate the extrusion pressure to shape the final product at the die;
- A Pharmalab Data to control the operating parameters.

Operating parameters and configuration are schematically represented in Figure 55. They were defined based on a previous studies developed in our laboratory. The temperature profile giving in Table 24 was defined, based on the EFV melting temperature and also preliminary experiments (not shown).

API and polymer were previously premixed during 12 min in a powder mixer Turbula T2F, also shown in Figure 54. The physical mixtures were then exposed to 55°C in a vacuum oven during approximately 2h to evaporate residual moisture from the samples.

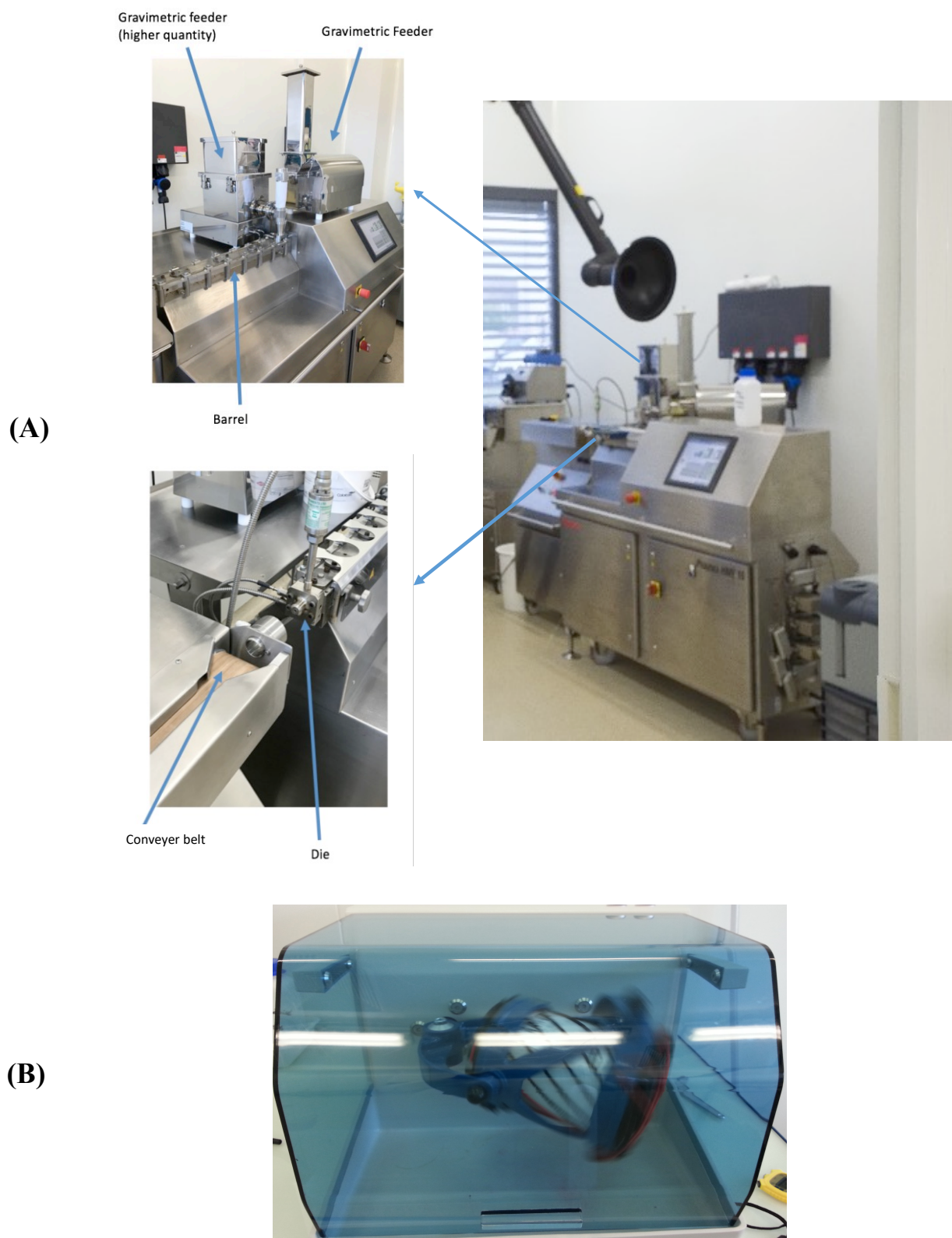


*Figure 54. (A) Thermo-Fisher Pharma 16 Extruder and (B) Powder mixer Turbula T2F*

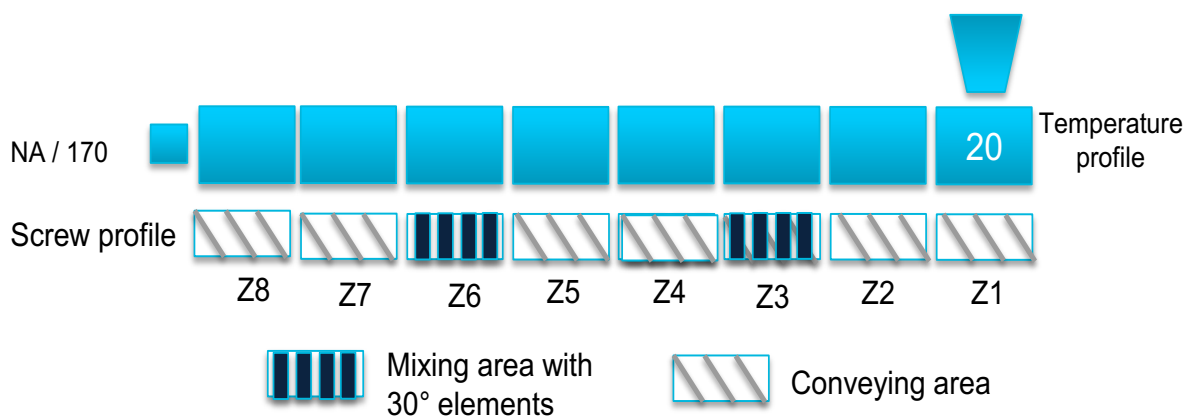


**Figure 55. Schematic representation of HME configuration u for extruded ASDs generation**  
*Process conditions: screw speed of 150 rpm; dosing rate of previously physically compounds of 0.25kg/h; die diameter of 1 mm)*

**Table 24. Temperature profile for ASDs production by Hot-Melt Extrusion process**

Sample	Die	Z7	Z6	Z5	Z4	Z3	Z2	Z1
<b>Pure Soluplus</b>	160	160	160	160	160	110	50	40
<b>20%EFV-80%SOL-HME</b>	135	135	135	135	135	90	50	20
<b>20%EFV-80%SOL-HME</b>	125	125	125	125	125	80	40	20
<b>20%EFV-80%SOL-HME</b>	110	110	110	110	110	70	40	20
<b>20%EFV-80%SOL-HME</b>	110	110	110	110	110	70	40	20

### 3. Characterization techniques

Extruded ASDs were characterized as previously performed with the spray-dried ADS samples. All techniques already described in Chapters 3 and 4, i.e., X-ray Scattering diffraction (XRD), differential scanning calorimetry (DSC), scanning electron microscopy (SEM), Raman mapping (RM) and performance behavior (in vitro drug release dissolution tests, physical stability) were also employed in this part of the work and are not presented here (see Chapters 3 and 4).

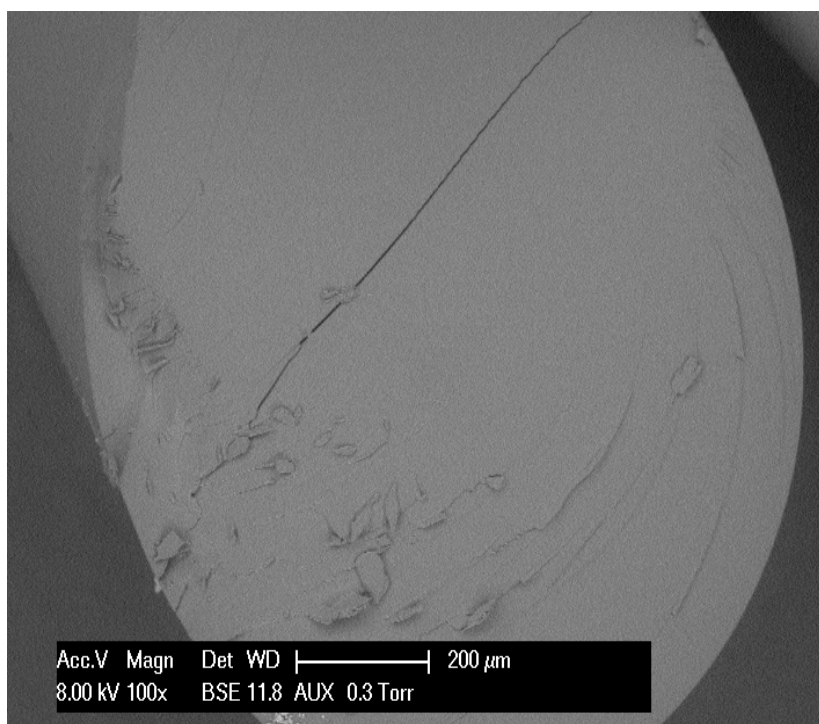
## 4. Results

### 4.1. Characterization of ASDs

#### 4.1.1. Microscopic observations

SEM and optical images were obtained from all extruded samples. The optical images were performed using a Keyence digital optical microscope equipped with polarized light. Figure 56 shows typical images of the extrudates, obtained by SEM and optical microscopy. The extruded products have around 1mm in diameter. From optical image, they are completely transparent and look like a glass (Fig. 3B). SEM image (Fig 3A) also shows uniform appearance, from which it is not possible to distinguish the two components (API and polymer).

(A)



(B)



*Figure 56. Images of extruded ASD with a charge of 70%EFV-30%SOL A) From SEM analysis and B) From optical microscopy.*

#### **4.1.2. Raman Spectroscopy**

Raman spectra of the extruded ASDs are exhibited in Figure 57.

In Chapter 4 (section 4.1.2), the characteristic peaks for pure compounds were already described. Raman spectra revealed all EFV and Soluplus vibrations bands in the ASDs, without modifications. Moreover, the intensity of Raman peaks increases with the concentration of each compound in the mixture.

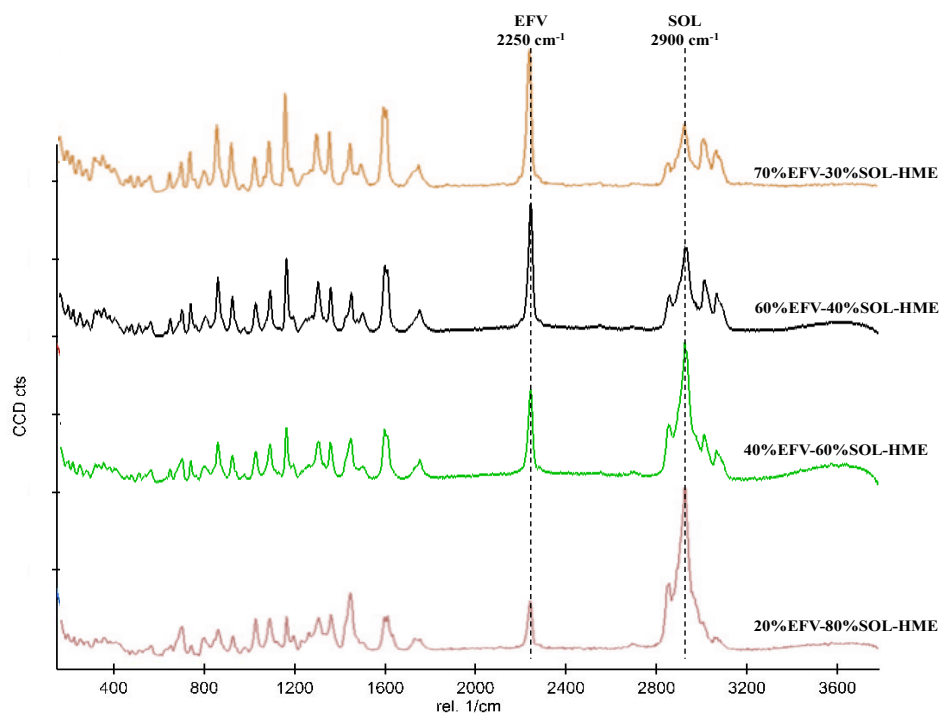


*Figure 57. Spectra from Raman Spectroscopy for extruded EFV-Soluplus ASDs*

### 4.1.3. Solid state (DRX)

The XRD patterns obtained for all extruded ASDs were depicted in Figure 58, including those for the pure compounds already presented (Chapter 3, section 2.2.1.3). The characteristic peaks of unprocessed EFV crystals disappeared in all extruded EFV-Soluplus ASDs, which means that EFV and Soluplus, after melting process, had given origin to a binary mixture between Soluplus and amorphous EFV.

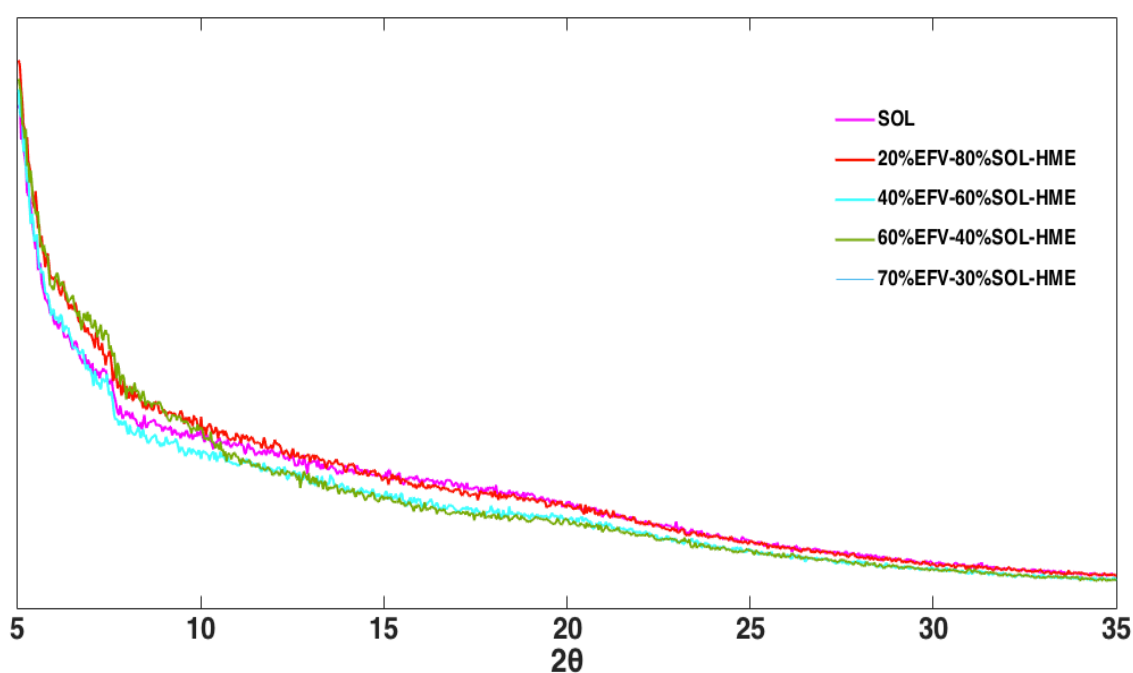


Figure 58. XRD diffractograms for extruded EFV-SOL ASDs

### 4.1.4. Glass transition temperature of binary mixtures (DSC)

Thermal analysis was performed to determine the experimental glass transition temperature of the extruded ASD systems. Figure 59 shows the experimental values of  $T_{mix}^g$  obtained from reversing heat flow signals in mDSC analysis as a function of the EFV load in the extruded ASDs. As already seen for spray-dried ASDs, a single  $T_{mix}^g$  was identified for each extruded formulation, a first indicative of only one amorphous phase in the binary mixture. Moreover, Figure 59 exhibits no deviations between the experimental values of  $T_{mix}^g$  for extruded ASDs and the theoretical values calculated from GT model.

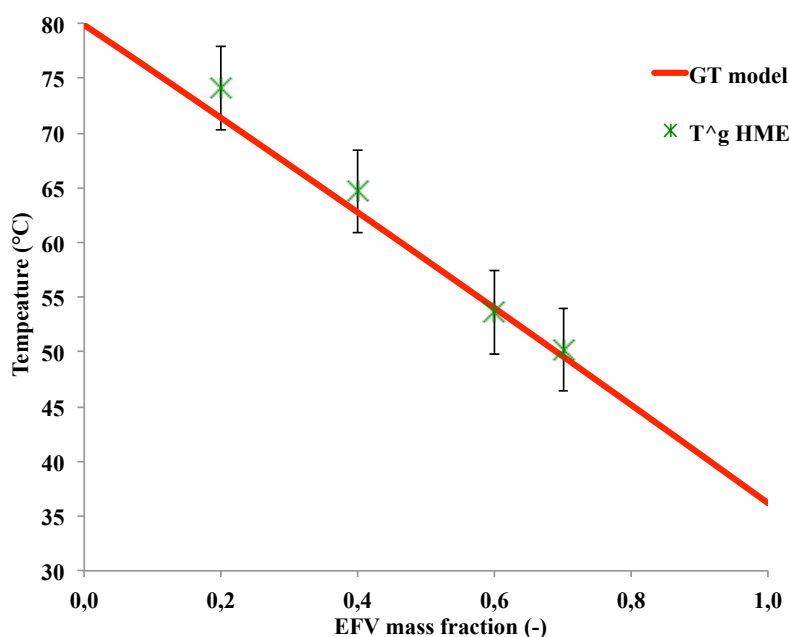
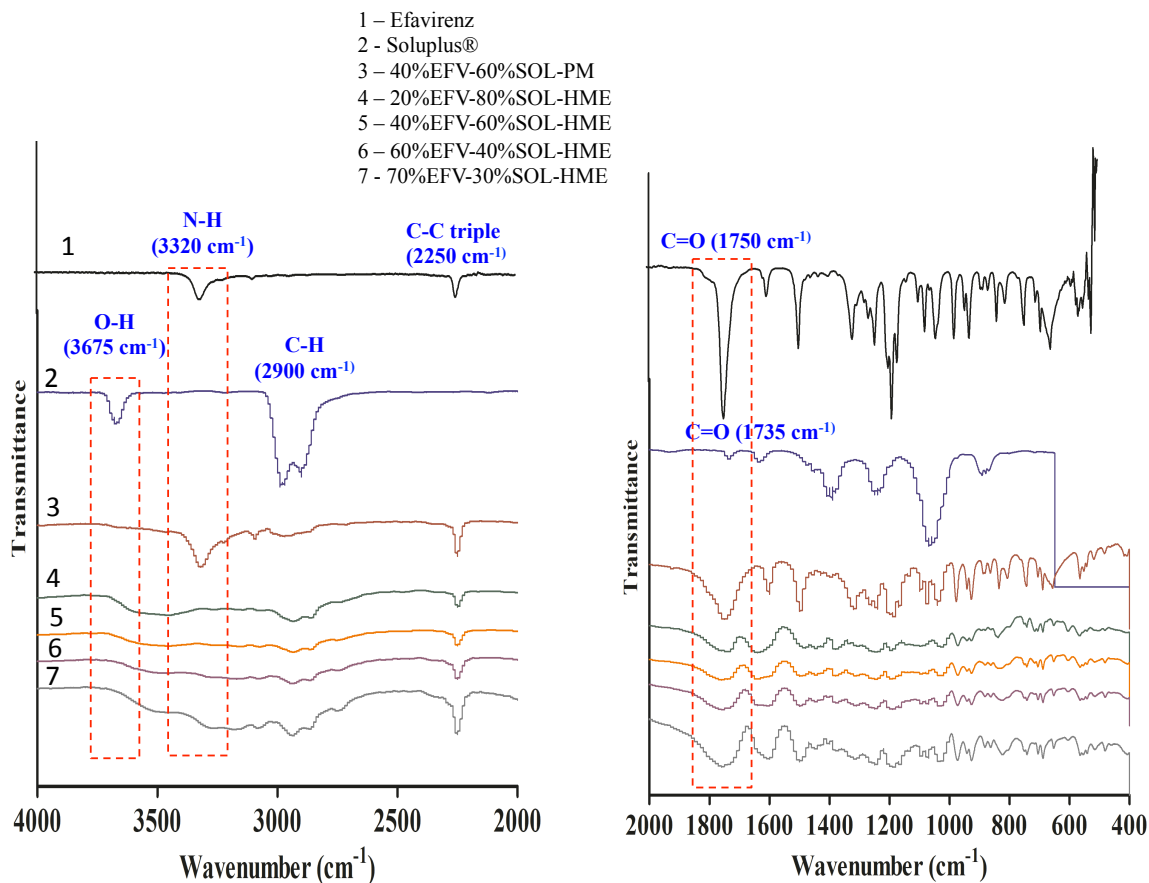


Figure 59. Mixture glass transition temperature ( $T_{mix}^g$ ): measured (green asterisks – HME and blue diamond - PM) and theoretical values by GT model (red line).

#### 4.1.5. Fourier Transform Infrared Spectroscopy (FTIR)

FTIR spectra of extruded ASDs were shown in Figure 60. FT-IR Spectra of pure EFV and pure Soluplus, also represented in Figure 7, have been already described in Chapter 4 (section 4.1.5).

Spectral analysis of extruded ASDs showed a peak at  $2250\text{ cm}^{-1}$  corresponding to C-C triple stretching vibrations of EFV, which the intensity increases as the ratio of EFV in these systems increased. Furthermore, it can be observed some modifications in the region between  $3700 - 2700\text{ cm}^{-1}$  as a disappearance of characteristic peak of Soluplus ( $3675\text{ cm}^{-1}$ ), disappearance of characteristic peak of EFV ( $3320\text{ cm}^{-1}$ ) and a broadening of Soluplus peaks at  $2987\text{ cm}^{-1}$  and  $2900\text{ cm}^{-1}$  due to C-H stretching bands. These modifications suggest some interaction between Soluplus and EFV in ASDs (possible interaction related to hydrogen bonds between the proton donating groups (-NH) of EFV and the proton accepting groups (C=O) in the Soluplus).



*Figure 60. FTIR spectra for pure components, physical mixture and ASDs.*

## 4.2. Performance behavior

### 4.2.1. Solubility studies

The ability of the extruded ASD systems to produce and maintain supersaturated EFV solution was evaluated by kinetic solubility studies in an aqueous medium containing 0.25% SLS at 37°C following the same protocol described in Chapter 3 (section 2.2.1.6).

Figure 61 shows the kinetic solubility profiles obtained over 48h. From these results, it is evident the EFV apparent solubility enhancement for all ASDs compared to the equilibrium solubility of crystalline EFV (dark dashed line).

As already observed with spray-dried ASDs, an oscillatory behavior is also detected for some samples during the first 2h, corresponding to events of solubilization and creation of a supersaturated solution followed by an instantaneous recrystallization, resolubilization... in an attempt of sample stabilisation. However, after that, no recrystallization was detected for all the extruded ASDs until the end of tests (48h).

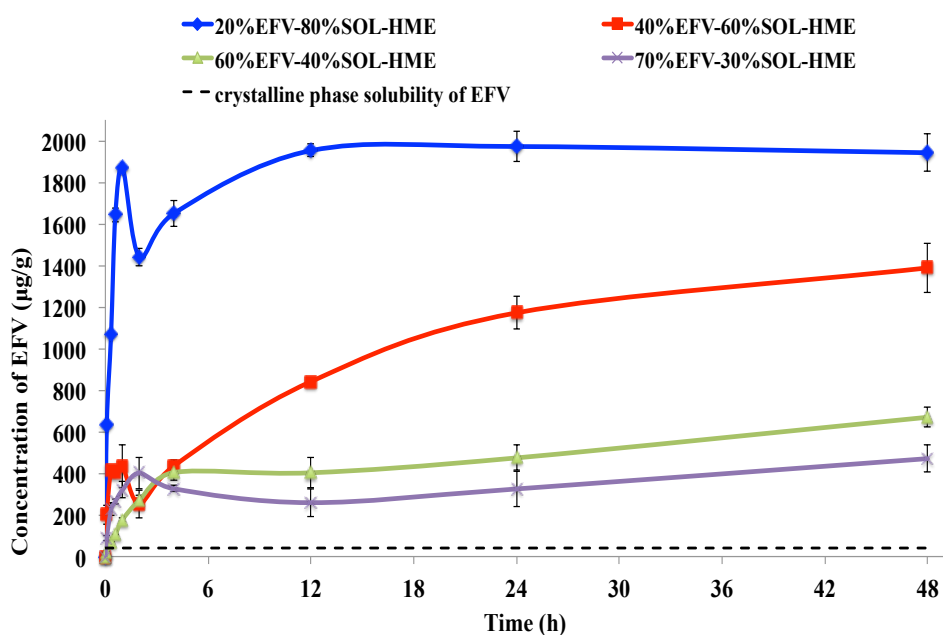


*Figure 61. Solubility profile for different ASD compositions generated by hot melt extrusion*

Figure 62 (A) and (B) compare the solubilizing effect of extruded ASDs (20 wt% and 40 wt% of EFV loading) with physical mixtures of EFV and Soluplus with similar compositions.

Once again, the solubilizing effect of Soluplus can be observed from physical mixtures of EFV with the polymer. This effect is proportional to the concentration of Soluplus. However, compared to the physical mixtures, this solubilizing power is still more pronounced with both ASDs showed in Figure 62, mainly due to the amorphous state of these formulations.

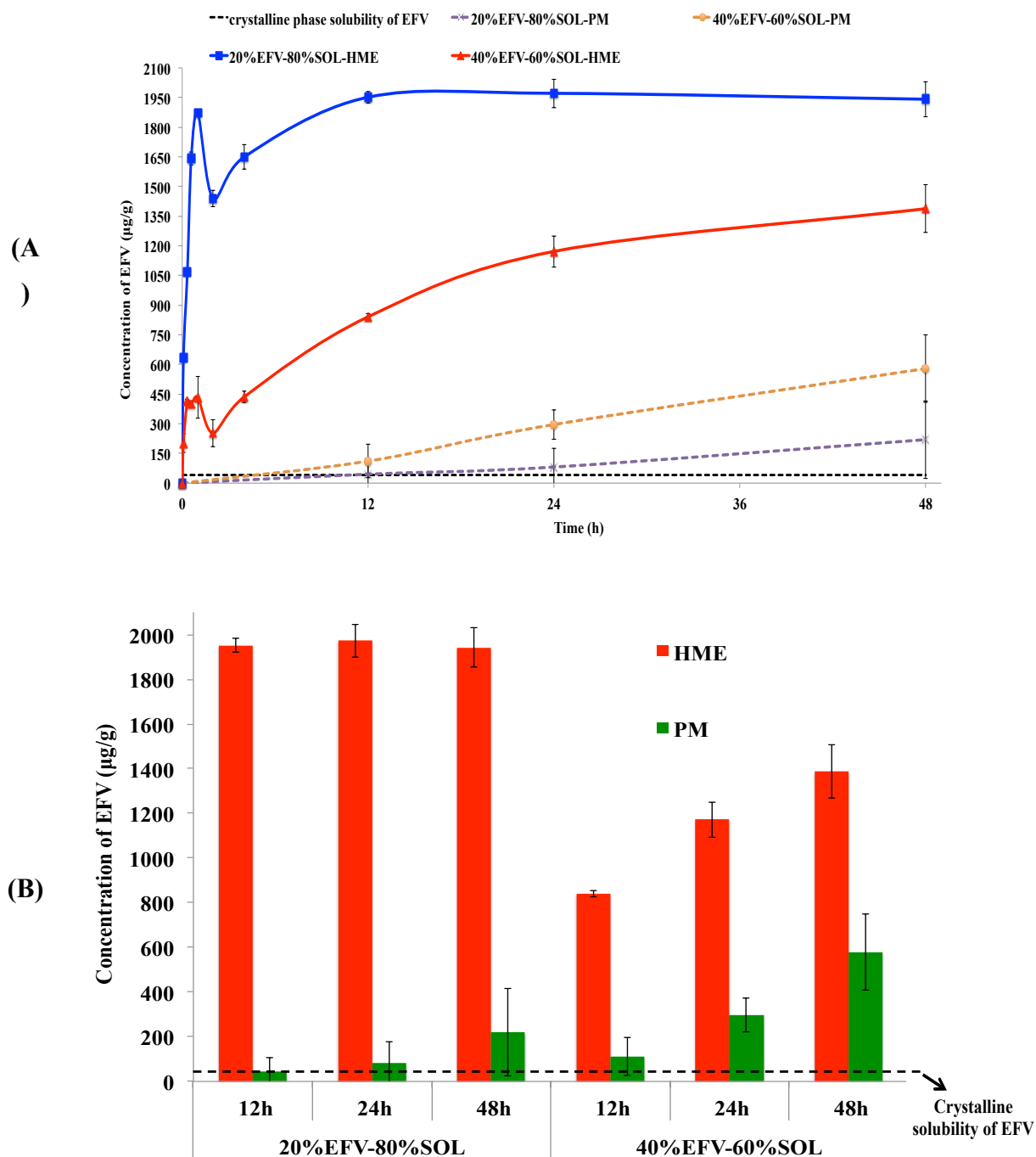
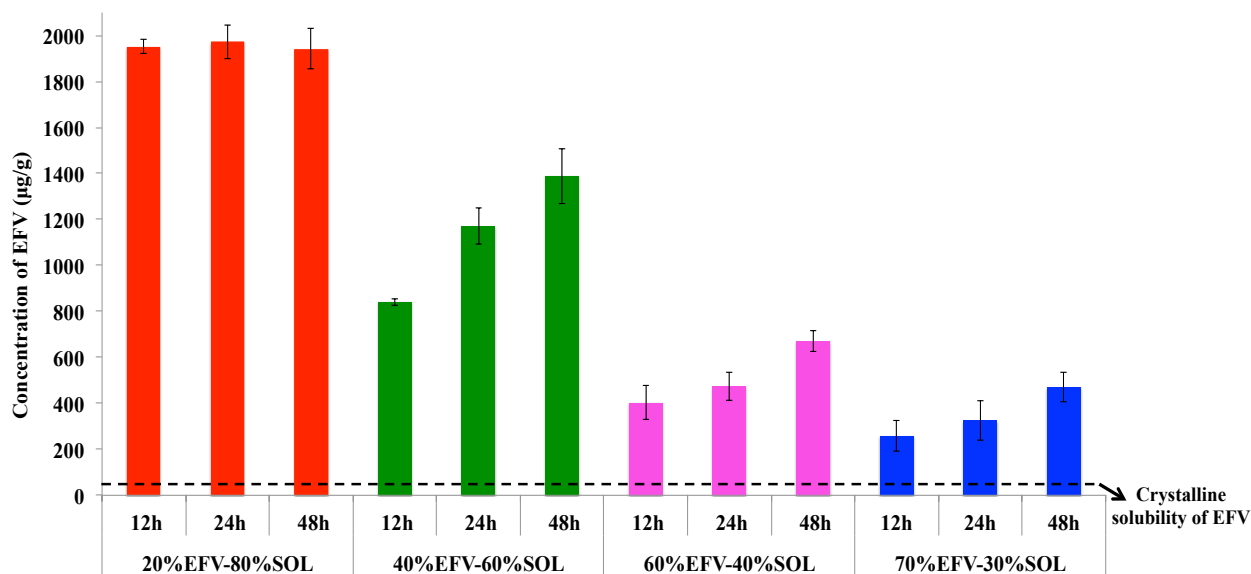


Figure 62. Comparison between kinetic solubility of extruded ASDs, and solubility of crystalline EFV, pure or physically mixed with Soluplus.

Figure 63 regroups the values of kinetic solubility for the four extruded ASDs systems studied in this work. Their positive impact in the improvement of kinetic solubility over 12, 24 and 48h is clearly demonstrated. A similar trend has also been found in several works in the literature [3], [8]–[12].



*Figure 63. Kinetic solubility profiles for all extruded ASDs*

#### **4.2.2. In vitro dissolution studies**

Dissolution tests of extruded ASDs were carried out following similar study already performed with spray-dried ASDs (Chapter 4, section 4.2.2).

To perform these tests, the physical dimension of extruded ASD samples were standardized in 1mm in diameter and 5mm in length, featuring a surface area of around 17.3 mm<sup>2</sup>.

Figure 64 displays the dissolution profiles for all extruded ASD systems. Dissolution parameters such as percentage of EFV dissolved in 360 minutes are given in Table 25.

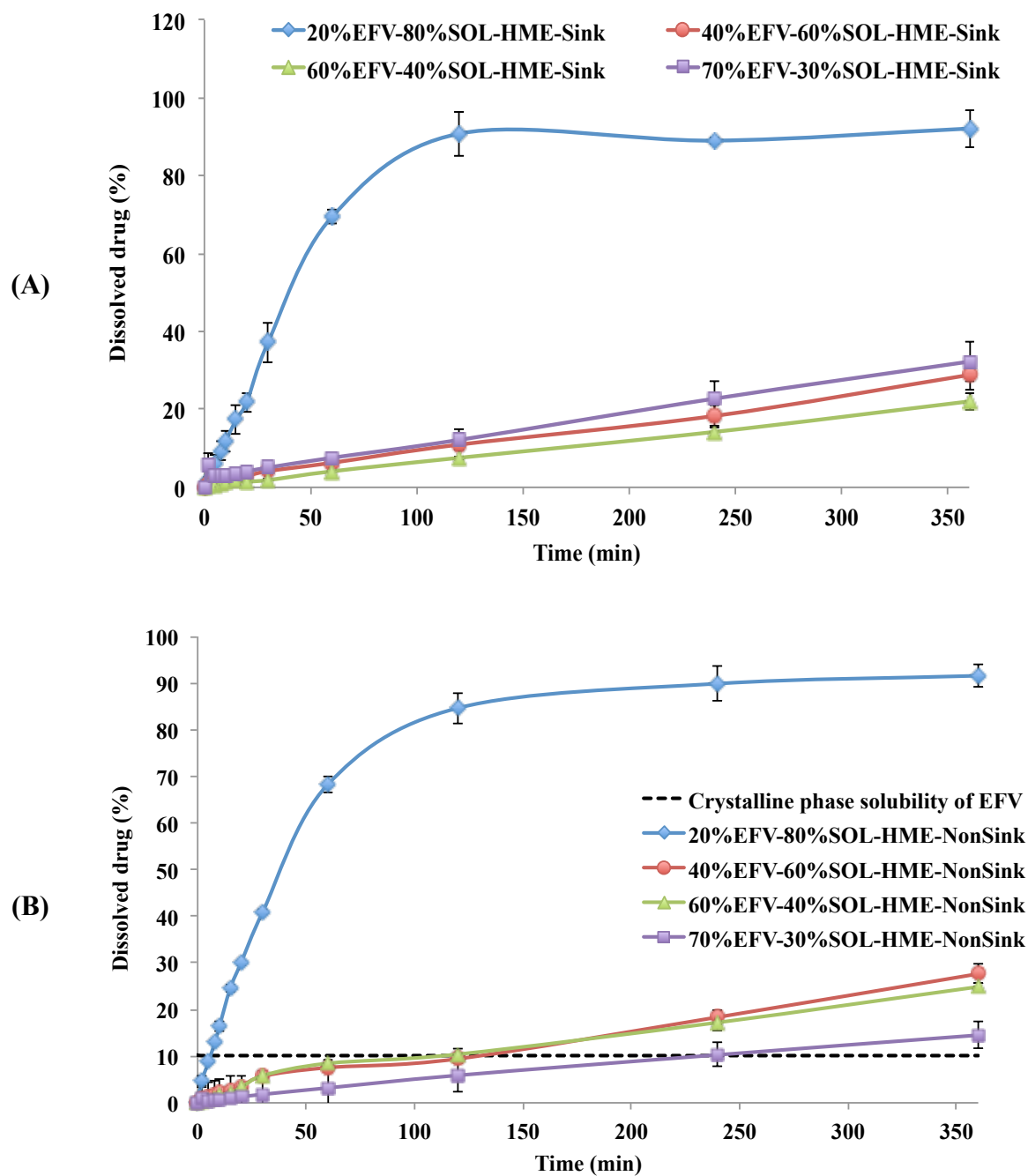


Figure 64. *In vitro* dissolution profiles of all samples including crystalline EFV and ASD's. (A) Under Sink dissolution conditions (B) under non-Sink dissolution conditions

*Table 25. Summary of dissolution key parameters under Sink and non-Sink conditions*

<b>Dissolution conditions</b>	<b>Sample</b>	<b>Cumulative Release<sub>360</sub> (%)</b>	
<b>Sink (SI=3)</b>	20%EFV-80%SOL-Sink	92.14	4.80
	40%EFV-60%SOL -Sink	28.87	3.98
	60%EFV-40%SOL -Sink	22.07	2.16
	70%EFV-30%SOL -Sink	32.29	5.12
<b>Non-Sink (SI=0.1)</b>	20%EFV-80%SOL- NonSink	91.57	2.39
	40%EFV-60%SOL- NonSink	27.65	2.03
	60%EFV-40%SOL- NonSink	24.87	0.76
	70%EFV-30%SOL- NonSink	14.51	0.82

- Values represent the mean of three independent determinations.

Figure 64 and Table 25 show that extruded ASD samples provided faster and increased dissolution for the ASD with 20%EFV-80%SOL compared with the others ASDs that exhibited a slow and progressive release. For non-Sink conditions, the dissolution profiles obtained showed that supersaturated solutions were generated and maintained for up to 360 min for all samples (no recrystallization was revealed). Moreover, the kinetic profile exhibited by 20 wt% EFV ASD was completely different from the others samples (40 wt%, 60wt% and 70wt%) for both conditions.

Table 26 shows that all extruded ASDs had a delayed release (<40%) under both, sink and non-sink conditions, within 30 min of experiment. This might be attributed to densification and reduction of polymeric-free volume during the hot-melt extrusion process [6]. Melt extruded materials are denser with less hydrophilic surface area. In this case, the thermoresponsive characteristic of Soluplus might be evidenced. Soluplus exhibits a lower critical solution temperature (LCST) near 40°C [13], above which it aggregates into larger micelles and displays gel-forming ability. The dissolution experiments were performed (37 ± 0.5°C) with temperature conditions close to the LCST. A possible gelling near to the extruded surface could be occur and promoted a barrier against API diffusion from the gelled surface.

A retard in the release of Ramipril and Chlorothiazide from Soluplus extruded was already observed in a previous work [3].

Indeed, the dissolution efficiency decreases gradually with increasing EFV load in extruded ASD samples.

Moreover, considering both conditions studied (sink and non-sink), the same order of magnitude in the dissolution profiles, cumulative release and DE was demonstrated.

*Table 26. EFV cumulative percentage released in the dissolution medium in 30 min*

<b>Dissolution conditions</b>	<b>Sample</b>	<b>Cumulative Release (%)</b>	
Sink (SI=3)	20%EFV-80%SOL-Sink	37.26	5.15
	40%EFV-60%SOL -Sink	4.17	0.17
	60%EFV-40%SOL -Sink	1.86	0.24
	70%EFV-30%SOL -Sink	5.10	1.22
Non-Sink (SI=0.1)	20%EFV-80%SOL- NonSink	40.90	0.57
	40%EFV-60%SOL- NonSink	5.72	0.68
	60%EFV-40%SOL- NonSink	5.85	0.82
	70%EFV-30%SOL- NonSink	1.81	0.17

EFV release from extruded ASD systems was also fitted with Korsmeyer–Peppas model, similarly to the mathematical treatment provided for spray-dried ASD systems (see Chap. 4). Just in reminder, the first 60% drug release data from all extruded ASDs formulations were fitted by the Equation 14 defined in Chapter 2 (section 1.3.6.7). Nonlinear regressions were applied for cumulative dissolved API.

From the obtained results (Table 27) it is confirmed that EFV release from ADSs is well described mathematically by the Korsmeyer-Peppas. The cylindrical extruded shape was considered when analysing the values for the exponent  $n$ , an indicative of mechanism release.

The exponent ( $n$ ) is higher than 0.89 for 20%EFV-80%SOL sample under sink dissolution conditions, suggesting a non-Fickian EFV release mechanism. In this case, the API release corresponds to zero-order release kinetics and the mechanism driving the API release is the swelling or relaxation of polymeric chains. The velocity of dissolution medium diffusion by the system (gellified region) is faster compared to the process of relaxation on the gel-vitreous polymeric interface, which marks the inner limit of penetration or solvent dispersion at a

determined time. The vitreous region has almost no medium penetration and the diffusivity of the medium in the gelled region is higher [14]. This behavior well represents the slow release of the API and its in good agreement with the thermoresponsive character of the Soluplus already presented.

The value of expoent (n) ranged in the interval  $0.45 < n < 0.89$ , suggesting also a non-fickian diffusion with anomalous transport for the other extruded samples. This type of mechanism refers to a combination of both diffusion and erosion controlled-API release. In this case, diffusion and swelling are comparable. The rearrangement of polymeric chains occurring slowly and the simultaneous diffusion process cause the time-dependent anomalous effects [14]. Non-fickian diffusion with anomalous transport was already reported in the litterature to explain the API release mechanism from extruded solid dispersions [15].

All fitting models are reunited in Appendix 3.

*Table 27. Summary of results obtained after after the kinetic fitting by Korsmeyer-Peppas model*

	Sample	K (min <sup>-n</sup> )	R <sup>2</sup>	n	AIC	RMSE
<b>Sink</b>	20%EFV-80%SOL-Sink	1.206	1.000	0.991	22.494	0.931
	40%EFV-60%SOL -Sink	0.206	0.998	0.833	21.967	0.610
	60%EFV-40%SOL -Sink	0.082	0.998	0.882	5.820	0.311
	70%EFV-30%SOL -Sink	0.427	0.985	0.729	46.664	1.708
<b>Non-Sink</b>	20%EFV-80%SOL- NonSink	2.825	0.999	0.780	20.369	0.828
	40%EFV-60%SOL- NonSink	0.332	0.996	0.743	33.436	0.984
	60%EFV-40%SOL- NonSink	0.409	0.999	0.693	29.155	0.823
	70%EFV-30%SOL- NonSink	0.110	0.994	0.829	0.349	0.248

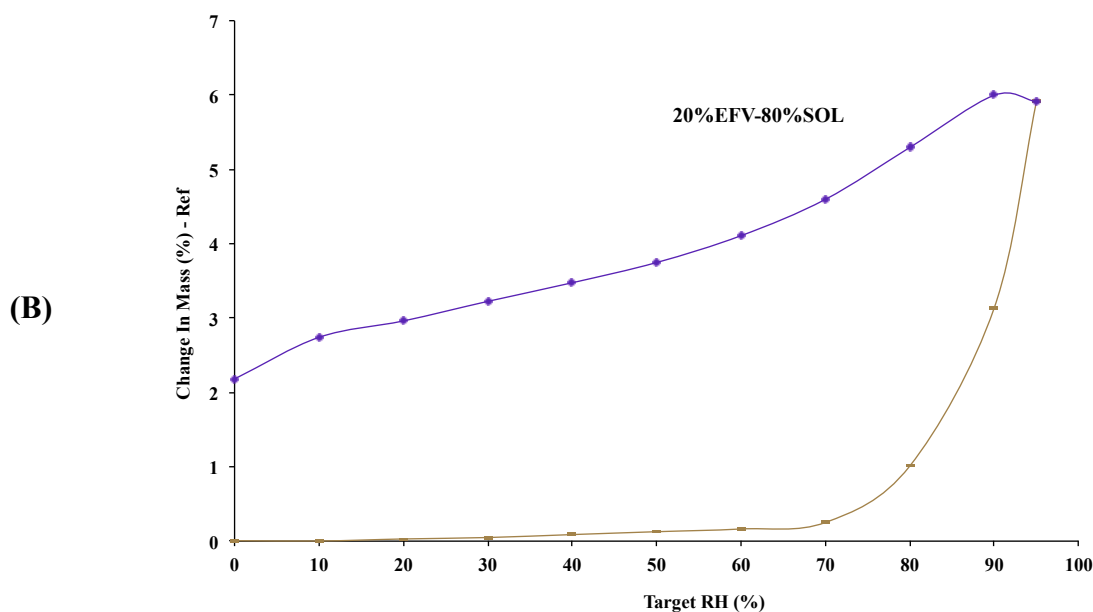
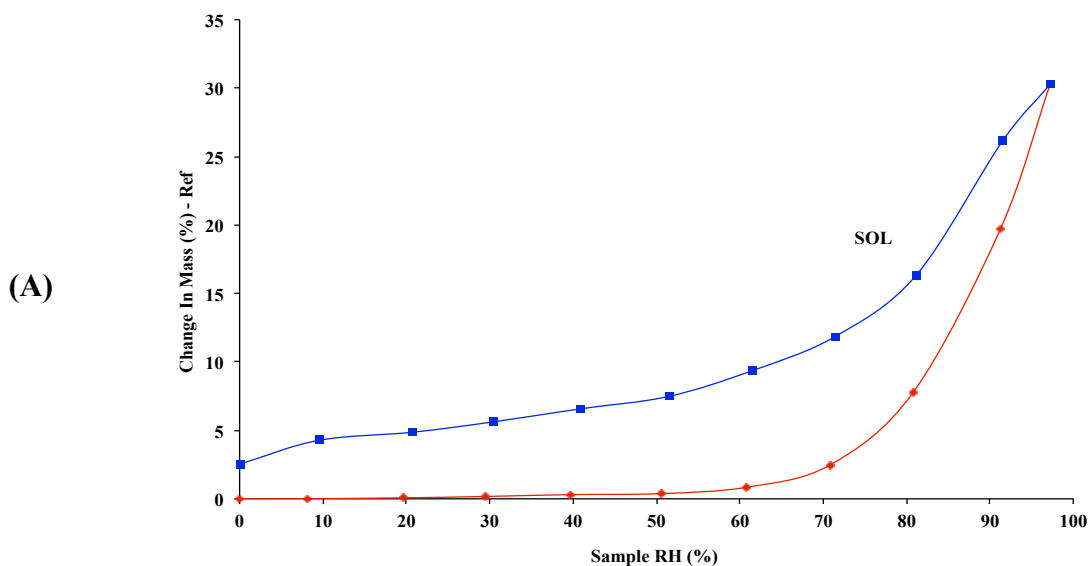
#### **4.2.3. Physical stability**

Stability of ASDs can be directly influenced by water uptake during downstream processing and storage. The aim of this study followed the same investigations already presented in Chapter 4 (section 4.2.3).

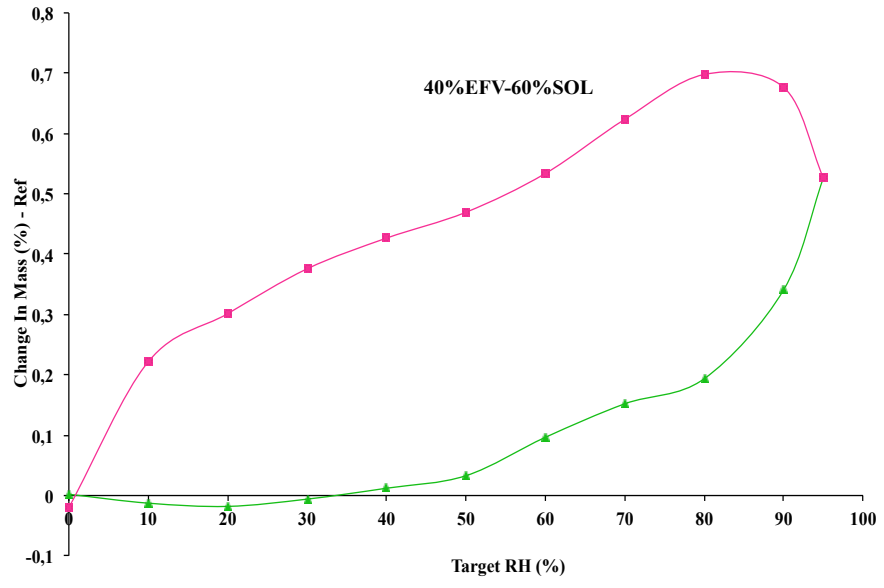
- Dynamic vapor sorption (DVS)

A water sorption isotherm at 25°C was used to obtain information about the affinity between the analyzed powders and water, upon exposure to stressed humidity. The general shape

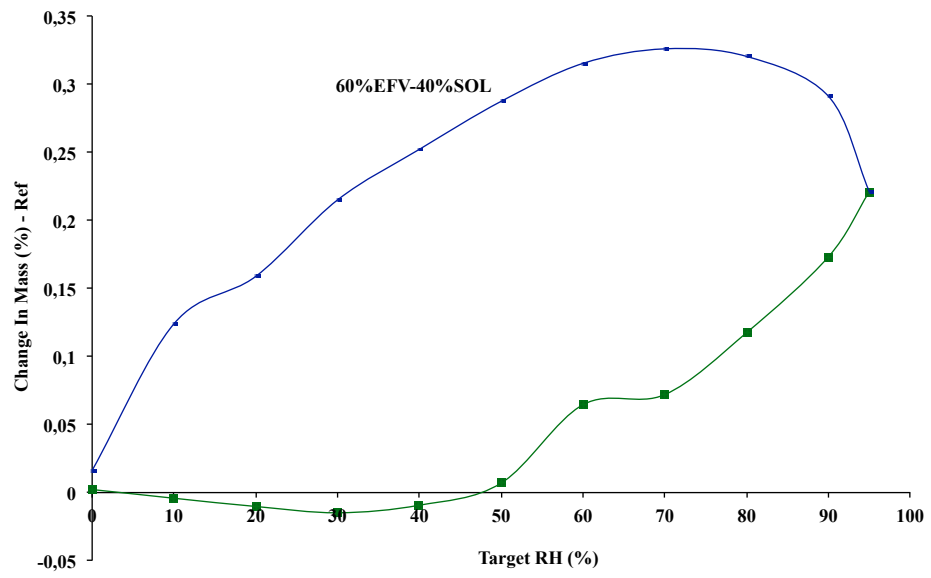
of the isotherm, reversibility of moisture uptake, presence and shape of a hysteresis loop provide information on the manner of interaction of the solid with water [16]. Figure 65 shows the DVS isotherm plots for the extruded ASDs exhibiting the change in mass percentage as a function of changing relative humidity (RH) in the range 0% to 95%RH.



(C)



(D)



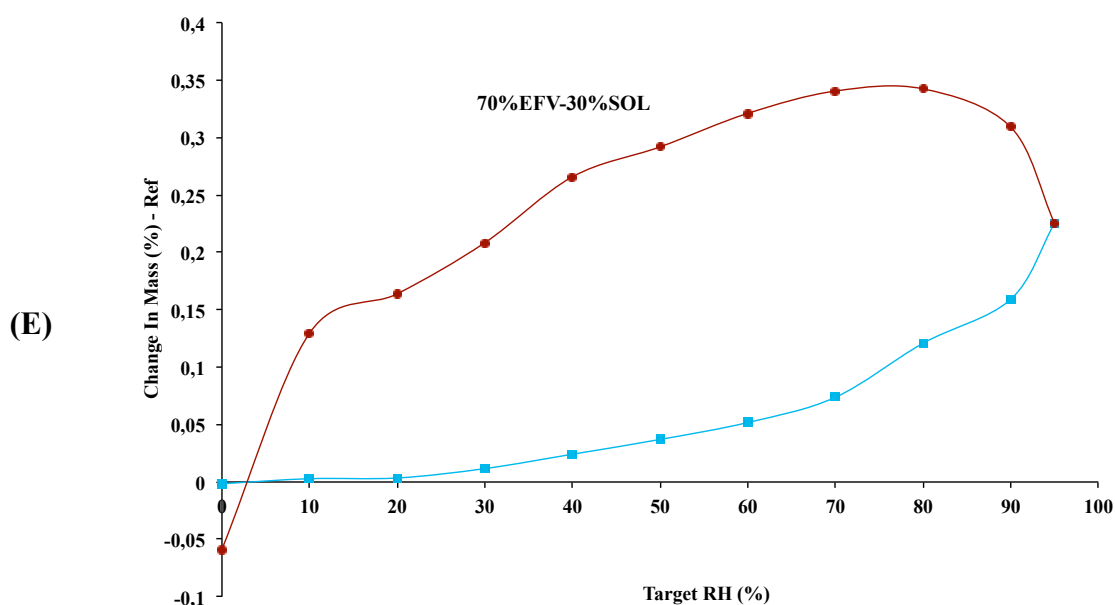


**Figure 65.** DVS isotherms at 25°C for extruded samples, demonstrating the weight change (%) as a function of the relative humidity (%) for each sample: (A) extruded Soluplus; (B) 20%EFV-80%SOL; (C) 40%EFV-60%SOL; (D) 60%EFV-40%SOL ASD; (E) 70%EFV-30%SOL ASD.

Figure 65 (A) and (B) shows the DVS isotherm for pure Soluplus and for 20%EFV-80%SOL ASD, respectively. Pure Soluplus can absorb 30.28% of water at 95%RH. When, the API is added in the formulation, the water uptake drops 5 fold for 20%EFV-80%SOL ASD (5.9% change of mass at 95% RH) and 50 fold for the others extruded ASDs (< 0.6% change of mass at 95% RH) as exhibited in Figure 65 (C), (D) and (E). All these results are summarized in Table 22. This behavior is attributed to the Soluplus amount in the samples. Soluplus has high hygroscopicity, which stimulates the uptake of a significant amount of water.

Large hysteresis between the sorption and the desorption isotherm are observed for all extruded ASDs studied (Figure 65 (A) to (D)). This is probably due to a slow diffusion-controlled bulk desorption process. As reported in an earlier work, amorphous materials can take up significant amount of moisture into their structure and not just on surface, which can result in a relevant hysteresis between sorption and desorption isotherm [17].

However, for pure Soluplus and 20%EFV-80%SOL ASD, an ‘open hysteresis’ is also detected. This type of hysteresis is normally attributed to an irreversible phenomenon (chemisorption) or diffusion-limited desorption. If the desorption branch doesn't reach the adsorption branch, it can mean that the equilibrium pressure is not established due to the slow diffusion rate of water in the micropores of ASDs materials [18].

**Table 28. Summary of water uptake (%) extruded ASDs in the different relative humidity (60%, 75%, 85% and 95% RH) at 25°C.**

Sample	Relative Humidity (RH), %			
	60	75	85	95
Soluplus	0.84	5.13	13.76	30.28
20%EFV-80%SOL	0.162	0.630	2.073	5.911
40%EFV-60%SOL	0.097	0.173	0.267	0.527
60%EFV-40%SOL	0.065	0.094	0.145	0.225
70%EFV-30%SOL	0.052	0.097	0.140	0.226

The water sorption isotherm of binary mixtures can be predicted as already presented in Chapter 4 (Equation 3, section 4.2.3) by assuming additivity of the individual component isotherms.

Figure 66 shows the water mass change of the extruded ASDs compared with theoretical water sorption at 95% RH. The water uptake for the extruded ASDs charged with higher than 40 wt% of EFV is close to zero. This low water absorption can be explained by the high densification of the extruded ASDs [6].

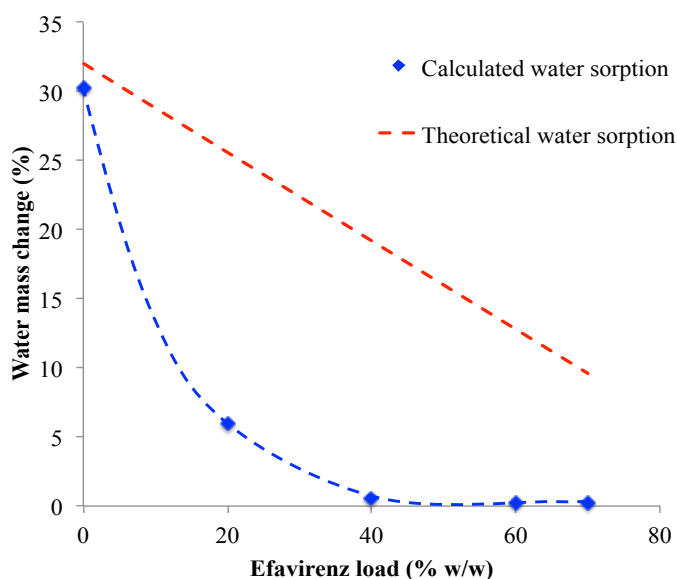


**Figure 66. Water mass change of the extruded ASDs compared with theoretical water sorption at 95% RH.**

- Stability studies at accelerated stability condition (40°C/75% RH)

Stability studies were performed following the methodology and the conditions already described in chapter 4 (section 4.2.3).

Samples were monitored by DSC analysis each 3 days, within 15 days. The results are grouped in Table 29. It is noticeable that the samples have evolved over time since  $T_{mix}^g$  increases in both cases, which could be an indicative of some evolution of the amorphous mixture composition. However, no particular signs of amorphous phase separation like emerging of a second  $T_g$ , or drug recrystallization were detected in both samples, from DSC analysis.

**Table 29. Stability results under stress conditions (40 °C/75 % RH) for EFV-SOL ASDs with drug loads of 40 % and 70 %**

	40%EFV- 60%SOL- HME	70%EFV- 30%SOL- HME
t (days)	$T_{mix}^g$ (°C)	$T_{mix}^g$ (°C)
3	60.60	53.93
6	64.24	54.02
9	64.16	56.68
15	61.59	56.76

## 5. Effect of the manufacturing process on the ASD properties

As already discussed in Chapter 2 (section 1.3.7.), the choice of the manufacturing process and its specific process variables can have a direct impact in the ASDs structure and provide ASD systems with different characteristics such as the level of molecular interactions between API and carrier. Here, we propose to compare the impact of process in the performance behavior of the ASDs with same compositions, generated by SD and HME processes.

Two compositions were selected: 40%EFV-60%SOL and 70%EFV-30%SOL.

## 5.1. Solid dispersion characteristics

### 5.1.1. Solid state, homogeneity, spatial distribution of EFV

As confirmed in Figure 67, amorphous binary mixtures with the following compositions: 40%EFV-60%SOL and 70%EFV-30%SOL were generated by SD and HME processes.

These amorphous mixtures are characterized by a single glass transition temperature ( $T_{mix}^g$ ) as assembled in a single figure (Figure 68). The values of  $T_{mix}^g$  measured for extruded ASDs were closer to the values  $T_{mix}^g$  calculated from GT equation. The deviations observed for spray dried ASDs might be due to the presence of some residual solvent in the spray-dried products.

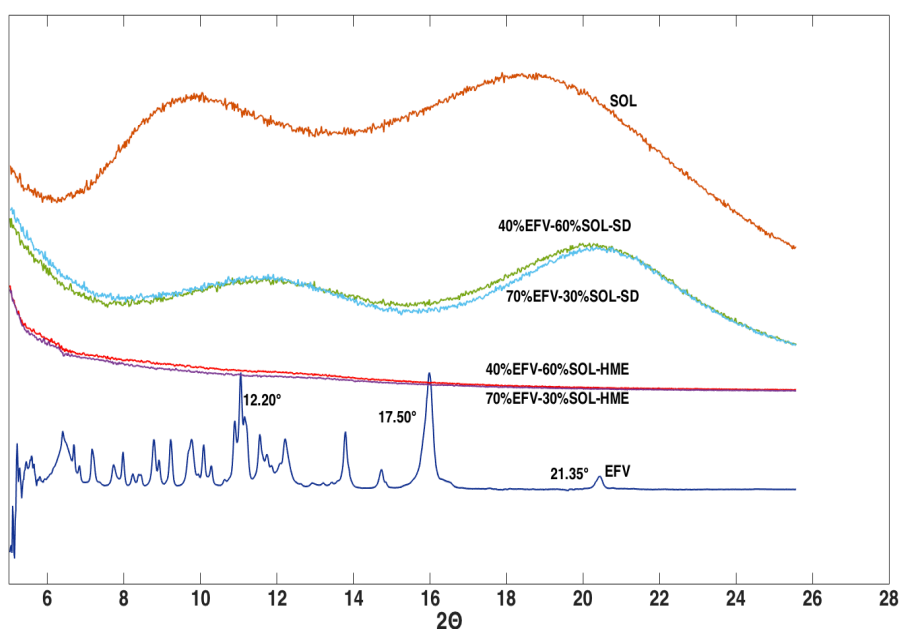
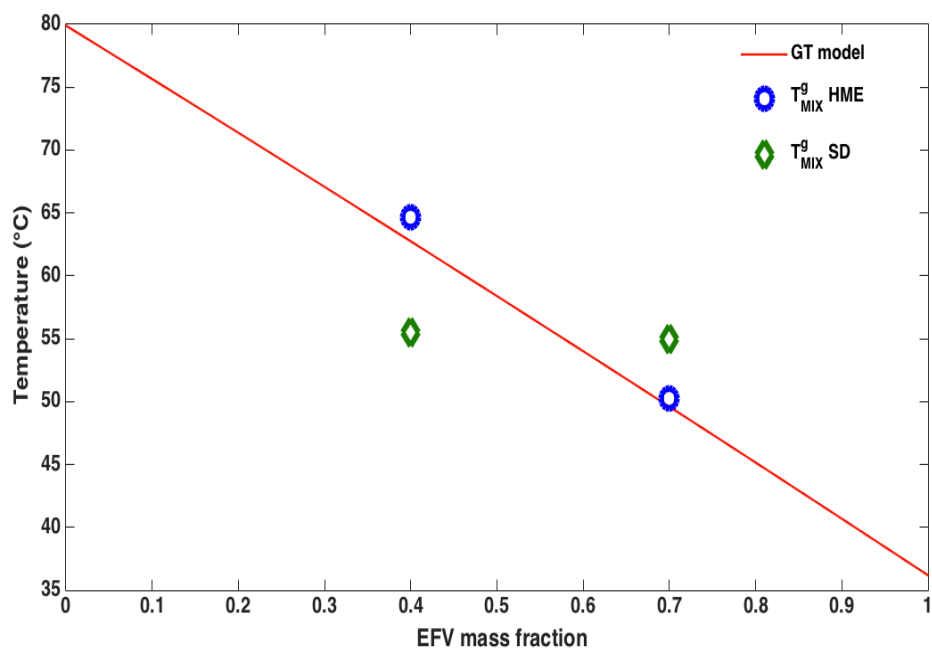
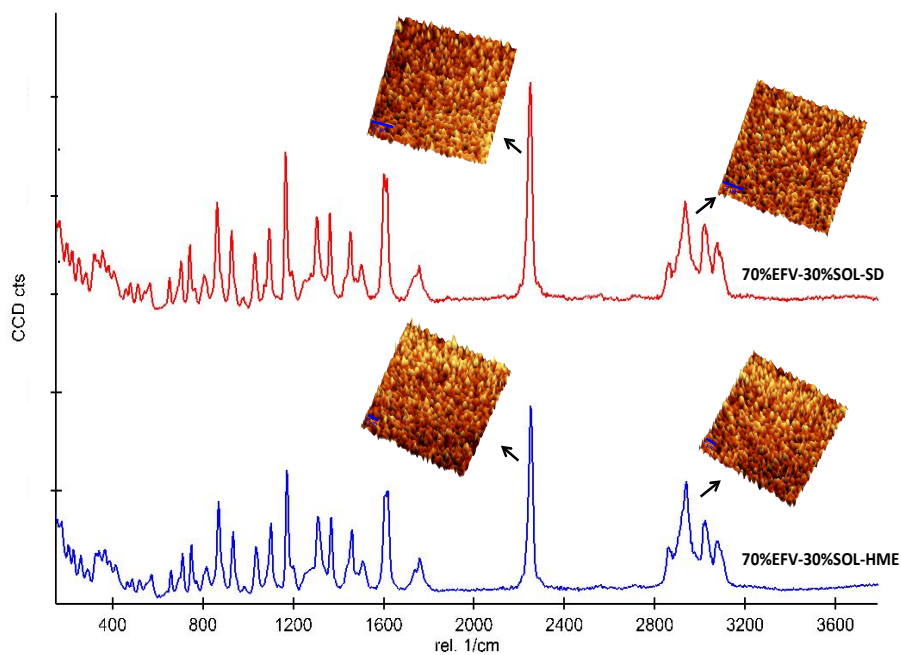


Figure 67. Comparative of XRD diffractograms for spray-dried and extruded ASDs.



**Figure 68.** Mixture glass transition temperature ( $T_{mix}^g$ ): measured (blue circles – HME and green diamonds-SD) and theoretical values by GT model (red line).

The mapping of individual components in spray-dried and extruded amorphous solid dispersions, provided by Raman microscopy, have confirmed a good EFV distribution within the polymeric matrix, as illustrated in Figure 69 for extruded and spray-dried 70%EFV-30%SOL ASDs, which is more likely to recrystallize.



**Figure 69. Raman Spectra of spray-dried and extruded 70%EFV-30%SOL ASD systems.**

### **5.1.2. EFV-Soluplus interactions**

EFV and Soluplus interactions were investigated by FTIR. Figure 70 represents FTIR of ASDs of two different compositions produced by SD and HME processes.

It can be seen that FTIR of spray-dried and extruded ASDs are quite similar, indicating the same modifications of some characteristic peaks of EFV and SOL as already discussed individually in Chapter 4 for spray-dried samples and before in the current chapter for extruded samples.

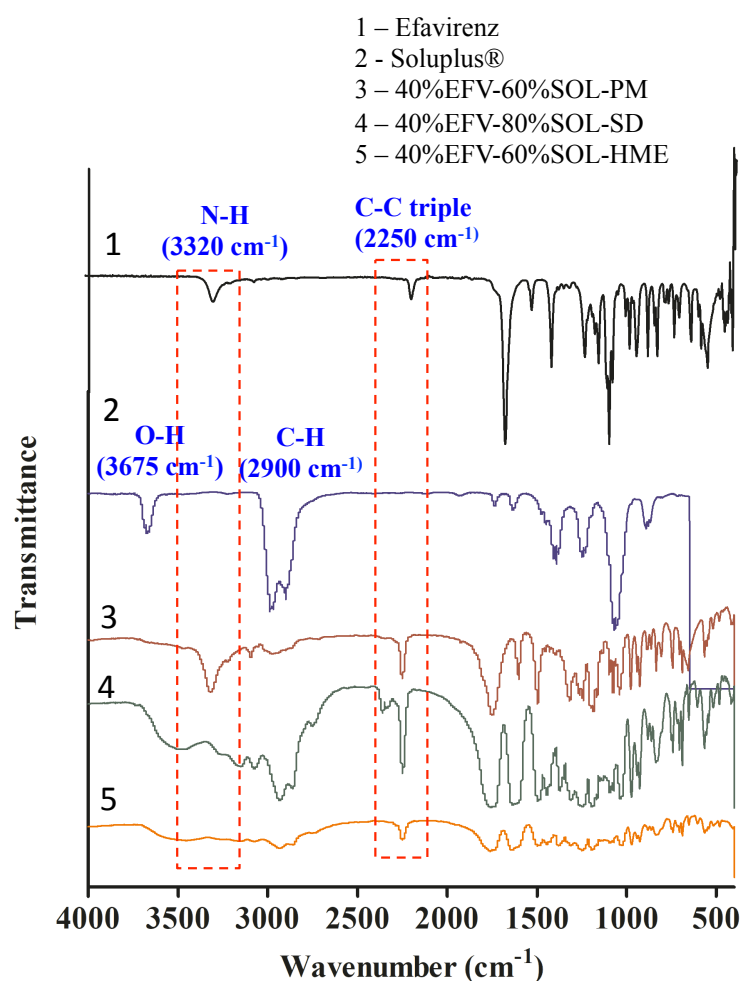


Figure 70. FTIR spectra for pure components, physical mixture and ASDs generated by SD and HME processes.

## 5.2. Performance behavior

### 5.2.1. Solubility studies

A comparative of the ability of spray-dried and extruded ASD systems to enhance EFV kinetic solubility in aqueous medium containing 0.25% SLS at 37°C is depicted in Figure 71 and Table 30. Both manufacturing processes were efficient to enhance the EFV kinetic solubility when compared with their similar physical mixtures. The API content in the ASDs have influenced on the kinetic solubility enhancement (Table 30).

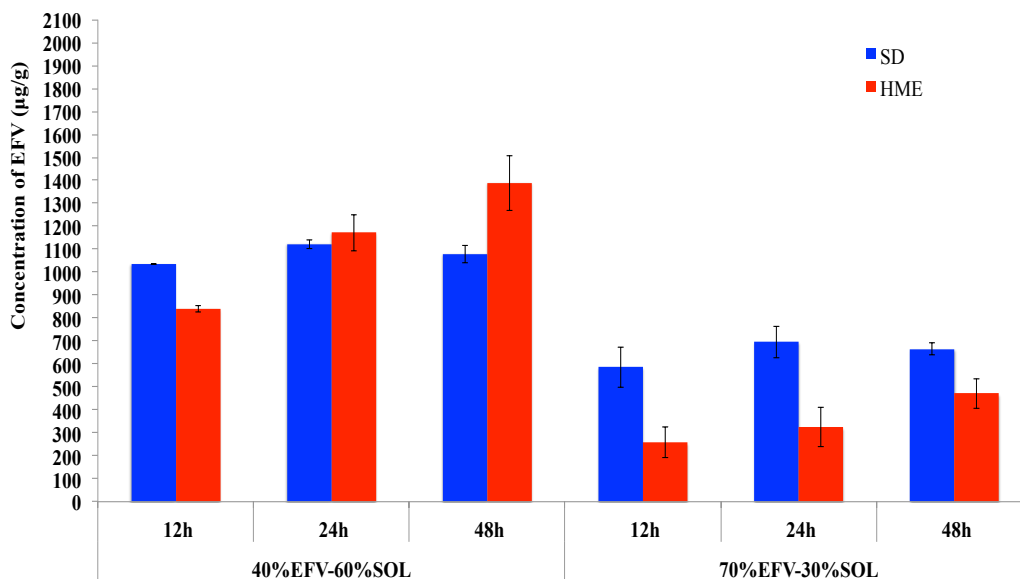


Figure 71. Comparison between kinetic solubility profiles for spray-dried and extruded ASDs with similar API-carrier compositions

Table 30. Comparative of apparent solubility enhancement for PM, HME and SD samples

API	Sample	API load (%)	Apparent solubility enhancement
Efavirenz	Physical mixture - PM	20	5.5 fold
	ASD-HME		48 fold
	ASD-SD		46 fold
	Physical mixture - PM	40	14 fold
	ASD-HME		34 fold
	ASD-SD		27 fold
	ASD-HME	70	11.5 fold
	ASD-SD		17 fold

The solubilizing effect of Soluplus is, clearly visualized in an increase relationship between the maximum supersaturated concentration of EFV reached in solution and the concentration of Soluplus in ASDs, as represented in Figure 72. The aqueous solubility of crystalline EFV in aqueous medium containing 0.25% SLS at 37°C of 41.019 – 9.38 µg/mL is also represented in this figure.

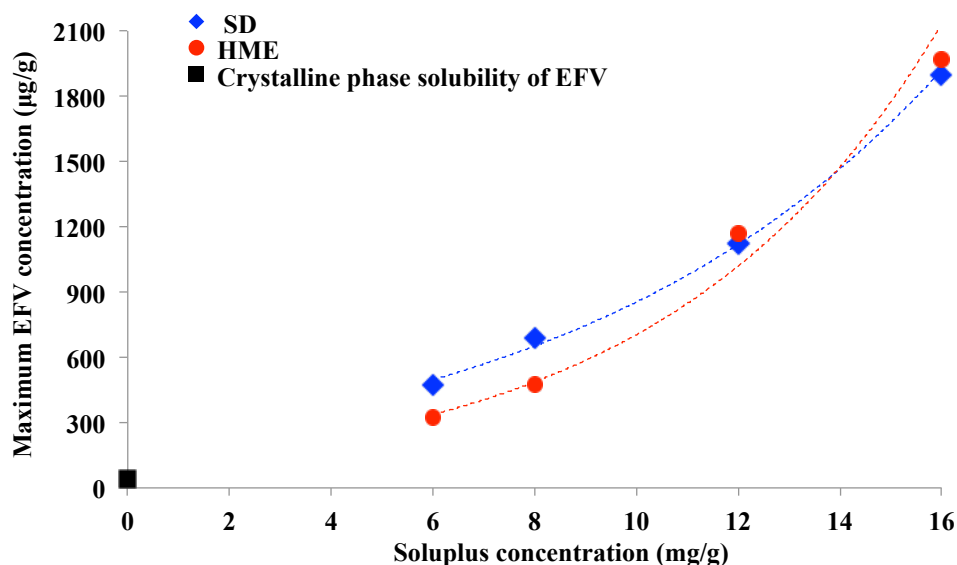


Figure 72. Effect of Soluplus in the ASDs generated by SD and HME

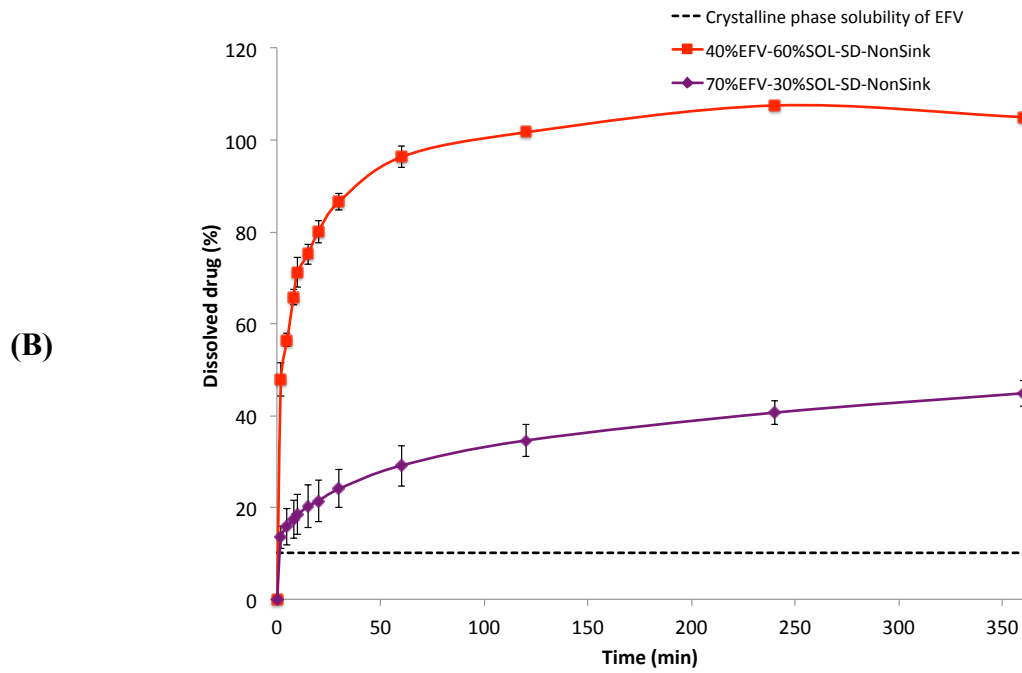
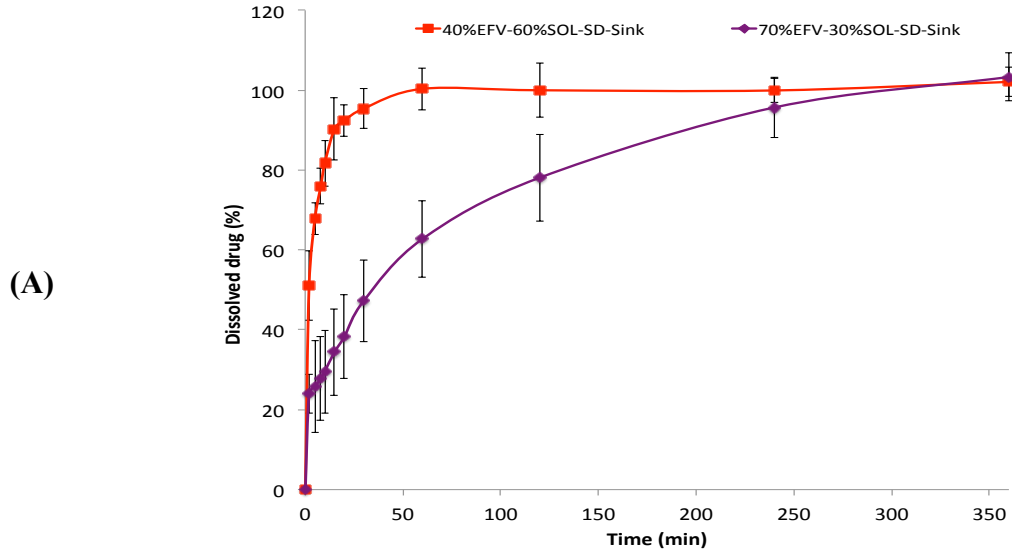
### 5.2.2. Dissolution studies

Figure 73 displays together the dissolution studies of different solid dispersions prepared by HME and SD processes. Dissolution parameters such as percentage of EFV dissolved in 360 minutes and  $DE_{360}$  are given in Table 31.

Besides a confirmed kinetic solubility enhancement, all ASDs contributed to a higher dissolution rate of EFV in the studied media. The API release from spray-dried ASDs was much faster and higher when compared with extruded samples. This effect is attributed mainly to differences of physical characteristics between extruded and spray dried ASDs. Indeed, shape factor (cylinder vs spherical particles), size and specific surface area of extruded and spray-dried samples are completely different. This latter point has a big influence on the release profiles since the surface of exchange with the dissolution media is much higher for spray dried samples than for extrudates (several orders of magnitude), which explains the kinetics difference.

Regardless of the dissolution conditions, favoring (non-sink) or not (sink) the supersaturation of the aqueous media, no signs of recrystallization represented by a decline in the EFV concentration in solution over time were observed. This is a positive result since the transformation of amorphous state into crystalline structures during the dissolution process has been considered a limiting factor in the development of amorphous solid dispersions since the

recrystallization in the biological environment can directly influences the drug absorption present in these systems [8].



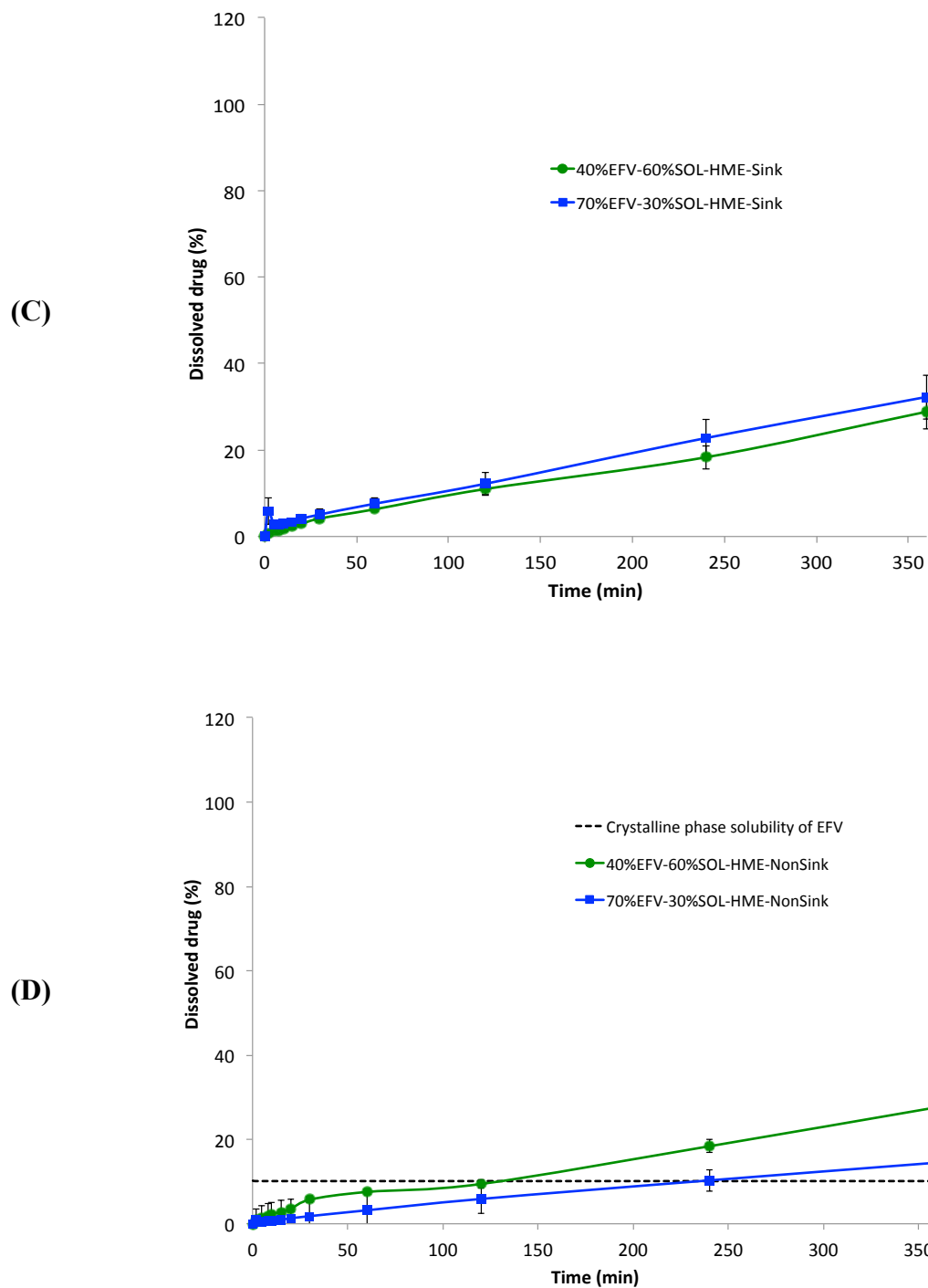


**Figure 73.** *In vitro* dissolution profiles of all samples including crystalline EFV, spray-dried and extruded ASDs. (A) SD ASD under Sink dissolution conditions, (B) SD ASD under non-Sink dissolution conditions, (C) HME ASDs under Sink dissolution conditions (D) HME ASD under non-Sink dissolution conditions.

**Table 31. Summary of dissolution key parameters under Sink and non-Sink conditions for spray-dried and extruded ASD**

<b>Dissolution conditions</b>	<b>Samples</b>	<b>Cumulative Release<sub>360</sub> (%)</b>	<b>Dissolution Efficiency<sub>360</sub> (DE - %) (n=3)*</b>
<b>Sink SI=3</b>	40%EFV-60%SOL-SD	102.09 3.6	98.20
	70%EFV-30%SOL-SD	103.32 6.0	80.70
	40%EFV-60%SOL-HME	28.87 4.0	-
	70%EFV-30%SOL-HME	32.29 5.1	-
<b>Non-Sink SI=0.1</b>	40%EFV-60%SOL-SD	104.99 0.5	96.51
	70%EFV-30%SOL-SD	44.86 2.8	-
	40%EFV-60%SOL-HME	27.65 2.0	-
	70%EFV-30%SOL-HME	14.51 0.8	-

\* Values represent the mean of three independent determinations.

### **5.2.3. Physical Stability**

The affinity with water is a critical attribute for physical stability. Presentation of DVS results for spray-dried and extruded samples have demonstrated that EFV is a very lipophilic API and that the association of this molecule with a hygroscopic polymer likes Soluplus could lead to a more hygroscopic amorphous binary mixture whose physical stability should be surveyed.

Figure 74 reunites the water amount up taken by the ASD systems, showing that spray-dried ASDs might be more hygroscopic, even if the amounts of water up taken by ASDs with EFV content higher than 40wt% remains low (lower than 5 wt%, in water mass change at 95%RH at 25°C).

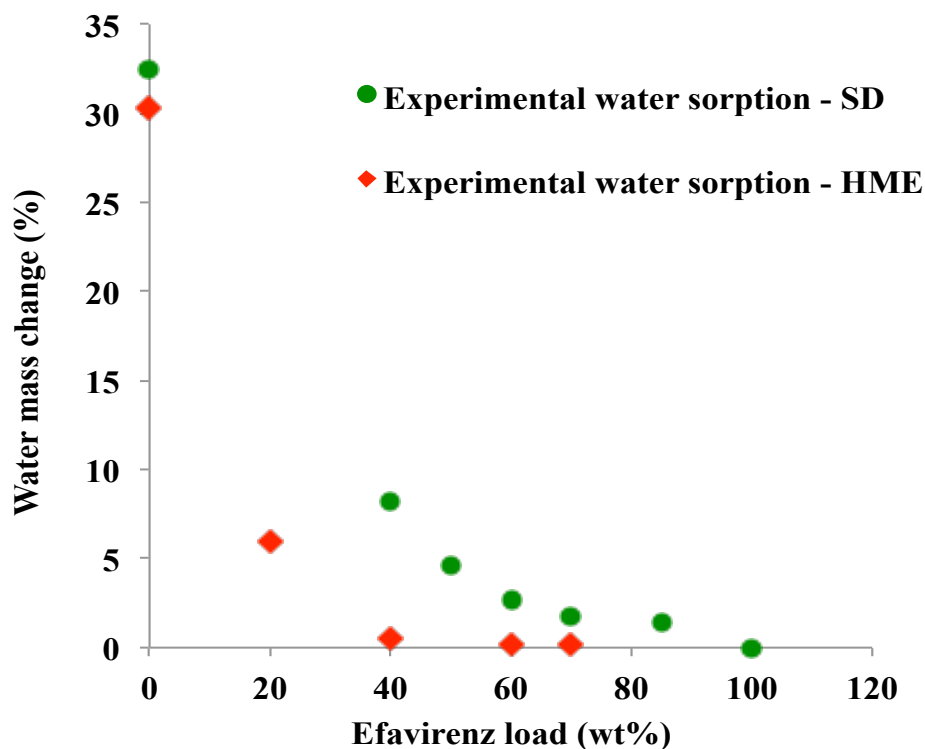


*Figure 74. Water mass change of the ASDs compare with theoretical water sorption at 95% RH, 25°C for spray-dried and extruded ASDs.*

The exposition of spray-dried and extruded ASD samples (40°C and 70% RH in an accelerated stability study) revealed different tendencies for the more concentrated sample studied (70 wt% EFV). While we did not observe any particular signs of amorphous phase separation or API recrystallisation for the sample loaded with 40%EFV-60%SOL for both spray-dried and extruded ASD samples, the spray-dried 70%EFV-30%SOL ASD sample revealed a partial EFV recrystallization.

The main reason for the absence of recrystallization for the HME ASDs is probably the effect that HME provides highly densification and consequently, reduction of polymeric-free volume during HME manufacturing compared with less dense SD samples as already reported in the literature [21]. Particle size plays a big role in the comparison of these two processes, as well [21]. In conclusion, HME ASDs compared with SD ASDs conducted to better product stability during the stress test conducted in this work.



## **6. Conclusion**

Here, we demonstrated that supersaturated ASDs, in a large range of API concentration, loaded up to 70 wt% in API, could be also generated by hot-melt extrusion. Amorphous behavior was confirmed through XRD and DSC analysis.

Raman Mapping exhibited a well spatially distribution of the two compounds for all extruded ASDs.

The apparent EFV solubility enhancement from extruded ASDs was also confirmed, as well as, the dependence on the Soluplus concentration.

Different dissolution profiles were generated depending on the dissolution conditions (sink or non-sink). Although these differences, all ASDs generated by hot-melt extrusion did not show signs of recrystallization in non-sink conditions. The results demonstrated a slow API release for all ASDs controlled by a Non-Fickian diffusion mechanism.

The highest concentrated EFV-Soluplus ASD with 70 wt% in EFV generated from both manufacturing processes, SD and HME, revealed a lower physical stability of the ASD produced by spray drying, already during the short duration of the stress test conducted (15 days at 40°C and 75% RH).



## 7. References

- [1] S. H. Surasarang, J. M. Keen, S. Huang, F. Zhang, J. W. McGinity, and R. O. W. III, 'Hot melt extrusion versus spray drying: hot melt extrusion degrades albendazole', *Drug Dev. Ind. Pharm.*, vol. 43, no. 5, pp. 797–811, May 2017.
- [2] J. M. Keen, J. S. LaFontaine, J. R. Hughey, D. A. Miller, and J. W. McGinity, 'Development of Itraconazole Tablets Containing Viscous KinetiSol Solid Dispersions: In Vitro and In Vivo Analysis in Dogs', *AAPS PharmSciTech*, vol. 19, no. 5, pp. 1998–2008, Jul. 2018.
- [3] J. F. Kelleher *et al.*, 'A comparative study between hot-melt extrusion and spray-drying for the manufacture of anti-hypertension compatible monolithic fixed-dose combination products', *Int. J. Pharm.*, vol. 545, no. 1–2, pp. 183–196, Jul. 2018.
- [4] Y. Song *et al.*, 'Acid-base interactions in amorphous solid dispersions of lumefantrine prepared by spray-drying and hot-melt extrusion using X-ray photoelectron spectroscopy', *Int. J. Pharm.*, vol. 514, no. 2, pp. 456–464, Dec. 2016.
- [5] A. M. Agrawal, M. S. Dudhedia, A. D. Patel, and M. S. Raikes, 'Characterization and performance assessment of solid dispersions prepared by hot melt extrusion and spray drying process', *Int. J. Pharm.*, vol. 457, no. 1, pp. 71–81, Nov. 2013.
- [6] O. Mahmah, R. Tabbakh, A. Kelly, and A. Paradkar, 'A comparative study of the effect of spray drying and hot-melt extrusion on the properties of amorphous solid dispersions containing felodipine', *J. Pharm. Pharmacol.*, vol. 66, no. 2, pp. 275–284, Feb. 2014.
- [7] M. T. Davis, C. B. Potter, and G. M. Walker, 'Downstream processing of a ternary amorphous solid dispersion: The impacts of spray drying and hot melt extrusion on powder flow, compression and dissolution', *Int. J. Pharm.*, vol. 544, no. 1, pp. 242–253, Jun. 2018.
- [8] Z. M. M. Lavra, D. Pereira de Santana, and M. I. Ré, 'Solubility and dissolution performances of spray-dried solid dispersion of Efavirenz in Soluplus', *Drug Dev. Ind. Pharm.*, vol. 43, no. 1, pp. 42–54, Jan. 2017.
- [9] R. N. Shamma and M. Basha, 'Soluplus®: A novel polymeric solubilizer for optimization of Carvedilol solid dispersions: Formulation design and effect of method of preparation', *Powder Technol.*, vol. 237, pp. 406–414, Mar. 2013.
- [10] J. Djuris, I. Nikolakakis, S. Ibric, Z. Djuric, and K. Kachrimanis, 'Preparation of carbamazepine-Soluplus solid dispersions by hot-melt extrusion, and prediction of drug-polymer miscibility by thermodynamic model fitting', *Eur. J. Pharm. Biopharm. Off. J. Arbeitsgemeinschaft Für Pharm. Verfahrenstechnik EV*, vol. 84, no. 1, pp. 228–237, May 2013.
- [11] A. Fini, C. Cavallari<sup>1</sup>, S. Ternullo<sup>2</sup>, F. Tarterini<sup>3</sup>, A. Fini<sup>1\*</sup>, and O. Internationals, 'Release Problems for Nifedipine in the Presence of Soluplus', *J. Pharm. Pharm.*, vol. 3, no. 2, pp. 0–0, Jun. 2016.
- [12] Y. Zhang *et al.*, 'Extruded Soluplus/SIM as an oral delivery system: characterization, interactions, in vitro and in vivo evaluations', *Drug Deliv.*, vol. 23, no. 6, pp.

1902–1911, Jul. 2016.

[13] M. Linn, ‘In vitro characterization of the novel solubility enhancing excipient Soluplus®’, *In vitro Charakterisierung des neuartigen Lösungsvermittlers Soluplus®*, 2011.

[14] M. L. Bruschi, Ed., ‘5 - Mathematical models of drug release’, in *Strategies to Modify the Drug Release from Pharmaceutical Systems*, Woodhead Publishing, 2015, pp. 63–86.

[15] J. S. Changdeo, M. Vinod, K. B. Shankar, and C. A. Rajaram, ‘Physicochemical characterization and solubility enhancement studies of allopurinol solid dispersions’, *Braz. J. Pharm. Sci.*, vol. 47, no. 3, pp. 513–523, Sep. 2011.

[16] S. Airaksinen, *Role of excipients in moisture sorption and physical stability of solid pharmaceutical formulations*. Helsinki: University of Helsinki, 2005.

[17] K. J. Crowley and G. Zografi, ‘Cryogenic grinding of indomethacin polymorphs and solvates: assessment of amorphous phase formation and amorphous phase physical stability’, *J. Pharm. Sci.*, vol. 91, no. 2, pp. 492–507, Feb. 2002.

[18] G. Aguirre-Álvarez, T. Foster, and S. E. Hill, ‘Modelling of isotherms and their hysteresis analysis in gelatin from different sources’, *CyTA - J. Food*, vol. 11, no. 1, pp. 68–74, Feb. 2013.

# Chapter 6 - General conclusion and perspectives

---



## General conclusion and perspectives

The main difficulty when an Active Pharmaceutical Ingredient (API) is orally administered is to guarantee that the clinical dose of the API will be dissolved in the available volume of gastrointestinal fluids. However, about 40% of APIs with market approval and nearly 90% of molecules in the discovery pipeline are poorly water-soluble and exhibits a poor oral absorption, which leads to a weak bioavailability.

Amorphous solid dispersions (ASDs) is considered as one of the most effective strategies to solve solubility limitations of poorly-water soluble compounds and hence, enhance their oral bioavailability. Despite their introduction as technical strategy to enhance oral APIs bioavailability more than 50 years ago, ASD formation and physical stability remains a subject of intense research.

In general, the advantages of amorphous form in pharmaceutical dosage forms are lost because of their inadequate thermodynamic stability and their tendency to recrystallize in the solid state or during dissolution. Therefore, to achieve the full advantage of ASDs, it is obligatory not only to maintain supersaturated concentration of the API during dissolution in the gastrointestinal tract, but also to stabilize the amorphous API during storage.

A relevant quantity of factors that have been noticed can influence the physical storage stability of ASDs, among them, the glass transition temperature of the API-carrier binary mixture, the apparent solubility of the API in the carrier, interactions between API and carrier, and the manufacturing process.

This thesis consisted of three parts that aim on developing new formulations of ASDs of an antiretroviral API, Efavirenz (EFV), dispersed in an amphiphilic polymer, Soluplus, by using two different processes, Spray-drying (SD) and Hot-melt extrusion (HME). EFV is the class II BCS API of our choice because it is a challenging API for new formulations. It needs more high-dosed ASDs, for which chemical and physical stability during storage and dissolution will be critical.

Aiming a rational development of high-loaded EFV-Soluplus ASDs, the first part focused on the construction of a temperature-composition EFV-Soluplus phase diagram. The phase-diagram was constructed from a thermal study of recrystallization of a supersaturated ASD (85 wt% in EFV), generated by spray drying. To our knowledge, this is the first study reporting a phase-diagram for this binary system. This phase-diagram is very useful and demonstrated that the EFV solubility in Soluplus ranges from 20 wt% (25°C) to 30 wt% (40°C). ASDs of EFV in Soluplus containing more than 30 wt% of EFV should be monitored

over storage under typical temperature conditions. This phase-diagram might be considered as a preformulation tool for researchers studying novel ASDs of EFV in Soluplus, to predict (thermodynamic and kinetic) stability.

ASDs prepared by different techniques can display differences in their physicochemical properties. Each of the two other studies focused on the manufacturing of ASDs by HME or SD processes. We demonstrated that supersaturated ASDs, in a large range of EFV concentration, loaded from 20 wt% up to 70 wt% EFV could be generated by HME. Indeed, more supersaturated ASD containing 85 wt% EFV was generated by spray drying, composition not investigated with HME. The amorphous state of all ASDs was confirmed by XRD and DSC analysis.

The two components seem to be well spatially distributed in all extruded ASDs and in most of the spray-dried ASDs as demonstrated by Raman mapping. However, high API loads might generate supersaturated systems in which the amorphous EFV in excess is distributed as amorphous clusters in the sample, as detected for the spray-dried ASD with 85 wt% EFV.

The manufacturing processes influenced the EFV apparent solubility enhancement, studied in an aqueous medium containing 0.25% SLS. For a same formulation (20%EFV-80%Soluplus), the results revealed an increase of 48 fold for spray-dried ASDs and 46 fold for extruded ASDs. No remarkable difference was observed in the maximum apparent solubility achieved for extruded and spray-dried ASDs (46-48 fold) with this EFV load (20 wt%). Nevertheless, the ‘parachute effect’ was limited over time for the spray-dried ASD. In 24 h experiment, a decline of the kinetic solubility was detected for this sample, a behavior not observed for the extruded ASD.

Soluplus has interesting characteristics to maintain supersaturation by forming micelles and ensuring a micellar API solubilization. However, very high concentrations in the aqueous medium can lead to other effects like gelling, changes of chains conformation related to a thermoresponsive behavior at temperatures near its LCST of 40°C. The gelling effect was already mentioned in other studies reported in the literature, although rarely.

To predict *in vitro* EFV dissolution behavior, different dissolution profiles were generated depending on the dissolution conditions (sink or non-sink). So far, few studies have reported the dissolution performance of EFV in Soluplus matrix and no studies were realized comparing sink and non-sink dissolutions. The transformation of amorphous state into crystalline structures during the dissolution process has been considered as a limiting factor in the development of ASDs. Indeed, the recrystallization in the biological environment can

directly influence the drug absorption present in these systems and non-sink conditions are better representative of the in vivo conditions. Although these differences, all ASDs have not shown signs of recrystallization in non-sink conditions. Moreover, the API release from spray-dried ASDs revealed to be much faster and higher when compared with extruded samples. This result is linked to differences in the particle size of spray dried and extruded particles, with a difference of, approximately, 90 fold in the surface area of the final product.

The release kinetics showed that the drug release mechanism involved in the EFV release from all spray-dried ASD formulations corresponds to a Fickian diffusion control. The penetration of the dissolution medium is controlled by the diffusion through the polymer layer around the EFV molecularly dispersed in the solid dispersions.

In contrast, the release kinetics from extruded ASDs with 20 wt% EFV under sink conditions suggests a non-Fickian release mechanism. In this case, the controlling mechanism could be the swelling or relaxation of polymeric chains. This behavior represented well the slow EFV release and is in good agreement with the thermoresponsive character of the Soluplus already mentioned. For the other extruded ASDs, the release kinetics seems to be driven by a non-Fickian diffusion, with anomalous transport marked by a combination of different mechanisms (diffusion, swelling, rearrangement of polymeric chains).

It will be interesting for the subsequent release studies of EFV-Soluplus ASDs to implement a downstream processing like jet milling, ball milling, mortar and pestle, or co-milling in order to reduce differences in particle size (surface area) between spray-dried powders and milled extrudates. Moreover, to carry out dissolution studies, intrinsic dissolution rate (IDR) or surface area normalized dissolution (for dispersions) rate might be a relevant strategy to properly compare the impact of manufacturing process in the final product generated by SD and HME processes.

The creation of a stable glass solution requires the equilibrium or thermodynamic solid solubility of the API in the carrier not to be exceeded. In practice, however, this thermodynamic solid solubility can be exceeded, creating glass solutions which are unstable over time (i.e., kinetically stable). According to our temperature-composition EFV-Soluplus phase diagram, the most of studied ASDs are supersaturated at typical storage temperature. Hence, physical stability can be considered as a critical parameter for them. However, the ASDs generated in this thesis present the following characteristics to favor physical stability:

- An antiplasticizing effect of the carrier used, confirmed by the increase of  $T_{\text{mix}}^{\text{g}}$  with the increased mass proportion of Soluplus in the binary mixtures,

- Possible interactions between EFV and Soluplus, confirmed by FTIR studies and probably due to hydrogen bonds interactions between the proton donating groups (-NH) of EFV and the proton accepting groups (C=O) of the Soluplus.

Moreover, a comparative analysis also revealed reduction of the intensity of characteristic compounds peaks for extruded ASDs. This might suggest a higher interaction between EFV and Soluplus in extruded compared to spray-dried ASDs. Melting process could generate ASDs with deeper interaction at the molecular level, however this clearly deserves further investigation.

It was also of interest to determine the feasibility of using high EFV loads. The more supersaturated the glass solution, the more prone it will be to crystallize. While it was demonstrated that the spray-dried ASD with 70 wt% EFV started to recrystallize in a short time experiment (15 days) at 40°C and 75%RH, no evolution was detected for extruded ASD with similar composition.

In future studies of EFV-Soluplus physical stability, it will be interesting to perform analysis in a prolonged time experiment (at least 6 months) to better investigate the physical stability performance for supersaturated EFV binary mixture.

Finally, this study clearly shows that ASD is a useful formulation strategy to improve the aqueous solubility and the dissolution rate of EFV from EFV-Soluplus binary mixtures. HME and SD manufacturing processes demonstrated to be efficient to generate ASDs in a large range of compositions and loads of EFV. The optimization of EFV to Soluplus ratio can be used to tailor the release kinetics from ASDs. The choice of a high EFV load exceeding the thermodynamic solid solubility in Soluplus is possible but it needs the consideration of its kinetic stability over time.

# Chapter 7 – Résumé étendu en français

---



## Résumé étendu en français

Lors de l'administration d'un ingrédient pharmaceutique actif (PA) par voie orale, les obstacles physico-chimiques à sa biodisponibilité orale comprennent une faible solubilité dans l'eau (propriété thermodynamique à l'équilibre) et une vitesse de dissolution lente (propriété cinétique). La faible solubilité dans l'eau d'un PA peut en effet limiter sa concentration dans les fluides gastriques et entraîner une faible absorption par l'intestin [1]. Une faible vitesse de dissolution peut également limiter l'absorption, en particulier lorsque la solubilité du PA est suffisamment faible. Il sera nécessaire de maintenir la concentration en PA proche de sa solubilité afin que l'absorption soit maximale au cours du temps limité pendant lequel le PA transite dans le tube digestif (Figure 75).

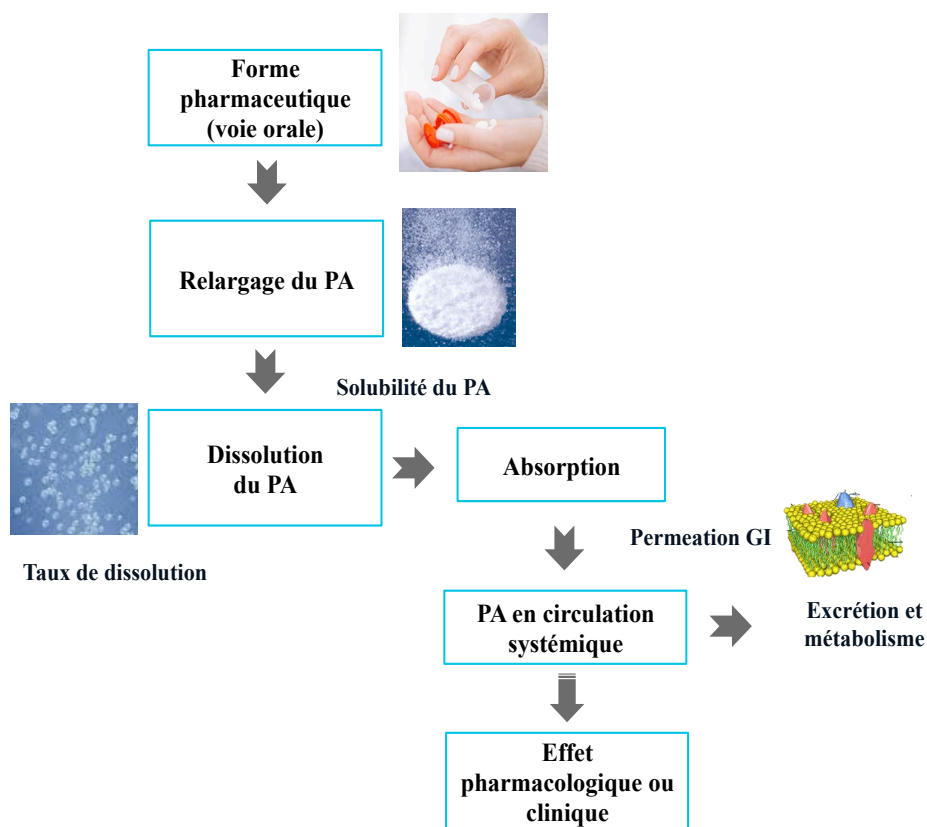
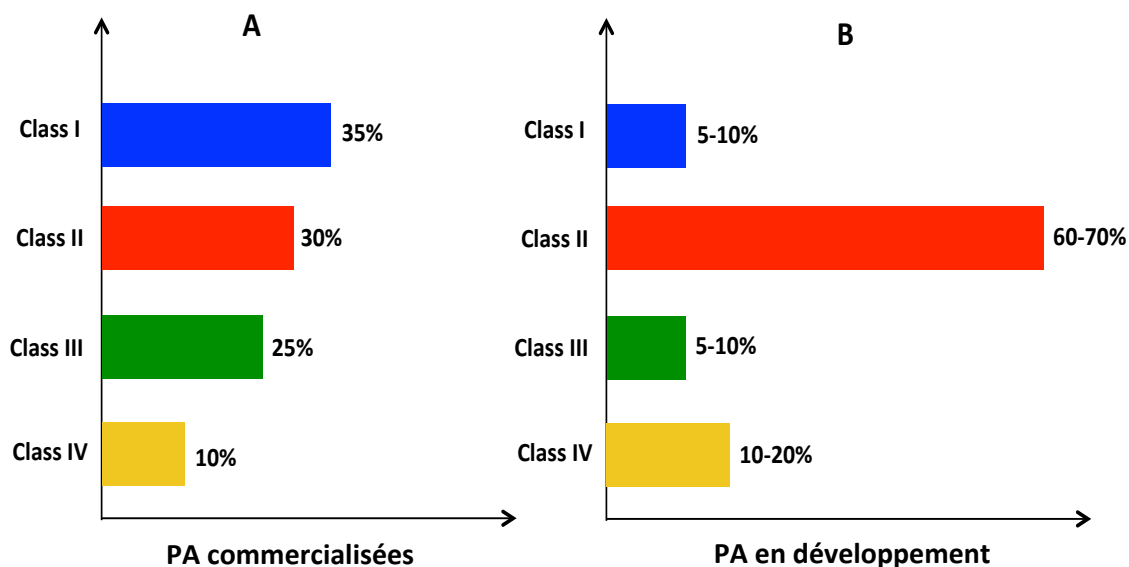


Figure 75. Représentation schématique du devenir d'un PA dans l'organisme après administration orale [2]–[4].

Les tendances émergentes dans la chimie combinatoire et le design des molécules actives d'intérêt pharmaceutique ont conduit au développement de candidats-médicaments ayant une lipophilicité plus importante et une faible solubilité dans l'eau [3], [5], [6]. Comme l'indique la Figure 76, environ 40% des PA approuvés par le marché et près de 90% des molécules-candidates en développement sont peu solubles dans l'eau. La plupart de ces composés appartiennent à la

classe II selon le Système de Classification Biopharmaceutique (BCS). Les composés de classe II se caractérisent par une faible solubilité dans l'eau et une perméabilité effective élevée [3].



*Figure 76. Défis de la solubilité dans le développement des PA pour une administration orale. A) PA commercialisés et B) PA en développement [3]*

Différentes approches (modifications de l'état du solide ou solubilisation/ complexation) ont été mises en œuvre pour développer des formes galéniques orales des PA peu solubles dans l'eau comme indiqué sur la Figure 77. Au cours des dernières années, les dispersions solides, qui impliquent la dispersion d'un composé faiblement soluble dans l'eau dans un support hydrophile ou amphiphile, sont apparues comme une stratégie prometteuse [7]–[9].

Plusieurs types de dispersions solides ont été développés selon l'état physique du PA dans le polymère. Les systèmes les plus courants et les plus attrayants sont les suspensions ou solutions solides amorphes, dans lesquelles le composé actif est sous forme amorphe ou dispersé au niveau moléculaire. L'état amorphe ou la dispersion moléculaire d'un PA montre généralement une biodisponibilité orale supérieure à celle de la forme cristalline [10]–[12].

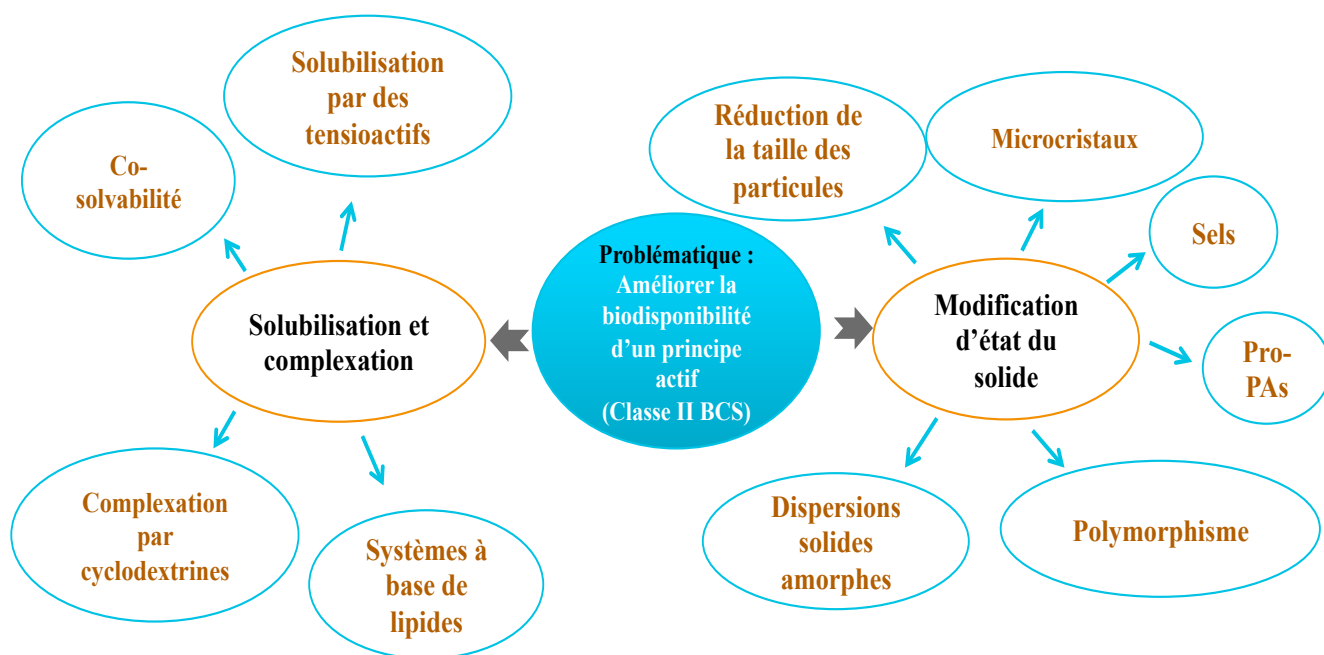


**Figure 77. Formulations stratégiques utilisées pour traiter la problématique d'amélioration de la biodisponibilité d'un principe actif d'intérêt pharmaceutique (Classe II BCS).**

Les dispersions solides amorphes (ASD) offrent un avantage potentiel dans la stabilisation d'une forme amorphe d'un PA. Cependant, la conversion de cette approche technologique en produits commerciaux performants reste un défi. Des problèmes tels qu'une mauvaise stabilité due à l'hygroscopicité, des écarts par rapport au comportement de dissolution attendu et une faible aptitude au traitement peuvent limiter leur utilité en tant que stratégie de formulation viable [11], [13]–[16].

Les performances des ASD (cinétique de solubilité et de dissolution, stabilité chimique et physique) sont affectées par les variables de formulation et de procédé. Les supports, en général les polymères [17], jouent un rôle important dans la stabilisation par divers mécanismes, comme l'anti-plastification ou des interactions intermoléculaires spécifiques [18], [19] sur la réduction de la mobilité moléculaire du PA amorphe [3], [11], [18], [20]–[22]. Les aspects moléculaires de la miscibilité et de l'interaction entre le PA et le polymère doivent donc être pris en compte lors de la formulation des dispersions solides. De plus, le choix approprié du support, la composition de la forme solide [17], [23] et le processus de fabrication peuvent aider à formuler un système amorphe stable, mais le contrôle minutieux de ces paramètres reste un défi scientifique. En particulier, la charge en PA dans ces structures solides représente un paramètre critique. exacerbé par le besoin sur le marché de formulations avec des doses plus élevées [15], [19], [24]. En effet, l'insertion sur le marché de dispersions solides amorphes à forte charge en PA peut réduire les doses ainsi que la production des industries pharmaceutiques afin de réaliser des économies de coûts. Au contraire, pour obtenir une stabilisation adéquate, les ASD sont

souvent produites avec une charge du PA relativement faible (<30 % m), nécessitant de fortes doses de la formulation pour assurer l'efficacité thérapeutique.

Divers procédés sont utilisés pour la fabrication des ASD en utilisant un procédé basé sur la fusion ou la solubilisation [25]. Néanmoins, l'extrusion à chaud (HME) et le séchage par atomisation (SD) sont les procédés de fabrication les plus courants [26]–[29]. Le SD est un procédé à base de solvant dans lequel la structure du réseau cristallin du PA est complètement détruite pendant le processus de préparation par sa solubilisation, généralement dans un solvant organique. C'est une technologie très efficace basée sur l'évaporation extrêmement rapide du solvant, conduisant à une transformation rapide du PA en une forme amorphisée dispersée dans des particules de support solides. L'extrusion à chaud est un processus sans solvant, dans lequel la structure cristalline du PA est détruite par les températures élevées et les contraintes mécaniques. Ces deux procédés de fabrication sont attrayants compte tenu des possibilités de changement d'échelle. Cependant, une amorphisation imparfaite des dispersions solides extrudées due à la présence de noyaux restants ou de petits cristaux, ou la présence de solvants résiduels dans des dispersions solides séchées par atomisation peut conduire à une recristallisation après la préparation. Certains points critiques doivent être contrôlés ou surveillés lors de la préparation de la suspension solide ou de la solution par ces procédés [27]–[29].

Le but de la caractérisation d'une ASD est donc de montrer la faisabilité de ce système complexe et sa capacité à améliorer la solubilité d'un PA, la vitesse de dissolution et également à maintenir les performances de la solution sursaturée en termes de stabilité, en contrôlant / réduisant sa tendance à la recristallisation [30]. Pour atteindre cet objectif, plusieurs techniques peuvent être utilisées afin d'explorer la structure physique, l'interaction moléculaire et le comportement des ASD [20], [27], [30] comme le montre la Figure 78.

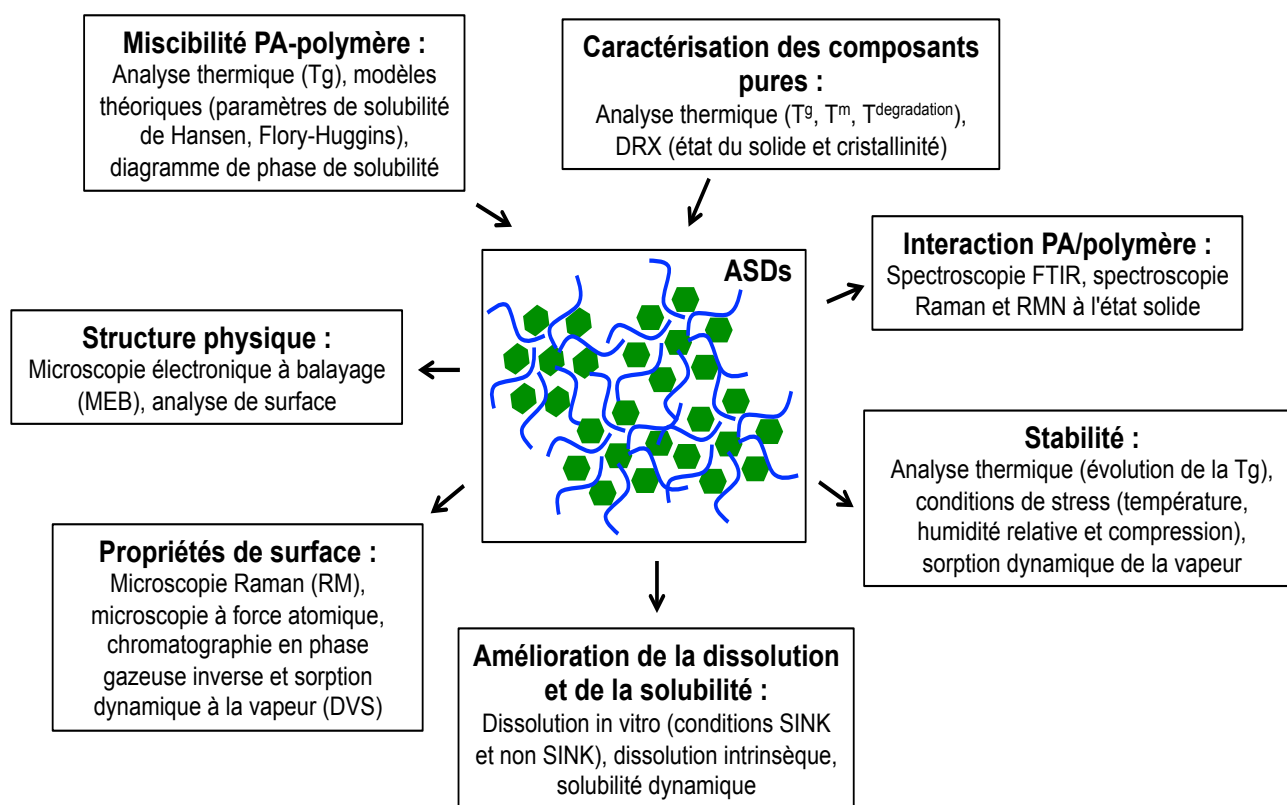
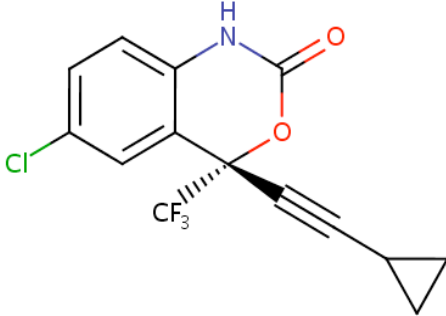


Figure 78. Résumé (non-exhaustif) des techniques de caractérisation des ASD.

Chaque molécule active d'intérêt pharmaceutique représente un cas spécifique et l'adaptation d'une technologie à un PA n'est généralement pas évidente. L'Efavirenz (EFV) est le PA de choix pour le développement de cette thèse car il représente un défi pour les nouvelles formulations : EFV, antirétroviral, appartient à la classe II du système BCS, c'est-à-dire qu'il a une faible solubilité dans l'eau (entre 1- 9  $\mu\text{g/mL}$  à la température ambiante), entraînant une mauvaise absorption gastro-intestinale et, par conséquent, une faible biodisponibilité orale [31]–[33].

La formule moléculaire de EFV est  $\text{C}_{19}\text{H}_{19}\text{ClF}_3\text{NO}_2$  (315,68 g/mol). Un résumé de ses caractéristiques physico-chimiques est présenté dans le Tableau 1.

*Tableau 1. Résumé des caractéristiques physicochimiques de l'Efavirenz*

<b>Masse moléculaire</b>	315,68 g/mol	<b>Structure chimique</b> 
<b>Point de fusion</b>	139-141 °C	
<b>pKa</b>	10,2	
<b>Log P</b>	4,6	
<b>Solubilité aqueuse</b>	1-9 µg/mL (25°C)	
<b>Accepteurs - PA</b>	5	
<b>Donneurs - PA</b>	1	

Plusieurs travaux de recherche portant sur l'amélioration de la solubilité/vitesse de dissolution de l'EFV, parmi lesquels les ASD, ont été publiés. Ils ont été développés en utilisant différents supports polymères et procédés de fabrication [20], [34]–[38] et les formulations obtenues ne sont pas comparables que ce soit au niveau de la composition ou de la structure physique. De plus, la stabilité physique est étudiée dans des conditions spécifiques, mais le comportement n'est pas toujours compris. L'EFV a également besoin d'ASD à plus forte dose, pour lesquelles la stabilité chimique et physique pendant le stockage et la dissolution sera essentielle [20], [34], [35], [39].

Dans ce contexte, cette thèse a été composée de trois parties qui visent à développer de nouvelles formulations d'ASD avec EFV (le PA) dispersé dans Soluplus (un polymère amphiphile), en utilisant deux procédés différents : le séchage par atomisation (SD) et l'extrusion à chaud (HME).

Dans le but de développer de manière rationnelle les ASD EFV-Soluplus fortement chargées en EFV, la première partie de cette thèse s'est concentrée sur la construction d'un diagramme de phase EFV-Soluplus. Le diagramme de phase représenté sur la Figure 79 a été construit à partir d'une étude thermique de la recristallisation d'une ASD sursaturée (85 % m en EFV), générée par SD. À notre connaissance, il s'agit de la première étude rapportant un diagramme de phase pour ce système binaire. Ce diagramme de phase est très utile et démontre que la solubilité de l'EFV dans le Soluplus va de 20 % m à 25 °C jusqu'à 30 % m (40 °C). Les ASD de l'EFV dans le Soluplus contenant plus de 30 % m d'EFV doivent donc être surveillées pendant le stockage dans des conditions de température ambiante. Ce diagramme de phase peut

être considéré comme un outil de pré-formulation pour les chercheurs qui étudient des ASD d'EFV dans le Soluplus afin de prédire la stabilité (thermodynamique et cinétique).

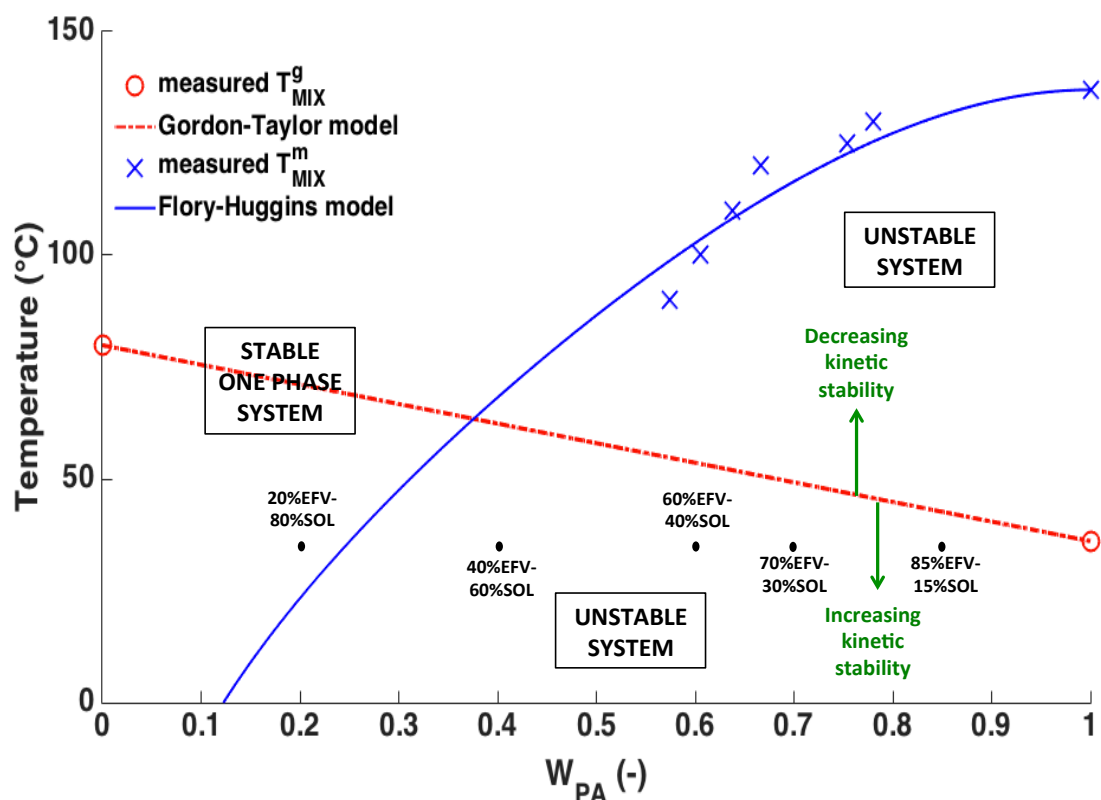


Figure 79. Diagramme de phase EFV(PA)/Soluplus. Les formulations des ASD étudiées dans cette thèse ont également été représentées à la température de  $T = 37^\circ\text{C}$  ( $T$  utilisée pour les essais de solubilité et dissolution)

Les ASD préparées par différents procédés peuvent montrer des différences dans leurs propriétés physico-chimiques. Chacune des deux autres études portait sur la fabrication d'ASD par les procédés HME ou SD. Nous avons démontré que les ASD sursaturées, dans une large gamme de concentration allant de 20 à 70 % m d'EFV, pouvaient être générées par HME et SD. Les ASD sursaturées les plus concentrées avec 85 % m en EFV ont été générées par SD, composition non étudiée avec HME. L'état amorphe de toutes les ASDs a été confirmé par analyses DRX et DSC.

Les deux composants semblent bien répartis spatialement dans toutes les ASD extrudées et dans la plupart des ASD séchées par atomisation, comme le montre la cartographie Raman (Chapitres 4 et 5). Cependant, des charges du PA élevées peuvent générer des systèmes sursaturés dans lesquels l'EFV amorphe en excès est distribué sous forme de clusters amorphes dans l'échantillon, comme détecté pour l'ASD séchée par atomisation avec 85 % m en EFV.

La solubilité apparente de l'EFV a été étudiée pour les différentes ASD dans un milieu aqueux contenant 0,25 % m de SLS. Aucune différence remarquable n'a été observée dans la

solubilité apparente maximale obtenue pour les ASD extrudées et séchées par atomisation (46 à 48 fois) avec une charge de EFV de 20 % m. Néanmoins, l'effet « parachute » a été limité dans le temps pour l'ASD générée par SD. En effet, pour une durée de 24h, une diminution de la solubilité cinétique a été détectée pour cet échantillon, comportement non observé pour l'ASD extrudée.

De plus, le Soluplus présente des caractéristiques intéressantes pour maintenir la sursaturation en formant des micelles et en assurant une solubilisation micellaire du PA. Cependant, des concentrations très élevées dans le milieu aqueux peuvent avoir d'autres effets, tels que la gélification, des modifications de la conformation des chaînes liées à un comportement thermo-réactif à des températures proches de sa valeur de Température de Solution Critique Inférieure (LCST) de 40 °C. L'effet gélifiant a déjà été mentionné dans d'autres études, bien que rarement[29], [40].

Pour prédire le comportement de la dissolution in vitro pour l'EFV, différents profils de dissolution ont été générés en fonction des conditions de dissolution (sink et non sink). Jusqu'à présent, peu d'études ont rapporté les performances de dissolution de l'EFV dans la matrice Soluplus et aucune étude n'a été réalisée comparant les dissolutions dans ces conditions. La transformation de l'état amorphe en structures cristallines au cours du processus de dissolution a été considérée comme un facteur limitant dans le développement des ASD. En effet, la recristallisation dans l'environnement biologique peut directement influencer sur l'absorption du principe actif présent dans ces systèmes, et les conditions non-sink sont plus représentatives des conditions in vivo. Toutes les ASDs ont montré des signes de recristallisation dans des conditions non-sink et ce relargage d'EFV s'est révélé beaucoup plus rapide et plus élevé pour les ADS séchées par atomisation que celle des échantillons extrudés. Ce résultat est essentiellement lié aux différences de granulométrie des particules séchées par atomisation et des particules extrudées, avec un facteur d'environ 90 entre les surfaces spécifiques des produits finaux.

La cinétique de relargage a montré que le mécanisme de libération d'EFV de toutes les formulations d'ASD séchées par atomisation correspond à la diffusion « fickienne ». La pénétration du milieu de dissolution est contrôlée par la diffusion à travers la couche de polymère autour de l'EFV dispersée moléculairement dans les dispersions solides. En revanche, la cinétique de relargage des ASD extrudées avec 20 % m en EFV dans des conditions sink suggère un mécanisme de libération non « fickien ». Dans ce cas, le mécanisme de contrôle pourrait être le gonflement ou la relaxation des chaînes de polymères, ce comportement étant en accord avec le caractère thermo-réactif du Soluplus déjà mentionné. Pour les autres ASD extrudées, la cinétique de libération semble être contrôlée par la diffusion non fickienne, avec un transport

anormal marqué par une combinaison de différents mécanismes (diffusion, gonflement, réarrangement des chaînes de polymères).

Il sera intéressant, pour les études à venir des ASD EFV-Soluplus, de mettre en œuvre un traitement en aval tel que le broyage à jets d'air, le broyage à billes, le mortier et le pilon, ou le co-broyage, afin de réduire les différences de taille des particules (surface spécifique) entre les matériaux obtenus par atomisation et extrudés. De plus, pour mener des études de dissolution, le taux de dissolution intrinsèque (IDR) ou le taux de dissolution normalisé par la surface (pour les dispersions solides) pourrait être une stratégie pertinente pour comparer correctement l'impact du processus de fabrication sur le produit final généré par les deux procédés, SD et HME. De plus, la variation des conditions de dissolution (pH, composition du milieu, ..) pourrait permettre de compléter cette comparaison entre les procédés.

La création d'une dispersion solide amorphe stable nécessite que la solubilité du PA dans le support ne soit pas dépassée afin de ne pas créer des solutions vitreuses cinétiquement instables. Selon notre diagramme de phase température-composition du mélange EFV-Soluplus, la plupart des ASDs étudiées sont sursaturées à une température de stockage proche de l'ambiante. Par conséquent, la stabilité physique peut être considérée comme un paramètre critique pour ces mélanges. Cependant, les ASD générées dans cette thèse présentaient les caractéristiques suivantes pour favoriser la stabilité physique :

- effet anti-plastifiant du support utilisé, confirmé par l'augmentation de la température de transition des mélanges binaires,  $T_g^{mix}$ , avec l'augmentation de la quantité de Soluplus,

- interactions possibles entre l'EFV et le Soluplus, confirmées par les études FTIR et probablement dues à des interactions de type liaison hydrogène entre les groupes donneurs de proton (-NH) de l'EFV et les groupes accepteurs de protons (C=O) du Soluplus.

En outre, une analyse comparative a également révélé une réduction de l'intensité des pics caractéristiques des composés pour les ASD extrudés. Cela suggère une interaction plus forte entre l'EFV et le Soluplus dans les ASD extrudées par rapport aux ASD séchées par atomisation. Le processus de fusion pourrait ainsi générer des ASDs avec une interaction plus profonde au niveau moléculaire, mais cela mérite clairement d'être confirmé par une étude plus approfondie.

Il était également intéressant de déterminer la faisabilité d'ASDs avec des charges élevées d'EFV. En effet, plus la solution vitreuse est sursaturée, plus elle sera susceptible de recristalliser. Il a été démontré que l'ASD séchée par atomisation avec 70 % m en EFV a commencé à recristalliser au cours d'une expérience de courte durée (15 jours) à 40 °C et à 75 % d'humidité

relative, alors qu'aucune évolution n'a été détectée pour une ASD extrudée de composition similaire.

Dans les futures études de stabilité physique EFV-Soluplus, il sera intéressant de réaliser une expérience à long terme (au moins 6 mois) afin de mieux étudier les performances de la stabilité physique du mélange binaire de l'EFV sursaturé.

Enfin, cette étude montre clairement que les ASD constituent une stratégie de formulation utile pour améliorer la solubilité dans l'eau et la vitesse de dissolution de l'EFV à partir de mélanges binaires EFV-Soluplus. Les procédés de fabrication, HME et SD, se sont révélés efficaces pour générer des ASD dans une large gamme de compositions d'EFV. L'optimisation du ratio EFV sur Soluplus peut être utilisée pour adapter la cinétique de libération des ASD. Le choix d'une charge d'EFV élevée dépassant la solubilité de l'EFV dans le Soluplus est possible, mais il convient de prendre en compte sa stabilité dans le temps.

## Références bibliographiques

- [1] A. Dokoumetzidis and P. Macheras, 'A century of dissolution research: from Noyes and Whitney to the biopharmaceutics classification system', *Int. J. Pharm.*, vol. 321, no. 1–2, pp. 1–11, Sep. 2006.
- [2] 19 November and 2007, 'The administration of medicines', *Nursing Times*. [Online]. Available: <https://www.nursingtimes.net/clinical-archive/medicine-management/the-administration-of-medicines/288560.article>. [Accessed: 01-Oct-2018].
- [3] J. M. Ting, W. W. Porter, J. M. Mecca, F. S. Bates, and T. M. Reineke, 'Advances in Polymer Design for Enhancing Oral Drug Solubility and Delivery', *Bioconjug. Chem.*, vol. 29, no. 4, pp. 939–952, Apr. 2018.
- [4] J. M. Ting *et al.*, 'High-Throughput Excipient Discovery Enables Oral Delivery of Poorly Soluble Pharmaceuticals', *ACS Cent. Sci.*, vol. 2, no. 10, pp. 748–755, Oct. 2016.
- [5] E. Gué, *Formes galéniques polymériques avec cinétiques de libération améliorée pour le kétoprofène et le fénofibrate*. Lille 2, 2013.
- [6] D. M. Oh, R. L. Curl, and G. L. Amidon, 'Estimating the fraction dose absorbed from suspensions of poorly soluble compounds in humans: a mathematical model', *Pharm. Res.*, vol. 10, no. 2, pp. 264–270, Feb. 1993.
- [7] A. Paudel, Z. A. Worku, J. Meeus, S. Guns, and G. Van den Mooter, 'Manufacturing of solid dispersions of poorly water soluble drugs by spray drying: Formulation and process considerations', *Int. J. Pharm.*, vol. 453, no. 1, pp. 253–284, Aug. 2013.
- [8] T. Vasconcelos, S. Marques, J. das Neves, and B. Sarmiento, 'Amorphous solid dispersions: Rational selection of a manufacturing process', *Adv. Drug Deliv. Rev.*, vol. 100, pp. 85–101, May 2016.
- [9] S. Sareen, G. Mathew, and L. Joseph, 'Improvement in solubility of poor water-soluble drugs by solid dispersion', *Int. J. Pharm. Investig.*, vol. 2, no. 1, pp. 12–17, 2012.
- [10] S. Baghel, H. Cathcart, and N. J. O'Reilly, 'Polymeric Amorphous Solid Dispersions: A Review of Amorphization, Crystallization, Stabilization, Solid-State Characterization, and Aqueous Solubilization of Biopharmaceutical Classification System Class II Drugs', *J. Pharm. Sci.*, vol. 105, no. 9, pp. 2527–2544, Sep. 2016.
- [11] N. Shah, H. Sandhu, D. S. Choi, H. Chokshi, and A. W. Malick, *Amorphous Solid Dispersions: Theory and Practice*. Springer, 2014.
- [12] C. L.-N. Vo, C. Park, and B.-J. Lee, 'Current trends and future perspectives of solid dispersions containing poorly water-soluble drugs', *Eur. J. Pharm. Biopharm.*, vol. 85, no. 3, Part B, pp. 799–813, Nov. 2013.

- [13] S. Baghel, H. Cathcart, and N. J. O'Reilly, 'Polymeric Amorphous Solid Dispersions: A Review of Amorphization, Crystallization, Stabilization, Solid-State Characterization, and Aqueous Solubilization of Biopharmaceutical Classification System Class II Drugs', *J. Pharm. Sci.*, vol. 105, no. 9, pp. 2527–2544, Sep. 2016.
- [14] Y. Chen *et al.*, 'Initial Drug Dissolution from Amorphous Solid Dispersions Controlled by Polymer Dissolution and Drug-Polymer Interaction', *Pharm. Res.*, vol. 33, no. 10, pp. 2445–2458, 2016.
- [15] M. E. Brewster, R. Vandecruys, G. Verreck, and J. Peeters, 'Supersaturating drug delivery systems: effect of hydrophilic cyclodextrins and other excipients on the formation and stabilization of supersaturated drug solutions', *Pharm.*, vol. 63, no. 3, pp. 217–220, Mar. 2008.
- [16] N.-Q. Shi *et al.*, 'Self-micellizing solid dispersions enhance the properties and therapeutic potential of fenofibrate: Advantages, profiles and mechanisms', *Int. J. Pharm.*, vol. 528, no. 1, pp. 563–577, Aug. 2017.
- [17] S. Sh, S. Sb, K. As, and A. Nh, 'SOLID DISPERSION: A NOVEL APPROACH FOR POORLY WATER SOLUBLE DRUGS', *Int. J. Curr. Pharm. Res.*, vol. 7, no. 4, pp. 1–8, 2015.
- [18] S. Baghel, H. Cathcart, and N. J. O'Reilly, 'Understanding the generation and maintenance of supersaturation during the dissolution of amorphous solid dispersions using modulated DSC and <sup>1</sup>H NMR', *Int. J. Pharm.*, vol. 536, no. 1, pp. 414–425, Jan. 2018.
- [19] S. A. Raina *et al.*, 'Trends in the Precipitation and Crystallization Behavior of Supersaturated Aqueous Solutions of Poorly Water-Soluble Drugs Assessed Using Synchrotron Radiation', *J. Pharm. Sci.*, vol. 104, no. 6, pp. 1981–1992, Jun. 2015.
- [20] S. K. Sathigari, V. K. Radhakrishnan, V. A. Davis, D. L. Parsons, and R. J. Babu, 'Amorphous-state characterization of efavirenz—polymer hot-melt extrusion systems for dissolution enhancement', *J. Pharm. Sci.*, vol. 101, no. 9, pp. 3456–3464, Sep. 2012.
- [21] N. Ogawa *et al.*, 'Improvement in the water solubility of drugs with a solid dispersion system by spray drying and hot-melt extrusion with using the amphiphilic polyvinyl caprolactam-polyvinyl acetate-polyethylene glycol graft copolymer and d-mannitol', *Eur. J. Pharm. Sci.*, vol. 111, pp. 205–214, Jan. 2018.
- [22] M. M. Knopp *et al.*, 'Comparative Study of Different Methods for the Prediction of Drug–Polymer Solubility', *Mol. Pharm.*, vol. 12, no. 9, pp. 3408–3419, Sep. 2015.
- [23] D. Q. M. Craig and J. M. Newton, 'The dissolution of nortriptyline HCl from polyethylene glycol solid dispersions', *Int. J. Pharm.*, vol. 78, no. 1, pp. 175–182, Jan. 1992.

- [24] T. Xie and L. S. Taylor, 'Dissolution Performance of High Drug Loading Celecoxib Amorphous Solid Dispersions Formulated with Polymer Combinations', *Pharm. Res.*, vol. 33, no. 3, pp. 739–750, Mar. 2016.
- [25] S. B. Teja, S. P. Patil, G. Shete, S. Patel, and A. K. Bansal, 'Drug-excipient behavior in polymeric amorphous solid dispersions', *J. Excip. Food Chem.*, vol. 4, no. 3, pp. 70–94, Sep. 2013.
- [26] S. Guns, A. Dereymaker, P. Kayaert, V. Mathot, J. A. Martens, and G. V. den Mooter, 'Comparison Between Hot-Melt Extrusion and Spray-Drying for Manufacturing Solid Dispersions of the Graft Copolymer of Ethylene Glycol and Vinylalcohol', *Pharm. Res.*, vol. 28, no. 3, pp. 673–682, Mar. 2011.
- [27] A. M. Agrawal, M. S. Dudhedia, A. D. Patel, and M. S. Raikes, 'Characterization and performance assessment of solid dispersions prepared by hot melt extrusion and spray drying process', *Int. J. Pharm.*, vol. 457, no. 1, pp. 71–81, Nov. 2013.
- [28] V. Bhardwaj, N. S. Trasi, D. Y. Zemlyanov, and L. S. Taylor, 'Surface area normalized dissolution to study differences in itraconazole-copovidone solid dispersions prepared by spray-drying and hot melt extrusion', *Int. J. Pharm.*, vol. 540, no. 1–2, pp. 106–119, Apr. 2018.
- [29] J. F. Kelleher *et al.*, 'A comparative study between hot-melt extrusion and spray-drying for the manufacture of anti-hypertension compatible monolithic fixed-dose combination products', *Int. J. Pharm.*, vol. 545, no. 1–2, pp. 183–196, Jul. 2018.
- [30] X. Liu, X. Feng, R. O. Williams, and F. Zhang, 'Characterization of amorphous solid dispersions', *J. Pharm. Investig.*, vol. 48, no. 1, pp. 19–41, Jan. 2018.
- [31] 'Efavirenz | C<sub>14</sub>H<sub>9</sub>ClF<sub>3</sub>NO<sub>2</sub> - PubChem'. [Online]. Available: <https://pubchem.ncbi.nlm.nih.gov/compound/64139>. [Accessed: 08-Jun-2018].
- [32] L. Fitriani, A. Haqi, and E. Zaini, 'Preparation and characterization of solid dispersion freeze-dried efavirenz u polyvinylpyrrolidone K-30', *J. Adv. Pharm. Technol. Res.*, vol. 7, no. 3, pp. 105–109, Sep. 2016.
- [33] E. Zaini, F. Rachmaini, F. Armin, and L. Fitriani, 'Preparation and Characterization of Binary Mixture of Efavirenz and Nicotinamide', *Orient. J. Chem.*, vol. 31, no. 4, pp. 2271–2276, Dec. 2015.
- [34] P. T. Koh, J. N. Chuah, M. Talekar, A. Gorajana, and S. Garg, 'Formulation Development and Dissolution Rate Enhancement of Efavirenz by Solid Dispersion Systems', *Indian J. Pharm. Sci.*, vol. 75, no. 3, pp. 291–301, 2013.

- [35] Z. M. M. Lavra, D. Pereira de Santana, and M. I. Ré, 'Solubility and dissolution performances of spray-dried solid dispersion of Efavirenz in Soluplus', *Drug Dev. Ind. Pharm.*, vol. 43, no. 1, pp. 42–54, Jan. 2017.
- [36] C. R. D. Hoffmeister *et al.*, 'Efavirenz dissolution enhancement III: Colloid milling, pharmacokinetics and electronic tongue evaluation', *Eur. J. Pharm. Sci. Off. J. Eur. Fed. Pharm. Sci.*, vol. 99, pp. 310–317, Mar. 2017.
- [37] M. A. da Costa, R. C. Seiceira, C. R. Rodrigues, C. R. D. Hoffmeister, L. M. Cabral, and H. V. A. Rocha, 'Efavirenz Dissolution Enhancement I: Co-Micronization', *Pharmaceutics*, vol. 5, no. 1, pp. 1–22, Dec. 2012.
- [38] L. Fitriani, M. Fadhila, and E. Zaini, 'Preparation of Efavirenz - PVP K-30 Solid Dispersion by Spray Drying Technique', *Res. J. Pharm. Biol. Chem. Sci.*, vol. 6, no. 6, pp. 925–930, Dec. 2015.
- [39] K. Kawakami, Y. Bi, Y. Yoshihashi, K. Sugano, and K. Terada, 'Time-dependent phase separation of amorphous solid dispersions: Implications for accelerated stability studies', *J. Drug Deliv. Sci. Technol.*, vol. 46, pp. 197–206, Aug. 2018.
- [40] A. Varela-Garcia, A. Concheiro, and C. Alvarez-Lorenzo, 'Soluplus micelles for acyclovir ocular delivery: Formulation and cornea and sclera permeability', *Int. J. Pharm.*, vol. 552, no. 1–2, pp. 39–47, Sep. 2018.

# Chapter 8 – Works made from this thesis

---



- 25<sup>th</sup> International Conference on Bioencapsulation – Nantes (France) at July 2016

✓ Award of the best poster contribution for this conference.

## EVALUATION OF DRUG LOADING IN AMORPHOUS SOLID DISPERSION FOR EFAVIRENZ DELIVERY

COSTA, B.L.A., SESCOUSSE, R., SAUCEAU, M., RÉ, M.I.- RAPSODEE Center, France. [blinsdea@mines-albi.fr](mailto:blinsdea@mines-albi.fr)



### INTRODUCTION AND OBJECTIVE

Poorly water-soluble drugs have steadily grown on the global pharmaceutical industry. The technological approach focused on rendering the drug amorphous in nature to improve apparent solubility, dissolution rate and bioavailability remains a challenge since amorphous state is metastable in nature with a potential to undergo recrystallization (Wlodarski, 2015). In order to prevent this conversion, amorphous materials have been stabilized as solid dispersions using generally polymeric materials for stabilization (Lu, 2016).

An amorphous solid dispersion (ASD) is basically a drug-polymer two-component system in which the mechanism of drug dispersion is the key to understanding its behavior. Such formulations impart an antiplasticizing effect on the amorphous compound yielding an increase in the glass transition temperature thereby reducing molecular mobility (Patel, 2013). However, in order to achieve adequate stabilization, solid dispersions are often produced with a relatively low drug load (<30% w/w) where the drug is dispersed in the polymer at the molecular level. The problem is that a low drug loaded ASD requires a large dose to ensure therapeutic efficacy.

The insertion of high drug load formulations on the market is expected to meet patients demand for fixed, unique and smaller dosage combinations products. Furthermore, the supersaturated combinations may reduce dosage amounts as well as decrease the production in the pharmaceutical industries to supply cost savings. The aim of the current work was to verify the possibility to formulate high drug loaded (>40%) ASD of Efavirenz (EFV) by spray drying. EFV is a non-nucleoside reverse transcriptase inhibitor used in the first-line treatment of HIV and a class 2 drug in the Biopharmaceutical Classification Systems (BCS) with low solubility (3-9  $\mu$ g/mL) and high permeability (Hoffmeister, 2016). To stabilize the amorphous drug, an amphiphilic and water-soluble copolymer named Soluplus® was used.

### MATERIALS AND METHODS

EFV was kindly supplied by Cristalia Ltd (Itapira, Brazil), Soluplus® (polyvinyl caprolactam-polyvinyl acetate-polyethylene glycol) was obtained from BASF corporation (Ludwigshafen, Germany) and Ethanol was used as organic solvent (Carlo Erba, Italy).

A Buchi B-290 minispray dryer (Buchi Labortechnik AG, Flawil, Switzerland) equipped with Inert Loop B-295 and an integrated two-fluid 0.7 mm nozzle was used to produce the ASD samples. Compressed nitrogen was used as the drying/carrying gas with a flow rate of 600 L/h. The solution feed rate was typically 3g/min, the inlet temperature was set to 80  $\pm$  2°C and the outlet temperature was maintained at 59°C  $\pm$  2°C. The feeding solution was prepared by dissolving EFV in a 10 (w/w) % solution of Soluplus in ethanol. Binary mixtures EFV-Soluplus containing 40wt%, 60wt% and 85wt% of EFV were formulated as spray-dried powders.

X-ray diffraction (XRD), modulated differential scanning calorimetry (mDSC), Raman spectroscopy, scanning electron microscopy (SEM) and dynamic vapor sorption (DVS) were

used to characterize the solid state of the spray-dried samples.

### RESULTS AND DISCUSSION

Firstly, the absence of Bragg peaks in X-ray diffractograms (Figure 1) of all spray-dried solids indicates the complete loss of the crystalline structure of EFV, which became amorphous during the spray-drying process.

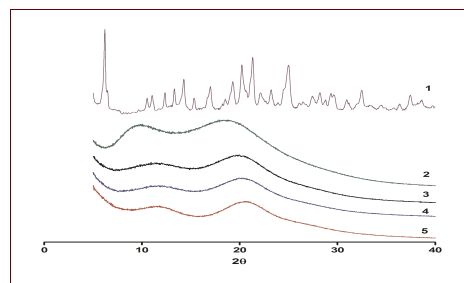


Figure 1. PXRD diffractograms of: (1) pure EFV; (2) pure Soluplus®; (3) ASD 40%EFV-Soluplus (w/w); (4) ASD 60%EFV-Soluplus (w/w) and (5) ASD 85%EFV-Soluplus (w/w)

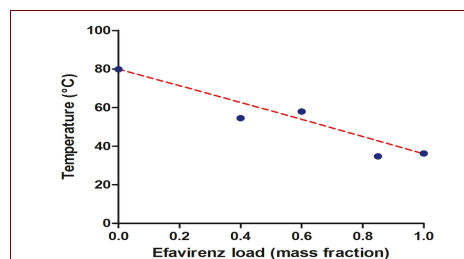


Figure 2. Glass temperature transition (T<sub>g</sub>) determined by mDSC (blue circles) and theoretical values by GT equation (dotted red line)

mDSC thermal analysis was performed to investigate the apparent EFV-Soluplus® miscibility. Figure 2 shows the single experimental glass transition temperature (T<sub>g</sub>) identified for each binary mixture EFV-Soluplus loaded with 40% to 85%(w/w) EFV, probably corresponding to the formation of an amorphous solid dispersions of EFV-Soluplus. The individual constituents (drug and polymer) were also spray-dried from ethanol solutions and used for comparison purposes (T<sub>g</sub> also in Figure 2). The T<sub>g</sub> of mixtures are placed as an intermediary between the pure drug and polymer values and are close to

# EVALUATION OF DRUG LOADING IN AMORPHOUS SOLID DISPERSION FOR EFAVIRENZ DELIVERY

Rapsodee Research Center, Université de Toulouse, École des Mines d'Albi, CNRS, Albi 81013 France



## Authors

Bhianca Lins de A. Costa  
Romain Sescousse  
Martial Sauceau  
Maria Inês Ré

## Contact

blinsdea@mines-albi.fr

## Acknowledgements

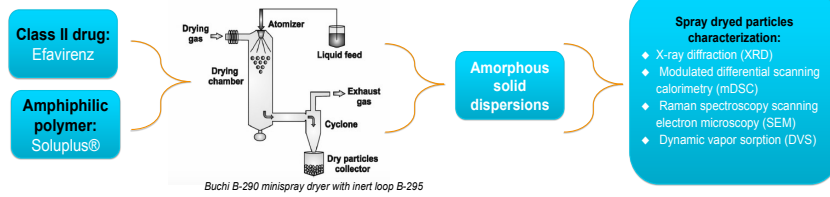
Rapsodee and Gala® platform (France) for technical support: Philippe Accart, Sylvie Delconetto, Véronique Nallet, Severine Patry, Christine Rolland and Laurene Haunie.



## INTRODUCTION AND OBJECTIVE

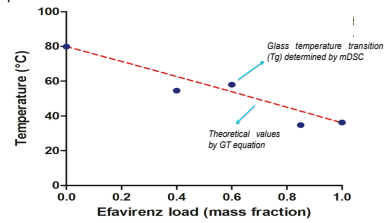
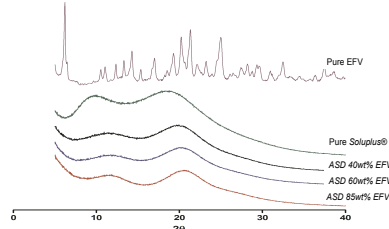
- The technological approach focused on rendering the drug amorphous in nature to improve apparent solubility, dissolution rate and bioavailability remains a challenge since amorphous state is metastable in nature with a potential to undergo recrystallization;
- In order, to achieve adequate stabilization, the strategic formulation of solid dispersions are often produced with a relatively low drug load (<30% w/w) where the drug is dispersed in the polymer at the molecular level. The problem is that a low drug loaded amorphous solid dispersions (ASD) requires a large dose to ensure therapeutic efficacy;
- The aim of the current work was to verify the possibility to formulate high drug loaded (>40%) ASD of Efavirenz (EFV) by spray drying.**

## MATERIALS AND METHODS

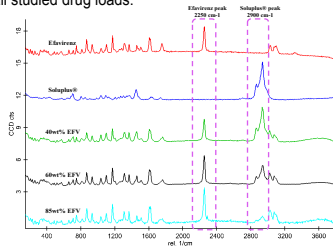


## RESULTS AND DISCUSSION

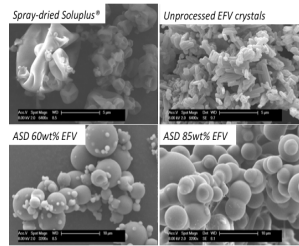
- X-ray diffraction (XRD):** Absence of Bragg peaks confirms the production of amorphous solid dispersions.
- Modulated differential scanning calorimetry (mDSC):** T<sub>g</sub> of mixture is close to the theoretical values of T<sub>g</sub> calculated by Gordon-Taylor (GT) equation.



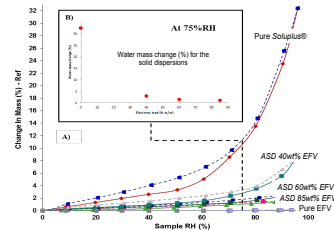
- Raman spectroscopy:** The presence of characteristic peaks of pure components in all ASD Raman spectra confirmed the good mixing between EFV-Soluplus® for all studied drug loads.



- Scanning electron microscopy (SEM):** The particles of ASD EFV-Soluplus® are predominantly spherical.



- Dynamic vapor sorption (DVS):** The decreased affinity to water with increased drug loading could be an interesting attribute for the amorphous phase physical stability.



## CONCLUSION AND PERSPECTIVES

- At the best of our knowledge, it is the first study reporting such levels of drug loading (>40%) in amorphous solid dispersions of EFV;
- Solubility and dissolution studies are currently being performed and stability studies are on going under stress conditions (40°C, 75%RH and compression tests).

## REFERENCES

Wordaski K., Sawicki W., Kozyra A. *et al.* 'Physical stability of solid dispersions with respect to thermodynamic solubility of tadalafil in PVP-VA' *Eur J Pharm Bio.* 2015, 96, 237-246.  
 Lu Z., Yang Y., Covington R. *et al.* 'Supersaturated controlled release matrix using amorphous dispersions of glipizide', *Int J Pharm.* 2016, 511, 957-968.  
 Patel B.B., Patel J.K., Chakraborty S., Shukla D., 'Revealing facts behind spray dried solid dispersions technology used for solubility enhancement', *Saudi Pharm J.* 2015, 23, 352-365.  
 Hoffmeister C. R. D., Fandaruff C., Costa M.A., *et al.* Efavirenz dissolution enhancement III: Colloid milling, pharmacokinetics and electronic tongue evaluation', *Eur J Pharm Sci.* 2017, 99, 310-317.





IDS'2018 – 21st International Drying Symposium  
València, Spain, 11-14 September 2018  
DOI: [http://dx.doi.org/10.4995/ids2018.2018.\\*\\*\\*\\*](http://dx.doi.org/10.4995/ids2018.2018.****)

**Generation of high drug loading amorphous solid dispersions by Spray Drying**

**B. L. A. Costa\***, M.Sauceau, R.Sescousse, M. I. Ré

Université de Toulouse; Ecole des Mines d'Albi; UMR CNRS 5302; Centre RAPSODEE, F-81013 Albi, France

\* [bhianca.lins\\_de\\_azevedo\\_costa@mines-albi.fr](mailto:bhianca.lins_de_azevedo_costa@mines-albi.fr)

---

**Abstract**

*Amorphous solid dispersions (ASDs) refers to drug - carrier systems, where the drug is dispersed in the carrier at a molecular level. In this work, ASDs were formulated by spray drying. The aim was to achieve high drug loads of an amorphous hydrophobic drug (Efavirenz - EFV) in the carrier Soluplus®. Solid state characterizations (mDSC, XRPD, DVS, Raman, SEM, stability and solubility studies) were done. EFV amorphisation in ASDs (20 to 85% EFV loads) resulted in improved drug solubility compared to unprocessed EFV crystals and tendency of properties evolution over time for ASDs with EFV loads higher than 70 wt%.*

**Keywords:** *amorphous solid dispersion, spray drying, high drug loading, soluplus, efavirenz.*

---





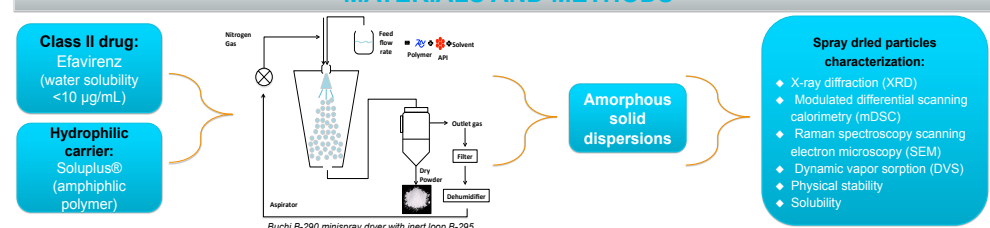
# GENERATION OF HIGH DRUG LOADING AMORPHOUS SOLID DISPERSIONS BY SPRAY DRYING

## MOTIVATION AND OBJECTIVE

### CONTEXT

- Amorphous solid dispersions (ASD) are a well-established strategy to improve apparent solubility, dissolution rate and bioavailability.
- High doses of APIs are suitable to achieve therapeutic efficacy with ASD.
- SCIENTIFIC CHALLENGE: Physical stability of ASD, in practice with high API load (> 40wt%).
- ✓ **AIM OF THIS STUDY:** To generate, by spray drying, ASDs comprising a hydrophobic drug class II BCS (Efavirenz) in a hydrophilic carrier (Soluplus®-SOL) expecting to achieve drug loads higher than 40 wt%.

## MATERIALS AND METHODS



### Authors

Bianca Lins de A. Costa  
Romain Sescousse  
Martial Sauceau  
Maria Inês Ré

### Contact

blinsdea@mines-albi.fr

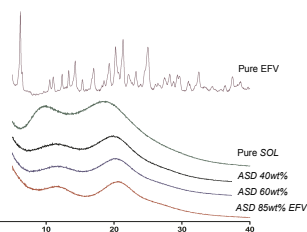
### Acknowledgements

Philippe Accart, Sylvie Delconferro, Véronique Nallet, Severine Patry, Christine Rolland and Laurene Haurie for technical support



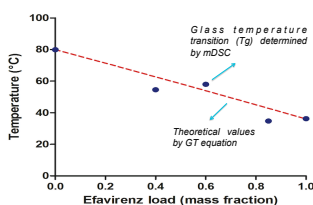
### XRD:

- Production of amorphous solid dispersions with 40 to 85wt% of EFV.



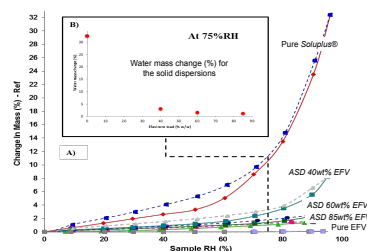
### mDSC:

- T<sub>g</sub> mixture close to the theoretical values calculated by Gordon-Taylor (GT) equation.



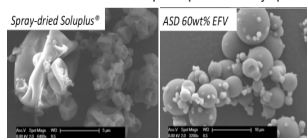
### DVS:

- Water affinity decreases with drug loading increase (interesting attribute for the amorphous phase stability).



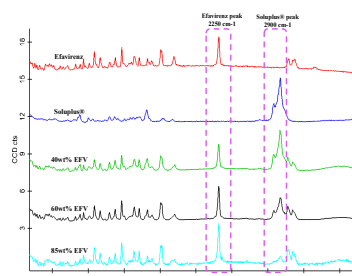
### SEM:

- Particles of ASD EFV-Soluplus® predominantly spherical.



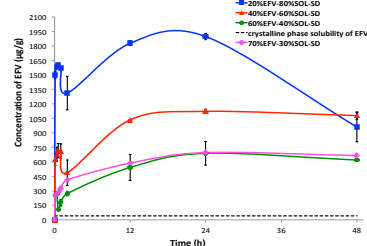
### Raman spectroscopy:

- Good mixing between EFV-Soluplus® for all drug loads.



### Solubility studies:

- EFV solubility decreases with drug load increases in ASDs



### Stability studies:

- No drug recrystallisation for 40 wt% EFV
- Partial EFV recrystallisation for 70wt % EFV

t (days)	40 % EFV-SOL		70 % EFV-SOL	
	T <sub>mix</sub> (°C)	T <sub>mix</sub> (°C)	Crystallization enthalpy ΔH (J/g)	Crystallization (%)
3	59.8	51.4	1.3	2.4
6	64.9	53.4	2.6	4.9
9	64.1	55.9	2.8	5.3
15	67.2	57.7	3.5	6.6

## CONCLUSION AND PERSPECTIVES

- At the best of our knowledge, it is the first study reporting such levels of drug loading (>40wt %) in amorphous solid dispersions of EFV;
- Solubility tests revealed a good solubility enhancement for all ASD compared with crystalline drug solubility;
- Physical stability should be a monitoring critical point for EFV-SOL ASDs with EFV loads higher than 70 wt% EFV.

## REFERENCES

Wlrodaski K., Sawicki W., Kozyra A. *et al.* 'Physical stability of solid dispersions with respect to thermodynamic solubility of tadalafil in PVP-VA' *Eur J Pharm Bio.* 2015, 96, 237-246.  
 Lu Z., Yang Y., Covington R. *et al.* 'Supersaturated controlled release matrix using amorphous dispersions of glipizide', *Int J Pharm.* 2016, 511, 957-968.  
 Patel B.B., Patel J.K., Chakraborty S., Shukla D., 'Revealing facts behind spray dried solid dispersions technology used for solubility enhancement', *Saudi Pharm J.* 2015, 23, 352-365.  
 Hoffmeister C. R. D., Fandanel C., Costa M.A., *et al.* 'Efavirenz dissolution enhancement III: Colloid milling, pharmacokinetics and electronic tongue evaluation', *Eur J Pharm Sci.* 2017, 99, 310-317.  
 J. A. Baird and L. S. Taylor, 'Evaluation of amorphous solid dispersion properties using thermal analysis techniques', *Adv. Drug Deliv. Rev.*, vol. 64, no. 5, pp. 396-421, Apr. 2012.

- Submitted article in an International Journal - 2018

**Determination of drug-polymer solubility from supersaturated spray-dried solid solutions: a case study with Efavirenz and Soluplus®**

## Manuscript Details

<b>Manuscript number</b>	EJPB_2018_825_R2
<b>Title</b>	Determination of drug-polymer solubility from supersaturated spray-dried solid solutions: a case study with Efavirenz and Soluplus®
<b>Article type</b>	Research Paper

### Abstract

Amorphous solid dispersions (ASDs) are found to be a well-established strategy for overcoming limited aqueous solubility and poor oral bioavailability of active pharmaceutical ingredients (APIs). One of the main parameters affecting ASDs physical stability is the API solubility in the carrier, because this value determines the maximal API load without a risk of phase separation and recrystallization. Phase-diagrams can be experimentally obtained by following the recrystallization of the API from a supersaturated homogeneous API-polymer solid solution, commonly produced by processes as solvent casting or comilling, which are very time-consuming (hours). The work deals with the construction of a temperature-composition EFV-Soluplus® phase diagram, from a thermal study of recrystallization of a supersaturated solid solution (85 wt% in EFV) generated by spray drying. This supersaturated solution is kept at a given annealing temperature to reach the equilibrium state and the amount that still remains dispersed in the polymer carrier at this equilibrium temperature is determined by means of the new glass transition temperature of the binary mixture. From our knowledge, this is the first study employing a fast process (spray drying) to prepare a supersaturated solid solution of an API in a polymer aiming to determine a temperature-composition phase diagram. The EFV solubility in Soluplus ranges from 20 wt% at 25 °C to 30 wt% at 40 °C. It can be a very useful preformulation tool for researchers studying amorphous solid dispersions of Efavirenz in Soluplus, to assist for predicting the stability of EFV-Soluplus ASDs at different EFV loadings and under different thermal conditions.

<b>Keywords</b>	amorphous solid dispersions, recrystallization method, Spray Drying, solubility, phase diagram, Efavirenz, Soluplus®
<b>Corresponding Author</b>	Bhianca Lins de Azevedo Costa
<b>Corresponding Author's Institution</b>	IMT Mines Albi-Carmaux

## Appendix

## Appendix 1- Contribution values of functional groups (Van Krevelen &amp; Te Nijenhuis, 2009)

Structural Group	$F_{di}$ (MJ.m <sup>3</sup> ) <sup>1/2</sup> .mol <sup>-1</sup>	$F_{pi}$ (MJ.m <sup>3</sup> ) <sup>1/2</sup> .mol <sup>-1</sup>	$E_{hi}$ (J.mol <sup>-1</sup> )
-CH <sub>3</sub>	420	0	0
-CH <sub>2</sub> -	270	0	0
>CH-	80	0	0
>C<	-70	0	0
=CH <sub>2</sub>	400	0	0
=CH-	200	0	0
=C<	70	0	0
C <sub>6</sub> H <sub>11</sub>	1620	0	0
C <sub>6</sub> H <sub>5</sub>	1430	110	0
C <sub>6</sub> H <sub>4</sub> (ortho/méta/para)	1270	110	0
-F	220	-	-
-Cl	450	550	400
-Br	550	-	-
-CN	430	1100	2500
-OH	210	500	20000
-O-	100	400	3000
-COH	470	800	4500
-CO-	290	770	2000
-COOH	530	420	10000

-COO-	390	490	7000
HCOO-	530	-	-
-NH <sub>2</sub>	280	-	8400
-NH-	160	210	3100
>N-	20	800	5000
-NO <sub>2</sub>	500	1070	1500
-S-	440	-	-
=PO <sub>4</sub>	740	1890	13000
Ring	190	-	-
Un plan de symétrie	NA	x 0,5	-
Deux plans de symétrie	NA	x 0,25	-
Plus de deux plans de symétrie	NA	x 0	x 0

## Appendix 2 – Approved procedure to EFV quantification by HPLC (Monograph posted on the Pharmacopeia USP)

### 1- Description of Chromatographic system

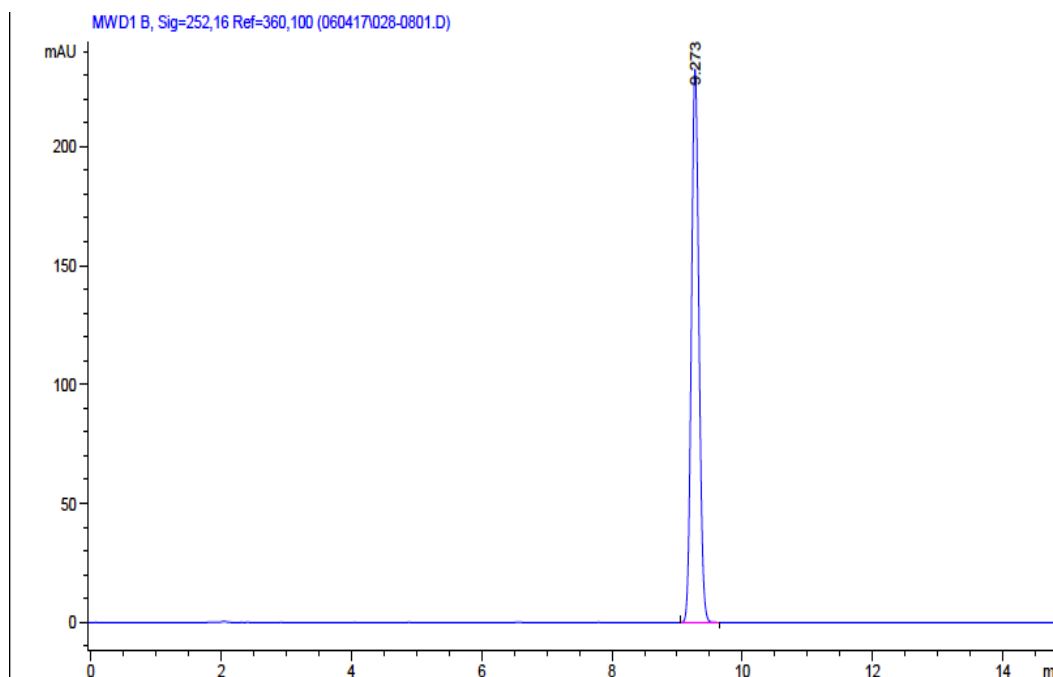
The liquid chromatograph is equipped with a column Phenomenex C18 kinetex (25 cm x 4.6 mm x 5  $\mu$ m) with a UV detector of 252 nm. The flow rate is about 1.0 mL per minute. The program used was based in an isocratic elution (mobile phase) with 50% of Acetonitrile (ACN) and 50% of an acetate buffer at pH 7.5.

Solution A: Dissolve 800 mg of ammonium acetate in 1000 mL of water, and then, the pH was adjust with 0.5% ammonia solution to a pH of 7.5  $\pm$  0.05.

Solution B: Acetonitrile

Mobile phase: Mixture of half of each solutions (A and B) and then, filtration with a polypropylene membrane of 0.45  $\mu$ m.

The column was maintained at 25°C and retention time of EFV was about 9.3 min, which is in good agreement with the EFV monograph.



*Example of EFV chromatogram obtained by HPLC*

## 2- Calibration curve

The calibration curve of EFV in Acetonitrile was prepared with different dilutions from the concentrated solution of EFV.

Firstly, a standard solution was prepared with a concentration of 1mg/g of EFV in ACN. Then, successive dilutions were performed in order to obtain the described calibration curve. Moreover, witnesses with EFV, ACN and aqueous medium containing 0.25% of SLS were also prepared to support the dissolution analysis by Sink an non-Sink conditions.

Preparation of witnesses:

- Sink conditions:

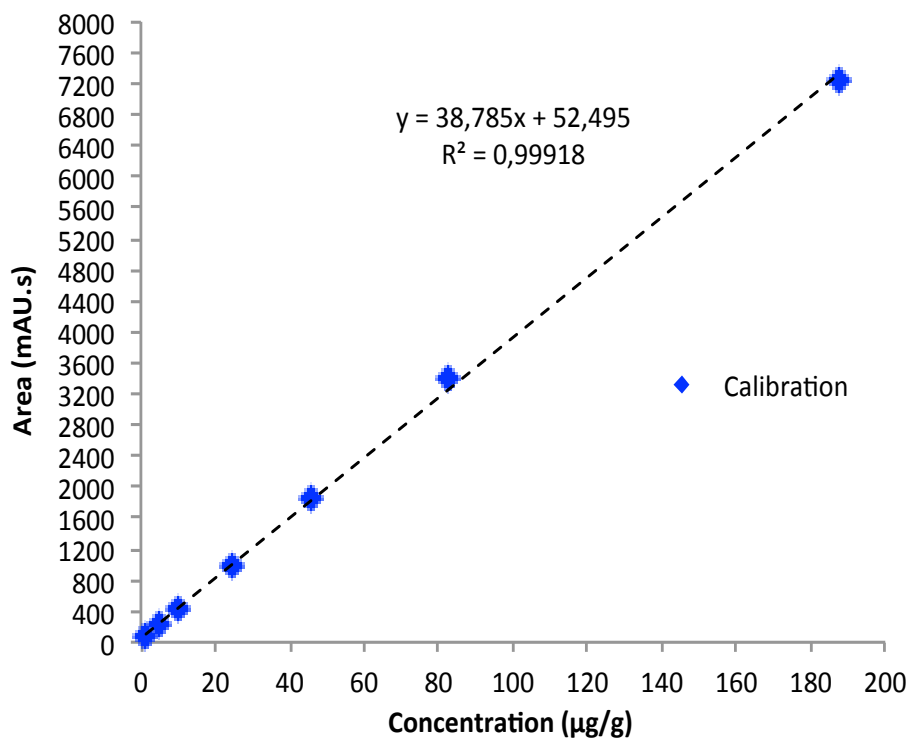
3.5 0.2 mg of EFV were adding to 15g of ACN and then, the volume was completed until reaching 250g with aqueous medium containing 0.25% of SLS.

- Non-Sink conditions:

42 0.2 mg of EFV were adding to 50g of ACN and then, the volume was completed until reaching 100g with aqueous medium containing 0.25% of SLS.

All analyses were performed in triplicate.

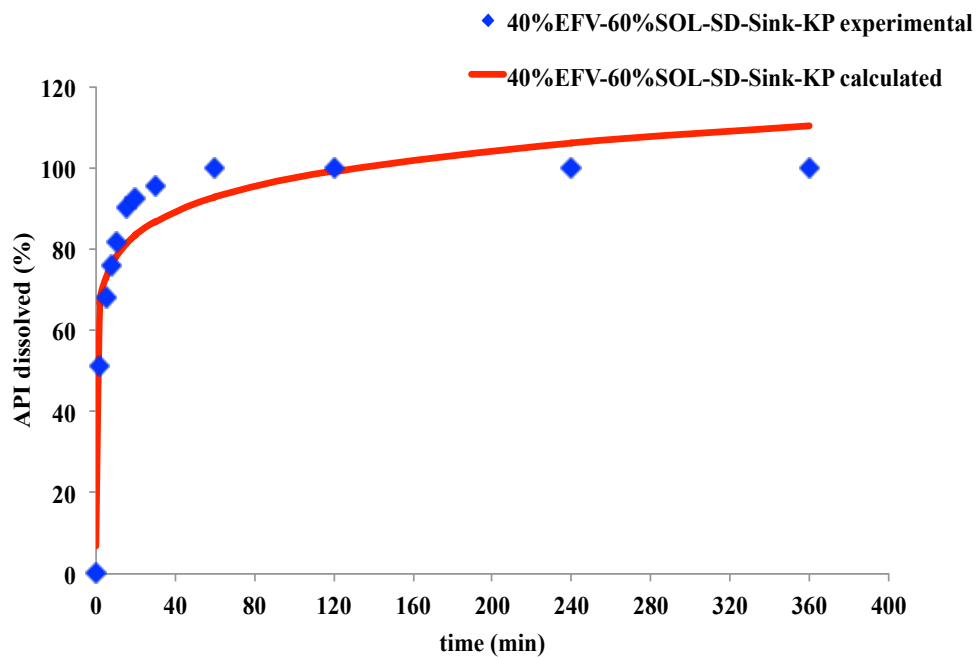
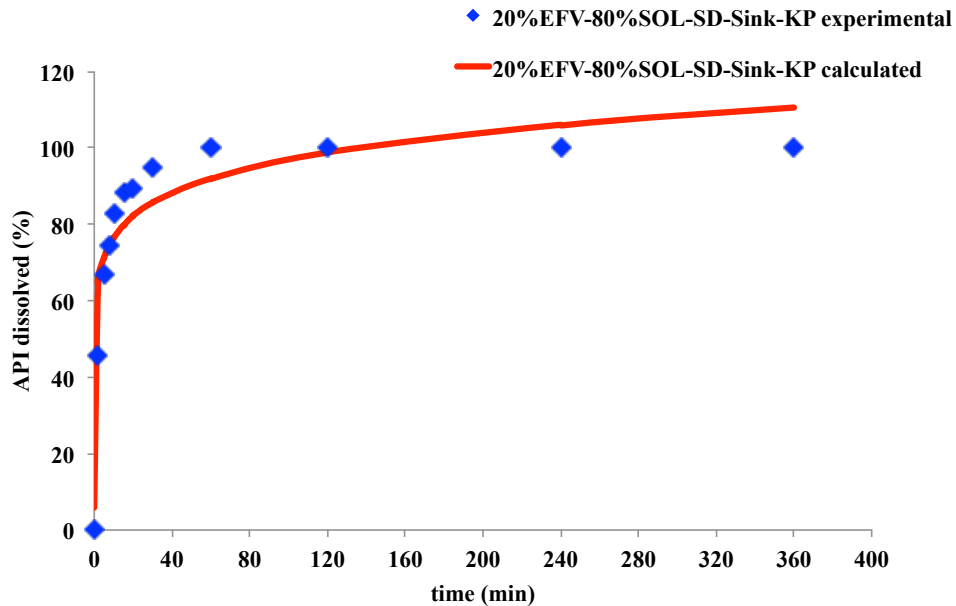
*Calibration curve in HPLC for EFV*

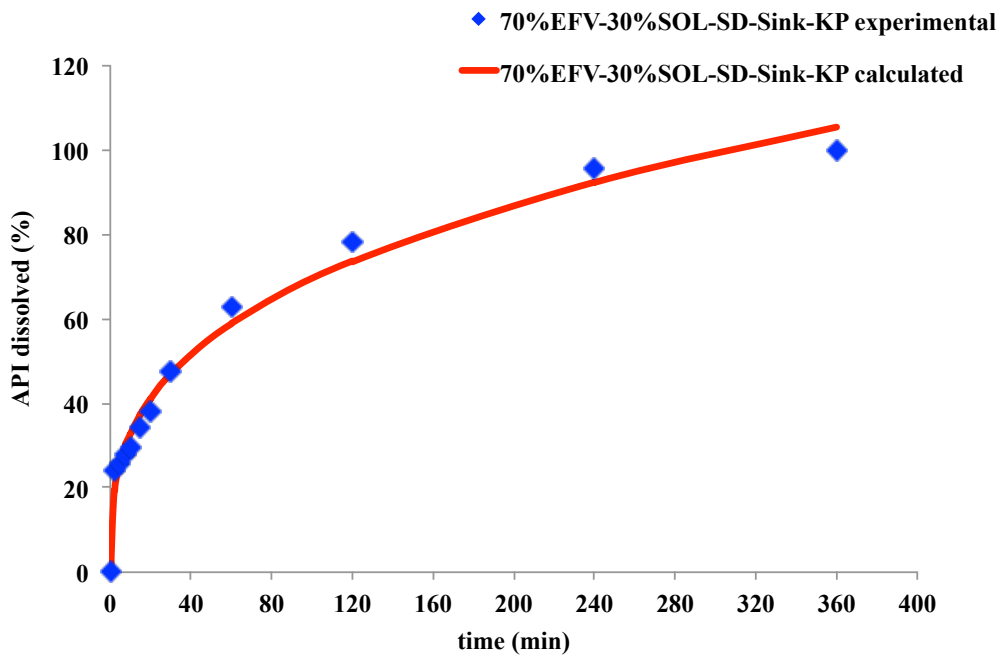
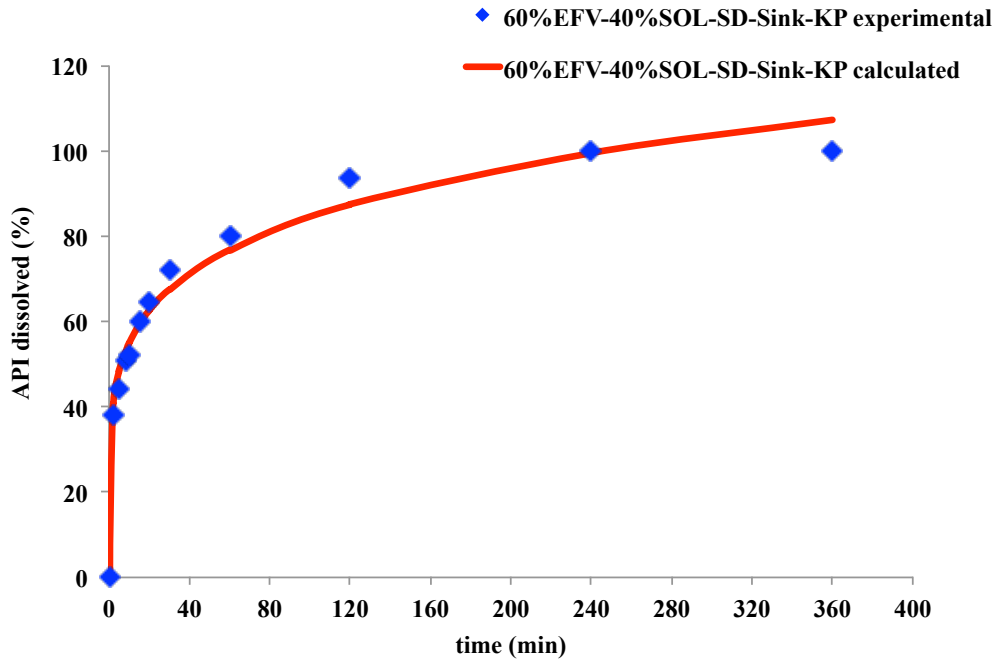


## Appendix 3 – API release fitting described mathematically by Korsmeyer-Peppas (KP) model

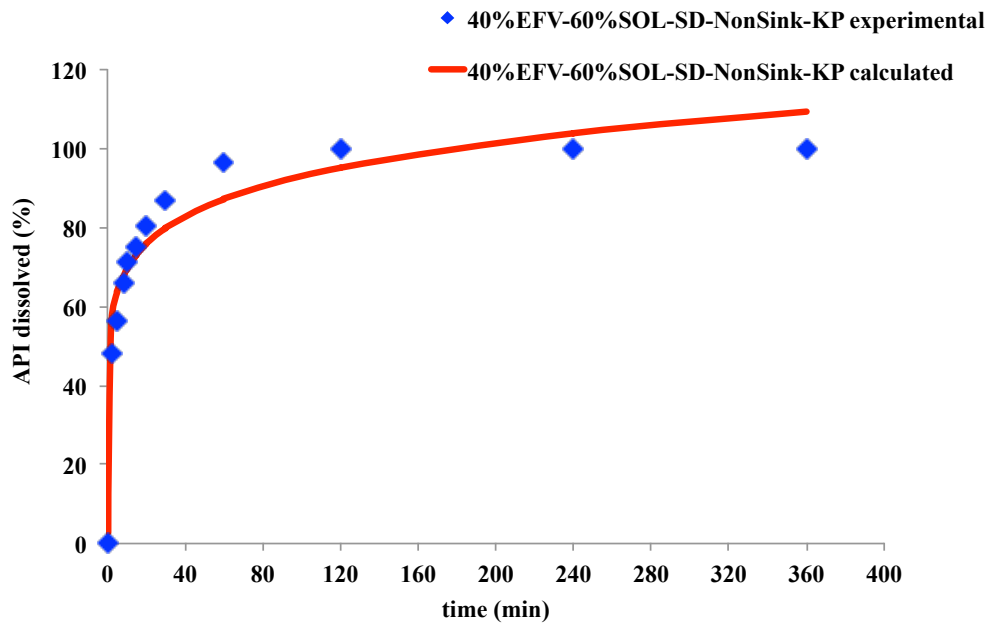
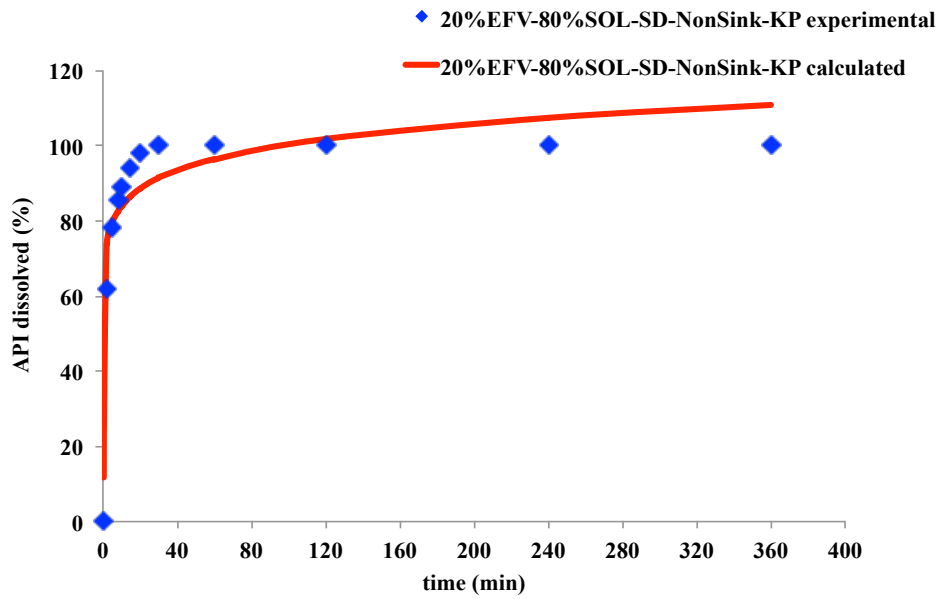
### 1- Spray Drying

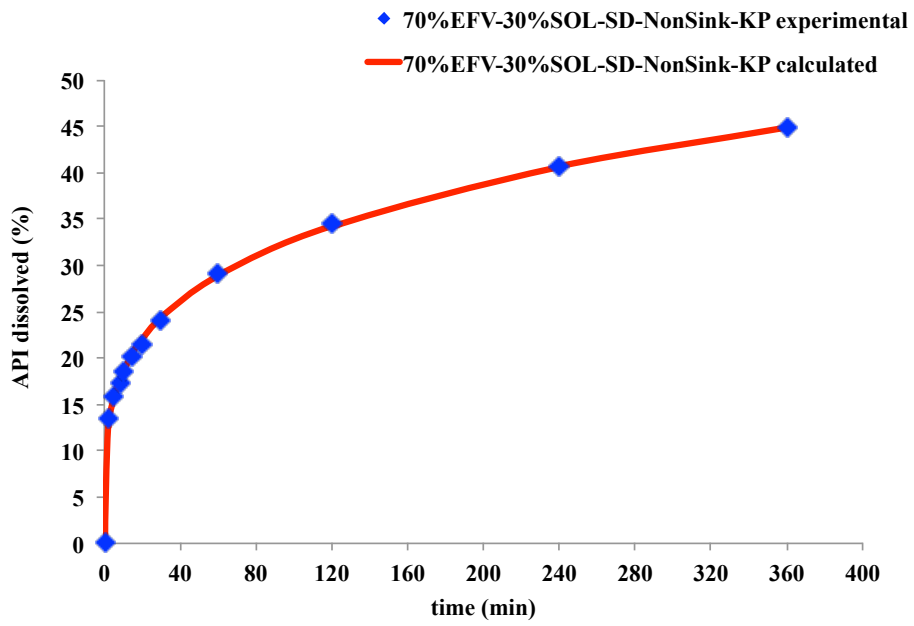
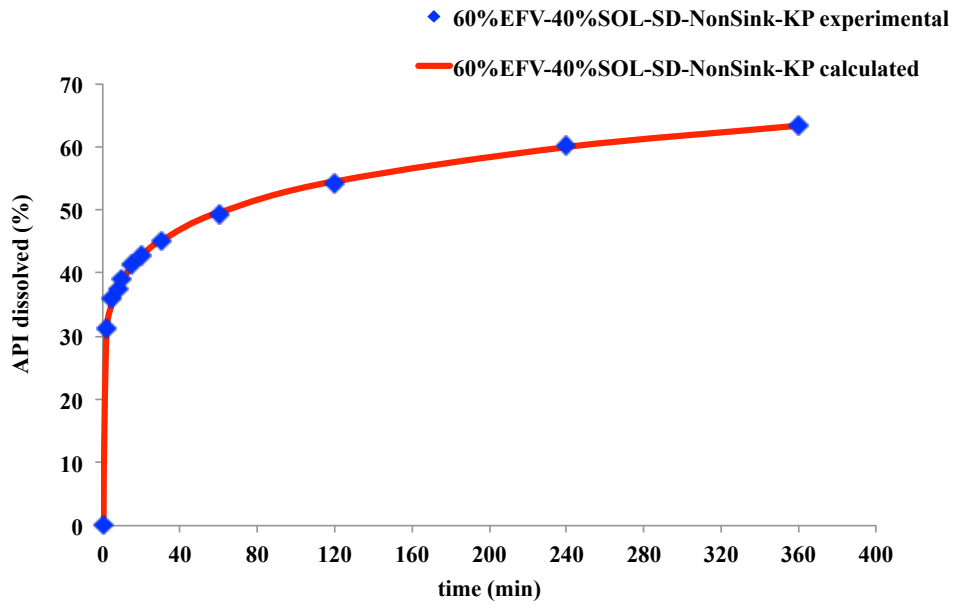
✓ Sink conditions





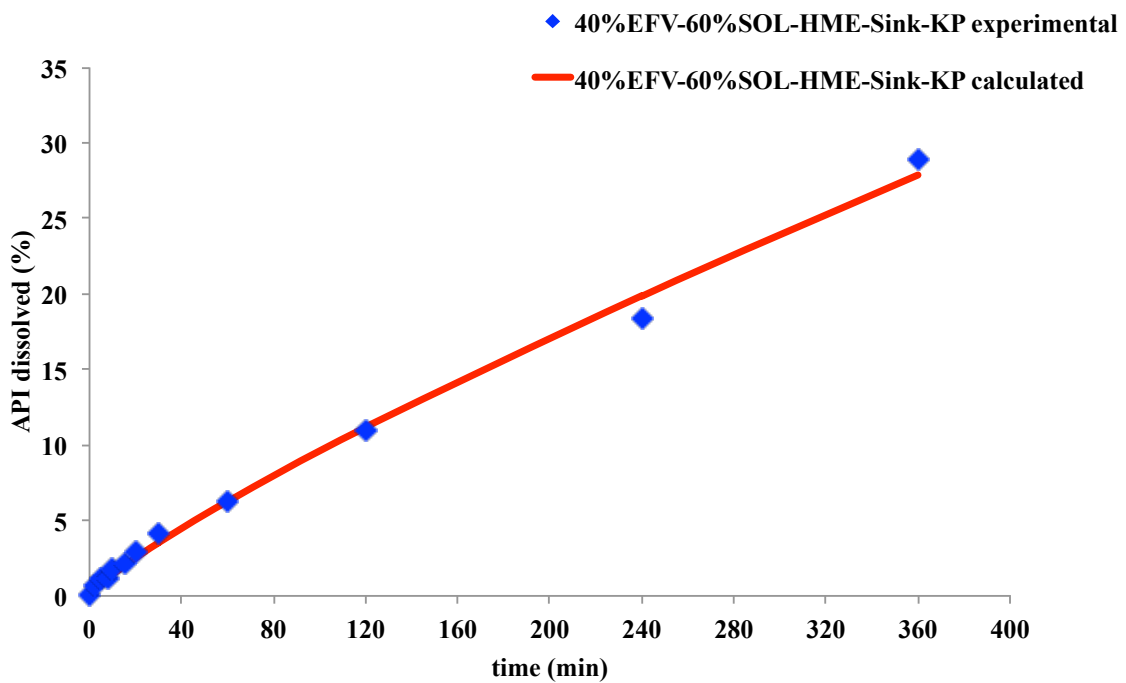
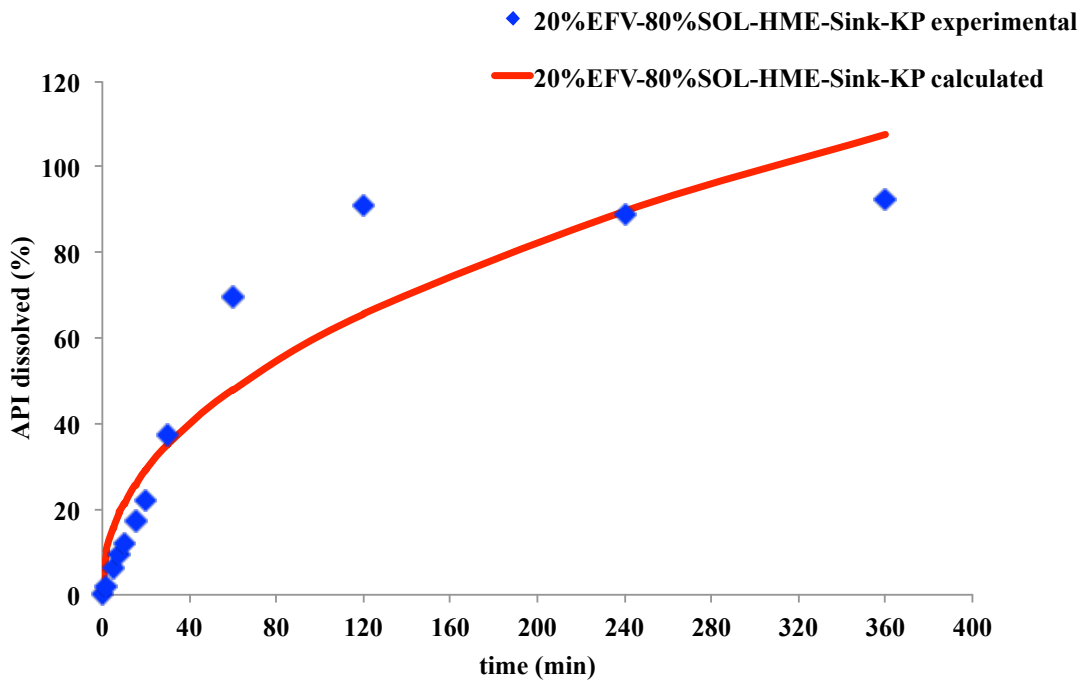
✓ Non-sink conditions

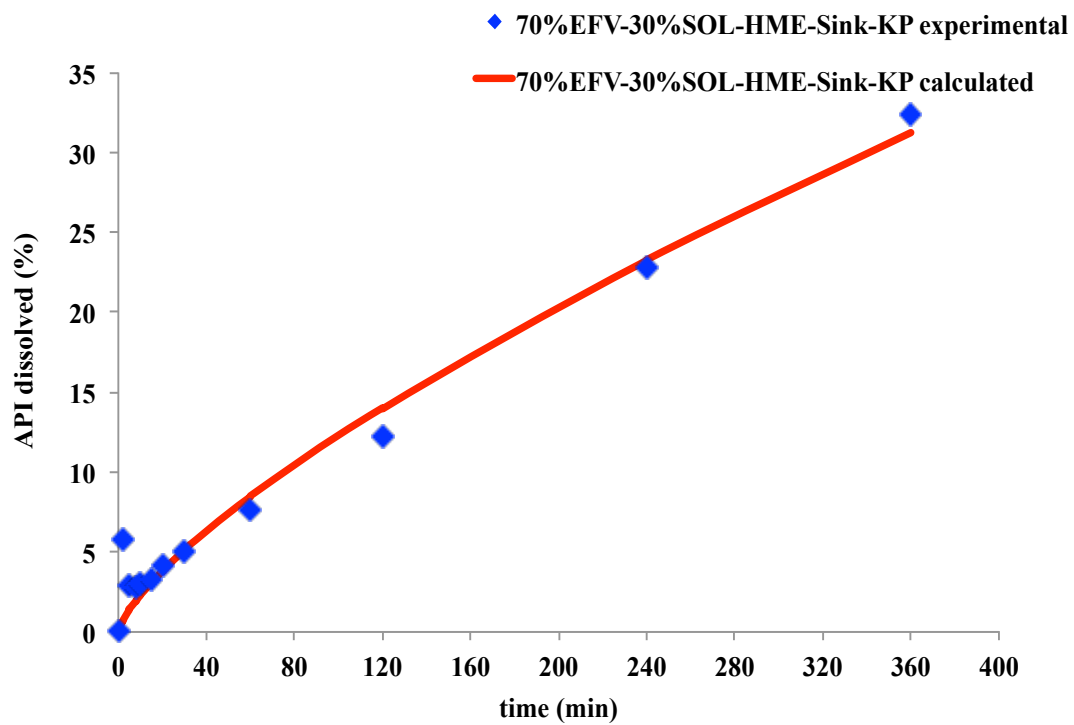
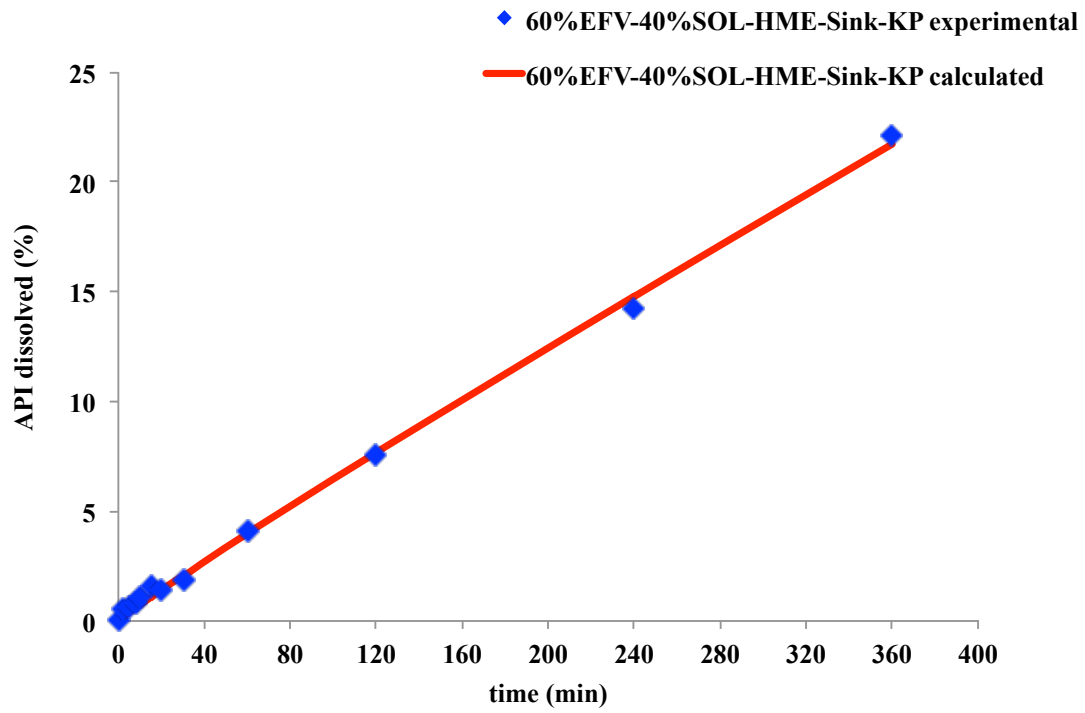




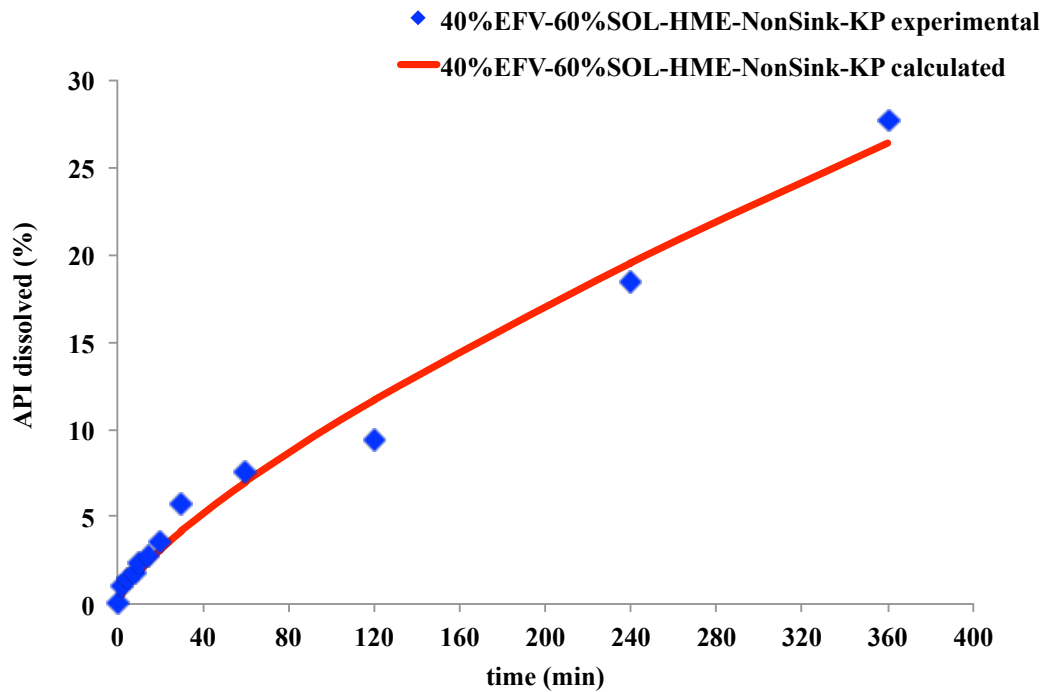
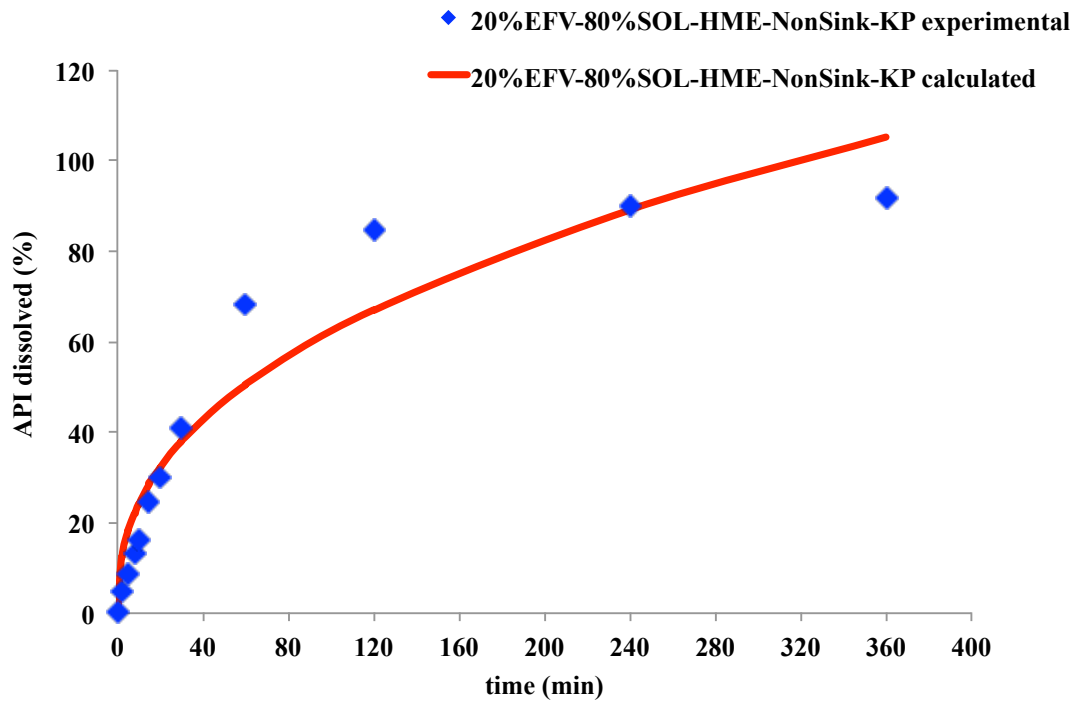
2- Hot-melt extrusion

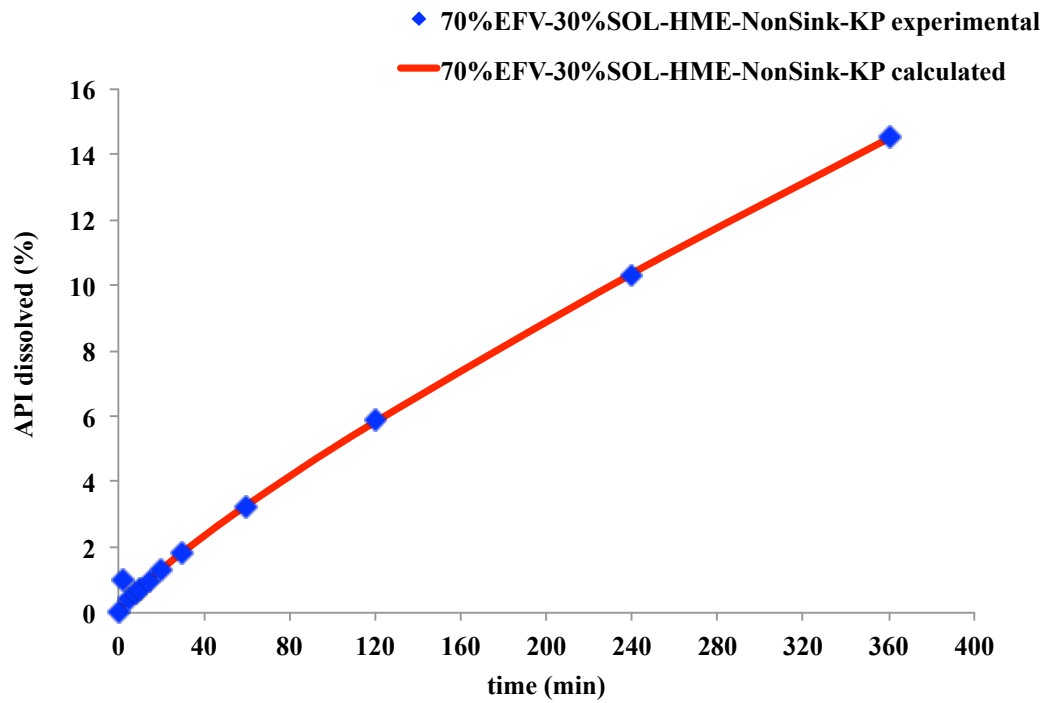
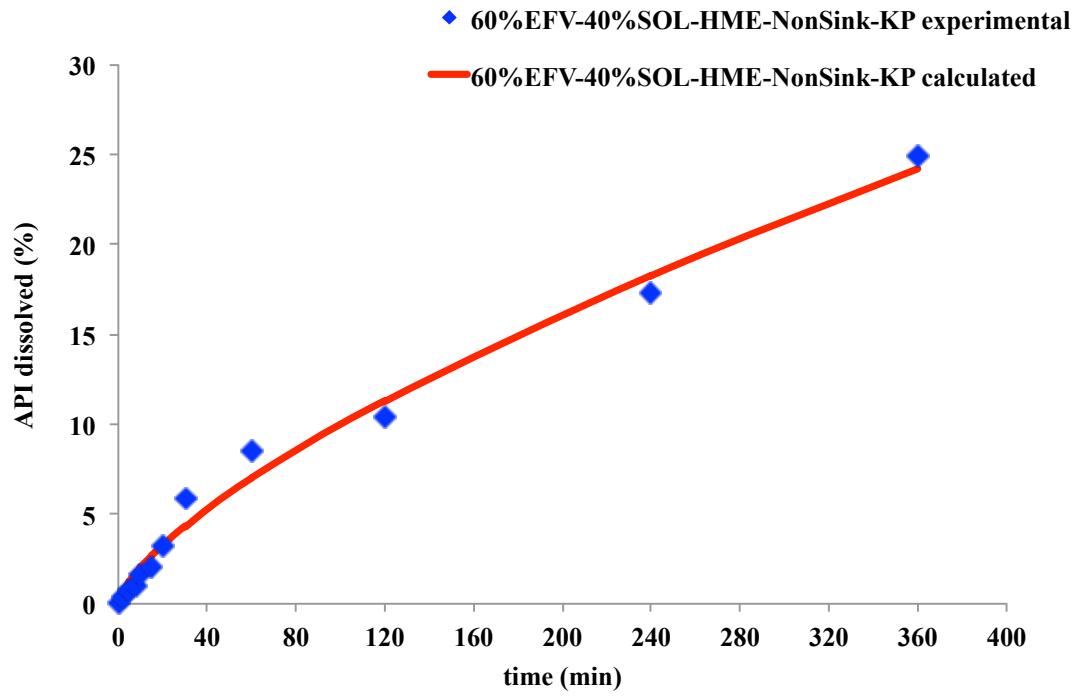
✓ Sink conditions





✓ Non-sink conditions





## Generation of high drug loading amorphous solid dispersions by different manufacturing processes

The main difficulty when an Active Pharmaceutical Ingredient (API) is orally administered is to guarantee that the clinical dose of the API will be dissolved in the available volume of gastrointestinal fluids. However, about 40% of APIs with market approval and nearly 90% of molecules in the discovery pipeline are poorly water-soluble and exhibits a poor oral absorption, which leads to a weak bioavailability. Amorphous solid dispersions (ASD) are considered as one of the most effective strategies to solve solubility limitations of poorly-water soluble compounds and hence, enhance their oral bioavailability. Despite their introduction as technical strategy to enhance oral APIs bioavailability more than 50 years ago, ASD formation and physical stability remains a subject of intense research. Indeed, several factors can influence the physical storage stability of ASD, among them, the glass transition temperature of the API-carrier binary mixture, the apparent solubility of the API in the carrier, interactions between API and carrier, and the manufacturing process. This thesis consisted of two parts that aim on developing new formulations of ASD of an antiretroviral API, Efavirenz (EFV), dispersed in an amphiphilic polymer, Soluplus, by using two different processes, Spray-drying (SD) and Hot-melt extrusion (HME). EFV is the class II BCS API of our choice because it is a challenging API for new formulations. It needs higher-dosed ASDs, for which chemical and physical stability during storage and dissolution will be critical. Aiming a rational development of high-loaded EFV-Soluplus ASDs, the first part focused on the construction of a temperature-composition EFV-Soluplus phase diagram. The phase-diagram was constructed from a thermal study of recrystallization of a supersaturated ASD (85 wt% in EFV), generated by spray drying. To our knowledge, this is the first study reporting a phase-diagram for this binary system. This phase-diagram is very useful and demonstrated that the EFV solubility in Soluplus ranges from 20 wt% (25 °C) to 30 wt% (40 °C). ASD of EFV in Soluplus containing more than 30 wt% of EFV should be monitored over storage under typical temperature conditions. This phase-diagram might be considered as a preformulation tool for researchers studying novel ASD of EFV in Soluplus, to predict (thermodynamic and kinetic) stability. ASD prepared by different techniques can display differences in their physicochemical properties. The second part of this thesis focused on the manufacturing of ASD by HME or SD processes. This study clearly shows that ASD is a useful formulation strategy to improve the aqueous solubility and the dissolution rate of EFV from EFV-Soluplus binary mixtures. HME and SD manufacturing processes demonstrated to be efficient to generate ASDs in a large range of compositions and loads of EFV. The optimization of EFV to Soluplus ratio can be used to tailor the release kinetics from ASD. The choice of a high EFV load exceeding the thermodynamic solid solubility in Soluplus is possible but it needs the consideration of its kinetic stability over time.

**Keywords:** *Amorphous solid dispersions, spray drying, hot-melt extrusion, solubility enhancement, phase diagram, drug release, Efavirenz, Soluplus.*